# **Springer Theses**Recognizing Outstanding Ph.D. Research

Hua-Sheng Shao

# Heavy Quarkonium Production Phenomenology and Automation of One-Loop Scattering Amplitud Computations



## **Springer Theses**

Recognizing Outstanding Ph.D. Research

#### Aims and Scope

The series "Springer Theses" brings together a selection of the very best Ph.D. theses from around the world and across the physical sciences. Nominated and endorsed by two recognized specialists, each published volume has been selected for its scientific excellence and the high impact of its contents for the pertinent field of research. For greater accessibility to non-specialists, the published versions include an extended introduction, as well as a foreword by the student's supervisor explaining the special relevance of the work for the field. As a whole, the series will provide a valuable resource both for newcomers to the research fields described, and for other scientists seeking detailed background information on special questions. Finally, it provides an accredited documentation of the valuable contributions made by today's younger generation of scientists.

#### Theses are accepted into the series by invited nomination only and must fulfill all of the following criteria

- They must be written in good English.
- The topic should fall within the confines of Chemistry, Physics, Earth Sciences, Engineering and related interdisciplinary fields such as Materials, Nanoscience, Chemical Engineering, Complex Systems and Biophysics.
- The work reported in the thesis must represent a significant scientific advance.
- If the thesis includes previously published material, permission to reproduce this must be gained from the respective copyright holder.
- They must have been examined and passed during the 12 months prior to nomination.
- Each thesis should include a foreword by the supervisor outlining the significance of its content.
- The theses should have a clearly defined structure including an introduction accessible to scientists not expert in that particular field.

More information about this series at http://www.springer.com/series/8790

# Heavy Quarkonium Production Phenomenology and Automation of One-Loop Scattering Amplitude Computations

Doctoral Thesis accepted by Peking University, Beijing, China



Author
Dr. Hua-Sheng Shao
School of Physics
Peking University
Beijing
China

Supervisor
Prof. Kuang-Ta Chao
School of Physics and State Key Laboratory
of Nuclear Physics and Technology
Peking University
Beijing
China

ISSN 2190-5053 ISSN 2190-5061 (electronic) Springer Theses ISBN 978-981-10-1623-3 ISBN 978-981-10-1624-0 (eBook) DOI 10.1007/978-981-10-1624-0

Library of Congress Control Number: 2016944407

#### © Springer Science+Business Media Singapore 2016

This work is subject to copyright. All rights are reserved by the Publisher, whether the whole or part of the material is concerned, specifically the rights of translation, reprinting, reuse of illustrations, recitation, broadcasting, reproduction on microfilms or in any other physical way, and transmission or information storage and retrieval, electronic adaptation, computer software, or by similar or dissimilar methodology now known or hereafter developed.

The use of general descriptive names, registered names, trademarks, service marks, etc. in this publication does not imply, even in the absence of a specific statement, that such names are exempt from the relevant protective laws and regulations and therefore free for general use.

The publisher, the authors and the editors are safe to assume that the advice and information in this book are believed to be true and accurate at the date of publication. Neither the publisher nor the authors or the editors give a warranty, express or implied, with respect to the material contained herein or for any errors or omissions that may have been made.

Printed on acid-free paper

This Springer imprint is published by Springer Nature
The registered company is Springer Science+Business Media Singapore Pte Ltd.

To my family For their continuous support and love

#### **Supervisor's Foreword**

Since the discovery of the first quarkonium state  $J/\psi$  in 1974 (Nobel Prize in 1976), it was thought as an ideal tool to measure fundamental parameters in quantum field theory (QFT) and to probe/understand many novel phenomena in quantum chromodynamics (QCD). Heavy quarkonium is composed of a heavy quark and an antiheavy quark, and it is a non-relativistic system of strong interactions. The production of heavy quarkonia provides a unique tool to test our understanding of strong interaction dynamics. However, for more than decades, the theoretical description for heavy quarkonium production is not satisfactory. The differential cross-sectional measurements of  $J/\psi$  and  $\psi(2S)$  production from proton–antiproton collisions by two experiments at the Tevatron were found to be more than an order of magnitude larger than theoretical predictions. It was thought as a "smoking gun" signal of a new heavy quarkonium production mechanism in QCD, the so-called color-octet mechanism (COM), which is usually thought to contribute at subleading level only. The importance of such a mechanism has been in debate since it was proposed. Although the introduction of COM can resolve the large discrepancies between experiment and theory for the yields, the polarization measurements of heavy quarkonium production at the Tevatron and the large Hadron collider (LHC) are far off the theoretical predictions based on COM. This polarization issue was thought as a long-standing puzzle in understanding QCD.

In recent years, great progress has been made at collider experiments of measuring quarkonia production. On the theory side, higher-order perturbative QCD corrections are found to be very crucial to account for the heavy quarkonium hadroproduction data. However, the perturbative calculations with QCD corrections by taking into account all important color-singlet and color-octet channels in an effective field theory are very challenging.

The first part of this thesis mainly focuses on the next-to-leading-order (NLO) QCD corrections to heavy quarkonium production. Based on the recursion relations, the thesis develops a new Monte Carlo event generator for investigating heavy quarkonium production processes, which were dubbed as HELAC-Onia. Such a technique helps to fulfill the complicated perturbative computations of

heavy quarkonium production processes. As a result, it was applied to accomplish a first complete NLO-level calculation of  $J/\psi$  polarization at Hadron colliders. With this new theoretical result, for the first time, both yields and polarizations of  $J/\psi$ can be explained within mid- and high-transverse momentum production regimes. The published results have been cited by almost all heavy quarkonium production measurements at hadron colliders later on. In the thesis, new comprehensive comparisons between experiment and theory are performed. So far, it gains the most satisfactory theoretical results compared to experimental data. This book also gives new insights into heavy quarkonium production mechanism by exploring the yields and polarizations of various heavy quarkonia from their different production processes at Hadron colliders and  $e^+e^-$  colliders at NLO QCD level. It points out that the COM can well account for the heavy quarkonium production in the large kinematical momentum transfer region, while the contributions from COM should not be important in the small kinematical momentum transfer region. Therefore, it sheds light on some unknown issues: non-perturbative effects, the possible violation of factorization theorem, our understanding of experimental measurements, etc.

In the second part of this thesis, it realizes the automation of computation of one-loop scattering amplitudes. In the higher-order perturbative computations of multileg scattering processes, the one-loop scattering amplitudes were thought as a bottleneck. Several modern loop techniques were proposed in the last 10 years. Based on these new techniques, Dr. Shao and his collaborators derived the complete Feynman rules for rational terms in the standard model and the minimal supersymmetric standard model, which should be derived once for all in each model. During his one-year visiting at CERN, he and his collaborators developed a new framework for the automated NLO-level Monte Carlo simulations in QFT, in which he is mainly in charge of developing one-loop module by applying the new loop techniques. This framework, MadGraph5\_aMC@NLO, is well known as one of the standard simulation tools in the high-energy phenomenology and the high-energy experiment communities. Since its first release on May 2014, the paper has been cited by more than 500 times.

The book has addressed several important scientific issues in the frontier of particle physics and opened new perspectives for scientific studies in this field. It also manifests the excellent physical insights, broad knowledge, good computational skills, and independent research capacity of the author. As the Ph.D. supervisor of Dr. Shao, I am glad to recommend this book and to express my congratulation to him on his very well-deserved thesis award.

Beijing, China May 2016 Prof. Kuang-Ta Chao

#### Acknowledgements

This thesis is based on the work in collaboration with Prof. Kuang-Ta Chao, Prof. Jean-Philippe Lansberg, Prof. Stefano Frixione, Prof. Fabio Maltoni, Prof. Tim Stelzer, Dr. Yu-Jie Zhang, Dr. Yan-Qing Ma, Dr. Kai Wang, Dr. Valentin Hirschi, Dr. Rikkert Frederix, Dr. Olivier Mattelaer, Dr. Marco Zaro, Dr. Paolo Torrielli, and Dr. Johan Alwall. Without their important contributions, I have no way to finish the majority parts of this dissertation. I am very pleasure to express my gratitude to all of them for the stimulating collaborations and for the fruitful discussions.

First of all, special thanks to my Ph.D. supervisor Prof. Kuang-Ta Chao. He provides me a free and active academic environment. His ongoing advice and support to me during my Ph.D. career is always invaluable. Thanks for his enthusiasm and insight in physics. Without his guidance, I might be lost in the literature. Thanks to him for many ideas he gave me and the solutions of my questions. Besides, I also want to thank him for taking care of me since I was an undergraduate student.

I would also like to give my special acknowledges to Prof. Michelangelo Mangano, Prof. Stefano Frixione, Prof. Fabio Maltoni, and Prof. Roberto Pittau. Thanks to all of you for providing me the opportunity to work with you, to stay at CERN for an amazing year from September 2012 to August 2013, and to get a job at CERN for my first postdoctoral career. I am happy to work with all of you and benefit a lot from you. I learned a lot from your talks and the discussions with you. Michelangelo, thanks to you for taking care of me when I was at CERN, for introducing me to other physicists, and for always providing me the opportunities in physics. Stefano, thanks to you for your very hard working in many aspects of the Madgraph5\_AMC@NLO projects and for your kind guidance for me when I was lost. Fabio, thanks to you for your enthusiasm in studying physics and for giving me a lot of ideas. Roberto, thanks to you for your nice encouragement when I was a junior Ph.D. student, for your invitation to Granada before I went to CERN, and for introducing me to develop the Madloop. Many many thanks to all of you.

x Acknowledgements

I want to thank Prof. Jean-Philippe Lansberg. Thanks to him for collaborating on several aspects of heavy quarkonium physics, for inviting me to visit Orsay when I was at CERN, and for many helps in my life.

I also thank Dr. Yu-Jie Zhang, who was initially guiding me when I started my Ph.D. research. I remembered you told me to read some paper on unitary methods when I was only an undergraduate student. Thanks to you for answering all of my questions patiently and for teaching me how to perform a next-to-leading-order computation. I am also grateful to all the guys in our group at my university: Dr. Ce Meng, Dr. Yan-Qing Ma, Dr. Kai Wang, Dr. Zhi-Guo He, Dr. Rong Li, Dr. Ying Fan, Dr. Dan Li, Dr. Li-Ping Sun, Jin-Zhao Li, Huai-Ke Guo, Sheng-Jin Sang, Hao Han, Wen-Zhe Yang, Peng Zhang, and Hao-Yu Liu. Thanks to all of you for the collaborations, discussions, and friendships.

I want to express my special gratitude to Dr. Valentin Hirschi. Thank you for allowing me to join you to develop MadLoop and for your amazing work on it. Thank you for explaining the code in detail to me when I just started working on it. Thank you for the stimulating discussions with you since then. Thanks for your helps and useful suggestions when I was stuck by the annoying bugs. I learned a lot from you both in softwares and in physics. I remembered we frequently linked over the sea to discuss physics this year. I like to collaborate with you and also appreciate the friendship with you. I thank Dr. Rikkert Frederix for patiently explaining the details of the MadFKS to me and for teaching me how to do FxFx merging with MadGraph5\_AMC@NLO. I also thank other guys in MadGraph team and FeynRules team: Dr. Olivier Mattelaer, Dr. Marco Zaro, Dr. Paolo Torrielli, Dr. Johan Alwall, Dr. Celine Degrande, Dr. Benjamin Fuks, and Dr. Claude Duhr. Thanks to all of you for the stimulating discussions and collaborations. I appreciate the friendship with Dr. Tom Melia, Dr. Franz Herzog, and Dr. Luca Barze at CERN.

I want to thank many persons who ever helped me. Thanks to Prof. Chong Sheng Li, who agreed to write a recommendation letter for me when I applied the fellowship at CERN. Thanks to the guys (like Dr. Hua Xing Zhu, Ding Yu Shao) in his group for useful discussions on physics. I also want to thank Prof. Costas Papadopoulos for encouraging me to upload HELAC-Onia to the HELAC Web page. Thanks to Dr. Qiang Li for the friendship and Dr. Qing-Hong Cao for the valuable suggestions. Forgive me if I forget anyone else.

### **Contents**

1			1	1 4
Pai	rt I H	Heavy Q	Quarkonium Production Phenomenology	
2	Back	ground	of Heavy Quarkonium Physics	9
	2.1		etical Framework	9
	2.2	Challe	enges	15
		2.2.1	Challenges in Proving NRQCD Factorization	15
		2.2.2	NRQCD Versus Experiments	15
	Refe	rences.		17
3	HEL	AC-On	ia	21
	3.1		etical Framework	21
		3.1.1	Recursive Computation of Helicity Amplitudes	21
		3.1.2	Heavy Quarkonium Amplitudes in NRQCD	25
	3.2	Monte	e Carlo Simulation with HELAC-Onia	27
		3.2.1	Usage	28
		3.2.2	Capability	31
		3.2.3	Validations	31
		3.2.4	Third-Party Codes in HELAC-Onia	32
		3.2.5	Status	33
		3.2.6	Robust on an Example: NNLO <sup>★</sup> QCD	
			Corrections to $\psi(2S)$ Hadroproduction in CSM	33
	Refe	rences .		34
4	Heav	vy Quar	konium Production in Hadronic Collisions	37
	4.1	Yields	s and Polarizations of Prompt $J/\psi$	
		and $\psi$	(2S) Production	37
		4.1.1	General Setup	38

xii Contents

		4.1.2 LDMEs	40
		4.1.3 Yields and Polarizations: NRQCD Versus	4.0
		Experiments	43
	4.0	4.1.4 Spin Density Matrix Elements	50
	4.2	Yields and Polarizations of Prompt $\chi_{c1}$ and $\chi_{c2}$ Production	51
		4.2.1 Motivation and Formulas	51
		4.2.2 LDMEs	54
		4.2.3 Numerical Results	55
	4.3	Double-Quarkonium Production at the LHC	58
		4.3.1 $J/\psi$ -pair Production	62
	D 0	4.3.2 $\Upsilon$ -pair Production	67
	Refe	rences	69
5		sive $J/\psi$ Production at B Factories	73
	5.1	Background	73
	5.2	Photon Shower from $e^{\pm}$ Beams	76
	5.3	Numerical Results: QCD, Relativistic and ISR Corrections	78
		5.3.1 $e^-e^+ \rightarrow J/\psi + c\bar{c} + X \dots$	78
		$5.3.2  e^-e^+ \to J/\psi + gg + X. \dots$	80
	Refe	rences	84
6	Sum	mary and Outlooks of Part I	87
Pai		Automation of One-Loop Scattering Amplitudes	
_		Computations	
7	NLO	Computations and Automation Philosophy	91
7	<b>NLO</b> 7.1	Computations and Automation Philosophy	91
7	<b>NLO</b> 7.1 7.2	Computations and Automation Philosophy	91 92
7	NLO 7.1 7.2 7.3	Computations and Automation Philosophy General Remarks Basic Concepts of NLO Computations Why Automation	91 92 96
7	NLO 7.1 7.2 7.3	Computations and Automation Philosophy	91 92
7 8	NLO 7.1 7.2 7.3 Refer	Computations and Automation Philosophy General Remarks Basic Concepts of NLO Computations Why Automation	91 92 96
	NLO 7.1 7.2 7.3 Refer One- 8.1	Computations and Automation Philosophy General Remarks Basic Concepts of NLO Computations Why Automation rences Loop Computations: OPP Versus TIR Generalities	91 92 96 97
	NLO 7.1 7.2 7.3 Refer	Computations and Automation Philosophy General Remarks Basic Concepts of NLO Computations Why Automation rences Loop Computations: OPP Versus TIR	91 92 96 97 101
	NLO 7.1 7.2 7.3 Refer One- 8.1 8.2 8.3	Computations and Automation Philosophy General Remarks Basic Concepts of NLO Computations Why Automation Tences  Loop Computations: OPP Versus TIR Generalities Rational Terms R <sub>2</sub> The Ossola–Papadopolous–Pittau Reduction	91 92 96 97 101 101
	NLO 7.1 7.2 7.3 Refer One- 8.1 8.2 8.3 8.4	Computations and Automation Philosophy General Remarks Basic Concepts of NLO Computations Why Automation rences  Loop Computations: OPP Versus TIR Generalities Rational Terms R <sub>2</sub> The Ossola–Papadopolous–Pittau Reduction Tensor Integral Reduction and IREGI	91 92 96 97 101 103 105 109
	NLO 7.1 7.2 7.3 Refer One- 8.1 8.2 8.3	Computations and Automation Philosophy General Remarks Basic Concepts of NLO Computations Why Automation Tences  Loop Computations: OPP Versus TIR Generalities Rational Terms R <sub>2</sub> The Ossola–Papadopolous–Pittau Reduction	91 92 96 97 101 103 105 109
	7.1 7.2 7.3 Refer One- 8.1 8.2 8.3 8.4 8.5	Computations and Automation Philosophy General Remarks Basic Concepts of NLO Computations Why Automation rences  Loop Computations: OPP Versus TIR Generalities Rational Terms R2 The Ossola–Papadopolous–Pittau Reduction Tensor Integral Reduction and IREGI Comparison Between OPP and TIR	91 92 96 97 101 103 105 109
8	7.1 7.2 7.3 Refer One- 8.1 8.2 8.3 8.4 8.5 Refer	Computations and Automation Philosophy General Remarks Basic Concepts of NLO Computations Why Automation rences  Loop Computations: OPP Versus TIR Generalities Rational Terms R2 The Ossola–Papadopolous–Pittau Reduction Tensor Integral Reduction and IREGI Comparison Between OPP and TIR rences  Loop5	91 92 96 97 101 103 105 109 114 119
8	7.1 7.2 7.3 Refer One- 8.1 8.2 8.3 8.4 8.5 Refer Mad 9.1	Computations and Automation Philosophy General Remarks Basic Concepts of NLO Computations Why Automation rences  Loop Computations: OPP Versus TIR Generalities Rational Terms R2 The Ossola–Papadopolous–Pittau Reduction Tensor Integral Reduction and IREGI Comparison Between OPP and TIR rences  Loop5 Notations and Conventions	91 92 96 97 101 103 105 109 114 114 119
	7.1 7.2 7.3 Refer 0ne- 8.1 8.2 8.3 8.4 8.5 Refer Mad 9.1 9.2	Computations and Automation Philosophy General Remarks Basic Concepts of NLO Computations Why Automation rences  Loop Computations: OPP Versus TIR Generalities Rational Terms R2 The Ossola—Papadopolous—Pittau Reduction Tensor Integral Reduction and IREGI Comparison Between OPP and TIR rences  Loop5 Notations and Conventions Basic Procedures	91 92 96 97 101 103 105 109 114 114 119 121
8	7.1 7.2 7.3 Refer  One- 8.1 8.2 8.3 8.4 8.5 Refer  Mad 9.1 9.2 9.3	Computations and Automation Philosophy General Remarks Basic Concepts of NLO Computations Why Automation rences  Loop Computations: OPP Versus TIR Generalities Rational Terms R2 The Ossola–Papadopolous–Pittau Reduction Tensor Integral Reduction and IREGI Comparison Between OPP and TIR rences  Loop5 Notations and Conventions Basic Procedures Improvements Compared to MadLoop4	91 92 96 97 101 103 105 109 114 114 119 121 121
8	7.1 7.2 7.3 Refer One- 8.1 8.2 8.3 8.4 8.5 Refer Mad 9.1 9.2 9.3 9.4	Computations and Automation Philosophy General Remarks Basic Concepts of NLO Computations Why Automation rences  Loop Computations: OPP Versus TIR Generalities Rational Terms R2 The Ossola–Papadopolous–Pittau Reduction Tensor Integral Reduction and IREGI Comparison Between OPP and TIR rences  Loop5 Notations and Conventions Basic Procedures Improvements Compared to MadLoop4 Optimizations	91 92 96 97 101 103 105 109 114 114 119 121 122 122
8	7.1 7.2 7.3 Refer  One- 8.1 8.2 8.3 8.4 8.5 Refer  Mad 9.1 9.2 9.3	Computations and Automation Philosophy General Remarks Basic Concepts of NLO Computations Why Automation rences  Loop Computations: OPP Versus TIR Generalities Rational Terms R2 The Ossola–Papadopolous–Pittau Reduction Tensor Integral Reduction and IREGI Comparison Between OPP and TIR rences  Loop5 Notations and Conventions Basic Procedures Improvements Compared to MadLoop4	91 92 96 97 101 103 105 109 114 114 119 121 121

Contents xiii

	9.7	Illustrative Stand-Alone Results	130
		9.7.1 High-Multiplicity QCD Process: $gg \rightarrow d\bar{d}b\bar{b}t\bar{t}$	131
		9.7.2 Mixed-Coupling Expansion I: $u\bar{d} \rightarrow d\bar{d}W^+ZH$	132
		9.7.3 Mixed-Coupling Expansion II: $u\bar{u} \rightarrow d\bar{d}t\bar{t}$	133
		9.7.4 A BSM Example: QCD Correction to $gg \rightarrow \tilde{t}_1 \tilde{t}_1^* g \dots$	134
	9.8	Summary of New Features in MadLoop5	136
	Refer	rences	136
10	Auto	mation of NLO Computations	139
	10.1	MadGraph5_aMC@NLO in a Nutshell	139
	10.2	How to Use MadGraph5_aMC@NLO	141
	10.3	Selected Results	144
		10.3.1 Total Cross Sections	144
		10.3.2 Differential Distributions	145
	Refer	rences	148
11	Sumi	mary and Prospects of Part II	151
Apj	pendix	A: Advanced Usage of HELAC-Onia	153
Apj	pendix	B: Validation of IREGI	157
Apj	pendix	C: Timing Scale of MadLoop5	163
Ind	ex		165

#### **Acronyms**

ALICE A LHC experiment/detector acronym for "A Large Ion Collider

Experiment"

ALOHA Automatic libraries of helicity amplitudes for Feynman diagram

computations

ATLAS A LHC experiment/detector acronym for "A Toroidal LHC

ApparatuS"

BABAR An experiment acronym for "B and B-Bar Experiment" at SLAC

Belle B detector at Koo Energy Ken in Japan

BLHA Binoth Les Houches Accord

BPHZ A renormalization procedure named after

Bogoliubov-Parasiuk-Hepp-Zimmermann

Br Branching ratio

BSM Beyond the Standard Model

CDF A Tevatron experiment/detector acronym for "Collider Detector at

Fermilab"

CEM Color Evaporation Model

CERN Conseil Europenne pour Recherches Nuclaires

CERN-NA3 An experiment on Super Proton Synchrotron at CERN

CKKW A leading-order merging scheme proposed by

"Catani-Krauss-Kuhn-Webber"

CKM A flavor mixing matrix proposed by "Cabibbo-Kobayashi-

Maskawa"

CLEO A general-purpose particle detector at the Cornell Electron Storage

Ring

CMS A LHC experiment/detector acronym for "Compact Muon

Solenoid"

CO Color Octet

COM Color-Octet Mechanism

CS Color Singlet

CSM Color-Singlet Model

xvi Acronyms

DGLAP An acronym of an equation proposed by

Dokshitzer-Gribov-Lipatov-Altarelli-Parisi

DPS Double-Parton Scattering

E1 Electric dipole E3 Electric octupole

EDM Extra-Dimensional Models
EPS Exceptional Phase Space point

EW Electroweak

FDH A dimensional regularization scheme called "Four-Dimensional

Helicity"

Fermilab Fermi National Accelerator Laboratory

FF Fragmentation Function

FKS A real subtraction method proposed by "Frixione–Kunszt–Signer"

FxFx A next-to-leading-order merging scheme proposed by

"Frederix-Frixione"

HEFT Higgs Effective Field Theory

HV A dimensional regularization scheme proposed by 't

Hooft-Veltman

IR Infrared

ISR Initial State Radiation

KLN A theorem named following Kinoshita–Lee–Nauenberg

LDME Long-Distance Matrix Element

LHC Large Hadron Collider

LHCb A LHC experiment/detector acronym for "Large Hadron Collider

beauty"

LHE Les Houches Event
LHM Little Higgs Models
LO Leading Order
M2 Magnetic quadrupole

iviagnetie quadrapole

MLM A leading-order merging scheme proposed by

"Michelangelo L. Mangano"

MSSM Minimal Supersymmetric Standard Model

NLO Next-to-Leading Order

NNLO Next-to-Next-to-Leading Order

NRQCD Non-Relativistic Quantum ChromoDynamics
OPP A one-loop integral reduction methods named after

Ossola–Papadopoulos–Pittau

PDF Parton Distribution Function

pQCD Perturbative Quantum ChromoDynamics

PSMC Parton Shower Monte Carlo
QCD Quantum ChromoDynamics
QED Quantum ElectroDynamics
QFT Quantum Field Theories
SCET Soft Collinear Effective Theory
SDC Short-Distance Coefficient

Acronyms xvii

SDME Spin-Density Matrix Element SLAC Stanford Linear Accelerator Center

SM Standard Model

SPS Single Parton Scattering SUSY SUper-SYmmetric

TIR Tensor Integral Reduction
UFO Universal FeynRules output
UPS Unstable Phase Space point

UV UltraViolet

# Chapter 1 Introduction

The ambition of high-energy collider physics is to probe the fundamental law of the universe via high-energy particle scattering processes. The modern high-energy physics studies are mainly focus on three aspects:

- study strongly interactive systems through the so-called Quantum Chromo Dynamics (QCD) theory;
- probe and/or validate electroweak (EW) symmetry breaking mechanism;
- search for Beyond the Standard Model (BSM) signals.

The theories in the first two items are unified into a modern Standard Model (SM) theory of elementary particles. In the SM, the strongly interactive systems are described by the unbroken SU(3) color gauge theory QCD, while the EW gauge theory is under SU(2)  $\times$  U(1) symmetry [1–3] and the symmetry is spontaneously broken through Higgs mechanism [4–7]. Moreover, many new theories were also proposed to replace the SM, such as SUper-SYmmetric (SUSY) theories (see, e.g., Ref. [8]), Extra-Dimensional Models (EDM) (see, e.g., Ref. [9]), and Little Higgs Models (LHM) (see, e.g., Ref. [10]), etc.

Before the 60th of last century, the picture of strong interactions only centered on the general principles of scattering amplitudes: analyticity, unitarity, crossing symmetry, etc., which is mainly due to unknown of the information on elementary constituents of hadrons. The experiments [11, 12] at the Stanford Linear Accelerator Center (SLAC) in the 1960s and the 1970s were the first ones to show the substructure of hadrons. The parton model [13, 14] and quark model [15, 16, 16, 17] were established to explain the experimental results. To avoid the apparent paradox in the quark model, a new quantum number "color" was postulated later [18, 19]. All these ideas were extending into a gauge theory [20–22]. However, the calculations and predictions in the theory are very difficult because the confinement is always required and perturbative method fails. The situation changes since the concept of asymptotic

1

2 1 Introduction

freedom was proposed [23, 24]. The asymptotic freedom makes it possible to study hadron inclusive production at colliders via perturbative calculations. The reliable of the perturbative QCD predictions is also relying on two key concepts: factorization [25–38] and infrared (IR) safety [39, 40]. Thanks to these pioneer works, the perturbative QCD has been developed a lot during the past 30 years and both experimental and theoretical results have been in the precision era. However, because of the presence of confinement, the understanding of non-perturbative QCD is still very limited. Modern non-perturbative approaches, such as QCD Sum Rules (see, e.g., Ref. [41]) and Lattice QCD (see, e.g., Refs. [42–45]), are not widely applied due to their limitations. Hence, the only powerful way to study non-perturbative physics is based on various factorizations, phenomenological models, and perturbative computations (see a recentreview Ref. [46]).

In contrast to QCD, since its establish, the EW theory has been tested to a very high accuracy. However, the EW symmetry broken mechanism is still unclear, and the last key missing piece in the SM, the Higgs boson, was discovered only recently [47, 48] at Large Hadron Collider (LHC). There are other open questions such as dark matter and hierarchy problem should be answered by the experiments at the LHC and the future colliders.

All of these studies are highly based on the precise perturbative calculations in quantum field theories (QFTs). My researches during my PhD are mainly focused on two aspects:

- 1. The first one is to study heavy quarkonium production mechanism via perturbative calculations. It provides a good way to study how the non-perturbative QCD physics plays role in the formation of heavy quarkonium.
- 2. The second aspect is to develop a way to automatically performing one-loop scattering amplitudes calculations with my collaborators, which is a key ingredient in the next-to-leading order (NLO) computations.

The thesis is organized into the following way:

- In the first part of this thesis, we will review the main background for the heavy quarkonium physics; then, we describe our method for calculating heavy quarkonium amplitudes and develop an automatic Monte Carlo generator HELAC-ONIA; we study the various heavy quarkonium production processes at hadron colliders and B factories in the next two chapters; finally, we present a summary and an outlook for this part.
- In the second part of this thesis, we recall the basic procedures for the NLO computations and then go into the modern one-loop integral reduction methods; with these algorithms for one-loop integrals, we develop an automatic one-loop program Madloop5 based on the tree-level generator Madgraph5 and describe a single framework Madgraph5\_AMC@NLO for the automation of NLO computation; a short summary is done at the end of this part.
- We also present some details about the relevant programs in the appendices.

1 Introduction 3

The thesis is mainly based on the work presented in the following publications:

- H.-S. Shao, "HELAC-Onia: An automatic matrix element generator for heavy quarkonium physics," *Comput.Phys.Commun.* 184 (2013) 2562–2570, arXiv:1212.5293 [hep-ph]. Copyright 2013 with permission from Elsevier.
- K.-T. Chao, Y.-Q. Ma, H.-S. Shao, K. Wang, and Y.-J. Zhang, " $J/\psi$  polarization at hadron colliders in nonrelativistic QCD," *Phys.Rev.Lett.* **108** (2012) 242004, arXiv:1201.2675 [hep-ph].
- H.-S. Shao, H. Han, Y.-Q. Ma, C. Meng, Y.-J. Zhang and K.-T. Chao, "Yields and polarizations of prompt  $J/\psi$  and  $\psi(2S)$  production in hadronic collisions," *JHEP* **1505** (2015) 103, arXiv:1411.3300 [hep-ph].
- H.-S. Shao and K.-T. Chao, "Spin correlations in polarizations of P-wave charmonia  $\chi_{cJ}$  and impact on  $J/\psi$  polarization," *Phys.Rev.* **D90** (2014) 014002, arXiv:1209.4610 [hep-ph].
- H.-S. Shao, Y.-Q. Ma, K. Wang, and K.-T. Chao, "Polarizations of  $\chi_{c1}$  and  $\chi_{c2}$  in prompt production at the LHC," *Phys.Rev.Lett.* **112** (2014) 182003, arXiv:1402.2913 [hep-ph].
- J.-P. Lansberg and H.-S. Shao, "Production of J/psi+eta(c) vs. J/psi+J/psi at the LHC: Impact of Real  $\alpha_s^5$  corrections," *Phys.Rev.Lett.* **111** (2013) 122001, arXiv:1308.0474 [hep-ph].
- H.-S. Shao, "Initial state radiation effects in inclusive  $J/\psi$  production at B factories," *JHEP* **04** (2014) 182, arXiv:1402.5840 [hep-ph].
- H.-S. Shao, Y.-J. Zhang, and K.-T. Chao, "Feynman Rules for the Rational Part of the Standard Model One-loop Amplitudes in the 't Hooft-Veltman  $\gamma_5$  Scheme," *JHEP* **09** (2011) 048, arXiv:1106.5030 [hep-ph].
- H.-S. Shao and Y.-J. Zhang, "Feynman Rules for the Rational Part of One-loop QCD Corrections in the MSSM," *JHEP* **1206** (2012) 112, arXiv:1205.1273 [hep-ph].
- J. Alwall, R. Frederix, S. Frixione, V. Hirschi, F. Maltoni, O. Mattelaer, H.-S. Shao, T. Stelzer, P. Torrielli, and M. Zaro, "The automated computation of tree-level and next-to-leading order differential cross sections, and their matching to parton shower simulations," *JHEP* **1407** (2014) 079, arXiv:1405.0301 [hep-ph].

The first 7 publications are devoted to the Part I and the remaining 3 publications contribute to the Part II. Some results are expanded into details and new, such as the new features of HELAC- ONIA version 1.2.X in second chapter of Part I, the yields and polarizations of prompt  $J/\psi$  and  $\psi(2S)$  production in Sect. 4.1,  $\Upsilon$  pair production in Sect. 4.3.2, the code of IREGI in the second chapter of Part II, and some details of MADLOOP5 in the third chapter of Part II.

4 1 Introduction

#### References

- 1. S. Glashow, Nucl. Phys. 22, 579 (1961). doi:10.1016/0029-5582(61)90469-2
- 2. S. Weinberg, Phys. Rev. Lett. 19, 1264 (1967). doi:10.1103/PhysRevLett.19.1264
- 3. A. Salam, Conf. Proc. C680519, 367 (1968)
- 4. P.W. Higgs, Phys. Lett. 12, 132 (1964). doi:10.1016/0031-9163(64)91136-9
- 5. P.W. Higgs, Phys. Rev. Lett. 13, 508 (1964). doi:10.1103/PhysRevLett.13.508
- 6. F. Englert, R. Brout, Phys. Rev. Lett. 13, 321 (1964). doi:10.1103/PhysRevLett.13.321
- G. Guralnik, C. Hagen, T. Kibble, Phys. Rev. Lett. 13, 585 (1964). doi:10.1103/PhysRevLett. 13.585
- 8. S. Ferrara (1987)
- 9. L. Randall, R. Sundrum, Phys. Rev. Lett. 83, 3370 (1999). doi:10.1103/PhysRevLett.83.3370
- N. Arkani-Hamed, A. Cohen, E. Katz, A. Nelson, JHEP 0207, 034 (2002). doi:10.1088/1126-6708/2002/07/034
- 11. E.D. Bloom, D. Coward, H. DeStaebler, J. Drees, G. Miller et al., Phys. Rev. Lett. 23, 930 (1969). doi:10.1103/PhysRevLett.23.930
- J.I. Friedman, H.W. Kendall, Ann. Rev. Nucl. Part. Sci. 22, 203 (1972). doi:10.1146/annurev. ns.22.120172.001223
- 13. R.P. Feynman, Phys. Rev. Lett. 23, 1415 (1969). doi:10.1103/PhysRevLett.23.1415
- 14. J. Bjorken, E.A. Paschos, Phys. Rev. 185, 1975 (1969). doi:10.1103/PhysRev.185.1975
- 15. M. Gell-Mann, Phys. Lett. **8**, 214 (1964). doi:10.1016/S0031-9163(64)92001-3
- 16. G. Zweig (1964)
- 17. J. Kokkedee, L. Van Hove, Nuovo Cim. 42, 711 (1966). doi:10.1007/BF02720548
- 18. O. Greenberg, Phys. Rev. Lett. 13, 598 (1964). doi:10.1103/PhysRevLett.13.598
- 19. M. Han, Y. Nambu, Phys. Rev. 139, B1006 (1965). doi:10.1103/PhysRev.139.B1006
- H. Fritzsch, M. Gell-Mann, H. Leutwyler, Phys. Lett. B 47, 365 (1973). doi:10.1016/0370-2693(73)90625-4
- 21. D.J. Gross, F. Wilczek, Phys. Rev. Lett. 30, 1343 (1973). doi:10.1103/PhysRevLett.30.1343
- 22. S. Weinberg, Phys. Rev. Lett. 31, 494 (1973). doi:10.1103/PhysRevLett.31.494
- 23. D. Gross, F. Wilczek, Phys. Rev. D 8, 3633 (1973). doi:10.1103/PhysRevD.8.3633
- 24. H.D. Politzer, Phys. Rev. Lett. 30, 1346 (1973). doi:10.1103/PhysRevLett.30.1346
- 25. A.H. Mueller, Phys. Rev. D 9, 963 (1974). doi:10.1103/PhysRevD.9.963
- 26. H.D. Politzer, Nucl. Phys. B 129, 301 (1977). doi:10.1016/0550-3213(77)90197-3
- 27. C.T. Sachrajda, Phys. Lett. B 73, 185 (1978). doi:10.1016/0370-2693(78)90831-6
- D. Amati, R. Petronzio, G. Veneziano, Nucl. Phys. B 140, 54 (1978). doi:10.1016/0550-3213(78)90313-9
- D. Amati, R. Petronzio, G. Veneziano, Nucl. Phys. B 146, 29 (1978). doi:10.1016/0550-3213(78)90430-3
- 30. S.B. Libby, G.F. Sterman, Phys. Rev. D 18, 4737 (1978). doi:10.1103/PhysRevD.18.4737
- 31. S.B. Libby, G.F. Sterman, Phys. Rev. D 18, 3252 (1978). doi:10.1103/PhysRevD.18.3252
- R.K. Ellis, H. Georgi, M. Machacek, H.D. Politzer, G.G. Ross, Nucl. Phys. B 152, 285 (1979). doi:10.1016/0550-3213(79)90105-6
- 33. A. Efremov, A. Radyushkin, Theor. Math. Phys. 44, 774 (1981). doi:10.1007/BF01029042
- 34. A. Efremov, A. Radyushkin, Theor. Math. Phys. 44, 664 (1981). doi:10.1007/BF01018445
- G.T. Bodwin, Phys. Rev. D 31, 2616 (1985). doi:10.1103/PhysRevD.34.3932, 10.1103/ PhysRevD.31.2616
- J.C. Collins, D.E. Soper, G.F. Sterman, Nucl. Phys. B 261, 104 (1985). doi:10.1016/0550-3213(85)90565-6
- J.C. Collins, D.E. Soper, G.F. Sterman, Nucl. Phys. B 308, 833 (1988). doi:10.1016/0550-3213(88)90130-7
- 38. J.C. Collins, D.E. Soper, G.F. Sterman, Adv. Ser. Direct. High Energy Phys. 5, 1 (1988)
- G.F. Sterman, S. Weinberg, Phys. Rev. Lett. 39, 1436 (1977). doi:10.1103/PhysRevLett.39.
   1436

References 5

 Y.L. Dokshitzer, D. Diakonov, S. Troian, Phys. Rept. 58, 269 (1980). doi:10.1016/0370-1573(80)90043-5

- 41. P. Colangelo, A. Khodjamirian (2000)
- 42. K.G. Wilson, Phys. Rev. D 10, 2445 (1974). doi:10.1103/PhysRevD.10.2445
- 43. A. Bazavov, D. Toussaint, C. Bernard, J. Laiho, C. DeTar et al., Rev. Mod. Phys. 82, 1349 (2010). doi:10.1103/RevModPhys.82.1349
- 44. D.J. Callaway, A. Rahman, Phys. Rev. Lett. 49, 613 (1982). doi:10.1103/PhysRevLett.49.613
- 45. D.J. Callaway, A. Rahman, Phys. Rev. D 28, 1506 (1983). doi:10.1103/PhysRevD.28.1506
- N. Brambilla et al., QCD and strongly coupled gauge theories: challenges and perspectives.
   Eur. Phys. J. C 74(10), 2981 (2014). doi:10.1140/epjc/s10052-014-2981-5. arXiv:1404.3723 [hep-ph]
- 47. G. Aad et al., Phys. Lett. B **716**, 1 (2012). doi:10.1016/j.physletb.2012.08.020
- 48. S. Chatrchyan et al., Phys. Lett. B **716**, 30 (2012). doi:10.1016/j.physletb.2012.08.021

## Part I Heavy Quarkonium Production Phenomenology

# **Chapter 2 Background of Heavy Quarkonium Physics**

**Abstract** Since the discovery of  $J/\psi$  in 1974 [1, 2], heavy quarkonium physics has played an important role in revealing and in investigating the QCD at the interplay between the perturbative regime and the non-perturbative regime. However, till now, we are still unable to understand the heavy quarkonium production mechanism very well. In particular, we do not know which theory can describe its production at various colliders. In this chapter, we review the main theoretical background, recent progress, and challenges in heavy quarkonium production physics. The organization of this chapter is: in Sect. 2.1, we will give an introduction of some basic theoretical ideas and establish the notations and nomenclature; in Sect. 2.2, we will present the challenges of theories in confront of experiments.

#### 2.1 Theoretical Framework

Heavy quarkonium is a kind of color-singlet (CS) bound state  $H_{Q\bar{Q}}$ , which is composed of a pair of heavy-flavor quarks  $Q\bar{Q}$ . For example,  $J/\psi(\Upsilon)$  is composed of a charm (bottom) quark and a charm (bottom) antiquark, while  $B_c^+$  meson is composed of a charm quark and a bottom antiquark. The mass of a heavy quarkonium is almost the sum of the masses in its constituent quarks, which indicates that heavy-flavor quarks in a heavy quarkonium meson are nonrelativistic and their relative velocity v in the rest frame of the meson should be a small parameter. For charmonium, <sup>1</sup> the typical  $v^2 \simeq 0.3$ , whereas for bottomonium,  $v^2 \simeq 0.1$ . Hence,there are three intrinsic scales in a heavy quarkonium meson: the heavy-flavor quark mass m, the relative momentum of the heavy quark pair mv, and the binding energy of the heavy quark pair  $mv^2$ .

Let us consider a process with a heavy quarkonium production at hadron colliders or  $e^-e^+$  colliders. Since the heavy-flavor quark pair  $Q\bar{Q}$  is produced in a hard-scattering process, a hard scale  $Q_{hard}$  should enter into the description of the production process. In a hadroproduction process, the hard-scattering scale  $Q_{hard}$  is

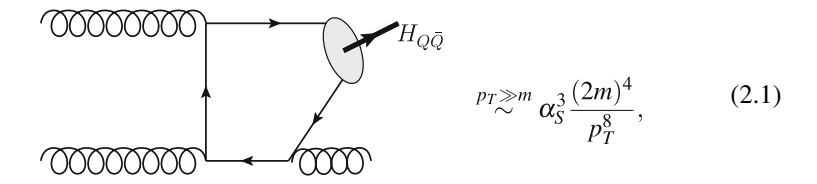
<sup>&</sup>lt;sup>1</sup>Charmonium is composed of a pair of charm quark and antiquark, whereas bottomonium is composed of a pair of bottom quark and antiquark.

<sup>©</sup> Springer Science+Business Media Singapore 2016 H.-S. Shao, *Heavy Quarkonium Production Phenomenology and Automation of One-Loop Scattering Amplitude Computations*, Springer Theses, DOI 10.1007/978-981-10-1624-0\_2

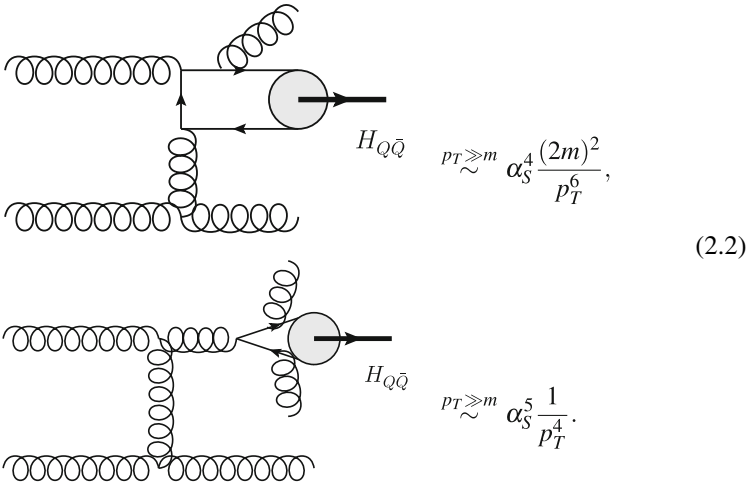
the order of the transverse momentum  $p_T$  of the heavy quarkonium, while in  $e^-e^+$  annihilation process,  $Q_{hard}$  is the order of the three-dimensional momentum  $p^*$  of the heavy quarkonium in the rest frame of the initial colliding particles. It would be imagined that the production could be understood in terms of two district steps. The first step is producing a quasi-collinear heavy quark pair  $Q\bar{Q}$  at hard scale  $Q_{hard} \gtrsim m$ . If the quark pair is moving too far away from each other, it would be difficult to bind together afterward. This scattering process should happen at "short" distance  $1/Q_{hard}$ . After the hard-scattering process,  $Q\bar{Q}$  will evolve into a color-singlet hadron state (i.e., a heavy quarkonium  $H_{Q\bar{Q}}$ ) with a probability smaller than unity. The dynamical scales involved in the second evolution process are mv and  $mv^2$ , and it happens at a relatively "long" distance.

The quantitative description of this physical picture relies on the validation of a factorization theorem; i.e., the short-distance physics at scale  $Q_{hard}$  can be completely separated from the long-distance physics at mv,  $mv^2$  and at the QCD scale  $\Lambda_{\rm OCD}$ . No important interference terms will contribute into the physical observables. To prove such factorization theorem, one must be able to express the heavy quarkonium amplitude into a sum of products of IR safe short-distance coefficients (SDCs) with well-defined long-distance matrix elements (LDMEs). Due to  $Q_{hard} \gg \Lambda_{\rm QCD}$ , the short-distance coefficients can be calculated in perturbative QCD (pQCD), while the long-distance terms are the only non-perturbative stuff. A better situation is the long-distance part has the less independent freedom than experiments and it can be determined once from some experiments and predicts the others. There are several approaches in describing the evolution of a heavy-flavor quark pair into a heavy quarkonium meson (see reviews in [3–5]): the color-singlet model (CSM)(see, e.g., Refs. [6–9]), the color-evaporation model (CEM) [10–15], the nonrelativistic QCD (NRQCD) effective theory [16] and the fragmentation-function (FF) approach [17–24].

In the CSM, the heavy quark pair  $Q\bar{Q}$  is produced in CS states at the hard-scattering process with scale  $Q_{hard}$ . The quantum numbers of the quark pair are the same with those of the heavy quarkonium. The LDME of the quarkonium  $H_{Q\bar{Q}}$  in the CSM can be estimated from its decay rates measurements or in a potential model [25]. The CSM was successful in describing the heavy quarkonium production rates at the relatively low-momentum transfer  $Q_{hard} \sim m$  [26–28] regime. However, it was found that the CSM underestimated the production rate of  $J/\psi$  and  $\psi(2S)$  at Tevatron [29–31] at larger  $p_T$ . The discrepancy can be reduced a lot if one includes higher-order contributions [32, 33]. Moreover, the polarization of  $J/\psi$  and  $\psi(2S)$  in the CSM will be changed from being transverse at leading order (LO) to be longitudinal at NLO [34]. This behavior is understood as new topologies only appear at higher orders. In specific, at LO, the parton-level distribution  $d\hat{\sigma}/dp_T^2$  is scaling as



whereas at NLO and next-to-next-to-leading order (NNLO), the corresponding scalings are

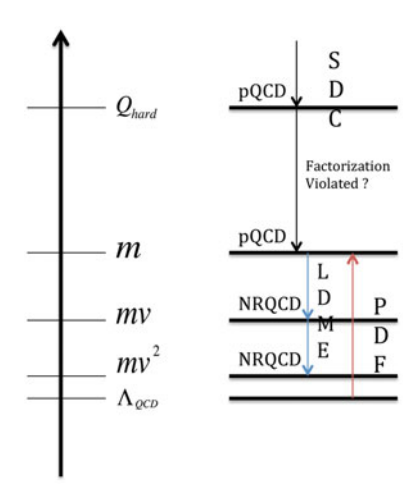


Because of the  $p_T$ -enhancement in the new topologies, the yields and polarization patterns of the heavy quarkonium will completely change in the CSM. After considering up to  $\mathcal{O}(\alpha_S^5)^2$  contributions [33, 35], the yields and polarizations of  $\psi$  are still in contradicted with the experimental data measured at the Tevatron and the LHC (e.g., see Ref. [36]). Moreover, in the production or the decay processes of the P-wave mesons, for example  $\chi_c$ , the CSM is known to be lacking the ability to cancel IR divergences.

The CEM is based on the principle of quark-hadron duality, in which the heavy-flavor quark pair evolves into a heavy quarkonium only when the invariant mass of the quark pair is less than the threshold for producing a pair of open-flavor heavy mesons. The probability of the quark pair evolving into a quarkonium is a universal and scale-independent constant. It also explores the large predictive power of the theory. However, the drawback of this model is that it predicts a fixed cross-sectional ratios of various heavy quarkonium productions, which is apparently in contradiction with the current experiments.

<sup>&</sup>lt;sup>2</sup>Only double real contribution is included at  $\mathcal{O}(\alpha_s^5)$ .

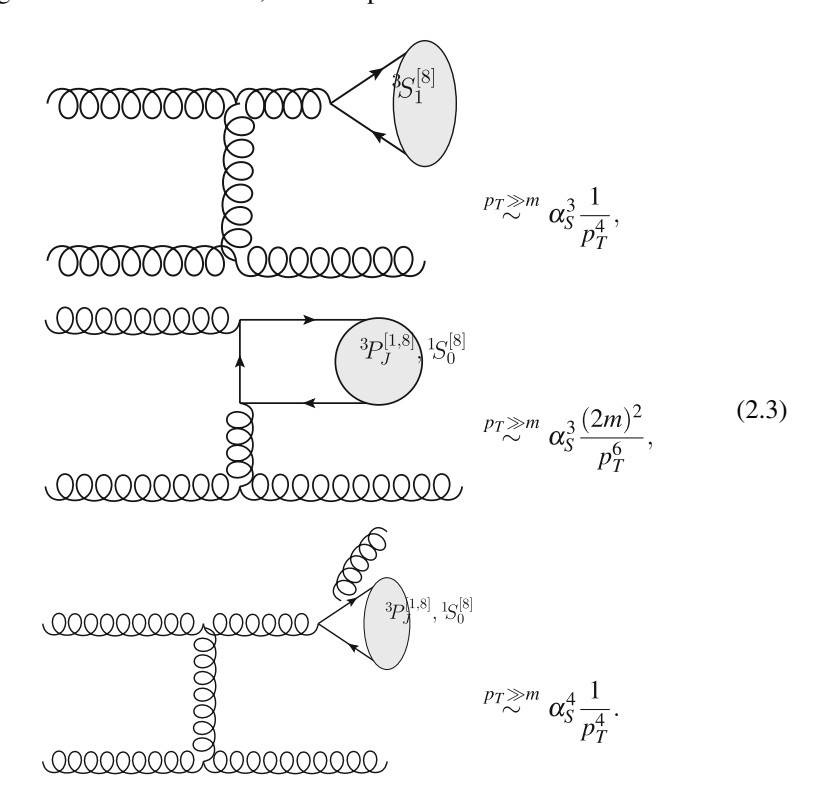
**Fig. 2.1** Various scales for the effective theory NRQCD setup



The FF approach is derived from the collinear factorization theorem that a heavy quarkonium production cross section can be factorized in terms of convolutions of parton-level production cross sections with light-cone like FFs [17–21] in the large  $p_T$  limit  $p_T\gg m$ . The leading power in  $m/p_T$  is coming from the terms of convolutions of a single parton production cross section with a single parton FF [17]. The factorization theorem of the subleading power of  $m/p_T$  contribution was introduced and proven in Refs. [18, 20]. Later, in Ref. [21], it was also proven in the Soft-Collinear Effective Theory (SCET) [37, 38]. The subleading contribution is given by  $Q\bar{Q}$  production cross sections convoluted by double parton FFs. The good thing in FF approach is that the collinear factorization theorem has been proven rigorously to subleading power of  $m/p_T$  and the large logarithms of  $\log \frac{p_T^2}{(2m)^2}$  can be systematically resumed via renormalization group running of FFs. However, it only applies in the large  $p_T$  regime and the predictive power relies heavily on the knowing of the non-perturbative FFs.

The state-of-the-art theory in describing the evolution of  $Q\bar{Q}$  in heavy quarkonium  $H_{Q\bar{Q}}$  is the NRQCD effective theory [16]. Its applicability to quarkonium production processes is based on the validity of NRQCD factorization theorem. NRQCD reproduces the complete QCD dynamics at the scales of mv and  $mv^2$ . The typical scales in NRQCD are shown in Fig. 2.1. In the regime of the dynamic scales at the order of mv and  $mv^2$ , the full QCD Lagrangian can be reorganized in the expansion of operators in different powers of v. The vacuum expectation values of some operators can be interpreted as the probability for a  $Q\bar{Q}$  pair evolving into a heavy quarkonium  $H_{Q\bar{Q}}$  and are the LDMEs in NRQCD. Hence, the inclusive cross section for a heavy quarkonium production at large momentum transfer can be written as a sum of SDCs times the NRQCD LDMEs. In addition to CS states, the hard-scattering production of  $Q\bar{Q}$  can also be in color-octet (CO) states. At the evolution stage, the CO  $Q\bar{Q}$  radiates mv gluon(s) to form CS mesons. We call such mechanism, which does not happen in CSM, as CO mechanism (COM). Although in general there are infinite

intermediate states<sup>3</sup> contributing to a heavy quarkonium  $H_{Q\bar{Q}}$  production process, according to the velocity scaling rule [16], its number is always finite when one truncates it at some specific accuracy. For example, in Table 2.1, we show the  $Q\bar{Q}$  Fock states contribute to some quarkonia up to  $\mathcal{O}(v^7)$ . Because the only unknown pieces in NRQCD are the vacuum expectation values of the NRQCD operators, the predictive power of NRQCD is much larger than that of the FF approach. Actually, the practical applications of the FF approach in heavy quarkonium production are based on NRQCD factorization [17, 22–24, 39–44]. The non-perturbative LDMEs play the similar role as the parton-distribution functions (PDFs) in QCD. Moreover, the non-cancellation of the IR divergences in the production of a P-wave quarkonium in the CSM can be naturally absorbed into the renormalization of the CO S-wave Fock state in NRQCD. Like the CSM, we have the similar  $p_T$  scaling behavior in producing CO intermediate states, for example



However, the statement that NRQCD can describe the quarkonium production heavily relies on the validity of NRQCD factorization theorem, which is now only a conjecture and is still lacking a compelling proof. Schematically, based on QCD factorization and NRQCD factorization, a heavy quarkonium hadroproduction cross section  $d\sigma(pp \to H_{O\bar{O}} + X)$  can be written as

<sup>&</sup>lt;sup>3</sup>We call the CS and CO intermediate states as Fock states.

Power counting	$\eta_c, \eta_b$	$J/\psi, \psi(2S), \Upsilon$	$h_c, h_b$	$\chi_{cJ}, \chi_{bJ}$
$v^3$	<sup>1</sup> S <sub>0</sub> <sup>[1]</sup>	<sup>3</sup> S <sub>0</sub> <sup>[1]</sup>	_	_
v <sup>5</sup>	_	_	${}^{1}P_{1}^{[1]}, {}^{1}S_{0}^{[8]}$	${}^{3}P_{J}^{[1]}, {}^{3}S_{1}^{[8]}$
$v^7$	${}^{1}S_{0}^{[8]}, {}^{3}S_{1}^{[8]}, {}^{1}P_{1}^{[8]}$	${}^{1}S_{0}^{[8]}, {}^{3}S_{1}^{[8]}, {}^{3}P_{J}^{[8]}$	_	_
	0 1 1	0 1 7		l

Table 2.1 Power counting of Fock states in NRQCD velocity scaling rule [16] for some quarkonia

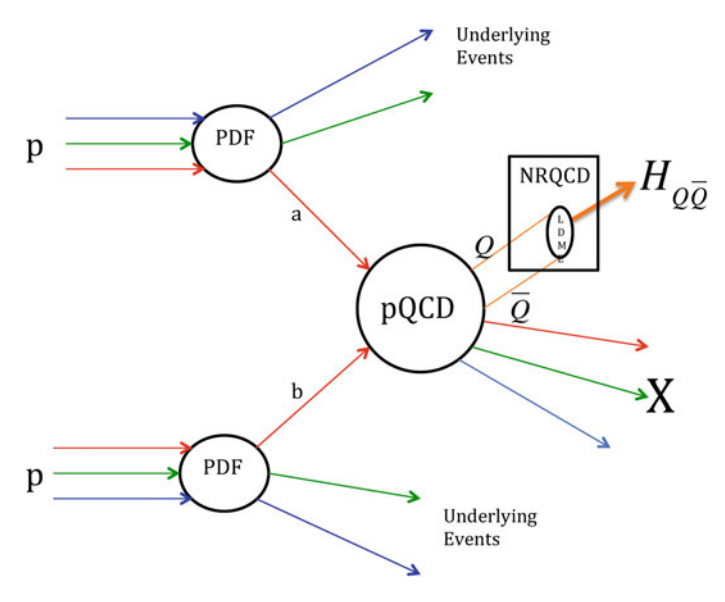


Fig. 2.2 An illustrative graph for the QCD factorization and the NRQCD factorization in describing a heavy quarkonium  $H_{Q\bar{Q}}$  production at a proton–proton collider

$$d\sigma(pp\to H_{Q\bar{Q}}+X)=\sum_n d\sigma(pp\to Q\bar{Q}[n]+X)\times\langle\mathcal{O}^{H_{Q\bar{Q}}}(n)\rangle, \quad (2.4)$$

where

$$d\sigma(pp \to Q\bar{Q}[n] + X) = \sum_{a,b} f_{a/p}(x_1) f_{b/p}(x_2) |\mathcal{A}(ab \to Q\bar{Q}[n] + X)|^2. \quad (2.5)$$

Its graphic representation is displayed in Fig. 2.2.

2.2 Challenges 15

#### 2.2 Challenges

#### 2.2.1 Challenges in Proving NRQCD Factorization

It is a difficult task to prove the validity of NRQCD factorization theorem. One difficulty is the NRQCD factorization formula [16] is only a perturbative expansion of  $\alpha_S$  and  $\nu$  in SDCs, which makes the NRQCD results usually suffer from large higher-order corrections. In other words, we need an optimal reorganization of the heavy quarkonium production cross sections into simultaneously  $\alpha_S$  and  $m/p_T$ . The FF approach provides such a reorganization. As proposed in Refs. [18, 19, 45], the proof can be done into two steps:

- 1. One should first prove that the inclusive heavy quarkonium production cross section can be written as convolutions of the heavy quarkonium FFs with the short-distance parton production cross sections. The factorization theorem in leading power of  $m/Q_{hard}$  was proven at electron–positron annihilation [46] and at hadronic collisions [18], whereas up to subleading power in hadroproduction, it was proven recently in Ref. [20].
- 2. One then tries to prove that the FFs can be written as a sum of SDCs times NRQCD LDMEs, which is the only obstacle to proving the NRQCD factorization theorem up to subleading power. A proof of the second step requires that all soft singularities can cancel or can be absorbed into the renormalization of NRQCD LDMEs and all collinear singularities and spectator interactions can be absorbed into PDFs to all orders in  $\alpha_S$ .

Two possible situations might violate the factorization at step 2. One difficulty is when there is a gluon with the momentum of order m in the heavy quarkonium rest frame, and it has nonvanishing soft exchanges in the FF [5, 47]. Another situation is when there are comoving heavy quark(s) with the  $Q\bar{Q}$  pair that forms  $H_{Q\bar{Q}}$ , the heavy quark(s) can have a soft-color exchange with the  $Q\bar{Q}$  pair [48, 49]. This process was not considered in the NRQCD factorization picture and would break its factorization.

If NRQCD factorization was proven to be valid to all orders in  $\alpha_S$  and up to subleading in  $m/Q_{hard}$ , one might expect that the non-factorizable corrections would be at least  $m^3/Q_{hard}^3$ . It indicates that NRQCD will fail to describe the heavy quarkonium production physics when  $Q_{hard}$  is not large enough compared to m.

#### 2.2.2 NRQCD Versus Experiments

It is apparent that NRQCD is a more rigorous theory than CSM and CEM. In particular, when one takes  $v \to 0$ , NRQCD will collapse into CSM. However, till now, it is still a debate how significant part will CO states contribute to the heavy quarkonium production physics. Since it is really a long story, we will try to recall it briefly.

More than a decade ago, the first measurements [29–31] by the CDF collaboration of the yields of  $J/\psi$  and  $\psi(2S)$  production at Tevatron Run I revealed an unexpected large discrepancy with the theoretical calculations. The observed production rates were more than an order of magnitude greater than the LO CSM theoretical result, which motivates a lot of theoretical studies on NROCD since the unknown CO contributions can compensate the large gap. At LO in  $\alpha_s$ , the dominant contribution at sufficiently large  $p_T$  is coming from a gluon fragmentating into a S-wave CO state. Consequently, LO NRQCD predicts a transverse polarization in its helicity frame [50–52]. It is in contradiction with the CDF measurements [53, 54], which was called "polarization puzzle" in NRQCD. On the other side, NLO QCD corrections to  $J/\psi$ and  $\Upsilon$  hadroproduction enhance the production rates substantially [32] due to the  $p_T$ -enhancement topologies. Later on, part of  $\mathcal{O}(\alpha_s^5)$  contribution was also taken into account [33]. All these efforts significantly reduce the discrepancy between CSM theoretical predictions and experiments [29–31]. After that, more and more theoretical advances are dedicated to higher-order computations in  $\alpha_S$  [24, 34, 55– 69] and in  $v^2$  [70, 71]. It explores that CSM cannot explain the polarization data as well as large  $p_T$  yields data [35, 57]. However, as far as the  $p_T$ -integrated yield is concerned, CSM contribution agree relatively well with the existing data [28, 72], which is dominated by  $p_T \sim m$  phase space. We guide the reader to a recent review [73] on heavy quarkonium polarization in hadronic collisions.

Based on our original works [66, 68, 74, 75], in the next few chapters, we will show that the NRQCD yields and polarizations of  $J/\psi$  and  $\psi(2S)$  in hadronic collisions are compatible with the Tevatron and the LHC data when  $p_T > 11 \, \text{GeV}$ . It is compatible with the recent observations by two theoretical groups [24, 69], which implies that NRQCD factorization may be only valid at large enough  $p_T \gg m$  regime. However, it is really tough to say that all of the available data outside this  $p_T$  constraints are lacking a theory to describe them. Given the large uncertainties, the data in small momentum transfer regime (including the data at B factories [76–83],in photoproduction [84–86], in fixed-target production [27, 87] and in hadroproduction [28, 72]) are described relatively well by CSM. A more severe thing is we do not have a satisfactory theory to describe the data between the small and large momentum transfer regions. Moreover, in exclusive heavy quarkonium production processes, only CS state can be taken into account.

More measurements on various heavy quarkonium production processes and on various observables are necessary in the future to assess the universality of NRQCD LDMEs. Theoretically, many interesting quarkonium-associated production processes have been promoted to NLO level in  $\alpha_s$ . They are  $J/\psi + \gamma$  [88, 89],  $J/\psi + Z$  [90, 91],  $J/\psi + W^{\pm}$  [92, 93] and  $J/\psi + J/\psi$  [94]. Finally, other interesting processes deserved mentioning here are  $J/\psi + c\bar{c}$  and  $\Upsilon + b\bar{b}$  [55], which may be important in understanding the factorization breakdown effects via the color-transfer mechanisms as proposed in Refs. [48, 49].

References 17

#### References

 J. Aubert et al., Phys. Rev. Lett. 33, 1404 (1974). doi:10.1103/PhysRevLett.33.1404. Technicalreport96

- 2. J. Augustin et al., Phys. Rev. Lett. 33, 1406 (1974). doi:10.1103/PhysRevLett.33.1406
- 3. N. Brambilla, et al. (2004)
- N. Brambilla, A. Pineda, J. Soto, A. Vairo, Rev. Mod. Phys. 77, 1423 (2005). doi:10.1103/ RevModPhys.77.1423
- N. Brambilla, S. Eidelman, B. Heltsley, R. Vogt, G. Bodwin et al., Eur. Phys. J. C 71, 1534 (2011). doi:10.1140/epjc/s10052-010-1534-9
- 6. M. Einhorn, S. Ellis, Phys. Rev. D 12, 2007 (1975). doi:10.1103/PhysRevD.12.2007
- S. Ellis, M.B. Einhorn, C. Quigg, Phys. Rev. Lett. 36, 1263 (1976). doi:10.1103/PhysRevLett. 36.1263
- 8. C. Carlson, R. Suaya, Phys. Rev. D 14, 3115 (1976). doi:10.1103/PhysRevD.14.3115
- 9. C.H. Chang, Nucl. Phys. B 172, 425 (1980). doi:10.1016/0550-3213(80)90175-3
- 10. H. Fritzsch, Phys. Lett. B 67, 217 (1977). doi:10.1016/0370-2693(77)90108-3
- 11. F. Halzen, Phys. Lett. B 69, 105 (1977). doi:10.1016/0370-2693(77)90144-7
- 12. M. Gluck, J. Owens, E. Reya, Phys. Rev. D 17, 2324 (1978). doi:10.1103/PhysRevD.17.2324
- V.D. Barger, W.Y. Keung, R. Phillips, Phys. Lett. B 91, 253 (1980). doi:10.1016/0370-2693(80)90444-X
- J. Amundson, O.J. Eboli, E. Gregores, F. Halzen, Phys. Lett. B 372, 127 (1996). doi:10.1016/ 0370-2693(96)00035-4
- J. Amundson, O.J. Eboli, E. Gregores, F. Halzen, Phys. Lett. B 390, 323 (1997). doi:10.1016/ S0370-2693(96)01417-7
- G.T. Bodwin, E. Braaten, G. Lepage, Phys. Rev. D 51, 1125 (1995). doi:10.1103/PhysRevD.51.
   1125, 10.1103/PhysRevD.55.5853, 10.1103/PhysRevD.51.1125, 10.1103/PhysRevD.55.5853
- E. Braaten, S. Fleming, T.C. Yuan, Ann. Rev. Nucl. Part. Sci. 46, 197 (1996). doi:10.1146/ annurev.nucl.46.1.197
- G.C. Nayak, J.W. Qiu, G.F. Sterman, Phys. Lett. B 613, 45 (2005). doi:10.1016/j.physletb. 2005.03.031
- G.C. Nayak, J.W. Qiu, G.F. Sterman, Phys. Rev. D 72, 114012 (2005). doi:10.1103/PhysRevD. 72.114012
- Z.B. Kang, J.W. Qiu, G. Sterman, Phys. Rev. Lett. 108, 102002 (2012). doi:10.1103/ PhysRevLett.108.102002 (Latex, 11 pages, 4 figures)
- S. Fleming, A.K. Leibovich, T. Mehen, I.Z. Rothstein, Phys. Rev. D 86, 094012 (2012). doi:10. 1103/PhysRevD.86.094012
- S. Fleming, A.K. Leibovich, T. Mehen, I.Z. Rothstein, Phys. Rev. D 87, 074022 (2013). doi:10. 1103/PhysRevD.87.074022
- Z.B. Kang, Y.Q. Ma, J.W. Qiu, G. Sterman, Phys. Rev. D 90(3), 034006 (2014). doi:10.1103/ PhysRevD.90.034006
- G.T. Bodwin, H.S. Chung, U.R. Kim, J. Lee, Phys. Rev. Lett. 113(2), 022001 (2014). doi:10. 1103/PhysRevLett.113.022001
- 25. E.J. Eichten, C. Quigg, Phys. Rev. D 52, 1726 (1995). doi:10.1103/PhysRevD.52.1726
- 26. G.A. Schuler, Phys. Rept. (1994)
- F. Maltoni, J. Spengler, M. Bargiotti, A. Bertin, M. Bruschi et al., Phys. Lett. B 638, 202 (2006). doi:10.1016/j.physletb.2006.05.010
- S.J. Brodsky, J.P. Lansberg, Phys. Rev. D 81, 051502 (2010). doi:10.1103/PhysRevD.81. 051502
- 29. F. Abe et al., Phys. Rev. Lett. **69**, 3704 (1992). doi:10.1103/PhysRevLett.69.3704
- 30. F. Abe et al., Phys. Rev. Lett. **79**, 572 (1997)
- 31. F. Abe et al., Phys. Rev. Lett. 79, 578 (1997)
- J.M. Campbell, F. Maltoni, F. Tramontano, Phys. Rev. Lett. 98, 252002 (2007). doi:10.1103/ PhysRevLett.98.252002

- P. Artoisenet, J.M. Campbell, J. Lansberg, F. Maltoni, F. Tramontano, Phys. Rev. Lett. 101, 152001 (2008). doi:10.1103/PhysRevLett.101.152001
- 34. B. Gong, J.X. Wang, Phys. Rev. D 78, 074011 (2008). doi:10.1103/PhysRevD.78.074011
- 35. J. Lansberg, J. Phys. **G38**, 124110 (2011). doi:10.1088/0954-3899/38/12/124110
- 36. S. Chatrchyan et al., Phys. Lett. B **727**, 381 (2013). doi:10.1016/j.physletb.2013.10.055
- C.W. Bauer, S. Fleming, M.E. Luke, Phys. Rev. D 63, 014006 (2000). doi:10.1103/PhysRevD.
   63.014006
- C.W. Bauer, S. Fleming, D. Pirjol, I.W. Stewart, Phys. Rev. D 63, 114020 (2001). doi:10.1103/ PhysRevD.63.114020
- 39. E. Braaten, T.C. Yuan, Phys. Rev. Lett. 71, 1673 (1993). doi:10.1103/PhysRevLett.71.1673
- E. Braaten, K.M. Cheung, T.C. Yuan. Phys. Rev. D48, 4230 (1993). doi:10.1103/PhysRevD. 48.4230
- 41. E. Braaten, S. Fleming, Phys. Rev. Lett. 74, 3327 (1995). doi:10.1103/PhysRevLett.74.3327
- 42. E. Braaten, J. Lee, Nucl. Phys. B 586, 427 (2000). doi:10.1016/S0550-3213(00)00396-5
- Y.Q. Ma, J.W. Qiu, H. Zhang, Phys. Rev. D 89(9), 094029 (2014). doi:10.1103/PhysRevD.89. 094029
- 44. Y.Q. Ma, J.W. Qiu, H. Zhang, Phys. Rev. D **89**(9), 094030 (2014). doi:10.1103/PhysRevD.89. 094030
- G.C. Nayak, J.W. Qiu, G.F. Sterman, Phys. Rev. D 74, 074007 (2006). doi:10.1103/PhysRevD. 74.074007
- 46. J.C. Collins, D.E. Soper, Nucl. Phys. B 194, 445 (1982), doi:10.1016/0550-3213(82)90021-9
- 47. G. Bodwin (2013). http://indico.ihep.ac.cn/conferenceOtherViews.py?view=standard&confId=2723
- 48. G.C. Nayak, J.W. Qiu, G.F. Sterman, Phys. Rev. Lett. **99**, 212001 (2007). doi:10.1103/ PhysRevLett.99.212001
- G.C. Nayak, J.W. Qiu, G.F. Sterman, Phys. Rev. D 77, 034022 (2008). doi:10.1103/PhysRevD. 77.034022
- 50. P.L. Cho, M.B. Wise, Phys. Lett. B 346, 129 (1995). doi:10.1016/0370-2693(94)01658-Y
- 51. A.K. Leibovich, Phys. Rev. D **56**, 4412 (1997). doi:10.1103/PhysRevD.56.4412
- E. Braaten, B.A. Kniehl, J. Lee, Phys. Rev. D 62, 094005 (2000). doi:10.1103/PhysRevD.62. 094005
- 53. T. Affolder et al., Phys. Rev. Lett. 85, 2886 (2000). doi:10.1103/PhysRevLett.85.2886
- 54. A. Abulencia et al., Phys. Rev. Lett. 99, 132001 (2007). doi:10.1103/PhysRevLett.99.132001
- 55. P. Artoisenet, J. Lansberg, F. Maltoni, Phys. Lett. B **653**, 60 (2007). doi:10.1016/j.physletb. 2007.04.031 (13 pages, 5 figures)
- B. Gong, X.Q. Li, J.X. Wang, Phys. Lett. B 673, 197 (2009). doi:10.1016/j.physletb.2009.
   02.026, 10.1016/j.physletb.2010.09.031, 10.1016/j.physletb.2009.02.026, 10.1016/j.physletb.
   2010.09.031
- B. Gong, J.X. Wang, Phys. Rev. Lett. 100, 232001 (2008). doi:10.1103/PhysRevLett.100.
   232001
- M. Butenschoen, B.A. Kniehl, Phys. Rev. Lett. 104, 072001 (2010). doi:10.1103/PhysRevLett. 104.072001
- Y.Q. Ma, K. Wang, K.T. Chao, Phys. Rev. D 83, 111503 (2011). doi:10.1103/PhysRevD.83. 111503
- Y.Q. Ma, K. Wang, K.T. Chao, Phys. Rev. Lett. 106, 042002 (2011). doi:10.1103/PhysRevLett. 106.042002
- M. Butenschoen, B.A. Kniehl, Phys. Rev. Lett. 106, 022003 (2011). doi:10.1103/PhysRevLett. 106.022003
- 62. Y.Q. Ma, K. Wang, K.T. Chao, Phys. Rev. D **84**, 114001 (2011). doi:10.1103/PhysRevD.84. 114001
- 63. M. Butenschoen, B.A. Kniehl (2011)
- M. Butenschoen, B.A. Kniehl, Phys. Rev. D 84, 051501 (2011). doi:10.1103/PhysRevD.84. 051501
- 65. M. Butenschoen, B.A. Kniehl, Phys. Rev. Lett. 108, 172002 (2012)

References 19

- 66. K.T. Chao, Y.O. Ma, H.S. Shao, K. Wang, Y.J. Zhang, Phys. Rev. Lett. 108, 242004 (2012)
- 67. B. Gong, L.P. Wan, J.X. Wang, H.F. Zhang, Phys. Rev. Lett. 110, 042002 (2013)
- H.S. Shao, Y.Q. Ma, K. Wang, K.T. Chao, Phys. Rev. Lett. 112(18), 182003 (2014). doi:10. 1103/PhysRevLett.112.182003
- 69. P. Faccioli, V. Knnz. Phys. Lett. **B736**, 98 (2014). doi:10.1016/j.physletb.2014.07.006
- Y. Fan, Y.Q. Ma, K.T. Chao, Phys. Rev. D 79, 114009 (2009). doi:10.1103/PhysRevD.79. 114009
- 71. G.Z. Xu, Y.J. Li, K.Y. Liu, Y.J. Zhang, Phys. Rev. D **86**, 094017 (2012). doi:10.1103/PhysRevD. 86.094017
- 72. J. Lansberg (2010)
- E. Braaten, J. Russ, Ann. Rev. Nucl. Part. Sci. 64, 221 (2014). doi:10.1146/annurev-nucl-030314-044352
- 74. H.S. Shao, K.T. Chao, Phys. Rev. D **90**(1), 014002 (2014). doi:10.1103/PhysRevD.90.014002
- H.S. Shao, H. Han, Y.Q. Ma, C. Meng, Y.J. Zhang, K.T. Chao, JHEP 05, 103 (2015). doi:10. 1007/JHEP05(2015)103
- Y.J. Zhang, K.T. Chao, Phys. Rev. Lett. 98, 092003 (2007). doi:10.1103/PhysRevLett.98. 092003
- 77. B. Gong, J.X. Wang, Phys. Rev. D 80, 054015 (2009). doi:10.1103/PhysRevD.80.054015
- Y.Q. Ma, Y.J. Zhang, K.T. Chao, Phys. Rev. Lett. 102, 162002 (2009). doi:10.1103/ PhysRevLett.102.162002
- B. Gong, J.X. Wang, Phys. Rev. Lett. 102, 162003 (2009). doi:10.1103/PhysRevLett.102. 162003
- Z.G. He, Y. Fan, K.T. Chao, Phys. Rev. D 81, 054036 (2010). doi:10.1103/PhysRevD.81. 054036
- 81. Y. Jia, Phys. Rev. D 82, 034017 (2010). doi:10.1103/PhysRevD.82.034017
- Y.J. Zhang, Y.Q. Ma, K. Wang, K.T. Chao, Phys. Rev. D 81, 034015 (2010). doi:10.1103/ PhysRevD.81.034015
- 83. H.S. Shao, JHEP **04**, 182 (2014)
- M. Kramer, J. Zunft, J. Steegborn, P. Zerwas, Phys. Lett. B 348, 657 (1995). doi:10.1016/0370-2693(95)00155-E
- 85. S.P. Baranov, Phys. Rev. D 66, 114003 (2002). doi:10.1103/PhysRevD.66.114003
- B. Kniehl, D. Vasin, V. Saleev, Phys. Rev. D 73, 074022 (2006). doi:10.1103/PhysRevD.73. 074022
- A. Petrelli, M. Cacciari, M. Greco, F. Maltoni, M.L. Mangano, Nucl. Phys. B 514, 245 (1998). doi:10.1016/S0550-3213(97)00801-8
- 88. R. Li, J.X. Wang, Phys. Rev. D 89(11), 114018 (2014). doi:10.1103/PhysRevD.89.114018
- 89. R. Li, J.X. Wang, Phys. Lett. B 672, 51 (2009). doi:10.1016/j.physletb.2008.12.050
- S. Mao, M. Wen-Gan, L. Gang, Z. Ren-You, G. Lei, JHEP 1102, 071 (2011). doi:10.1007/ JHEP12(2012)010, 10.1007/JHEP02(2011)071
- 91. B. Gong, J.P. Lansberg, C. Lorce, J. Wang, JHEP **1303**, 115 (2013). doi:10.1007/ JHEP03(2013)115
- 92. G. Li, M. Song, R.Y. Zhang, W.G. Ma, Phys. Rev. D 83, 014001 (2011). doi:10.1103/PhysRevD. 83.014001
- 93. J. Lansberg, C. Lorce, Phys. Lett. B 726, 218 (2013). doi:10.1016/j.physletb.2013.07.059
- J.P. Lansberg, H.S. Shao, Phys. Rev. Lett. 111, 122001 (2013). doi:10.1103/PhysRevLett.111.
   122001

# Chapter 3 HELAC-Onia

**Abstract** In this chapter, we will describe an automatic tree-level matrix elements and events generator for heavy quarkonium physics, which is dubbed as HELAC-ONIA [1]. It will be used to do the heavy quarkonium phenomenological analysis in the following chapters. The package is already available on the Web page http://helac-phegas.web.cern.ch/helac-phegas. It is a first realization of automation for heavy quarkonium production at  $e^-e^+$  and pp,  $p\bar{p}$  collisions based on recursion relations. This chapter is organized as follows: In the first section, we will describe the theoretical framework for the realization of HELAC-ONIA and then go to the details of HELAC-ONIA in the next section.

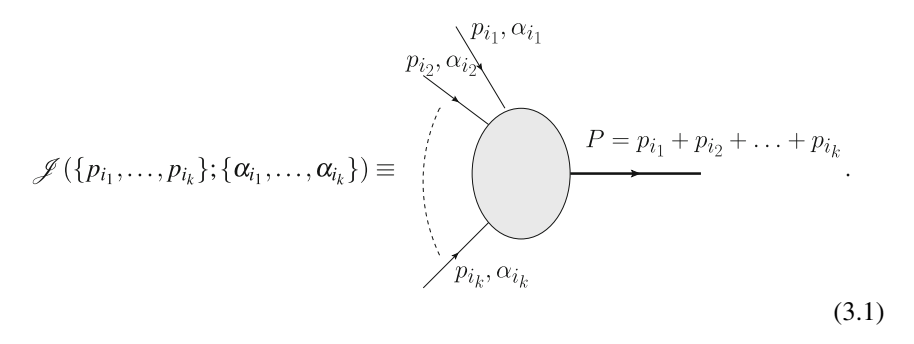
#### 3.1 Theoretical Framework

Before we describe the details of HELAC-ONIA, we will present the basic theoretical framework in this section.

#### 3.1.1 Recursive Computation of Helicity Amplitudes

HELAC-ONIA is based on a public package HELAC [2–4], which uses the Dyson–Schwinger equations [5–7] to calculate the helicity amplitude in the SM at the parton level. It is a generalized version of the well-known Berends–Giele off-shell recursive relation [8]. In this section, we will describe how to calculate a helicity amplitude for a general process with n external legs. We denote the momenta of these external legs as  $p_1, p_2, \ldots, p_n$ , and their quantum numbers, such as color and helicity, are symbolized as  $\alpha_1, \alpha_2, \ldots, \alpha_n$ . Any k external legs can form an off-shell current in the following way

22 3 HELAC-Onia



All possible subgraphs that are able to transfer the k external legs into such offshell current  $\mathscr{J}$  have been contained in the shade bubble. We can assign each current  $\mathscr{J}$  a number l, which is called "level" in the context. It is defined as the number of external legs involved in the current  $\mathscr{J}$ . In other words, the "level" of  $\mathscr{J}(\{p_{i_1},\ldots,p_{i_k}\};\{\alpha_{i_1},\ldots,\alpha_{i_k}\})$  is k. In such a case, we see that the "level" of each external leg should be 1. Our construction of the higher "level" currents is starting from the lower "level" ones in a recursive way. The starting point of the recursion relation is the external legs, i.e., the "level" l=1 currents. We take the corresponding current for the lth leg as its wave function

$$\mathscr{J}(\{p_i\};\{\alpha_i\}) \equiv \xrightarrow{p_i, \alpha_i} . \tag{3.2}$$

For example, for a vector boson, it is

$$\mathscr{J}(\{p_i\};\{\mu,\lambda\}) \equiv \varepsilon_{\lambda}^{\mu}(p_i),\tag{3.3}$$

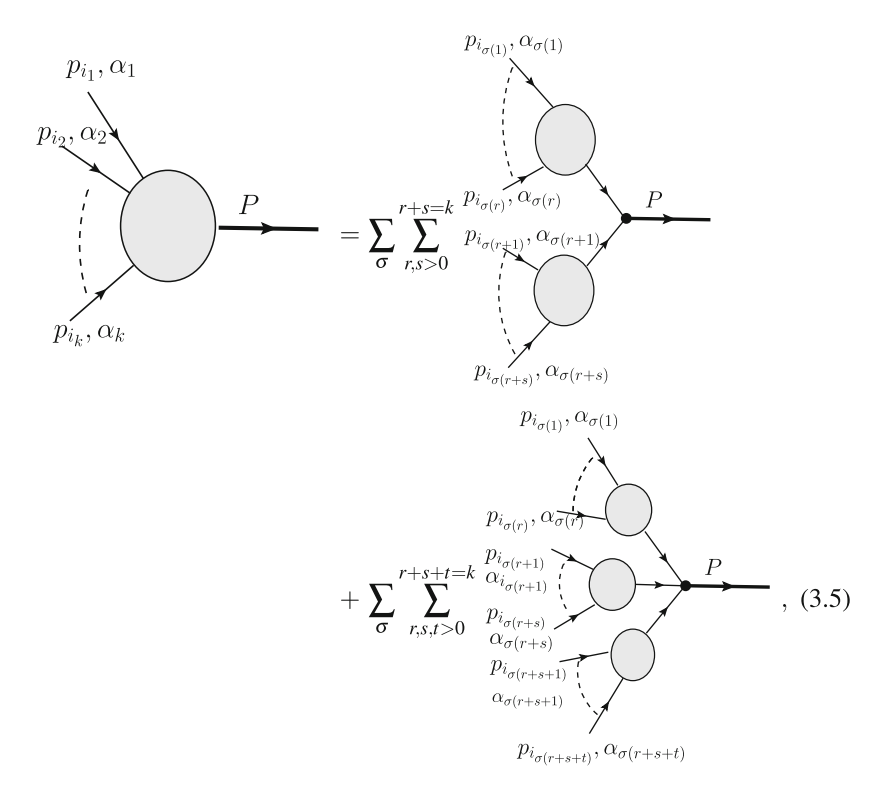
where  $\mu$  is the Lorentz index and  $\lambda$  is the helicity of the vector boson. For simplicity, we have suppressed symbols for other possible quantum numbers like color. For a spin- $\frac{1}{2}$  fermion, we have

$$\mathcal{J}(\{p_i\}; \{+1, \lambda\}) \equiv \begin{cases} u_{\lambda}(p_i) & \text{when } p_i^0 \ge 0 \\ v_{\lambda}(-p_i) & \text{when } p_i^0 \le 0 \end{cases},$$

$$\mathcal{J}(\{p_i\}; \{-1, \lambda\}) \equiv \begin{cases} \bar{u}_{\lambda}(p_i) & \text{when } p_i^0 \ge 0 \\ \bar{v}_{\lambda}(-p_i) & \text{when } p_i^0 \le 0 \end{cases},$$
(3.4)

where +1(-1) means fermion (antifermion) flow and  $\lambda=\pm 1$  is its helicity index. The explicit expressions of these external wave functions are formulated in Ref. [2]. The algorithms are relying on the observation that a current with l=k>1 can be constructed from the currents with lower l. For illustration, we only include trilinear and quadri-linear couplings here, though it is possible to take into account higher-point vertices. It is schematically written as follows

 $<sup>^{1}\</sup>lambda=\pm1$  for a massless vector, whereas  $\lambda=\pm1,0$  for a massive vector.



where  $\sigma$  exhausts all possible generating "level" r, s(r, s, t) trilinear (quadri-linear) currents that are formed by the  $i_1, \ldots, i_k$  external legs. In the expression of each off-shell current, we have already multiplied its propagator. The endpoint of the recursion is obtaining the "level" n current. In our treatment, we will choose all possible l=n-1 currents to multiply it with the wave function of the first external particle. If the flavor of the first external particle does not match to the flavor of the l=n-1 current, the current should be dropped. Afterward, we arrive at the final amplitude. One of the advantages by working in this way is that one is able to avoid computing identical subgraphs contributing to different Feynman diagrams more than once. The summation of all subgraphs contributing to a specific current reduces the total number of objects that should be used in the next recursion procedure. The computation complexity is reduced from  $\sim n!$  in the Feynman-diagram-based algorithm to  $\sim a^n$  in the Dyson–Schwinger-based recursive algorithm, where  $a \sim 3$  [2–4].

Technically, inherited from the original HELAC program [2], we will use a binary representation of the momenta involved in a process [9] in HELAC-ONIA. For any the external momenta  $p_i(i=1,2,\ldots,n)$ , its binary representation is  $2^{i-1}$ , whereas we express  $\sum_{j=1}^k 2^{j-1}$  for a "level" l=k current  $\mathscr{J}(\{p_{i_1},\ldots,p_{i_k}\};\{\alpha_{i_1},\ldots,\alpha_{i_k}\})$ . In this way, each momenta  $P^{\mu}=\sum_{i=1}^n m_i p_i$  can uniquely correspond to an integer

24 3 HELAC-Onia

 $m = \sum_{j=1}^{n} 2^{j-1} m_j$ , where  $m_j = 0$  or 1. The "level" of a current with momenta  $P^{\mu} = \sum_{j=1}^{n} m_j p_j$  can be calculated directly by  $l = \sum_{j=1}^{n} m_j$ . We can also determine the sign factor from the antisymmetric property of fermions in binary representation. It can be obtained by

$$\varepsilon(P_1, P_2) = (-1)^{\chi(P_1, P_2)}, \chi(P_1, P_2) = \sum_{i=n}^{2} \hat{m}_{1i} \sum_{j=1}^{i-1} \hat{m}_{2j},$$
(3.6)

with

$$P_{1} = \sum_{j=1}^{n} m_{1j} p_{j},$$

$$P_{2} = \sum_{j=1}^{n} m_{2j} p_{j},$$

$$\hat{m}_{1j} = \begin{cases} 0 & \text{when particle } j \text{ is a boson} \\ m_{1j} & \text{when particle } j \text{ is a fermion}, \end{cases}$$

$$\hat{m}_{2j} = \begin{cases} 0 & \text{when particle } j \text{ is a boson} \\ m_{2j} & \text{when particle } j \text{ is a fermion}. \end{cases}$$
(3.7)

The sign factor for the current, which is constructed from a trilinear coupling with the lower "level" currents  $P_1$  and  $P_2$ , is  $\varepsilon(P_1, P_2)$ . If the current is constructed from a quadri-linear coupling with the momenta of the lower "level" currents  $P_1, P_2$ , and  $P_3$ , it is  $\varepsilon(P_1, P_2, P_3) = \varepsilon(P_1, P_2)\varepsilon(P_1 + P_2, P_3)$ . In the following part of this section, we will describe how the color and helicity of particles will be treated in HELAC-ONIA.

First, we describe the color treatment. In HELAC-ONIA, we decompose the color factors into the so-called color-flow basis, which was first proposed in Ref. [10] and then applied to pQCD computations in Refs. [11, 12]. The basic idea is based on the fact that a color-octet (CO) gluon field  $A^a_\mu$  can be replaced by a 3 × 3 matrix  $(\mathscr{A}_\mu)^i_j = \frac{1}{\sqrt{2}}A^a_\mu(\lambda^a)^i_j$ , where  $\lambda^a$  is the Gell-Mann matrix. It is usually denoted as  $\mathbf{8} = \mathbf{3} \otimes \mathbf{\bar{3}} - \mathbf{1}$ . On the other hand, the incoming quarks or outgoing antiquarks maintain the  $\mathbf{3}$  representations of non-abelian group SU(3), and the outgoing quarks or incoming antiquarks are in the  $\mathbf{\bar{3}}$  representation. With this transformation, there is only the Kronecker notation  $\delta \mathbf{s}$  in the Feynman rules. From the Lagrangian level, all of the QCD Feynman rules in the color-flow basis have been established in Ref. [12]. In a process with  $n_g$  external gluons (denote as  $1, 2, \ldots, n_g$ ) and  $n_q$  external quark-antiquark pairs (denoted as  $n_g + 1, n_g + 2, \ldots, n_g + n_q$ ), the color basis for the amplitude will be decomposed in the form of

$$\mathscr{C}_i = \delta^1_{\sigma_i(1)} \dots \delta^{n_g + n_q}_{\sigma_i(n_e + n_e)},\tag{3.8}$$

where  $\sigma_i$  means the *i*th permutation of  $1, 2, \ldots, n_g + n_q$ . The total number of the color basis is  $(n_g + n_q)!$  despite that some of them may vanish. Afterward, one is able to calculate the color matrix via

$$M_{ij} = \sum \mathscr{C}_i \mathscr{C}_j^*, \tag{3.9}$$

and to obtain the final square of matrix elements by

$$|\mathcal{M}|^2 = \sum_{i,j=1}^{(n_g + n_q)!} A_i M_{ij} A_j^*, \tag{3.10}$$

where  $A_i$  and  $A_i$  are the color-stripped amplitudes.

Finally, we turn to the helicity issue. In a general way, the number of helicity configurations in a process grows as the number of external legs increases. Sometimes, it is a disaster because too many helicity configurations should be computed in a single-phase space point in a sufficiently complicated process. In order to improve the computation efficiency, one usually devotes to a Monte Carlo sampling over the helicity configurations in the program [2] to perform the helicity summation. Let us take a massive vector boson for example. A massive vector boson has three helicity states, i.e.,  $\lambda=\pm 1,0$ , with wave functions  $\varepsilon_+^\mu,\varepsilon_-^\mu$ , and  $\varepsilon_0^\mu$ . We take its amplitude in helicity  $\lambda$  as  $\mathscr{A}_\mu \varepsilon_\lambda^\mu$ . Then, the square of matrix elements would be  $\mathscr{A}_\mu(\mathscr{A}_\nu)^* \sum_{\lambda=\pm,0} \varepsilon_\lambda^\mu(\varepsilon_\lambda^\nu)^*$ . The strategy of Monte Carlo sampling over helicity in HELAC-Onia is that we will put the concrete helicity summation of  $\sum_{\lambda=\pm,0} \varepsilon_\lambda^\mu(\varepsilon_\lambda^\nu)^*$  into a continue integration by defining  $\varepsilon_\phi^\mu \equiv \sum_{\lambda=\pm,0} e^{i\lambda\phi} \varepsilon^\mu$ . The concrete summation would become  $\int_0^{2\pi} \mathrm{d}\phi \varepsilon_\phi^\mu(\varepsilon_\phi^\nu)^*$ , which is in a much suitable form to be calculated in a Monte Carlo way.

# 3.1.2 Heavy Quarkonium Amplitudes in NRQCD

Based on the NRQCD factorization, the cross section for a heavy quarkonium production process can be factorized into the perturbative short-distance components and the non-perturbative LDMEs. Let us have a look at a heavy quarkonium  $\mathcal{Q}$  production process at a proton–proton collider. Its cross section can be written as

$$\sigma(pp \to \mathcal{Q} + X) = \sum_{i,j,n} \int dx_1 dx_2 f_{i/p}(x_1) f_{j/p}(x_2) \hat{\sigma}(ij \to Q\bar{Q}[n] + X) \langle \mathcal{O}_n^{\mathcal{Q}} \rangle,$$
(3.11)

where  $f_{i/p}$  and  $f_{j/p}$  are the PDFs and  $\hat{\sigma}(ij \to Q\bar{Q}[n] + X)$  is the short-distance coefficient (SDC) of producing a heavy quark pair  $Q\bar{Q}$  in the specific quantum state n.

26 3 HELAC-Onia

Following the usual notation, we write the Fock states n in the spectroscopic form  $n = {}^{2S+}L_J^{[c]}$ , where S, L, and J identify the spin, orbital momentum, and total angular momentum states, respectively, and c=1, 8 means that the intermediate state  $Q\bar{Q}$  can be in a CS or CO state. The LDMEs are denoted as  $\langle \mathcal{O}_n^{\mathcal{Q}} \rangle$ . Its physical interpretation is the probability of a heavy quark pair in Fock state n evolving into a heavy quarkonium. The power counting rules in NRQCD result in the fact that for any heavy quarkonium, there are only limited Fock states contributing up to a specific order of v. We take  $J/\psi$  production for instance. Four Fock states  ${}^{\{1\}}_{1}$ ,  ${}^{\{1\}}_{2}$ ,  ${}^{\{2\}}_{1}$ , and  ${}^{\{5\}}_{0}$  will contribute to its production cross section up to  $v^7$ .

#### 3.1.2.1 Projection Method

Since the heavy quarkonium amplitudes require the heavy quark pair  $Q\bar{Q}$  produced in a specific quantum state n, we will show how to achieve it in a convenient way in what follows. We use the projection method to achieve it.

First, we concern the color. The color projectors to the process  $ij \to Q\bar{Q}[^{2S+}L_J^{[c]}] + X$  are [13]  $\frac{\delta_{ij}}{N_c}$  in CS and  $\sqrt{2}\lambda_{ij}^a$  in CO, respectively, where i and j are the color indices of the heavy quark pair  $Q\bar{Q}$  and  $\lambda^a$  is the well-known Gell-Mann matrix. The Gell-Mann matrix in CO projector will be decomposed into the color-flow basis as introduced in Sect. 3.1.1. After projecting, there will be no color indices for the heavy quark pair in CS as it should be.

Another important constraint of the heavy quark pair is their total spin, where the spin projectors were first derived in Ref. [14]. The general form of the projectors is<sup>3</sup>

$$-\frac{1}{2\sqrt{2}(E+m_0)}\bar{v}(p_2,\lambda_2)\Gamma_S \frac{p+2E}{2E}u(p_1,\lambda_1),$$
(3.12)

where  $m_Q$  is the mass of the heavy quark,  $p_1$  and  $p_2$  and  $\lambda_1$  and  $\lambda_2$  are the momenta and helicity of the heavy quarks, respectively. The total momentum of the heavy quark pair is  $P^\mu = p_1^\mu + p_2^\mu$  and  $E = \frac{\sqrt{P^2}}{2}$ . The  $\Gamma_S$  is  $\gamma_5$  in a spin-singlet state S=0 and is  $\varepsilon_\mu^{\lambda_s} \gamma^\mu$  in a spin-triplet state S=1. In the latter case, we take  $\lambda_s=\pm,0$  as the helicity of the heavy quarkonium  $\mathcal Q$  and  $\varepsilon_\mu^{\lambda_s}$  as the polarization vector for the spin-triplet state. E can be safely set as  $m_Q$ , since we only consider S-wave and P-wave here. However, after applying such a spin projection, the two external wave functions for quarks Q and  $\bar{Q}$  will be glued together. It might result in a problem in the recursion relation. In order to cure it, we have cut the glued fermion chain at the place of P + 2E in the projector shown in Eq. (3.12). Using the completeness relation of  $P + 2E = \sum_{\lambda'=\pm} u(P,\lambda')\bar{u}(P,\lambda')$ , we take the new "level" l=1 current for Q as  $\frac{1}{m_Q}\bar{u}(P,\lambda')(\not p_1+m_Q)$  and for  $\bar{Q}$  as  $-\frac{1}{8\sqrt{2}m_Q}(\not p_2-m_Q)u(P,\lambda')$ .

<sup>&</sup>lt;sup>2</sup>Note that, v is the relative velocity of the heavy quark pair.

<sup>&</sup>lt;sup>3</sup>In HELAC-ONIA, we generalize the projectors in the case of the heavy quarks in different flavors that form a heavy quarkonium like  $B_c^{\pm}$ .

#### 3.1.2.2 P-Wave State Treatment

The P-wave Fock states are necessary in probing the mechanism of heavy quarkonium production, because P-wave states will contribute to CS part of  $h_{c/b}$ ,  $\chi_{c/b}$  as well as CO components of  $J/\psi$ ,  $\Upsilon$ ,  $\eta_{c/b}$ . For example, the CO P-wave Fock states  ${}^3P_J^{[8]}$  are very important in determination of yields and polarizations of prompt  $J/\psi$  from hadroproduction [15–20] and from photoproduction [21, 22]. Hence, HELAC-ONIA is designed to be cable of handling P-wave states. We will introduce the extra numerical stable P-wave currents in the following.

Let us recall the computation of the amplitude for P-wave states production first. It can be obtained by expanding the relative momentum  $q^{\nu} = \frac{p_1^{\nu} - p_2^{\nu}}{2}$  between the heavy quark pair in the amplitude  $\mathscr{A}(ij \to Q(p_1)\bar{Q}(p_2) + X)$  into the nonrelativistic approximation, i.e.,  $\nu \ll 1$ . The formula for the computation of P-wave amplitude is

$$(\varepsilon_{\nu}^{\lambda_{I}})^{*} \frac{\partial}{\partial q_{\nu}} \mathscr{A}(ij \to Q(p_{1})\bar{Q}(p_{2}) + X) \bigg|_{q=0},$$
 (3.13)

where  $\lambda_l = \pm$ , 0 is the helicity of the polarization vector  $\varepsilon_{\nu}^{\lambda_l}$  of P-wave states.

A direct numerical derivation of the small relative momentum q of the quark and antiquark in Eq. (3.13) might result in numerical instability potentially especially when there are several P-wave states involved in the process. Alternatively, the introduction of new P-wave currents, which is extended from the original off-shell currents at the parton level, is able to avoid such a dangerous problem. In HELAC-ONIA, we assign each current with a derivation index and represent such index in binary representation. For example, let us assume there are  $n_P$  P-wave states in the considered process. The relative momentum of the ith heavy quark pair in P-wave state is denoted as  $q_i$  where  $i = 1, \ldots, n_P$ . Then, the general derivation index form for a current is  $b = \sum_{i=1}^{n_P} b_i 2^{i-1}$  with  $b_i = 0$  or 1. If the current has been derived by  $q_i$  as done like in Eq. (3.13),  $b_i$  is 1; otherwise,  $b_i$  is 0. We only keep the amplitudes with  $b = 2^{n_P} - 1$ . A numerical stable form of P-wave current successfully avoids the large numerical cancellation in the amplitude computations.

#### 3.2 Monte Carlo Simulation with HELAC-Onia

The program can be split into two major phases, which we call *initialization phase* and *computation phase* following Ref. [2]. During the *initialization phase*, HELAC-Onia will select all the subamplitudes and evaluate the color matrix  $M_{ij}$ , while during the *computation phase*, it will compute the Feynman amplitude in each phase space point kinematics, generate unweighted or weighted events, drive the Monte Carlo programs to do shower, and analyze the relevant observables on the fly. The program requires only minimal inputs from a user and achieves the automation.

28 3 HELAC-Onia

**Table 3.1** The identity numbers for the SM partonic particles in HELAC-ONIA

$\overline{\nu_e, e^-, u, d, \nu_\mu, \mu^-, c, s, \dots}$	1, , 12
$\bar{\nu_e}, e^+, \bar{u}, \bar{d}, \bar{\nu}_\mu, \mu^+, \bar{c}, \bar{s}, \dots$	$-1, \dots, -12$
$\gamma, Z, W^+, W^-, g$	31,, 35
$H, \chi, \phi^+, \phi^-$	41, , 44

# 3.2.1 *Usage*

We are trying to design the program to be user friendly. In versions 1.1.X, it could run under both Unix and Windows, whereas in versions 1.2.X, we only support Unix environment. One can follow the following steps to run HELAC-ONIA.

- 1. Provide process information in input/process.inp.
- 2. Specify the input parameters in input/user.inp following the format in input/default.inp.
- 3. Edit configurations for external libraries such as LHAPDF [23] in input/ho configuration.txt.
- 4. If one wants to plot histograms on the fly, edit the user's plot file analysis/user/plot\_user.f90.
- 5. If one wants to change the renormalization and factorization scales, edit the file src/setscale.f90.
- 6. Compile and run the program with the command lines<sup>4</sup>:

```
./config
./Helac-Onia
```

In item 1, the user should tell the program the information on the process. The information includes the number of external particles in the first line of the file and the identities of the particles in the second line. Since we only support scattering processes in the program, the first two particles are always interpreted as initial states, while the remaining particles are understood as final states. Following the notations in HELAC, we present the identity numbers of the partonic particles in Table 3.1. Our naming rules of the identities for the heavy quarkonium in HELAC-ONIA are summarized as:

- The number for each heavy quarkonium is in 6 digits.
- The first two digits are 44 for charmonium, 55 for bottomonium, and 45 for  $B_c^{\pm}$  system.
- The remaining four digits represent the Fock states. The four digits are in the order of (2S+1)LJc for  $^{2S+1}L_J^{[c]}$ .

<sup>&</sup>lt;sup>4</sup>The output file will be generated in the output directory.

, ,							
$c\bar{c}[S_0^{[1]}]$	$c\bar{c}[{}^{1}\!S_{0}^{[8]}]$	$c\bar{c}[{}^3\!\!S_1^{[1]}]$	$c\bar{c}[{}^3\!\!S_1^{[8]}]$	$c\bar{c}[P_1^{[1]}]$	$c\bar{c}[P_1^{[8]}]$	$c\bar{c}[{}^{3}\!P_{J}^{[1]}]$	$c\bar{c}[{}^{3}\!\!P_{J}^{[8]}]$
441001	441008	443011	443018	441111	441118	4431 <i>J</i> 1	4431 <i>J</i> 8
$b\bar{b}[S_0^{[1]}]$	$b\bar{b}[S_0^{[8]}]$	$b\bar{b}[{}^3\!\!S_1^{[1]}]$	$b\bar{b}[{}^{3}\!\!\!S_{1}^{[8]}]$	$b\bar{b}[{}^{1}\!\!P_{1}^{[1]}]$	$b\bar{b}[{}^{1}\!\!P_{1}^{[8]}]$	$b\bar{b}[{}^{3}\!\!P_{J}^{[1]}]$	$b\bar{b}[{}^{3}\!\!P_{J}^{[8]}]$
551001	551008	553011	553018	551111	551118	5531 <i>J</i> 1	5531 <i>J</i> 8
$c\bar{b}[{}^{1}\!S_{0}^{[1]}]$	$c\bar{b}[S_0^{[8]}]$	$c\bar{b}[{}^3\!\!S_1^{[1]}]$	$c\bar{b}[{}^3\!\!S_1^{[8]}]$	$c\bar{b}[{}^{1}\!P_{1}^{[1]}]$	$c\bar{b}[{}^{1}\!P_{1}^{[8]}]$	$c\bar{b}[{}^{3}\!P_{J}^{[1]}]$	$c\bar{b}[{}^{3}\!\!P_{J}^{[8]}]$
451001	451008	453011	453018	451111	451118	4531 <i>J</i> 1	4531 <i>J</i> 8
$\bar{c}b[{}^{1}\!\!S_{0}^{[1]}]$	$\bar{c}b[S_0^{[8]}]$	$\bar{c}b[{}^3\!\!S_1^{[1]}]$	$\bar{c}b[{}^{3}\!\!S_{1}^{[8]}]$	$\bar{c}b[{}^{1}\!\!P_{1}^{[1]}]$	$\bar{c}b[{}^{1}\!\!P_{1}^{[8]}]$	$\bar{c}b[{}^{3}\!\!P_{J}^{[1]}]$	$\bar{c}b[{}^{3}\!\!P_{J}^{[8]}]$
-451001	-451008	-453011	-453018	-451111	-451118	-4531 <i>J</i> 1	-4531 <i>J</i> 8

**Table 3.2** The identity numbers for the quarkonia in various Fock states in HELAC-ONIA, where J = 0.1.2

• For the non-self-conjugated mesons, i.e.,  $B_c^{\pm}$  mesons, an extra minus sign is used to represent the antiparticle. In HELAC-ONIA, we take  $B_c^+$  as the particle and  $B_c^-$  as the antiparticle.

With these rules, we are able to assign a unique number to each Fock state. We have listed the identity numbers for quarkonia in various Fock states in Table 3.2. Let us take an example. If we want to calculate a process  $gg \to c\bar{c}[{}^3\!P_1^{[8]}] + c\bar{c}[{}^3\!c_1^{[8]}] + g$ , we should specify the first line of input/process.inp as 5 and write the second line as

In item 2, one should provide the running parameters to the program. The parameters include the information of the running program, input parameters as well as kinematic cutoffs. All of these parameters are explained in the comment lines in input/default.inp. We summarized some of them in version 1.2.X in what follows:

- collar represents the type of colliding particles, i.e., 1 for pp, 2 for  $p\bar{p}$ , and 3 for  $e^+e^-$  colliders.
- energy\_beam1 and energy\_beam2 are the energies (in the unit of GeV) of the first and second beams, respectively. We have improved it in the case that the laboratory frame is not the same as the center-of-mass frame in the initial collisions.
- gener specifies the Monte Carlo generator, i.e., 0 for PHEGAS [24], 1 for RAMBO [25], 2 for DURHAM, and 3 for VEGAS [26]. We also provide the option to users to compute a single-phase space as long as they specify gener to be -1.
- ranhel is a parameter to determine whether the program uses the Monte Carlo sampling over the helicity configurations. In specific, if one sets it to be 0, it does the helicity summation explicitly, whereas if its value is larger than 0, it does the Monte Carlo sampling over helicity at various levels. All of these are explained in detail in Ref. [1] and in the file input/default.inp.

30 3 HELAC-Onia

• The value of qcd determines the amplitude should be calculated in which theory, i.e., 0 for only EW, 1 for EW and QCD, 2 for only QCD, 3 for only Quantum ElectroDynamics (QED) and 4 for QCD and QED.

- alphasrun is a parameter to determine whether the strong coupling constant  $\alpha_S$  will run or not. If alphasrun is 1,  $\alpha_S$  will run via renormalization equation during the computation. Otherwise, it will not.
- Flags such as gauge, ihiggs, and widsch determine the gauge (0 is in Feynman gauge, whereas 1 is in unitary gauge), the inclusion of Higgs or not, and using the fixed or complex scheme for the widths of  $W^{\pm}$  and Z bosons.
- mmc is the total number of the Monte Carlo iterations.
- pdf is the PDF set number proposed in pdf/pdflist.txt or LHAPDF. Entering 0 means no PDF is convoluted. If one wants to use LHAPDF, please edit input/ho\_configuration.txt and set lhapdf to be T.
- ptdisQ is a flag to determine it and calculates the  $p_T$  distribution  $\frac{d\sigma}{dp_T}$  for the first final quarkonium (T) or total cross section (F). If ptdisQ is set to be T, one should also specify which  $p_T$  value (the parameter Pt1) should be calculated.
- Scale specifies which renormalization and PDF factorization scale should be used. If the user decides to choose the fixed-value scheme, he/she should also supply the corresponding value of the scale via parameter FScaleValue.
- exp3pjQ is a flag to decide whether summing over J in Fock states  ${}^3P_J^{[8]}$  or  ${}^3P_J^{[1]}$ . It would be quite useful, for example, in  $J/\psi$  production. In practice, we only need the summation of  ${}^3P_J^{[8]}(J=0,1,2)$  instead of the separate components.
- modes determines whether the evaluated result is the polarized one (1) or not (0). If it is 1, the user should also provide the values of SDME1<sup>5</sup> and SDME2 to let HELAC-ONIA know to calculate which spin-density matrix element (SDME). Meanwhile, the value of LSJ represents to specify which "spin" (S,L,or J) in the heavy quarkonium. The user should also specify the corresponding polarization frame via parameter PolarFrame.
- The parameters of the physical cutoffs in computing the cross section should be input by the user if he/she wishes to use his/her own values.
- The default LDMEs are provided in input/default.inp. The user can use his/her own values by specifying the corresponding parameters in the file input/user.inp.
- topdrawer\_output, gnuplot\_output, and root\_output are plotting flags to let HELAC-ONIA plot histograms and output the corresponding files at the end of the *computation phase*.

If the user do not understand the exact meaning of the parameters, please have a look at the comment lines in input/default.inp. The format of the parameters in input/user.inp should be the same with those in input/default.inp.

<sup>&</sup>lt;sup>5</sup>"SDME" is an acronym for "spin-density matrix element".

# 3.2.2 Capability

In general, HELAC-Onia is able to perform any tree-level multileg SM processes computations with or without heavy quarkonium. Because it is based on the recursion relation, it is expected to be more efficient than the codes based on Feynman diagrams, such as Madonia [27]. In a simple example  $gg \to J/\psi + c\bar{c}$ , we have already tested that the timing of one unweighted event generating by Madonia is almost 4 times longer than by HELAC-Onia. Moreover, to the best of our knowledge, HELAC-Onia is the only general event generator on the market for studying multi-quarkonium production. We summarized the main aspects of what HELAC-Onia can do in what follows:

- 1. One or more heavy quarkonium, including  $B_c^{\pm}$  system and up to P-wave states, production in hadronic collisions and in electron–positron annihilations.
- 2. Unweighted events generation in the standard Les Houches Event (LHE) format [28] and analysis at differential levels.
- 3. Spin-density matrix elements (SDMEs) computations in the helicity frame, Collins-Soper frame, Gottfried-Jackson frame, and target frame [29].
- 4. Complex-mass scheme for electroweak particles and inclusive  $k_T$  clustering for jet(s) production.
- 5. Inclusion of QED photon showering from initial  $e^{\pm}$  beams by interfacing to QEDPS [30, 31].

Several applications, described in the next few chapters, will show some of these capabilities in the detail examples. Moreover, we want to emphasize that the QED photon showering is only done in versions 1.2.X.

#### 3.2.3 Validations

HELAC-ONIA has been checked widely before it was released [1]. First, we have make sure all of our modifications do not change the results for the partonic processes with HELAC. Second, we have checked several single-phase-space points with the analytic computations [15, 32]. Third, we have checked some conclusions from symmetries, for example, parity conservation in QCD. At integrated level, we have checked the various processes with those present in the literature. We will not repeat them again in the thesis, but only refer the interested readers to Ref. [1]. For completeness, we just summarized all of the benchmark processes presented in Ref. [1] as follows:

- $B_c^{\pm}$  meson, in  ${}^{1}\!S_{0}^{[8]}$ ,  ${}^{1}\!S_{0}^{[1]}$ ,  ${}^{3}\!S_{1}^{[1]}$ ,  ${}^{3}\!S_{1}^{[8]}$ ,  ${}^{1}\!P_{1}^{[1]}$ ,  ${}^{1}\!P_{1}^{[8]}$ ,  ${}^{3}\!P_{J}^{[8]}$ ,  ${}^{3}\!P_{J}^{[1]}$ , production at the LHC via gluon fusion and quark–antiquark annihilation.
- Charmonia production processes at B factories. They include the processes

32 3 HELAC-Onia

$$e^{+}e^{-} \rightarrow \gamma^{*} \rightarrow \eta_{c}c\bar{c},$$

$$e^{+}e^{-} \rightarrow \gamma^{*} \rightarrow \eta_{c}ggg,$$

$$e^{+}e^{-} \rightarrow \gamma^{*} \rightarrow J/\psi c\bar{c},$$

$$e^{+}e^{-} \rightarrow \gamma^{*} \rightarrow J/\psi gg,$$

$$e^{+}e^{-} \rightarrow \gamma^{*} \rightarrow J/\psi \eta_{c},$$

$$e^{+}e^{-} \rightarrow \gamma^{*} \rightarrow h_{c}\eta_{c},$$

$$e^{+}e^{-} \rightarrow \gamma^{*} \rightarrow h_{c}\chi_{cJ},$$

$$e^{+}e^{-} \rightarrow \gamma^{*} \rightarrow h_{c}\chi_{cJ},$$

$$e^{+}e^{-} \rightarrow J/\psi J/\psi,$$

$$e^{+}e^{-} \rightarrow J/\psi h_{c}.$$

• Quarkonium-pair production at the Tevatron:

$$\begin{split} p\bar{p} &\to \eta_c + \eta_c, \\ p\bar{p} &\to J/\psi + J/\psi, \\ p\bar{p} &\to \eta_b + \eta_b, \\ p\bar{p} &\to \Upsilon + \Upsilon, \\ p\bar{p} &\to B_c^+ + B_c^-, \\ p\bar{p} &\to B_c^+ + B_c^{-*}, \\ p\bar{p} &\to B_c^{+*} + B_c^{-*}. \end{split}$$

- Differential distributions for  $J/\psi + c\bar{c}$  and  $\Upsilon + b\bar{b}$  at the Tevatron and the LHC.
- Yields of  $J/\psi$  and  $\chi_{cJ}$  at hadron colliders at  $\mathcal{O}(\alpha_S^3)$  and  $\mathcal{O}(\alpha_S^4)$ .

We have successfully applied HELAC-ONIA to the NRQCD polarization predictions for  $J/\psi$  [18] and  $\chi_{cJ}$  [33, 34] at  $\mathcal{O}(\alpha_S^3)$  and  $\mathcal{O}(\alpha_S^4)$ , some of which have been confirmed by other theoretical groups [17, 19]. With the new code, we were able to quickly obtain the new  $\mathcal{O}(\alpha^2\alpha_S^2 + \alpha^3\alpha_S + \alpha^4)$  results for  $e^-e^+ \to \eta_c + c\bar{c}$  and  $e^-e^+ \to J/\psi + c\bar{c}$  as done in Ref. [1].

# 3.2.4 Third-Party Codes in HELAC-Onia

HELAC-ONIA is completely self-contained and ready to run. There are several third-party codes included in it. Thanks to these public codes, we are able to perform physical analysis directly with one command only. They are listed as follows: PHEGAS [24], VEGAS [26], RAMBO [25], MINT [35], QEDPS [30, 31], and LHAPDF [23]. We have improved PHEGAS capable of dealing with quarkonium kinematics. For

LHAPDF, it is not installed internally by HELAC-ONIA but asking users to install it themselves. If the program cannot find the LHAPDF, it will use the internal PDF sets. This would supply the maximal flexible freedom to the users.

#### 3.2.5 Status

We have improved HELAC-ONIA a lot since it was first released [1]. The main changes include:

- 1. Two completely independent generators based on PHEGAS [24] and VEGAS [26] are established. Both of them can be used to calculate cross sections and to generate unweighted events for  $2 \to n$  processes when  $n \ge 2$  at pp,  $p\bar{p}$  and  $e^-e^+$  collisions. However, for  $2 \to 1$  processes at hadron colliders, only VEGAS is available.
- 2. More internal PDFs are added. The program also can be interfaced to LHAPDF.
- 3. Analysis is done on the fly. Differential distributions are plotted at the end of *computation phase*.
- 4. The laboratory frame is not restricted to the center-of-mass frame of initial collision anymore.
- 5. An interface from QEDPS to HELAC-ONIA is done. One can include the QED photon showering effects from the initial  $e^{\pm}$  beams.

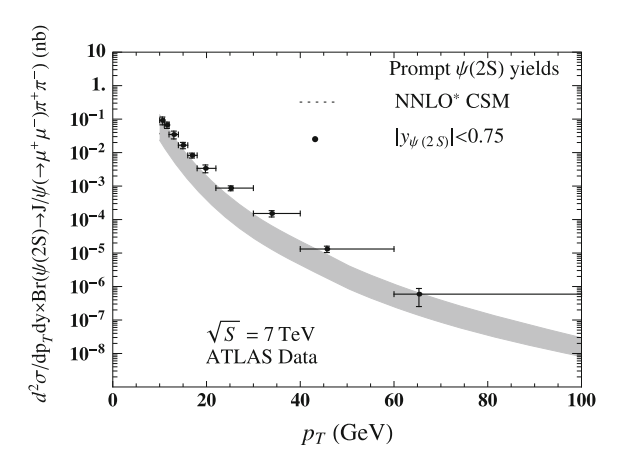
For item 1, in versions 1.1.X, the unweighted events can only be generated by PHEGAS[24].  $2 \rightarrow 1$  processes are also not achievable in the old versions. The improvement allows us to get rid of a lot of restrictions. Concerning for item 2, there is only CTEQ6 [36] available in versions 1.1.X. It paves a way for us to apply it to nucleon collisions and to estimate PDF uncertainties. With the improvement presented in item 4, we are able to apply HELAC-ONIA to more experiments such as the fixed-target experiments [37] in the versions 1.2.X. Item 5 allows us to consider initial radiation effects at  $e^-e^+$  collision, which might be not small in several important processes, such as  $e^-e^+ \rightarrow J/\psi + gg$  [38].

Due to the large higher-order QCD corrections in heavy quarkonium production, we are planning to improve HELAC-ONIA to perform NLO-level computations. Moreover, it is quite interesting to see how HELAC-ONIA can be applied to more broder physics, such as heavy ion collisions [39] and transverse momentum factorization [40].

# 3.2.6 Robust on an Example: NNLO\* QCD Corrections to $\psi(2S)$ Hadroproduction in CSM

At the end of this chapter, we will present an example to show the robust of HELAC-ONIA, i.e., NNLO\* QCD corrections to  $\psi(2S)$  production at the LHC. It is the highest 34 3 HELAC-Onia

Fig. 3.1 NNLO\* CSM prediction for prompt  $\psi(2S)$  production at the LHC  $\sqrt{S} = 7$  TeV and |y| < 0.75. The ATLAS data are obtained from Ref. [44]



multiplicity quarkonium process that has been calculated and studied so far [41]. Other similar but in lower complexity process is  $J/\psi + \gamma$  [42]. Due to its complications, it is difficult to do an analytic computation. We will do it completely numerically with the help of HELAC-ONIA. For phase space integration, we used the multichannel techniques [43], which was already implemented in PHEGAS [24]. There are almost 180 channels in the most complicated subprocess  $gg \to c\bar{c}[\hat{S}_1^{(1)}] + ggg$ . The convergence is fast, and it costs only several hours to achieve 2% accuracy. The timing indicated is for a single core of a 2.3 GHz i7 CPU, with the gfortran compiler v4.6.2 without optimization flags. Apart from  $gg \to c\bar{c}[\hat{S}_1^{(1)}] + ggg$ , at  $\mathcal{O}(\alpha_S^5)$ , we have included other important subprocesses such as  $gg \to c\bar{c}[\hat{S}_1^{(1)}] + ggg$ .

We have shown the NNLO\* result calculated by HELAC-ONIA in Fig. 3.1. To compare with the experimental data, we have also put the preliminary ATLAS data [44] in the plot. We have used  $\text{Br}(\psi \to J/\psi + \pi^+\pi^-) = 34.0\,\%$ ,  $\text{Br}(J/\psi \to \mu^+\mu^-) = 5.94\,\%$ , and  $\langle \mathcal{O}^{\psi(2S)}({}^3\!\!S_1^{[1]}) \rangle = 0.95\,\,\text{GeV}^3$ , and have taken  $m_c = 1.5 \pm 0.1\,\text{GeV}$ , 0.5  $\sqrt{4m_c^2 + p_T^2} \le \mu_F = \mu_R \le 2\sqrt{4m_c^2 + p_T^2}$ ,  $s_{ij}^{\text{min}}$  dependence as our theoretical uncertainties. The result presented here has been checked with the result calculated by MADONIA [27] up to 40GeV.

## References

- 1. H.S. Shao, Comput. Phys. Commun. **184**, 2562 (2013). doi:10.1016/j.cpc.2013.05.023
- A. Kanaki, C.G. Papadopoulos, Comput. Phys. Commun. 132, 306 (2000). doi:10.1016/S0010-4655(00)00151-X
- 3. C. Papadopoulos, M. Worek, pp. 507–510 (2006)
- A. Cafarella, C.G. Papadopoulos, M. Worek, Comput. Phys. Commun. 180, 1941 (2009). doi:10.1016/j.cpc.2009.04.023
- 5. F. Dyson, Phys. Rev. 75, 1736 (1949), doi:10.1103/PhysRev.75,1736
- 6. J.S. Schwinger, Proc. Nat. Acad. Sci. 37, 452 (1951)

References 35

- 7. J.S. Schwinger, Proc. Nat. Acad. Sci. **37**, 455 (1951)
- F.A. Berends, W.T. Giele, Nucl. Phys. B 306, 759 (1988). doi:10.1016/0550-3213(88)90442-7
- F. Caravaglios, M. Moretti, Phys. Lett. B 358, 332 (1995). doi:10.1016/0370-2693(95)00971-M
- 10. G. 't Hooft, Nucl. Phys. **B72**, 461 (1974). doi:10.1016/0550-3213(74)90154-0
- 11. A. Kanaki, C.G. Papadopoulos (2000)
- F. Maltoni, K. Paul, T. Stelzer, S. Willenbrock, Phys. Rev. D 67, 014026 (2003). doi:10.1103/ PhysRevD.67.014026
- A. Petrelli, M. Cacciari, M. Greco, F. Maltoni, M.L. Mangano, Nucl. Phys. B 514, 245 (1998). doi:10.1016/S0550-3213(97)00801-8
- 14. E.L. Berger, D.L. Jones, Phys. Rev. D 23, 1521 (1981). doi:10.1103/PhysRevD.23.1521
- Y.Q. Ma, K. Wang, K.T. Chao, Phys. Rev. Lett. 106, 042002 (2011). doi:10.1103/PhysRevLett. 106.042002
- M. Butenschoen, B.A. Kniehl, Phys. Rev. Lett. 106, 022003 (2011). doi:10.1103/PhysRevLett. 106.022003
- 17. M. Butenschoen, B.A. Kniehl, Phys. Rev. Lett. 108, 172002 (2012)
- 18. K.T. Chao, Y.Q. Ma, H.S. Shao, K. Wang, Y.J. Zhang, Phys. Rev. Lett. 108, 242004 (2012)
- 19. B. Gong, L.P. Wan, J.X. Wang, H.F. Zhang, Phys. Rev. Lett. 110, 042002 (2013)
- H.S. Shao, H. Han, Y.Q. Ma, C. Meng, Y.J. Zhang, K.T. Chao, JHEP 05, 103 (2015). doi:10. 1007/JHEP05(2015)103
- M. Butenschoen, B.A. Kniehl, Phys. Rev. Lett. 104, 072001 (2010). doi:10.1103/PhysRevLett. 104.072001
- 22. M. Butenschoen, B.A. Kniehl (2011)
- 23. M. Whalley, D. Bourilkov, R. Group (2005)
- C.G. Papadopoulos, Comput. Phys. Commun. 137, 247 (2001). doi:10.1016/S0010-4655(01)00163-1
- R. Kleiss, W. Stirling, S. Ellis, Comput. Phys. Commun. 40, 359 (1986). doi:10.1016/0010-4655(86)90119-0
- G. Lepage, J. Comput. Phys. 27, 192 (1978). doi:10.1016/0021-9991(78)90004-9 (Revised version)
- P. Artoisenet, F. Maltoni, T. Stelzer, JHEP 0802, 102 (2008). doi:10.1088/1126-6708/2008/ 02/102 (17 pages, 7 figures)
- 28. E. Boos, M. Dobbs, W. Giele, I. Hinchliffe, J. Huston, et al. (2001)
- M. Beneke, M. Kramer, M. Vanttinen, Phys. Rev. D 57, 4258 (1998). doi:10.1103/PhysRevD. 57.4258
- J. Fujimoto, Y. Shimizu, T. Munehisa, Prog. Theor. Phys. 90, 177 (1993). doi:10.1143/PTP.90.
   177
- 31. T. Munehisa, J. Fujimoto, Y. Kurihara, Y. Shimizu, Prog. Theor. Phys. **95**, 375 (1996). doi:10. 1143/PTP.95.375
- Y.Q. Ma, K. Wang, K.T. Chao, Phys. Rev. D 83, 111503 (2011). doi:10.1103/PhysRevD.83. 111503
- 33. H.S. Shao, K.T. Chao, Phys. Rev. D 90(1), 014002 (2014). doi:10.1103/PhysRevD.90.014002
- 34. H.S. Shao, Y.Q. Ma, K. Wang, K.T. Chao, Phys. Rev. Lett. **112**(18), 182003 (2014). doi:10. 1103/PhysRevLett.112.182003
- 35. P. Nason (2007)
- 36. J. Pumplin, D. Stump, J. Huston, H. Lai, P.M. Nadolsky et al., JHEP **0207**, 012 (2002)
- S. Brodsky, F. Fleuret, C. Hadjidakis, J. Lansberg, Phys. Rept. 522, 239 (2013). doi:10.1016/j.physrep.2012.10.001
- 38. H.S. Shao, JHEP **04**, 182 (2014)
- E. Ferreiro, F. Fleuret, J. Lansberg, A. Rakotozafindrabe, Phys. Rev. C 88, 047901 (2013). doi:10.1103/PhysRevC.88.047901
- W.J. den Dunnen, J.P. Lansberg, C. Pisano, M. Schlegel, Phys. Rev. Lett. 112, 212001 (2014). doi:10.1103/PhysRevLett.112.212001

36 3 HELAC-Onia

41. P. Artoisenet, J.M. Campbell, J. Lansberg, F. Maltoni, F. Tramontano, Phys. Rev. Lett. 101, 152001 (2008). doi:10.1103/PhysRevLett.101.152001

- 42. J. Lansberg, Phys. Lett. B **679**, 340 (2009). doi:10.1016/j.physletb.2009.07.067 43. R. Kleiss, R. Pittau, Comput. Phys. Commun. **83**, 141 (1994). doi:10.1016/0010-4655(94)90043-4
- 44. T.A. Collaboration (2013)

# Chapter 4 Heavy Quarkonium Production in Hadronic Collisions

**Abstract** In this chapter, we will apply HELAC-ONIA to study heavy quarkonium production processes at hadron colliders. Since the large samples of charmonia and bottomonia accumulated at the LHC, all of the LHC experiments such as A Toroidal LHC ApparatuS (ATLAS), Compact Muon Solenoid (CMS), Large Hadron Collider beauty (LHCb) and A Large Ion Collider Experiment (ALICE) have released their measurements on heavy quarkonium production. Theoretically, it is still unclear what is the production mechanism of heavy quarkonium. HELAC-ONIA provides us a good opportunity to investigate the production mechanism of heavy quarkonium with less manpower. In this chapter, we will show CO intermediate states will be quite important to explain the yields and polarizations of heavy quarkonium in the high- $p_T$  regime. By contrast, from B factories data, it indicates a completely different conclusion. We devote it to the next chapter. We organized this chapter into three interesting processes happening at the LHC. They are prompt  $J/\psi$  and  $\psi(2S)$  production, prompt  $\chi_c$  production and double-quarkonium production.

# 4.1 Yields and Polarizations of Prompt $J/\psi$ and $\psi(2S)$ Production

We take our attention to the yields and polarizations of prompt  $J/\psi$  and  $\psi(2S)^1$  at the Tevatron and the LHC in this section. Here, we are trying to study the phenomenology of  $\psi$  production up to  $\mathcal{O}(\alpha_S^4 v^4)$  in the framework of NRQCD. Four important Fock states  ${}^3\!\!\!S_1^{[1]}, {}^3\!\!\!S_1^{[8]}, {}^1\!\!\!S_0^{[8]}, {}^3\!\!\!P_J^{[8]}$  contribute to  $\psi$  production at this order. For prompt  $J/\psi$  production, there are also significant feed-down contributions from  $\psi(2S)$  and  $\chi_{cJ}(J=0,1,2)$  decay.  $\chi_{cJ}$  have two Fock states  ${}^3\!\!\!S_1^{[8]}$  and  ${}^3\!\!\!P_J^{[1]}$  contributions.

<sup>&</sup>lt;sup>1</sup>Note that, people also usually call  $\psi(2S)$  as  $\psi'$  in the literature.

<sup>&</sup>lt;sup>2</sup>Following the initial submission of this thesis, the results presented in this section are published in Ref.[1].

<sup>3&</sup>quot;Prompt" charmonium production means it excludes the contributions from bottom quark/meson decays.

Several groups, including us, have done a lot of theoretical works at this level [1–7]. In particular, a consistent yield and polarization predictions for prompt  $J/\psi$  production at the Tevatron and the LHC have been given by us in Ref. [6]. However, we did not include feed-down contributions in our previous NRQCD predictions. We pointed out later in Ref. [8] that in our case the feed-down contributions will not alter our conclusion (but it will really modify the possible extraction of CO LDMEs). Recently, there are new theoretical progress appearing in studying  $J/\psi$  and  $\psi(2S)$  production at the LHC [9, 10]. In Ref. [9], Bodwin et al. calculated the leading- $p_T$  resummation contribution for  $J/\psi$  production. They ignored the feed-down contributions and drew a similar conclusion as ours [6]:  ${}^3\!{}^{[8]}_1$  and  ${}^3\!{}^{[8]}_J$  should be canceled to guarantee the unpolarized  $J/\psi$  result. In Ref. [10], Faccioli et al. used a data-driven method to fix CO LDMEs of  $\psi(2S)$  based on NLO NRQCD. They pointed out that a large  $p_T$  cutoff was necessary for explaining the polarization data of  $\psi(2S)$ . In this section, we present our complete NRQCD results for prompt  $J/\psi$  and  $\psi(2S)$  production and compare them with experiments.

# 4.1.1 General Setup

Before proceeding, we first specify the general setup in our computations. The starting point is the cross section for a quarkonium  $\mathcal{Q}$  production in pp collision

$$\sigma(pp \to \mathcal{Q} + X) = \sum_{n} \sigma(pp \to Q\bar{Q}[n] + X) \times \langle \mathcal{O}^{\mathcal{Q}}(n) \rangle, \tag{4.1}$$

where  $\sigma(pp \to Q\bar{Q}[n] + X)$  is the SDC for producing a heavy quark pair  $Q\bar{Q}$  in the quantum number n.  $\langle \mathcal{O}^{\mathcal{Q}}(n) \rangle$  in Eq. (4.1) is the non-perturbative LDME for the heavy quarkonium  $\mathcal{Q}$ , which means the probability of a quark pair in n evolving into the heavy quarkonium  $\mathcal{Q}$ . In QCD factorization formula, the SDC can be computed perturbatively as

$$\sigma(pp \to Q\bar{Q}[n] + X) = \sum_{a,b} \int dx_1 dx_2 d\text{LIPS} f_{a/p}(x_1) f_{b/p}(x_2)$$
$$|\mathscr{A}(ab \to Q\bar{Q}[n] + X)|^2, \tag{4.2}$$

where a, b exhaust all possible partonic species in the colliding protons, dLIPS is the Lorentz-invariant phase space measurement,  $x_1, x_2$  are the Bjorken fractions,  $f_{a/p}(x_1), f_{b/p}(x_2)$  are PDFs, and  $\mathscr{A}(ab \to Q\bar{Q}[n] + X)$  denotes as the amplitude of the parton-level process  $ab \to Q\bar{Q}[n] + X$ .

$J/\psi$	$\psi(2S)$	Xc0	Xc1	Xc2
3.097	3.686	3.415	3.511	3.556

Table 4.1 Physical masses (in the unit of GeV) for various charmonia [12]

**Table 4.2** Branching ratios for various decay processes involved in this section [12]

Decay channel	Branching ratio ( $\times 10^{-2}$ )
$J/\psi \to \mu^+\mu^-$	5.93
$\psi(2S) \to \mu^+ \mu^-$	0.75
$\psi(2S) \to J/\psi + X$	57.4
$\psi(2S) \to J/\psi \pi^+ \pi^-$	34.0
$\psi(2S) \to \chi_{c0} + \gamma$	9.84
$\psi(2S) \to \chi_{c1} + \gamma$	9.30
$\psi(2S) \to \chi_{c2} + \gamma$	8.76
$\chi_{c0}  o J/\psi + \gamma$	1.28
$\chi_{c1}  o J/\psi + \gamma$	36.0
$\chi_{c2}  o J/\psi + \gamma$	20.0

In this section, we will use CTEQ6M [11] in our NLO computations. The mass of charm quark is fixed as  $m_c=1.5 \, {\rm GeV}$  and the masses of charmonia are  $2m_c$ . The renormalization and factorization scales are taken as  $\mu_R=\mu_F=\sqrt{(2m_c)^2+p_T^2}$  and the NRQCD scale is  $\mu_A=m_c$ . For the feed-down contributions from higher-excited charmonia, i.e.,  $\chi_{cJ}$ , J=0, 1, 2 and  $\psi(2S)$ , we will take a  $p_T$  spectrum shifting in their decay. In a general decay process  $\mathcal{Q}_1\to\mathcal{Q}_0+X$ , it is approximated by the relation  $\frac{p_T^{\mathcal{Q}_0}}{M_{\mathcal{Q}_0}}=\frac{p_T^{\mathcal{Q}_1}}{M_{\mathcal{Q}_1}}$ , where  $M_{\mathcal{Q}_0}$ ,  $M_{\mathcal{Q}_1}$  are the physical masses of particles  $Q_0$ ,  $Q_1$  and  $p_T^{\mathcal{Q}_0}$ ,  $p_T^{\mathcal{Q}_1}$  are their transverse momenta in the laboratory frame. In Tables 4.1 and 4.2, we establish the physical masses for relevant charmonia and the branching ratios (Br) for various charmonia decay processes in our analysis.

A very clean decay mode for  $J/\psi$  and  $\psi(2S)$  is decaying into a lepton pair, which is almost free of background. The angular distribution of the lepton pair may expose the spin information of its mother particles. It provides us the opportunity to count how many events are generated in the transverse-polarized pattern or in the longitudinal-polarized pattern. Therefore, it may reveal more information on the heavy quarkonium production mechanism. We can express the polar angular distribution of the di-lepton in the rest frame of  $\psi$  as  $1 + \lambda_{\theta} \cos \theta$ , where  $\theta$  is the polar angle of one lepton via its z-axis. Then, the polarization observable  $\lambda_{\theta}$  can be expressed in the SDMEs of  $\psi$  as follows<sup>4</sup>

$$\lambda_{\theta} = \frac{d\sigma_{11} - d\sigma_{00}}{d\sigma_{11} + d\sigma_{00}}. (4.3)$$

<sup>&</sup>lt;sup>4</sup>We have assumed  $d\sigma_{11} = d\sigma_{-1-1}$ , which is always true in a QCD process.

The value of  $\lambda_{\theta}$  depends on the z-axis definition. We only choose the helicity frame in the context, in which the z-axis is defined as the flight direction of  $\psi$ .

### 4.1.2 LDMEs

The most involved thing in  $\psi$  production is how to extract the non-perturbative CO LDMEs from experimental data. Different experimental inputs really impact the extraction of CO LDMEs [2–7]. Sometimes, it is indeed dangerous because it is unclear on the theoretical side to know what large  $p_T$  is sufficient for the validity of NRQCD factorization. The inclusion of inappropriate experimental data may result in unstable and/or unphysical CO LDMEs. For example, a negative value of CO LDME  $\langle \mathcal{O}^{J/\psi}({}^3\!P_0^{[8]})\rangle$  may result in negative yields of  $J/\psi+\gamma$  [13]. In this subsection, we will take a careful investigation on this issue and try to avoid trapping in such a problem.

Let us recall what we have learned from the previous studies [3, 4, 6, 14]. The LDMEs  $\langle \mathcal{O}^{\chi_{cJ}}(\mathring{S}_1^{[8]}) \rangle$  and  $\langle \mathcal{O}^{\chi_{cJ}}(\mathring{P}_J^{[1]}) \rangle$  for  $\chi_{cJ}$  have the spin symmetry relations:  $\langle \mathcal{O}^{\chi_{cJ}}(\mathring{S}_1^{[8]}) \rangle = (2J+1)\langle \mathcal{O}^{\chi_{c0}}(\mathring{S}_1^{[8]}) \rangle$  and  $\langle \mathcal{O}^{\chi_{cJ}}(\mathring{P}_J^{[1]}) \rangle = (2J+1)\langle \mathcal{O}^{\chi_{c0}}(\mathring{P}_0^{[1]}) \rangle$ . CS LDME  $\langle \mathcal{O}^{\chi_{c0}}(\mathring{P}_0^{[1]}) \rangle$  is closely related to the derivation of wave function at origin R'(0) via  $\langle \mathcal{O}^{\chi_{c0}}(\mathring{P}_0^{[1]}) \rangle = \frac{3}{4\pi}|R'(0)|^2$ .  $|R'(0)|^2$  is estimated to be 0.075 GeV<sup>5</sup> [15] in Buchmuller-Tye potential model [16]. Moreover, the only independent CO LDME  $\langle \mathcal{O}^{\chi_{c0}}(\mathring{S}_1^{[8]}) \rangle$  for  $\chi_c$  should be determined from the experimental data. Following Ref. [4], it is a good choice to determine  $\langle \mathcal{O}^{\chi_{c0}}(\mathring{S}_1^{[8]}) \rangle$  from the ratio  $\sigma_{\chi_{c2} \to J/\psi\gamma}/\sigma_{\chi_{c1} \to J/\psi\gamma}$ . As shown in Sect. 4.2.2, by using this ratio, the CO LDME  $\langle \mathcal{O}^{\chi_{c0}}(\mathring{S}_1^{[8]}) \rangle$  is insensitive to the  $p_T$  cutoff. Hence, we simply take the value from Ref. [4], i.e.,

$$\begin{split} \langle \mathcal{O}^{\chi_{c0}}({}^3\!\!\!\!\!S_1^{[8]}) \rangle &= (2.2^{+0.48}_{-0.32}) \times 10^{-3} \text{GeV}^3, \\ \frac{\langle \mathcal{O}^{\chi_{c0}}({}^3\!\!\!\!P_0^{[1]}) \rangle}{m_c^2} &= 7.96 \times 10^{-3} \text{GeV}^3, \end{split}$$
(4.4)

in which we use the Collider Detector at Fermilab (CDF) data [17] only.

The CS LDME for  $\psi$  can also be estimated in potential model [15]. However, due to the smallness of the SDC in our interested  $p_T$  regime, its value in our analysis is indeed not important. For completeness, we establish it in the following

$$\langle \mathcal{O}^{J/\psi}(\mathring{S}_{1}^{[1]}) \rangle = 1.16 \text{ GeV}^{3},$$
  
 $\langle \mathcal{O}^{\psi(2S)}(\mathring{S}_{1}^{[1]}) \rangle = 0.76 \text{ GeV}^{3}.$  (4.5)

The determination of three unknown CO LDMEs for  $\psi$  is much involved. From our previous studies [3, 6, 18], we are able to summarize the following facts:

<sup>&</sup>lt;sup>5</sup>We drop a factor  $2N_c$  for convenience here.

• The SDC of P-wave CO Fock state  ${}^3P_J^{[8]}$  can be decomposed into a linear combination of the SDCs of  ${}^1S_0^{[8]}$  and  ${}^3S_1^{[8]}$  as follows:

$$d\hat{\sigma}(^{3}P_{J}^{[8]}) = r_{0}\frac{d\hat{\sigma}(^{5}S_{0}^{[8]})}{m_{c}^{2}} + r_{1}\frac{d\hat{\sigma}(^{3}S_{1}^{[8]})}{m_{c}^{2}},$$
(4.6)

where  $r_0$  and  $r_1$  change slightly with the rapidity interval, but they are almost insensitive to the center-of-mass energy  $\sqrt{S}$  (see Table I in Ref. [18]). Therefore, it would be difficult to fix three independent CO LDMEs precisely by fitting the helicity-summed yield data at hadron colliders. Alternatively, one is able to extract two linear combinations of the three CO LDMEs within convincing accuracy. We denote them as

$$M_{0,r_0}^{J/\psi(\psi(2S))} \equiv \langle \mathcal{O}^{J/\psi(\psi(2S))}(\mathring{S}_0^{[8]}) \rangle + r_0 \frac{\langle \mathcal{O}^{J/\psi(\psi(2S))}(\mathring{P}_0^{[8]}) \rangle}{m_c^2}$$

$$M_{1,r_1}^{J/\psi(\psi(2S))} \equiv \langle \mathcal{O}^{J/\psi(\psi(2S))}(\mathring{S}_1^{[8]}) \rangle + r_1 \frac{\langle \mathcal{O}^{J/\psi(\psi(2S))}(\mathring{P}_0^{[8]}) \rangle}{m_c^2}. \tag{4.7}$$

Here,  $M_{0,r_0}^{J/\psi(\psi(2S))}$  and  $M_{1,r_1}^{J/\psi(\psi(2S))}$  can be viewed as the coefficients of two different  $p_T$  curves. The curve corresponding to  $M_{1,r_1}^{J/\psi(\psi(2S))}$  is much harder than the one corresponding to  $M_{0,r_0}^{J/\psi(\psi(2S))}$ .

- The SDC  $d\hat{\sigma}_{11}({}^3\!P_J^{[8]})$  in the helicity frame<sup>6</sup> has the similar decomposition into  $d\hat{\sigma}_{11}({}^3\!S_0^{[8]})$  and  $d\hat{\sigma}_{11}({}^3\!S_1^{[8]})$ . The non-trivial thing is that  $r_1$  in  $d\hat{\sigma}_{11}({}^3\!P_J^{[8]})$  decomposition is quite close to that in the helicity-summed  $d\hat{\sigma}({}^3\!P_J^{[8]})$  decomposition [6]. Hence, it still does not help a lot to fix the three CO LDMEs individually by including polarization data in our fit. This fact was already emphasized in Ref. [6]. It implies that the value of  $M_{1,r_1}^{J/\psi(\psi(2S))}$  defined in Eq. (4.7) almost controls the weight of the transverse-polarized component. Hence, the unpolarized data would require a (very) small  $M_{1,r_1}^{J/\psi(\psi(2S))}$ .
- We can assume that all of the CO LDMEs are positive [6], which is in contrast to those given in Refs. [5, 7]. Because  $r_1$  in the forward rapidity interval is smaller than that in the central rapidity interval, a positive  $\langle \mathcal{O}^{J/\psi(\psi(2S))}(^2P_0^{(8)})\rangle$  guarantees the forward rapidity  $\frac{d\sigma}{dp_T}$  and  $\lambda_\theta$  lower than those in the central rapidity. This assumption will be justified later by the experimental data.

Based on these observations, we are now in the position to determine  $M_{0,r_0}^{J/\psi(\psi(2S))}$  and  $M_{1,r_1}^{J/\psi(\psi(2S))}$  from Tevatron yield data only. In Ref. [3], they were determined from the CDF yield data [19, 20] with  $p_{T\text{cut}} = 7$  GeV. They are [3]

<sup>&</sup>lt;sup>6</sup>In this chapter, we only consider the helicity frame.

$$M_{0,r_0}^{J/\psi} = (7.4 \pm 1.9) \times 10^{-2} \text{ GeV}^3,$$
  
 $M_{1,r_1}^{J/\psi} = (0.05 \pm 0.02) \times 10^{-2} \text{ GeV}^3,$  (4.8)

$$M_{0,r_0}^{\psi(2S)} = (2.0 \pm 0.6) \times 10^{-2} \text{ GeV}^3,$$
  
 $M_{1,r_1}^{\psi(2S)} = (0.12 \pm 0.03) \times 10^{-2} \text{ GeV}^3.$  (4.9)

We take this set of CO LDMEs as our default set. However, as we discussed at the beginning of this subsection, it is unclear from theory to know which  $p_{T\text{cut}}$  is enough to make sure NRQCD factorization maintain. Hence, we would like to see the  $p_{T\text{cut}}$  dependence of  $M_{0,r_0}^{J/\psi(\psi(2S))}$  and  $M_{1,r_1}^{J/\psi(\psi(2S))}$  in our fit. For  $\psi(2S)$ , we have summarized our results for  $M_{0,r_0}^{\psi(2S)}$  and  $M_{1,r_1}^{\psi(2S)}$  with different  $p_{T\text{cut}}$  in Table 4.3, from which we see that the values are sensitive to  $p_{T\text{cut}}$  when  $p_{T\text{cut}} \geq 7$  GeV. The minimal  $\chi^2$  arrives when  $p_{T\text{cut}} = 11$  GeV, where we also obtain a relatively stable values for  $M_{0,r_0}^{\psi(2S)}$  and  $M_{1,r_1}^{\psi(2S)}$ . In contrast, for  $J/\psi$ , the values of  $M_{0,r_0}^{J/\psi}$  and  $M_{1,r_1}^{J/\psi}$  are insensitive to  $p_{T\text{cut}}$  when  $p_{T\text{cut}} \geq 7$  GeV. It reflects that the feed-down contribution from  $\psi(2S)$  decay is not significant in the CDF fiducial region. Therefore, we will only use the default set of  $M_{0,r_0}^{J/\psi}$  and  $M_{1,r_1}^{J/\psi}$  for the  $J/\psi$  production process. The new set of CO LDMEs for  $\psi(2S)$  we will adopt in this chapter is

$$M_{0,r_0}^{\psi(2S)} = (3.82 \pm 0.78) \times 10^{-2} \text{ GeV}^3,$$
  
 $M_{1,r_0}^{\psi(2S)} = (0.059 \pm 0.029) \times 10^{-2} \text{ GeV}^3,$  (4.10)

**Table 4.3** Values of  $M_{0,r_0}^{\psi(2S)}$  and  $M_{1,r_1}^{\psi(2S)}$  extracted from CDF data [20] with different  $p_{T\text{cut}}$ , where  $r_0 = 3.9, r_1 = -0.56$ 

$p_{T\mathrm{cut}}^{\psi(2S)}(\mathrm{GeV})$	$M_{0,m}^{\psi(2S)}(\times 10^{-2} \text{ GeV}^3)$	$M_{1,r_1}^{\psi(2S)}(\times 10^{-2} \text{ GeV}^3)$	$\chi^2/d.o.f$
5	$1.3754 \pm 0.118931$	$0.159987 \pm 0.0117348$	37.2068/16 = 2.32542
6	$1.93677 \pm 0.17044$	$0.128511 \pm 0.0135506$	14.0112/14 = 1.0008
7	$2.23162 \pm 0.23115$	$0.109918 \pm 0.0155178$	7.21501/12 = 0.601251
8	$2.253154 \pm 0.301835$	$0.100531 \pm 0.0175978$	5.46679/10 = 0.546679
9	$2.7258 \pm 0.401123$	$0.0932409 \pm 0.0201979$	4.92587/8 = 0.615734
10	$3.23067 \pm 0.58727$	$0.0763209 \pm 0.0247166$	3.37617/6 = 0.562696
11	$3.81594 \pm 0.784395$	$0.0585894 \pm 0.0293102$	2.10933/5 = 0.421866
12	$3.67631 \pm 1.00394$	$0.0625013 \pm 0.0341653$	2.05968/4 = 0.514919
13	$3.48695 \pm 1.30212$	$0.0673741 \pm 0.0402811$	2.00752/3 = 0.669175
14	$3.02071 \pm 1.7219$	$0.0784274 \pm 0.0483324$	1.83628/2 = 0.918141
15	$1.04558 \pm 2.34914$	$0.121791 \pm 0.0597233$	0.308538/1 = 0.308538

$r_0 = 3.5, r_1 =$	0.50		
$p_{T\mathrm{cut}}^{J/\psi}(\mathrm{GeV})$	$M_{0,r_0}^{J/\psi} (\times 10^{-2} \text{ GeV}^3)$	$M_{1,r_1}^{J/\psi} (\times 10^{-2} \text{ GeV}^3)$	$\chi^2/d.o.f$
5	$5.59062 \pm 0.28429$	$0.0996893 \pm 0.0226048$	23.7515/8 = 2.96894
6	$6.5255 \pm 0.387526$	$0.0557103 \pm 0.026131$	6.90798/6 = 1.15133
7	$7.42525 \pm 0.560786$	$0.0168421 \pm 0.0320113$	1.2102/4 = 0.30255
8	$7.60831 \pm 0.681376$	$0.0113182 \pm 0.0360441$	0.985812/3 = 0.328604
9	$7.56822 \pm 0.885713$	$0.0111586 \pm 0.0425265$	0.970201/2 = 0.4851
10	$6.8639 \pm 1.21425$	$0.0381292 \pm 0.0525473$	0.428409/1 = 0.428409

**Table 4.4** The values of  $M_{0,r_0}^{J/\psi}$  and  $M_{1,r_1}^{J/\psi}$  extracted from CDF data [19] with different  $p_{T\text{cut}}$ , where  $r_0 = 3.9, r_1 = -0.56$ 

where  $p_{T\text{cut}} = 11$  GeV. We will call this new set of CO LDMEs for  $\psi(2S)$  as "set II" in the remaining context. Finally, we point out that  $r_0 = 3.9$ ,  $r_1 = -0.56$  in the CDF fiducial region (i.e.,  $\sqrt{S} = 1.96$  TeV, |y| < 0.6).

In order to present our theoretical predictions for yields and polarizations in various rapidity intervals, we have to know the three CO LDMEs individually. The strategy we adopt here is based on the item 3 which was pointed out before; i.e., all CO LDMEs are positive. With the values of  $M_{0,r_0}^{J/\psi(\psi(2S))}$  and  $M_{1,r_1}^{J/\psi(\psi(2S))}$  extracted from the CDF data, we vary  $0 \leq \langle \mathcal{O}^{J/\psi(\psi(2S))}({}^{l}S_0^{[8]}) \rangle \leq M_{0,r_0}^{J/\psi(\psi(2S))}$  to determine the three CO LDMEs. The uncertainty from this variation and the errors in the  $M_{0,r_0}^{J/\psi(\psi(2S))}$ ,  $M_{1,r_1}^{J/\psi(\psi(2S))}$  and  $\langle \mathcal{O}^{\chi_{c0}}(\mathring{\mathfrak{F}}_1^{[8]}) \rangle$  values will be considered in the theoretical uncertainties (Table 4.4).

# 4.1.3 Yields and Polarizations: NRQCD Versus Experiments

After the long preparation, we want to discuss the phenomenology of prompt  $J/\psi$  and  $\psi(2S)$  production at the Tevatron and the LHC in this subsection. The NLO NRQCD results will be compared with the currently available experimental data.

### 4.1.3.1 Yields and Polarizations of $\psi(2S)$

First of all, we consider the relatively simple case, i.e., prompt  $\psi(2S)$  hadroproduction. Unlike prompt  $J/\psi$ , no significant feed-down contribution smears the prompt  $\psi(2S)$  production.

The  $\psi(2S)$  resonance can be reconstructed via  $\psi(2S) \to \mu^+\mu^-$  or  $\psi(2S) \to J/\psi(\to \mu^+\mu^-)\pi^+\pi^-$ . In the past few years, several experiments have released their results on the prompt  $\psi(2S)$  yield measurements [20–23]. One of the main uncertainties in their measurements comes from the unknown spin alignment of

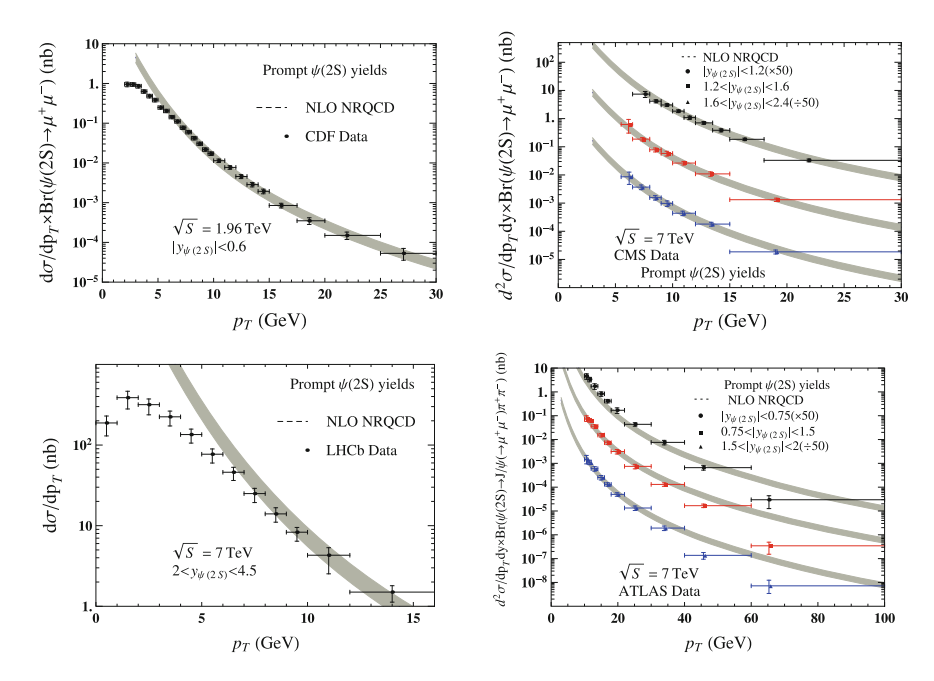


Fig. 4.1 Comparison of NLO NRQCD results (with the default set of CO LDMEs in Eq. (4.9)) and CDF [20],CMS [21], LHCb [22] and ATLAS [23] data for the yields of prompt  $\psi(2S)$  production

 $\psi(2S)$ .<sup>7</sup> Therefore, a good understanding of the polarization would, of course, improve the measurement.

First of all, let us compare our NLO NRQCD results of prompt  $\psi(2S)$  with the helicity-summed yield data. In Figs. 4.1 and 4.2, we compare our theoretical results with CDF [20], CMS [21], LHCb [22] and ATLAS [23] data by using two sets of CO LDMEs in Eqs. (4.9, 4.10). It is shown that NLO NRQCD results are in good agreement with the experimental data measured at the LHC and the Tevatron in the transverse momentum region from  $p_{T\text{cut}}$  to 40GeV. In the regime of  $p_T < p_{T\text{cut}}$ , the experimental data hint that NRQCD factorization is violated. From the preliminary ATLAS data [23], we see that our NRQCD prediction overshots the data in the last two bins, where  $p_T$  is larger than 40 GeV. However, for such a large  $p_T$ , the perturbative computation is not reliable due to the presence of large logarithms like  $\log \frac{p_T^2}{(2m_c)^2}$ . Hence, resummation of such logarithms is necessary to understand the data in this regime in the NRQCD framework [9]. One thing we want to point out is that the experimental data in the central rapidity interval are larger than those in forward rapidity interval and it is consistent with our assumption of the positive CO LDME  $\langle \mathcal{O}^{\psi(2S)}({}^2P_0^{(8)})\rangle$  illustrated in Sect. 4.1.2.

<sup>&</sup>lt;sup>7</sup>It will impact the determination of the detecting efficiency estimation.

<sup>&</sup>lt;sup>8</sup>Note that, we use  $p_{T\text{cut}} = 7 \text{ GeV}$  in the default set (Eq. (4.9) and Fig. 4.1) and  $p_{T\text{cut}} = 11 \text{ GeV}$  in the set II (Eq. (4.10) and Fig. 4.2).

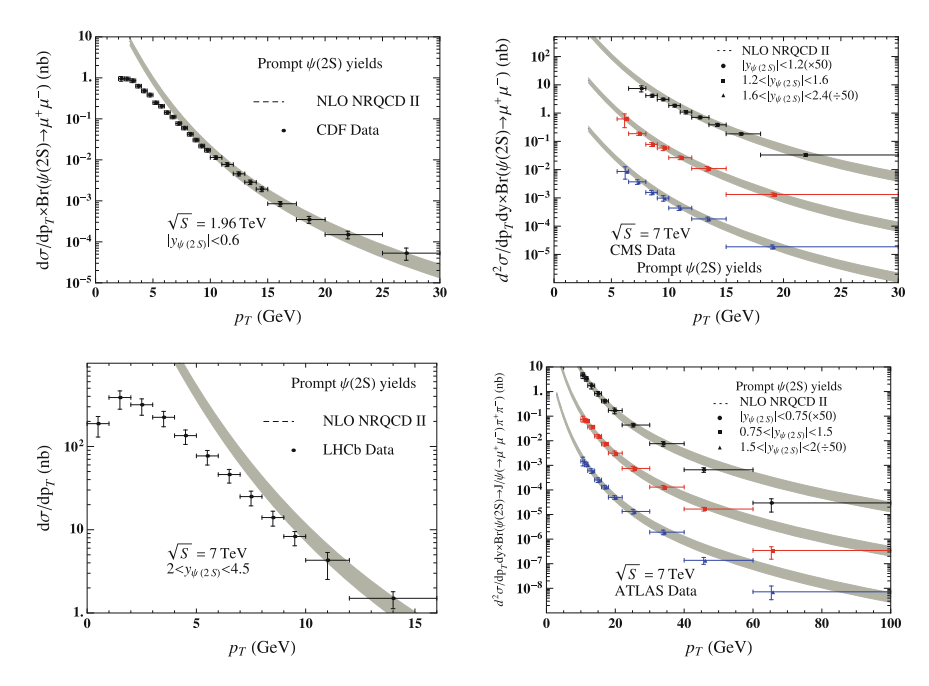
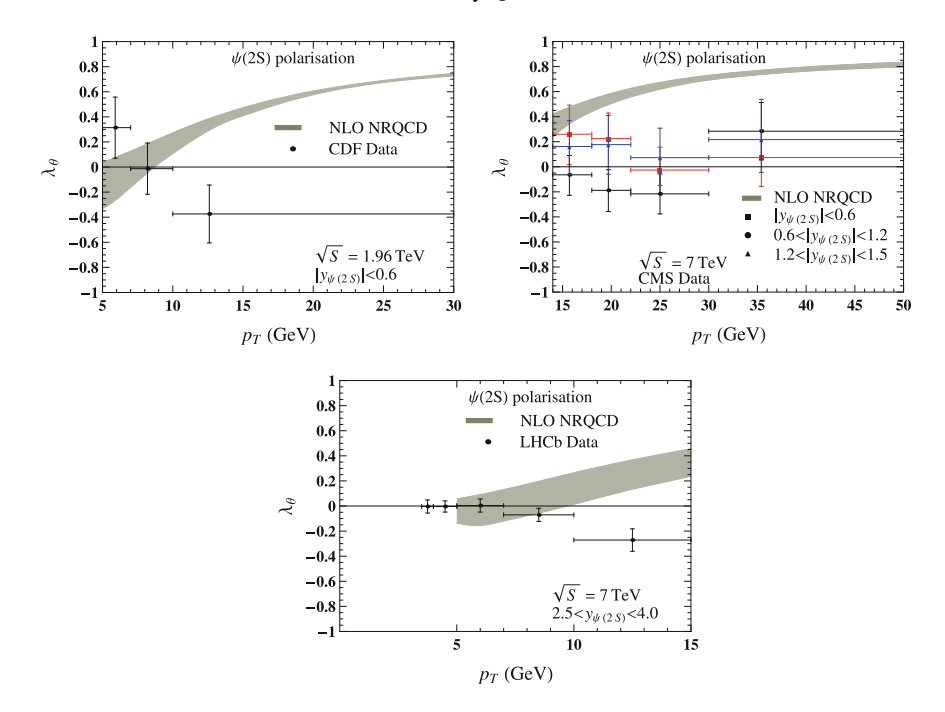


Fig. 4.2 Comparison of NLO NRQCD results (with the set II of CO LDMEs in Eq. (4.10)) and CDF [20], CMS [21], LHCb [22] and ATLAS [23] data for the yields of prompt  $\psi(2S)$  production

Now, we go to study the polarization observable  $\lambda_{\theta}$  for prompt  $\psi(2S)$  production. We have established our NLO NRQCD results in companion with CDF [24], CMS [25] and LHCb [26] data in Figs. 4.3 and 4.4. In Fig. 4.3, we use the default set of CO LDMEs (see Eq. (4.9)), whereas in Fig. 4.3 we use the set II (see Eq. (4.10)). Apparently, the polarization  $\lambda_{\theta}$  is sensitive to  $p_{T\text{cut}}$ . With  $p_{T\text{cut}} = 7\text{GeV}$ , the NLO NRQCD polarization prediction is far from the unpolarized data because of a large  $M_{1,r_1}^{\psi(2S)}$ . In contrast, the NLO NRQCD result is compatible with the LHC experiments when using the set II of CO LDMEs with  $p_{T\text{cut}} = 11$  GeV, which is shown in Fig. 4.4. NRQCD is difficult to explain the Tevatron polarization data in both sets of CO LDMEs at NLO level. However, we want to remind readers that there is a little bit inconsistence between the CDF [24] data and the CMS [25] data, though the uncertainties are still large. It may be attributed to the fact that the measurement at the Tevatron [10] is incomplete.

## 4.1.3.2 Yields and Polarizations of Prompt $J/\psi$

The prompt  $J/\psi$  production at hadron colliders is much involved. It receives contributions from  $\chi_{cJ}$  (J = 0, 1, 2) and  $\psi$  (2S) decays, which makes the physical analysis more complicated than that in the case of prompt  $\psi$  (2S) production.



**Fig. 4.3** Comparison of NLO NRQCD results (with the default set Eq. (4.9) of CO LDMEs) and CDF [24], CMS [25] and LHCb [26] data for prompt  $\psi(2S)$  polarization  $\lambda_{\theta}$  in the helicity frame

Experimentalists usually reconstruct the  $J/\psi$  resonance in the decay channel  $J/\psi \to \ell^+\ell^-$ , where  $\ell^\pm = e^\pm$  or  $\mu^\pm$ . The branching ratio is  $\sim\!\!6\%$ . This decay channel has the virtue that it is almost free of background. The polarization of  $J/\psi$  can be determined from its di-lepton angular distribution.

Due to the complication in the NLO computation, the feed-down contributions missed in our previous study [6]. We pointed out in Ref. [6] that the unpolarized result can be guaranteed when the cancellation of  ${}^{3}C_{1}^{[8]}$  and  ${}^{3}C_{1}^{[8]}$  happens or equivalently a sufficiently small  $M_{1,r_{1}}^{J/\psi}$  is obtained. In a later publication [8], we estimated the impact of feed-down contribution from  $\chi_{cJ}$  decay to  $J/\psi$  polarization. With the help of Eq. (C4) in Ref. [8], we know that the feed-down contribution from  $\chi_{c1}$  decay to  $J/\psi$  polarization is in the interval  $[-\frac{1}{3},1]$ , whereas that from  $\chi_{c2}$  decay is in the interval  $[-\frac{3}{5},1]$ . This argument is regardless of the production mechanism of  $\chi_{c}$ . We estimated that the smearing effect from  $\chi_{c}$  feed-down did not alter our conclusion based on our direct  $J/\psi$  polarization.

In this subsection, we are intending to present a rigorous computation for prompt  $J/\psi$  yields and polarizations after including the feed-down contribution from  $\chi_{cJ}$  and  $\psi(2S)$  decay. As we have discussed in Sect. 4.1.2, the LDMEs of  $M_{0,r_0}^{J/\psi}$  and

<sup>&</sup>lt;sup>9</sup>The  $J/\psi$  polarization  $\lambda_{\theta}$  from the scalar  $\chi_{c0}$  is always zero.

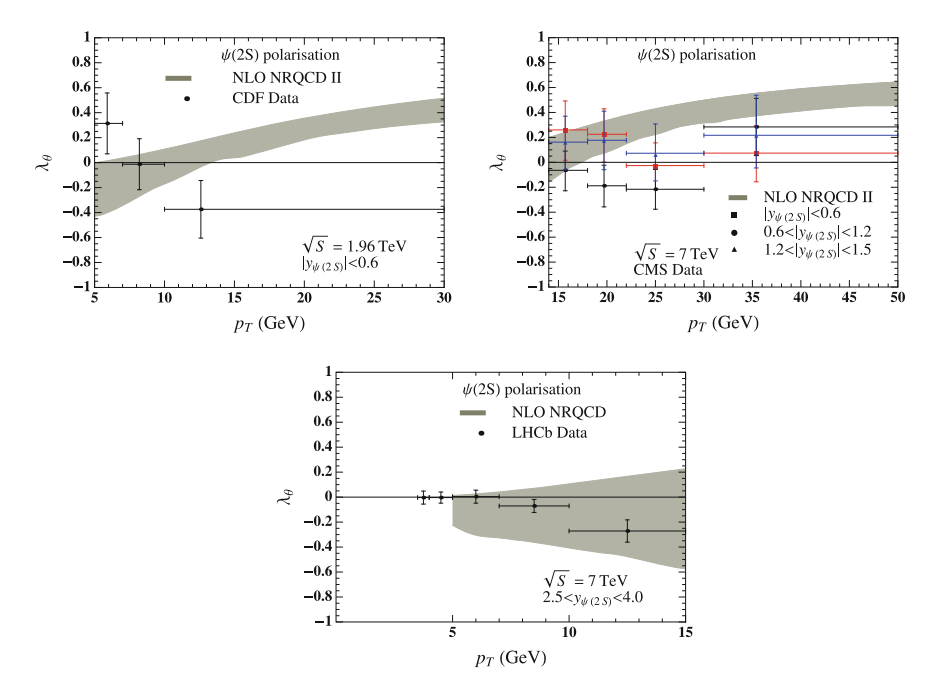


Fig. 4.4 Comparison of NLO NRQCD results (with the set II Eq. (4.10) of CO LDMEs) and CDF [24], CMS [25] and LHCb [26] data for prompt  $\psi(2S)$  polarization  $\lambda_{\theta}$  in the helicity frame

 $M_{1,r_1}^{J/\psi}$  are not sensitive to the  $p_{T{\rm cut}}$  when  $p_{T{\rm cut}}>7$  GeV. We only use the values of  $M_{0,r_0}^{J/\psi}$  and  $M_{1,r_1}^{J/\psi}$  in Eq. (4.8).

We show our NLO NRQCD results for prompt  $J/\psi$  yields in Fig. 4.5. Our results are compared with CDF [19], ATLAS [27], CMS [21] and LHCb [28] measurements. Satisfactory agreement is gained in the whole  $p_T$  regime and various rapidity intervals. As we have mentioned before, the feed-down contribution from  $\psi(2S)$  is limited. Hence, we do not establish the results by using CO LDMEs for  $\psi(2S)$  in Eq. (4.10) here. We have checked numerically that the yields and polarizations of prompt  $J/\psi$  only change slightly by using different CO LDMEs of  $\psi(2S)$ . In order to understand the fraction of feed-down contribution from  $\chi_c$  decay in prompt  $J/\psi$ , we show the NLO NRQCD results of  $\sigma(\chi_c \to J/\psi \gamma)/\sigma(J/\psi)$  in Fig. 4.6 in the LHCb fiducial region. The curve implies that the transverse momentum spectrum of prompt  $\chi_c$  is harder than that of direct  $J/\psi$ , because  $\chi_c$  is dominated by  ${}^3\Sigma_1^{[8]}$ . Moreover, we also plot the ratio R of prompt  $\psi(2S)$  yields and prompt  $J/\psi$  yields in Fig. 4.7, which is defined in Refs. [21, 22] as

$$R \equiv \frac{\sigma(\psi(2S) \to \mu^+ \mu^-)}{\sigma(J/\psi \to \mu^+ \mu^-)}.$$
 (4.11)

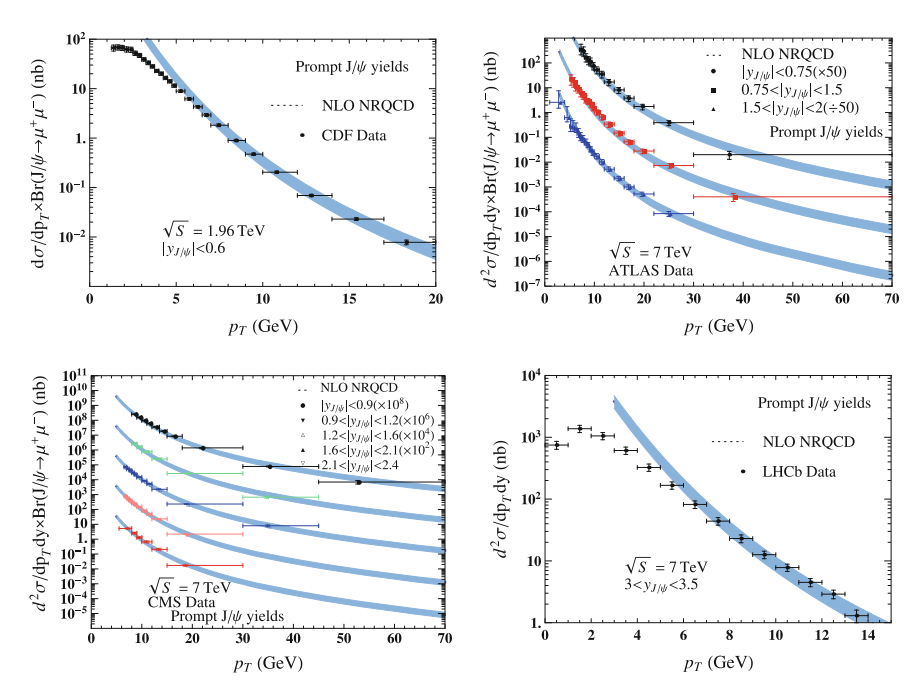


Fig. 4.5 Comparison of NLO NRQCD results and CDF [19], ATLAS [27], CMS [21] and LHCb [28] data for the yields of prompt  $J/\psi$  production

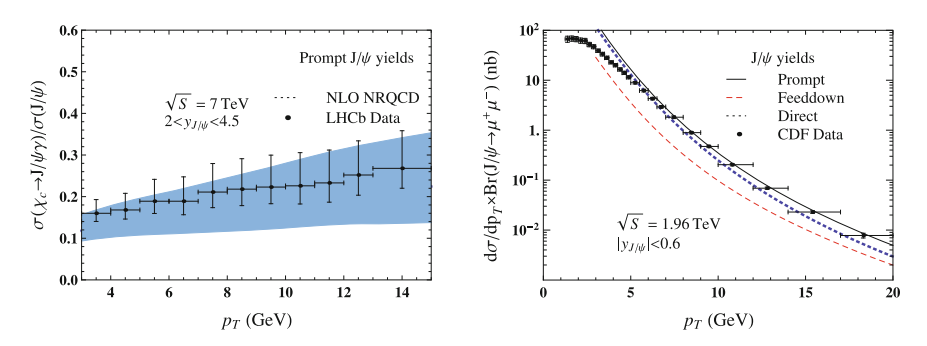


Fig. 4.6 Comparison of NLO NRQCD results and LHCb [29] and CDF [19] data for the yields of  $J/\psi$  production

This observable represents the  $p_T$  spectrum of the feed-down contribution from  $\psi(2S)$  in prompt  $J/\psi$  yields. With the default set of CO LDMEs for  $\psi(2S)$  in Eq. (4.9), the ratio R increases as  $p_T$  is larger. In contrast, with the set II of CO LDMEs for  $\psi(2S)$  in Eq. (4.10), the ratio R is flat in  $p_T$  spectrum. In Fig. 4.6, we divide the prompt  $J/\psi$  yields into the direct  $J/\psi$  yields and the feed-down part from excited charmonia decay. It shows that the  $p_T$  spectrum of the feed-down part is indeed harder than that of the direct one.

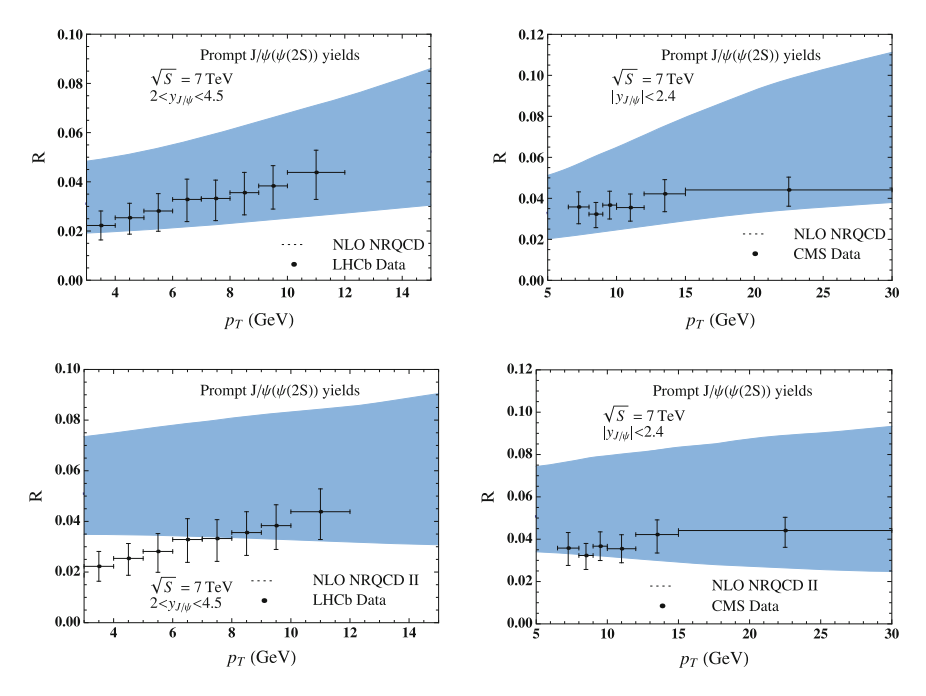


Fig. 4.7 Comparison of NLO NRQCD results and LHCb [22] and CMS [21] data for R. We use the default set of CO LDMEs for  $\psi(2S)$  in the upper two panels, while the lower two panels are obtained by using the set II of CO LDMEs for  $\psi(2S)$ 

The polarization observable  $\lambda_{\theta}$  of  $J/\psi$  in its prompt production is expected to be close to 0 because of the values of  $M_{0,r_0}^{J/\psi}$  and  $M_{1,r_1}^{J/\psi}$  in Eq. (4.8). The comparison of the theoretical results with the measurements by various experiments (i.e., CDF [24], CMS [25], LHCb [30] and ALICE [31]) is done in Fig. 4.8.  $\lambda_{\theta}$  in different rapidity bins are close to 0, which is consistent with our previous claim [6, 32]. Similar to the case of  $\psi(2S)$  in Fig. 4.4, our NLO NRQCD results are consistent with the measurements [25, 30, 31] performed at the LHC, while the NLO NRQCD result is not consistent with the CDF data [24].

Our positive LDMEs assumption is justified by the LHC experiments. From Fig. 4.8, it is easy to observe that the LHCb data are a bit lower than the CMS data. In our definite-positive assumption, the  $\lambda_{\theta}$  will be smaller in the forward rapidity bin than that in the central rapidity bin. It can be attributed to the fact that the  $M_{1,r_1}^{J/\psi}$  is smaller when the rapidity y becomes larger. In contrast, negative values of  $\langle \mathcal{O}^{J/\psi}({}^3\!P_0^{[8]}) \rangle$  are extracted by other two groups [5, 7]. Hence, they will give larger values of  $\lambda_{\theta}$  in the forward rapidity bin, which apparently is in conflict with the LHC data.

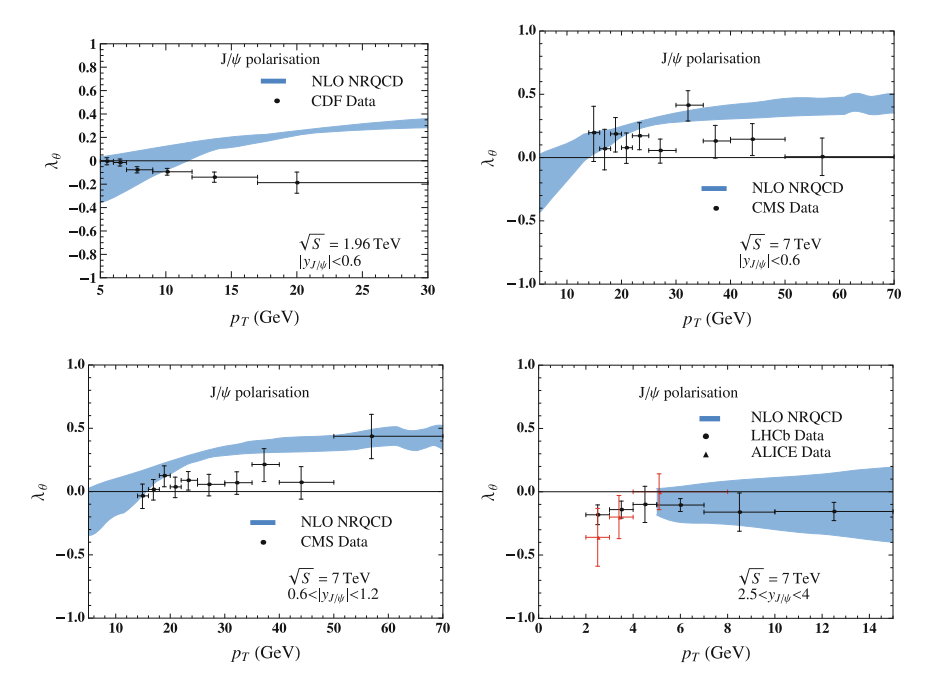
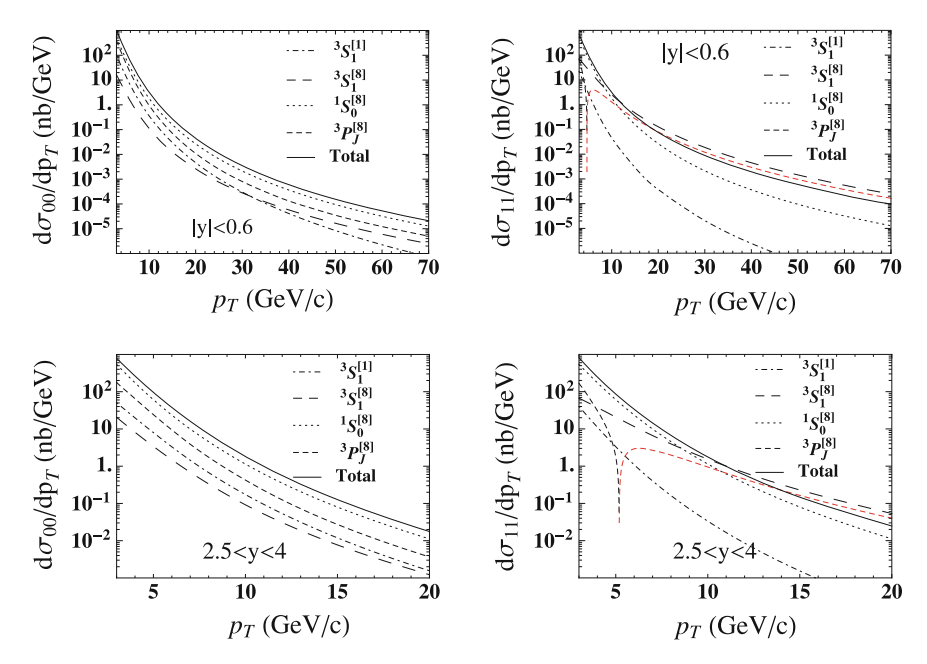


Fig. 4.8 Comparison of NLO NRQCD results and CDF [24], CMS [25], LHCb [30], and ALICE [31] data for prompt  $J/\psi$  polarization  $\lambda_{\theta}$  in helicity frame. The ALICE [31] data are for the inclusive  $J/\psi$ 

# 4.1.4 Spin Density Matrix Elements

Finally, we establish here the SDMEs of  $\psi(2S)$  in various Fock states. In Fig. 4.9, we present the results in the central rapidity |y| < 0.6 and forward rapidity 2.5 < y < 4.0 at the LHC with  $\sqrt{S} = 7$  TeV. We take a special set of LDMEs  $\langle \mathcal{O}^{\psi(2S)}({}^{S}_1^{[1]}) \rangle = 0.76 \, \text{GeV}^3, \langle \mathcal{O}^{\psi(2S)}({}^{S}_0^{[8]}) \rangle = 2.82 \times 10^{-2} \, \text{GeV}^3, \langle \mathcal{O}^{\psi(2S)}({}^{S}_1^{[8]}) \rangle = 0.20259 \times 10^{-2} \, \text{GeV}^3, \langle \mathcal{O}^{\psi(2S)}({}^{3}_0^{[8]}) \rangle / m_c^2 = 0.25641 \times 10^{-2} \, \text{GeV}^3$ . The perturbative SDCs can be easily read from the curves, where we marked the negative values red. We leave it for whom interested in it and wanted to use their own CO LDMEs in the future.



**Fig. 4.9**  $d\sigma_{00}/dp_T$  and  $d\sigma_{11}/dp_T$  for  $pp \to \psi(2S) + X$  with  $\sqrt{S} = 7$  TeV and |y| < 0.6 (upper panels), 2.5 < y < 4.0 (lower panels) in the helicity frame at NLO in NRQCD. Negative values are marked red. We take one special set of LDMEs here, i.e.,  $\langle \mathcal{O}^{\psi(2S)}(\mathring{S}_1^{[1]}) \rangle = 0.76 \text{ GeV}^3$ ,  $\langle \mathcal{O}^{\psi(2S)}(\mathring{S}_0^{[8]}) \rangle = 2.82 \times 10^{-2} \text{ GeV}^3$ ,  $\langle \mathcal{O}^{\psi(2S)}(\mathring{S}_1^{[8]}) \rangle = 0.20259 \times 10^{-2} \text{ GeV}^3$ ,  $\langle \mathcal{O}^{\psi(2S)}(\mathring{S}_0^{[8]}) \rangle / m_c^2 = 0.25641 \times 10^{-2} \text{ GeV}^3$ 

# 4.2 Yields and Polarizations of Prompt $\chi_{c1}$ and $\chi_{c2}$ Production

## 4.2.1 Motivation and Formulas

The prompt  $J/\psi$  production at the Tevatron and the LHC is usually affected substantially by higher-excited charmonia  $\chi_{cJ}$  and  $\psi(2S)$  transition to  $J/\psi$ . Hence, the determination of the yields and polarizations of  $\chi_{cJ}$  is very important. For the  $\psi$  system, there are at least three CO LDMEs that should be extracted from experimental data. It makes the unique determination of them individually difficult. On the other hand, there is only one independent CO LDME  $\langle \mathcal{O}^{\chi_{c0}}(\mathring{S}_1^{[8]}) \rangle$  in  $\chi_c$ , because others can be fixed by using the spin symmetry relation  $\langle \mathcal{O}^{\chi_{c0}}(\mathring{S}_1^{[8]}) \rangle = (2J+1)\langle \mathcal{O}^{\chi_{c0}}(\mathring{S}_1^{[8]}) \rangle$ . The spin symmetry violation effect is a pure higher-order  $v^2$  correction. Therefore, it would make the theoretical prediction of  $\chi_{cJ}$  easier than  $\psi$  (at least at the level of less input experimental data are necessary). Theoretically, the higher-order QCD correction to the P-wave CS Fock states  ${}^3P_J^{[1]}$  suffers from IR divergences. In the framework of NRQCD factorization, these IR divergences would be naturally absorbed into the

renormalization of the non-perturbative CO LDMEs  $\langle \mathcal{O}^{\chi_{cJ}}({}^3\!\!\!\!S_1^{[8]})\rangle$ . From this point of view, CSM is not enough to describe the production mechanism of  $\chi_{cJ}$ . Upon these reasons, we think it is very crucial (and even provides a unique opportunity) to test the validity of NRQCD factorization and to probe the CO mechanism by investigating the  $\chi_{cJ}$  production process at the LHC.

The aim of this section was to study both yields and polarizations of prompt  $\chi_{c1}$  and  $\chi_{c2}$  production at NLO level in QCD. It is an extensive investigation of the work present in Ref. [4]. The main results we presented here are already published in Ref. [14].

Similar to the  $\psi$  meson, the measurements of the polarization observables of  $\chi_{c1}$  and  $\chi_{c2}$  should provide us more important and complete information for their production mechanism. Therefore, several authors [8, 33, 34], including us, have proposed various polarization observables for  $\chi_{c1}$  and  $\chi_{c2}$ . Experimentally,  $\chi_{cJ}$  is usually reconstructed via the cascade decay chain  $\chi_{cJ} \to (J/\psi \to \mu^+\mu^-)\gamma$ . People have opportunities to measure the polarizations of  $\chi_{c1}$  and  $\chi_{c2}$  either through the angular distribution of  $J/\psi$  (or  $\gamma$ ) or through that of  $\mu^{\pm}$ .

The angular distribution with respect to the polar angle  $\theta$  of  $J/\psi$  in the rest frame of  $\chi_{cJ}$  can be formulated as [8]

$$\frac{\mathrm{d}\mathcal{N}^{\chi_{cJ}}}{\mathrm{d}\cos\theta} \propto 1 + \sum_{k=1}^{J} \lambda_{k\theta} \cos^{2k}\theta, \tag{4.12}$$

where the polar asymmetry coefficients  $\lambda_{k\theta}$  can be expressed as the rational function of the SDMEs  $d\sigma_{ii}^{\chi_{cJ}}$  of  $\chi_{cJ}$  production. In specific, we have

$$\lambda_{\theta} = (1 - 3\delta) \frac{N_{\chi_{c1}} - 3d\sigma_{00}^{\chi_{c1}}}{(1 + \delta)N_{\chi_{c1}} + (1 - 3\delta)d\sigma_{00}^{\chi_{c1}}},\tag{4.13}$$

for  $\chi_{c1}$ , where  $N_{\chi_{c1}} \equiv d\sigma_{11}^{\chi_{c1}} + d\sigma_{00}^{\chi_{c1}} + d\sigma_{-1-1}^{\chi_{c1}}$  and

$$\lambda_{\theta} = 6[(1 - 3\delta_{0} - \delta_{1})N_{\chi_{c2}} - (1 - 7\delta_{0} + \delta_{1})(d\sigma_{11}^{\chi_{c2}} + d\sigma_{-1-1}^{\chi_{c2}}) - (3 - \delta_{0} - 7\delta_{1})d\sigma_{00}^{\chi_{c2}}]/R,$$

$$\lambda_{2\theta} = (1 + 5\delta_{0} - 5\delta_{1})[N_{\chi_{c2}} - 5(d\sigma_{11}^{\chi_{c2}} + d\sigma_{-1-1}^{\chi_{c2}}) + 5d\sigma_{00}^{\chi_{c2}}]/R,$$

$$(4.14)$$

with

$$\begin{split} N_{\chi_{c2}} &\equiv d\sigma_{22}^{\chi_{c2}} + d\sigma_{11}^{\chi_{c2}} + d\sigma_{00}^{\chi_{c2}} + d\sigma_{-1-1}^{\chi_{c2}} + d\sigma_{-2-2}^{\chi_{c2}}, \\ R &\equiv (1 + 5\delta_0 + 3\delta_1)N_{\chi_{c2}} \\ &+ 3(1 - 3\delta_0 - \delta_1)(d\sigma_{11}^{\chi_{c2}} + d\sigma_{-1-1}^{\chi_{c2}}) \\ &+ (5 - 7\delta_0 - 9\delta_1)d\sigma_{00}^{\chi_{c2}}. \end{split} \tag{4.15}$$

The parameters  $\delta$ ,  $\delta_0$ , and  $\delta_1$  in Eqs. (4.13) and (4.14) are determined from the normalized multipole amplitudes. We denote the normalized electric dipole (E1) transition amplitude and magnetic quadrupole (M2) amplitude as  $a_1^{J=1}$ ,  $a_2^{J=1}$  for  $\chi_{c1}$ , whereas the normalized E1 amplitude, M2 amplitude, and electric octupole (E3) amplitude are denoted as  $a_1^{J=2}$ ,  $a_2^{J=2}$ ,  $a_3^{J=2}$ . Because these amplitudes are normalized, we have the following identities:

$$(a_1^{J=1})^2 + (a_2^{J=1})^2 = 1$$
  

$$(a_1^{J=2})^2 + (a_2^{J=2})^2 + (a_3^{J=2})^2 = 1.$$
 (4.16)

The explicit expressions for  $\delta$ ,  $\delta_0$ ,  $\delta_1$  in terms of these multipole amplitudes are

$$\delta \equiv (1 + 2a_1^{J=1}a_2^{J=1})/2,$$

$$\delta_0 \equiv [1 + 2a_1^{J=2}(\sqrt{5}a_2^{J=2} + 2a_3^{J=2}) + 4a_2^{J=2}(a_2^{J=2} + \sqrt{5}a_3^{J=2}) + 3(a_3^{J=2})^2]/10,$$

$$\delta_1 \equiv [9 + 6a_1^{J=2}(\sqrt{5}a_2^{J=2} - 4a_3^{J=2}) - 4a_2^{J=2}(a_2^{J=2} + 2\sqrt{5}a_3^{J=2}) + 7(a_3^{J=2})^2]/30.$$
(4.17)

An alternative way to study the polarizations of  $\chi_{cJ}$ , J=1,2 is to study the di-lepton angular distributions. Two choices are discussed in Refs. [8, 34] for dilepton angular distributions. As discussed in Ref. [8], we only choose the one in which the z-axis in the rest frame of  $J/\psi$  coincides with the direction of the spin quantization axis in the  $\chi_c$  rest frame. Thus, we will have a general lepton polar angle  $\theta'$  dependence

$$\frac{\mathrm{d}\mathscr{N}^{\chi_{G}}}{\mathrm{d}\cos\theta'} \propto 1 + \lambda_{\theta'}\cos^{2}\theta',\tag{4.18}$$

where

$$\lambda_{\theta'}^{\chi_{c1}} = \frac{-N_{\chi_{c1}} + 3d\sigma_{00}^{\chi_{c1}}}{R_1},$$

$$\lambda_{\theta'}^{\chi_{c2}} = \frac{6N_{\chi_{c2}} - 9(3\sigma_{11}^{\chi_{c2}} + d\sigma_{-1-1}^{\chi_{c2}}) - 12d\sigma_{00}^{\chi_{c2}}}{R_2},$$
(4.19)

and

$$\begin{split} R_1 &\equiv [(15 - 2(a_2^{J=1})^2)N_{\chi_{c1}} \\ &- (5 - 6(a_2^{J=1})^2)d\sigma_{00}^{\chi_{c1}}]/(5 - 6(a_2^{J=1})^2), \\ R_2 &\equiv [2(21 + 14(a_2^{J=2})^2 + 5(a_3^{J=2})^2)N_{\chi_{c2}} \\ &+ 3(7 - 14(a_2^{J=2})^2 - 5(a_3^{J=2})^2)(d\sigma_{11}^{\chi_{c2}} + d\sigma_{-1-1}^{\chi_{c2}}) \\ &+ 4(7 - 14(a_2^{J=2})^2 - 5(a_3^{J=2})^2)d\sigma_{00}^{\chi_{c2}}] \\ &/ [7 - 14(a_2^{J=2})^2 - 5(a_3^{J=2})^2]. \end{split}$$
(4.20)

Given that the higher-order multipole amplitudes are  $v^2$  suppressed, there are the hierarchy relations  $a_2^{J=1} \ll a_1^{J=1}$  and  $a_3^{J=2} \ll a_2^{J=2} \ll a_1^{J=2}$  in the limitation of  $v^2 \ll 1$ . One observes that the angular distribution  $\frac{d_{\infty} \chi_{cJ}}{d\cos\theta}$  is  $a_2^J$  dependent, while the angular distribution  $\frac{d_{\infty} \chi_{cJ}}{d\cos\theta}$  is  $(a_2^J)^2$  dependent. It guarantees that  $\frac{d_{\infty} \chi_{cJ}}{d\cos\theta}$  should be affected little by nonzero higher-order multipole transition contributions, while the nonzero M2 and E3 transition probability would be important in the determination of  $\frac{d_{\infty} \chi_{cJ}}{d\cos\theta}$ . Therefore, the later ones are good observables to extract or to check the values of these higher-order multipole amplitudes at the LHC. The current measurements of these values from various experiments are still in contradiction with each other. We use the newest measurement by CLEO collaboration [35]. They are  $a_2^{J=1} = (-6.26 \pm 0.68) \times 10^{-2}$ ,  $a_2^{J=2} = (-9.3 \pm 1.6) \times 10^{-2}$ ,  $a_3^{J=2} = 0$ . From the single-quark radiation hypothesis [36, 37], the E3 amplitude  $a_3^{J=2}$  is kept to be zero. From Eq. (4.14),  $\lambda_{2\theta}$  for  $\chi_{c2}$  is suppressed by  $a_2^{J=2}$ ,  $a_3^{J=2}$ . Hence, we expect these values are close to zero. In this section, we will refrain ourselves from establishing such a observable.

### 4.2.2 LDMEs

In the numerical computation, same input parameters are chosen as presented in Sect. 4.1.1. In particular, we determine the CO LDMEs by fitting the Tevatron data [4], i.e.,  $\langle \mathcal{O}^{\chi_{cJ}}(\mathring{S}_1^{[8]}) \rangle = (2J+1) \times (2.2^{+0.48}_{-0.32}) \times 10^{-3} \text{ GeV}^3$ . The CS LDMEs are estimated from potential model [15] as  $\langle \mathcal{O}({}^3\!P_J^{[1]}) \rangle = (2J+1) \frac{3|R'(0)|^2}{4\pi}$  with  $|R'(0)|^2 = 0.075 \text{GeV}^5$ . Here, we are trying to see whether the new LHC data are able to improve the NRQCD predictions. It would be convenient to define a dimensionless quantity r [4] as follows:

$$r \equiv \frac{\langle \mathcal{O}^{\chi_{c0}}({}^3\!S_1^{[8]})\rangle}{\langle \mathcal{O}^{\chi_{c0}}({}^3\!P_0^{[1]})\rangle/m_c^2}.$$
(4.21)

In Ref. [4], its value was determined as  $r=0.27\pm0.6$ . The theoretical uncertainties including scale dependence and charm quark mass dependence are all embodied in the uncertainty of the r value. Its central value and  $\chi^2/d.o.f$  are shown in Table 4.5. We only apply  $p_T$  cutoff of the  $J/\psi$  in  $\chi_{cJ} \rightarrow J/\psi + \gamma$  4 GeV to the Tevatron data [17]. We cannot enlarge the  $p_T$  cutoff at the Tevatron because the released data lack high- $p_T$  data. The CDF measurement [17] was performed under the unpolarized hypothesis. With the LHCb data [38] only, <sup>10</sup> we present the fitted r values with various  $p_{T\text{cut}}^{J/\psi}$  in Table 4.6. Its value varies from 0.33 to 0.30 when  $p_{T\text{cut}}^{J/\psi} \geq 8$  GeV. Moreover, CMS collaboration have performed a more careful analysis on the measurement of  $\sigma(\chi_{c2})/\sigma(\chi_{c1})$  [39]. They have seriously considered the uncertainties from different polarization hypothesis. In Tables 4.7 and 4.8, we present the extracted r values with

<sup>&</sup>lt;sup>10</sup>Note that, LHCb data [38] are also measured under unpolarized hypothesis.

**Table 4.5** r value extracted from CDF data [17]

$p_{T\mathrm{cut}}^{J/\psi}(\mathrm{GeV})$	r	$\chi^2/d.o.f$
4	0.267115	10.6769/2 = 5.33846

**Table 4.6** r value extracted from LHCb data [38]

$p_{T\mathrm{cut}}^{J/\psi}(\mathrm{GeV})$	r	$\chi^2/d.o.f$
4	0.446941	9.4456/8 = 1.1807
5	0.398909	6.67584/7 = 0.953692
6	0.371	4.54149/6 = 0.756916
7	0.350187	2.74159/5 = 0.548319
8	0.333301	1.22078/4 = 0.305195
9	0.323163	0.86712/3 = 0.28904
10	0.320056	0.84792/2 = 0.402396
11	0.306659	0.460704/1 = 0.460704

**Table 4.7** r value extracted from CMS data [39] after including the uncertainties from polarization hypothesis

$p_{T\mathrm{cut}}^{J/\psi}(\mathrm{GeV})$	r	$\chi^2/d.o.f$
7	0.247441	1.00808/4 = 0.252021
9	0.245041	0.710214/3 = 0.236738
11	0.24205	0.468795/2 = 0.234797
13	0.238609	0.21089/1 = 0.271089

the data under unpolarized hypothesis. In the former table, we take into account the uncertainty from unknown  $\chi_c$  polarization in the  $\chi^2$  fit, whereas we do not include such a polarization uncertainty in the latter table. From these two tables, we understand that the central value of r is almost independent of  $p_{T\text{cut}}^{J/\psi}$  and it is close to  $\sim 0.25$ . The largest uncertainty in determining r comes from the various polarization hypotheses. From Tables 4.9 and 4.10, it is observed that the different polarization hypotheses change the value of r from 0.21 to 0.32. All the results in these tables show that the r value is well embodied in the original uncertainty  $0.27 \pm 0.06$ . This conclusion can also be easily justified from the plots of  $\sigma(\chi_{c2})/\sigma(\chi_{c1})$  in Fig. 4.10, where the NRQCD results use the LDMEs presented at the beginning of this section.

#### 4.2.3 Numerical Results

In this section, we present our main numerical results for the yields and polarizations of  $\chi_{c1}$  and  $\chi_{c2}$ .

CSIS		
$p_{T\mathrm{cut}}^{J/\psi}(\mathrm{GeV})$	r	$\chi^2/d.o.f$
7	0.253408	13.1953/4 = 3.29884
9	0.251778	10.8483/3 = 3.61611
11	0.248219	7.85111/2 = 3.92855
13	0.243029	5.06465/1 = 5.06465

**Table 4.8** r value extracted from CMS data [39] without the uncertainties from polarization hypothesis

**Table 4.9** r value extracted from CMS data [39] with the extreme polarization hypothesis  $(m_{\chi_{c1}}, m_{\chi_{c2}}) = (0, 0)$ 

$p_{T\mathrm{cut}}^{J/\psi}(\mathrm{GeV})$	r	$\chi^2/d.o.f$
7	0.214647	1.31167/4 = 0.327918
9	0.214636	1.31116/3 = 0.437052
11	0.214362	1.24125/2 = 0.62062
13	0.213629	1.05769/1 = 1.05769

**Table 4.10** r value extracted from CMS data [39] with the extreme polarization hypothesis  $(m_{X,1}, m_{X,2}) = (\pm 1, \pm 2)$ 

$(\cdots \lambda_{c1}, \cdots \lambda_{c2})$ $(,)$		
$p_{T\mathrm{cut}}^{J/\psi}(\mathrm{GeV})$	r	$\chi^2/d.o.f$
7	0.324315	25.6817/4 = 6.42042
9	0.318204	20.4471/3 = 6.81572
11	0.307108	14.7442/2 = 7.37211
13	0.292948	9.85555/1 = 9.85555

First, we just focus on the yields, i.e., helicity-summed results. Figure 4.10 shows the cross-sectional ratios  $\sigma(\chi_{c2})/\sigma(\chi_{c1})$  at the Tevatron Run II and the LHC Run I. In order to make a rich comparison, besides the NLO NRQCD results, we also plot the LO NRQCD results and the CSM results in the figure. In contrast to the LO NRQCD results and the CSM results, the NLO NRQCD results are consistent with the CDF data [17] and CMS data [39] in the whole  $p_T^{J/\psi}$  region. In the forward rapidity, the NLO NRQCD result agrees with LHCb data [38] when  $p_T^{J/\psi} \geq 8$ GeV. This is fine because NRQCD factorization may be not valid when  $p_T$  is not large enough, which was already pointed out in the  $\psi$  case. It is shown in Fig. 4.10 that the LO CSM and LO NRQCD results are conflict with the experiments. We present the NLO NRQCD predictions for the yields of  $\chi_{c1}$  and  $\chi_{c2}$  at the LHC in the central (|y| < 2.4) and forward (2 < y < 4.5) rapidity intervals in Fig. 4.11, which can be tested in the future by the experiments.

In Fig. 4.12, we present the curves of the SDMEs  $d\sigma_{00}/dp_T$ ,  $d\sigma_{11}/dp_T$  (and  $d\sigma_{22}/dp_T$ ) of  $\chi_{c1}(\chi_{c2})$  at  $\sqrt{S}=7$  TeV and |y|<2.4,2< y<4.5. With the chosen LDMEs, we also display the curves in different Fock states. These results are valuable

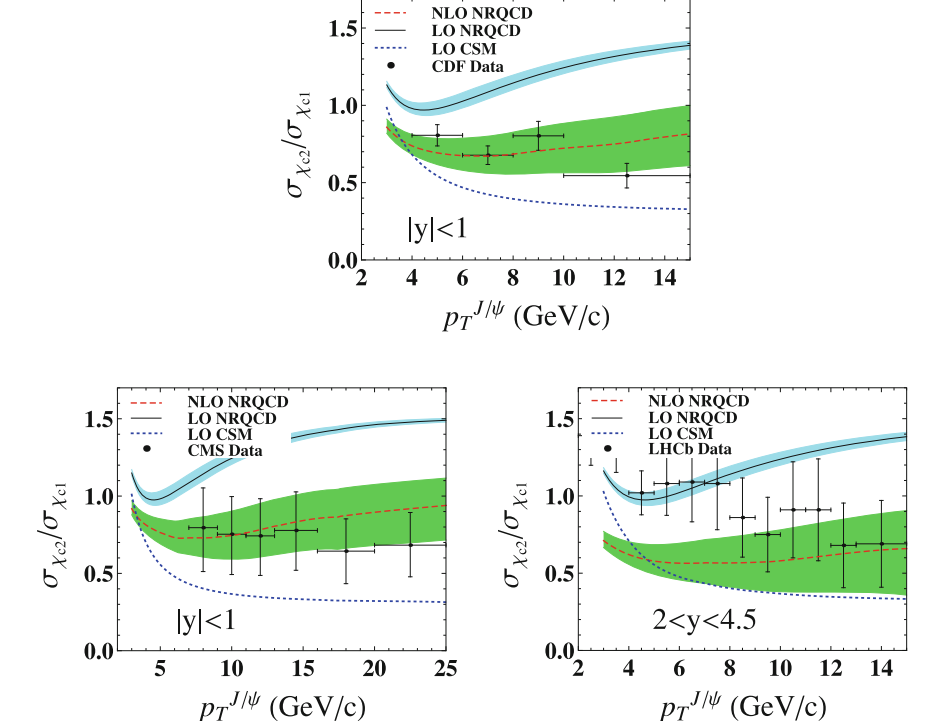
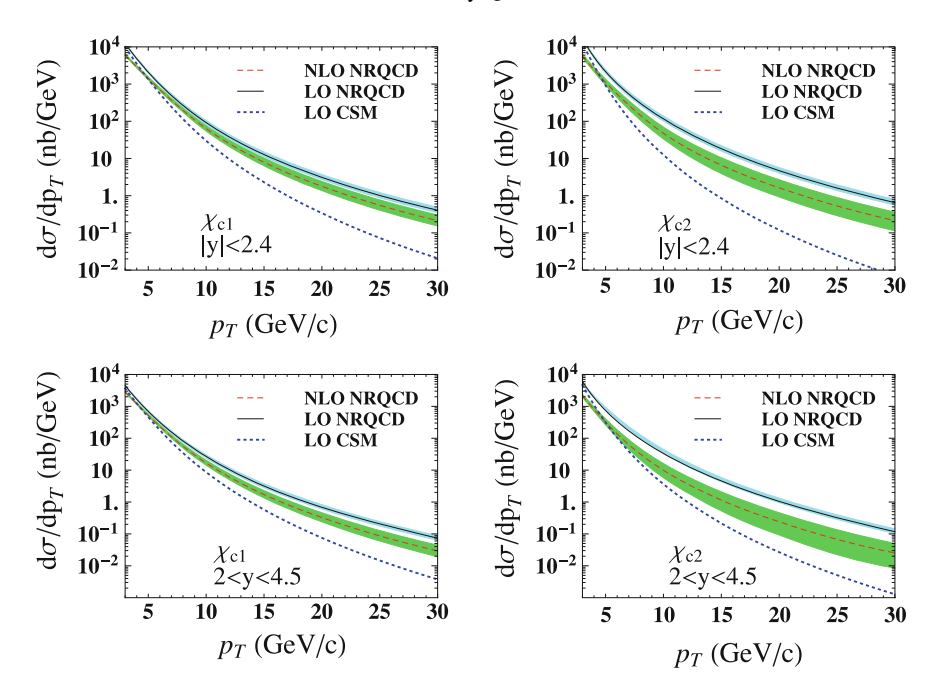


Fig. 4.10 The cross-sectional ratio  $\sigma_{\chi c2}/\sigma_{\chi c1}$  versus the transverse momentum  $p_T^{J/\psi}$  at the Tevatron with  $\sqrt{S}=1.96$  TeV (*upper panel*) and the LHC with  $\sqrt{S}=7$  TeV (*lower two panels*). The rapidity cutoffs are the same as the experiments [17, 38, 39]. Results for LO NRQCD (*solid line*), NLO NRQCD (*dashed line*), and LO CSM (*dotted line*) are shown

in the future if the experiments are already able to constraint the LDMEs in a more accuracy way. People can rescale these curves to obtain the results with their own values of LDMEs. In order to study the polarization observables  $\lambda_{\theta}$  and  $\lambda_{\theta'}$  defined in Sect. 4.2.1, let us have a look at the lower and upper bound values of  $\lambda_{\theta}$  and  $\lambda_{\theta'}$  for  $\chi_{c1}$  and  $\chi_{c2}$  from Eqs. (4.13, 4.14, 4.19) first. Regardless of the  $\chi_c$  production mechanism, the bounds of these observables are presented in Table 4.11. The polar observables for  $\chi_{c1}$  approach to their maximal values when  $d\sigma_{11}^{\chi_{c1}} = d\sigma_{-1-1}^{\chi_{c1}} \ll d\sigma_{00}^{\chi_{c1}}$ , and to their minimal values when  $d\sigma_{11}^{\chi_{c1}} = d\sigma_{-1-1}^{\chi_{c1}} \gg d\sigma_{00}^{\chi_{c1}}$ . For  $\chi_{c2}$ , the polarization observables  $\lambda_{\theta}$  and  $\lambda_{\theta'}$  are maximum when  $d\sigma_{22}^{\chi_{c1}} = d\sigma_{-2-2}^{\chi_{c1}} \gg d\sigma_{11}^{\chi_{c2}} = d\sigma_{-1-1}^{\chi_{c2}}$ ,  $d\sigma_{00}^{\chi_{c2}}$  and minimum when  $d\sigma_{22}^{\chi_{c2}} = d\sigma_{-2-2}^{\chi_{c1}} = d\sigma_{-1-1}^{\chi_{c2}} \ll d\sigma_{00}^{\chi_{c2}}$ . The transverse momentum distributions of  $\lambda_{\theta}$  and  $\lambda_{\theta'}$  are shown in Figs. 4.13 and 4.14. The error bands in these figures can be attributed to the uncertainties of the CO LDMEs and errors in the E1,M2, and E3 amplitudes. It is very interesting that these observables can be compared to the corresponding experiments at the LHC in the near future.



**Fig. 4.11** Predictions of  $p_T$  spectra for the helicity-summed  $\chi_{c1}$  (*left column*) and  $\chi_{c2}$  (*right column*) at the LHC with  $\sqrt{S} = 7$  TeV. Cross sections in the central rapidity region (|y| < 2.4) and forward rapidity region (2 < y < 4.5) for  $\chi_c$  are plotted. Results for LO NRQCD (*solid line*), NLO NRQCD (*dashed line*), and LO CSM (*dotted line*) are shown

# 4.3 Double-Quarkonium Production at the LHC

The LHC data for prompt  $J/\psi$  and  $\psi(2S)$  may be not enough to pin down the complexity of quarkonium production mechanism. In this section, we put our hope into the study of a pair of quarkonium production. We know that  $\mathcal{O}(\alpha_S^4)$  and  $\mathcal{O}(\alpha_S^5)$  corrections in CSM are significant. They cannot be overlooked if one tries to understand the transverse momentum  $p_T$  dependence of the  $J/\psi$  and  $\Upsilon$  cross sections at hadron colliders [40–45]. On the other hand, for the total cross sections at hadron colliders and the quarkonium production processes at B factories, the CSM contributions agree relatively well with the existing experimental data (see, e.g., Refs. [46, 47]). Hence, we wonder whether CSM also applies to quarkonium-pair production. Moreover, due to the double suppression of CO LDMEs in CO+CO+X production channels, CO contributions may not be important in double-quarkonium production. A strict conclusion can only be drawn after considering the mixed CS+CO+X production channels rigorously. However, from a naive estimation, there is no obvious  $p_T$  enhancement in the mixed channels compared to that in CSM, but they are suppressed by the values of CO LDMEs. Therefore, we think that the CS contribution

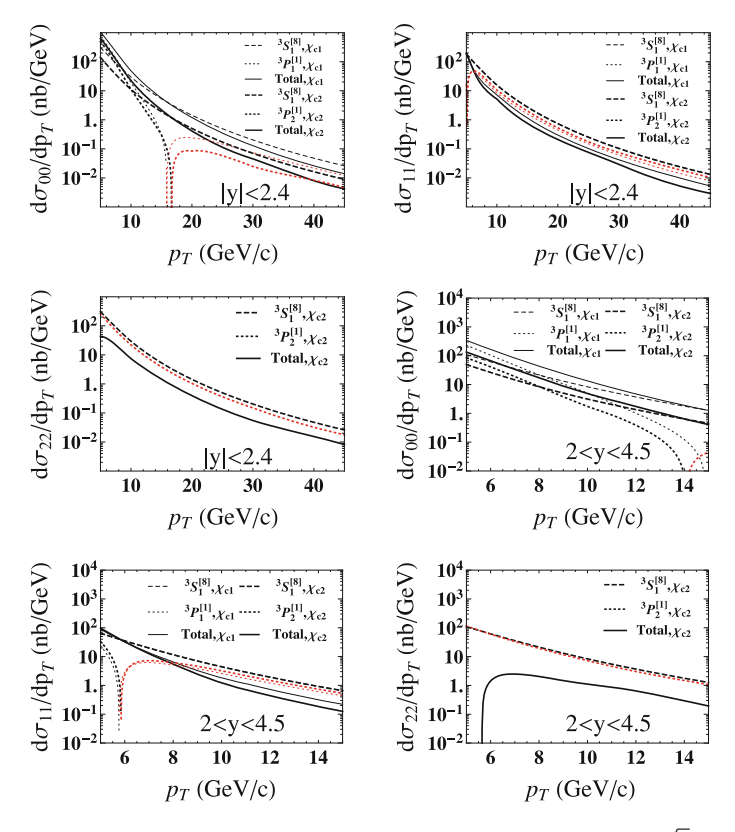


**Fig. 4.12**  $d\sigma_{00}/dp_T$ ,  $d\sigma_{11}/dp_T$  and  $d\sigma_{22}/dp_T$  for  $pp \to \chi_{cJ} + X$ , J=1,2 with  $\sqrt{S}=7$  TeV and |y| < 2.4 (upper panels), 2 < y < 4.5 (lower panels) in the helicity frame at NLO in NRQCD. The thin lines represent  $\chi_{c1}$  while the thick lines represent  $\chi_{c2}$ . Negative values are marked red

**Table 4.11** Upper and lower bound values of the observables  $\lambda_{\theta}$  and  $\lambda_{\theta'}$  for  $\chi_{c1}$  and  $\chi_{c2}$ 

Observable	$\lambda_{ heta}^{\chi_{c1}}$	$\lambda_{ heta}^{\chi_{c2}}$	$\lambda_{\theta'}^{\chi_{c1}}$	$\lambda_{\theta'}^{\chi_{c2}}$
Upper bound	0.556	1.61	0.994	0.928
Lower bound	-0.217	-0.803	-0.332	-0.574

would play the dominant role in understanding double-quarkonium production data at the LHC at least  $p_T < 30$  GeV.

Before our investigation [48], all the double-quarkonium production studies were restricted to  $\mathcal{O}(\alpha_S^4)$ , i.e., LO in  $\alpha_S$  [49–59]. However, bear in mind that there are already many examples [44, 45, 48, 60–62] showing that higher-order QCD corrections are important due to new  $p_T$ -enhanced topologies beyond LO. For the first time, we try to include  $\mathcal{O}(\alpha_S^5)$  contribution into double- $J/\psi$  hadroproduction process [48]. Because of the robust and automation of HELAC-ONIA, it is easy for us to study  $\mathcal{O}(\alpha_S^5)$  real correction directly. Because the missing virtual correction is the same

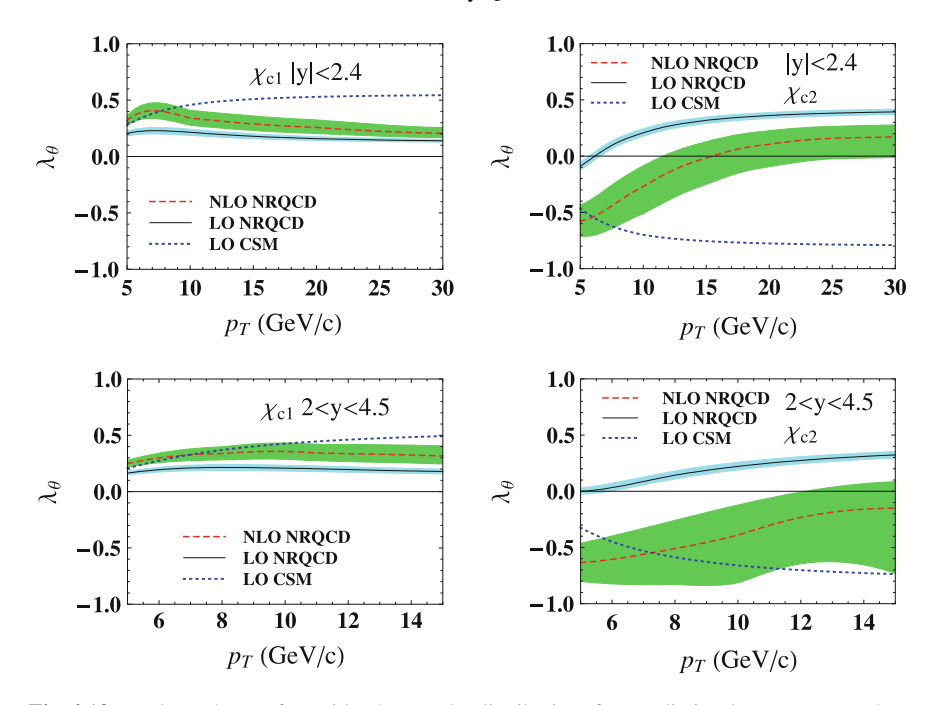


Fig. 4.13  $p_T$  dependence of  $\lambda_\theta$  with  $J/\psi$  angular distributions from radiative decays  $\chi_{c1} \to J/\psi \gamma$  (left column) and  $\chi_{c2} \to J/\psi \gamma$  (right column) in the helicity frame at the LHC with  $\sqrt{S} = 7 \text{TeV}$ . Results in central and forward rapidity regions are plotted. The LO NRQCD (solid line), NLO NRQCD (dashed line), and LO CSM (dotted line) predictions are shown

 $p_T$  behavior as the LO one, we think the virtual correction only contributes a pure  $\mathcal{O}(\alpha_S)$  correction. This fact will be emphasized later in more details.

On the physical side, there are several motivations to study the associated production channels of  $J/\psi$ . Recently, LHCb collaboration has measured two associated production channels, i.e.,  $J/\psi$  +charm quark [63] and  $J/\psi+J/\psi$  [64]. The  $J/\psi$  pair production process was measured for the first time by the CERN-NA3 collaboration in the eighties [65, 66]. The rates were higher than expected. It was explained by the coalescence of double intrinsic charm quark pair in the proton projectile [67]. It is believed that  $J/\psi+\eta_c$  and  $J/\psi+\chi_c$  production is suppressed at the hadron colliders due to C-parity conservation. Hence, in Ref. [68], authors suggested to use the ratio of  $J/\psi+\chi_c$  and  $J/\psi+J/\psi$  to investigate the effect of double-parton-scattering (DPS). It is believed that DPS could be a significant source of quarkonium-pair production at the LHC [56].

In this section, we will present the leading  $p_T$  NLO contributions to  $J/\psi + J/\psi$  and  $\Upsilon + \Upsilon$ . Our computation consists of the real emission NLO corrections regulated by a cutoff, which is denoted as NLO\* [44]. In order to avoid IR divergences appearing in real emissions, we have imposed the invariant mass of any light-parton pair  $s_{ij}$  to be larger than an IR cutoff  $s_{ij}^{\min}$ . We emphasize that our IR treatment is expected to

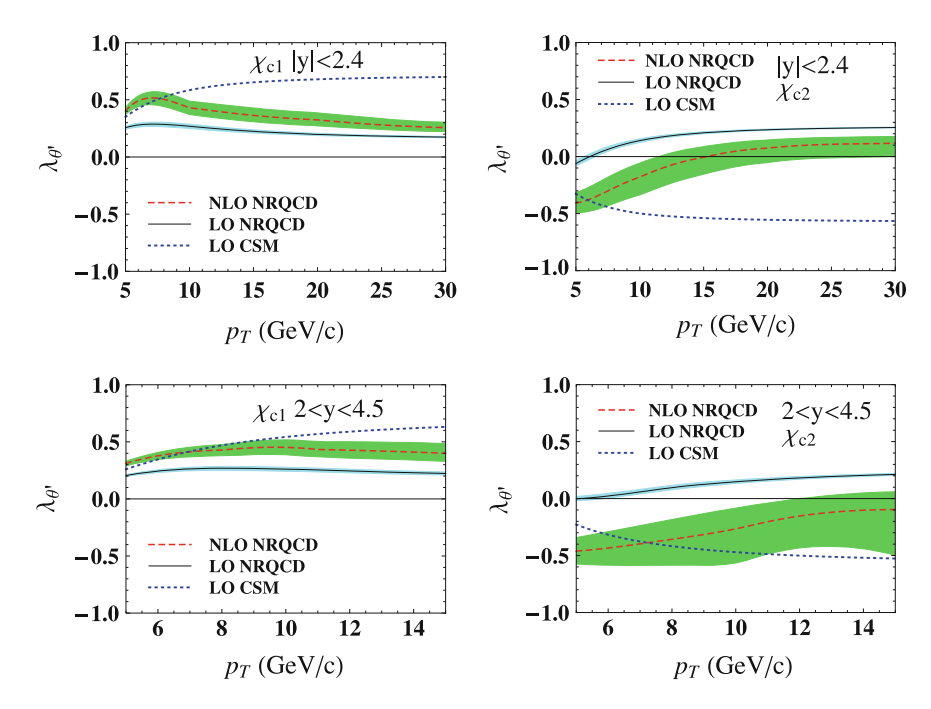
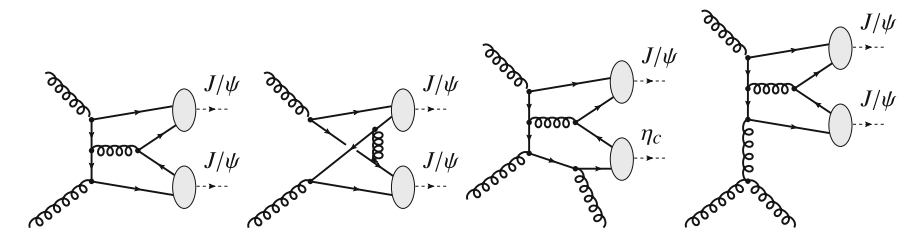


Fig. 4.14  $p_T$  dependence of  $\lambda_{\theta'}$  with di-lepton angular distributions from cascade decays  $\chi_{c1} \rightarrow J/\psi \gamma \rightarrow l^+ l^- \gamma$  (left column) and  $\chi_{c2} \rightarrow J/\psi \gamma \rightarrow l^+ l^- \gamma$  (right column) in the helicity frame at the LHC with  $\sqrt{S} = 7$  TeV. Results in central rapidity and forward rapidity regions are plotted, and the LO NRQCD (solid line), NLO NRQCD (dashed line), and LO CSM (dotted line) predictions are shown

give a reliable estimation of the NLO result at least when  $p_T$  is large for the following reasons.

- If one inspects all propagators, he/she can easily see that the IR cutoff  $s_{ij} > s_{ij}^{\min}$  is already sufficient to regulate all the collinear and soft divergences in real emission diagrams.
- The key point is that for the new  $p_T$ -enhanced topologies appearing at NLO, for example, the t-channel diagram shown in Fig. 4.15.  $s_{ij}$  will be large for any light-parton pair at high  $p_T$  in such diagrams.
- For the remaining topologies, large logarithms  $\log(s_{ij}/s_{ij}^{\min})$  will appear, but there are  $p_T$  suppressed factors in such topologies. Therefore, the dependence on  $s_{ij}^{\min}$  should vanish when  $p_T$  increases.
- The virtual corrections, which have the same  $p_T$ -scaling as the Born ones, are also  $p_T$  suppressed compared to the real emission contributions. They can also be neglected as we have anyhow regulated the IR divergences.



**Fig. 4.15** Representative diagrams to the hadroproduction of a pair of quarkonium in the CSM at  $\mathcal{O}(\alpha_S^4)$  for  $J/\psi + J/\psi$  (the first two), and  $\mathcal{O}(\alpha_S^5)$  for  $J/\psi + \eta_c$  (the third one) and for  $J/\psi + J/\psi$  (the last one)

The reliability of the NLO\* approximation has been explicitly verified in the  $J/\psi$  and  $\Upsilon$  hadroproduction [44, 45],  $J/\psi + \gamma$  and  $\Upsilon + \gamma$  [62] and  $J/\psi + Z$  [69]. 11

In the next two subsections, we will go into the phenomenological part of the direct  $J/\psi$  and  $\Upsilon$  pair production. The result of the  $J/\psi$ -pair production is already presented in a published paper [48], while the result for the  $\Upsilon$ -pair production is completely new.

### 4.3.1 $J/\psi$ -pair Production

In this subsection, we present the results in Ref. [48]. To enrich the comparison, we have also calculated the yield and polarization of  $J/\psi$  in association with  $\eta_c$  at  $\mathcal{O}(\alpha_s^5)$ . Moreover, some kinematic correlations based on unweighted events generated by HELAC-Onia are also analyzed. This analysis of the kinematic correlations may help to study the DPS contributions. Finally, we present the polarization of  $J/\psi$  in  $J/\psi + J/\psi$ .

Here, we are only working in CSM. The CS LDME can be estimated via  $\langle \mathcal{O}^{J/\psi}({}_S^{[1]}) \rangle = \frac{2N_c|R(0)|^2}{4\pi}$ , where  $|R(0)|^2 = 0.81$  GeV<sup>3</sup>. Because only CS results are presented in this section, if people want to use their own CS LDME, they can just make a rescaling to the curves presented here. We have considered the processes of  $J/\psi$ -pair and  $J/\psi + \eta_c$  production at  $\mathcal{O}(\alpha_S^4)$  via gluon–gluon collisions (see the first two diagrams in Fig. 4.15) and  $gg \to J/\psi + \eta_c + g$  at  $\mathcal{O}(\alpha_S^5)$  (see the third diagram in Fig. 4.15). Because of C-parity conservation, the radiated final gluon only attaches to the heavy quark lines in  $gg \to J/\psi + \eta_c + g$ . For the  $\mathcal{O}(\alpha_S)$  correction to  $J/\psi$ -pair hadroproduction, we have to consider more subprocesses such as  $gg \to J/\psi + J/\psi + g$ ,  $gg \to J/\psi + J/\psi + q$ ,  $gg \to J/\psi + J/\psi + q$  and  $q\bar{q} \to J/\psi + J/\psi + g$ , where q represents light quark or antiquark. In the nonrelativistic framework, all heavy quarks are generated on-shell, and we have  $M_{J/\psi,\eta_c} = 2m_c$ .

<sup>&</sup>lt;sup>11</sup>After comparing our result with a full complete NLO QCD correction to  $pp \to J/\psi + J/\psi + X$  done by L.-P.Sun et al. recently, it seems that our NLO\* result indeed gives a very good agreement with theirs when  $p_T > 5$  GeV.

The combined variations of charm quark mass  $m_c = 1.5 \pm 0.1$  GeV and the factorization scale  $\mu_F$  and renormalization scale  $\mu_R$  as  $0.5\mu_0 \le \mu_F = \mu_R \le 2\mu_0$  are considered as the theoretical uncertainties, where  $\mu_0 = \sqrt{(4m_c)^2 + p_T^2}$ . We use the CTEQ6L1 and CTEQ6M [11] for the LO and NLO\* computations, respectively.

#### 4.3.1.1 Transverse Momentum Differential Distribution

We present the transverse momentum differential distribution  $d\sigma/dp_T$  for  $J/\psi$  in Fig. 4.16. We have considered the largest rapidity intervals |y| < 3 covered by CMS and ATLAS detectors and 2 < v < 4.5 covered by LHCb detector. At low  $p_T$ region, it is shown that the yield of  $J/\psi + \eta_c$  is about ten times lower than that of double  $J/\psi$  production. To understand it, we have a factor three comes from the spin-state counting and another factor from a single power of  $\alpha_s$ . Concerning to the  $p_T$  spectrum, the  $p_T$  falloff for  $J/\psi + \eta_c$  is slower than that for  $J/\psi$ -pair at LO. The yield of  $J/\psi + \eta_c$  catches up with that of LO  $J/\psi$ -pair at about 17 GeV. However, one should not restrict oneself to do the comparison by using the LO result of  $J/\psi$ -pair hadroproduction only. From Fig. 4.16, we indeed see that there is a large enhancement between the  $p_T$  distribution of LO and NLO\*, which is very similar to the case in  $J/\psi$  and  $\Upsilon$  hadroproduction processes. In all of the known cases, the NLO\* yield is able to accurately reproduce the full NLO yield as long as the  $p_T$  is a few times of  $m_Q$ . Recently, we have compared our result with the full NLO result provided by others. We gain a very good agreement with theirs when  $p_T > 5$  GeV. On our own side, which was done before this comparison, we separately plot the sensitivity on the IR cutoff  $s_{ij}^{min}$  in the last panel of Fig. 4.17. The uncertainty from  $s_{ii}^{\min}$  is negligible at  $p_T > 10$  GeV, and it is also smaller than a factor of two when  $p_T > 5 \text{ GeV}.$ 

To understand the  $p_T$  scaling of  $J/\psi + J/\psi$  and  $J/\psi + \eta_c$  production, we have added a curve for the leading- $p_T$  CO channel  $\mathring{S}_1^{[8]} + \mathring{S}_1^{[8]}$  in Fig. 4.17. The  $p_T$  power of partonic distribution  $d\sigma/dp_T^2$  is expected to be  $p_T^{-4}$  at high  $p_T$ , which is mainly due to

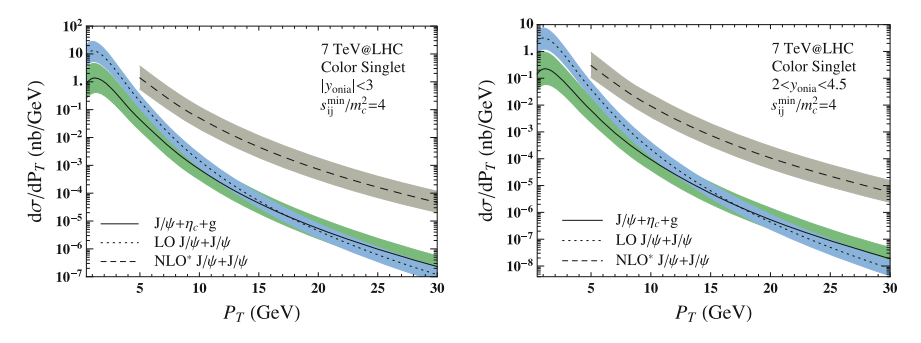
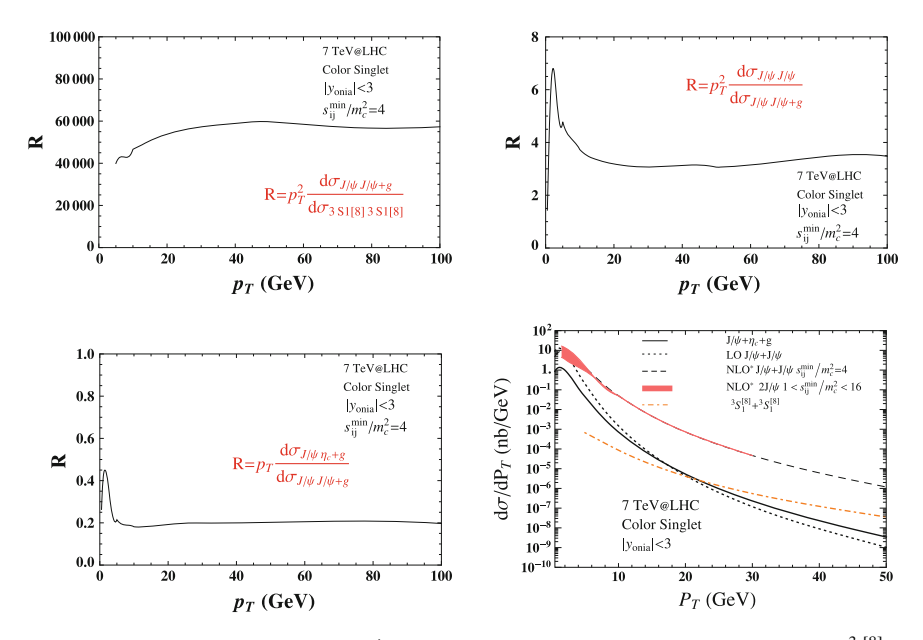


Fig. 4.16  $d\sigma/dp_T$  for  $J/\psi + J/\psi$  at LO and NLO\*, and for  $J/\psi + \eta_c + g$  at the LHC with  $\sqrt{S} = 7 \text{ TeV}$ 



**Fig. 4.17** Cross-sectional ratios and  $s_{ij}^{min}$  dependence for  $J/\psi + J/\psi$  at NLO\*. We also put  $\mathring{S}_{1}^{[8]} + \mathring{S}_{1}^{[8]}$  contribution in plot with  $\langle \mathcal{O}^{J/\psi}(\mathring{S}_{1}^{[8]}) \rangle = 2 \times 10^{-3} \text{ GeV}^{3}$ 

the double-gluon-fragmentation channels. Considering the PDF smearing effect on  $p_T$  scaling, we take this channel as our benchmark. The  $p_T$  scalings of other processes can be obtained from the ratios of its cross sections over that of  ${}^{5}1^{[8]} + {}^{3}5^{[8]}1^{[8]}$ , since the ratios will cancel the PDF smearing effect between the numerator and denominator. From the first panel in Fig. 4.17, the  $d\sigma/dp_T^2$  at  $\mathcal{O}(\alpha_S^5)$  for  $J/\psi$ -pair production is  $p_T^{-6}$ , whereas that at  $\mathcal{O}(\alpha_S^4)$  for  $J/\psi$ -pair production is  $p_T^{-8}$ , which is easily seen from the second panel. From the third plot in Fig. 4.17, the  $J/\psi - p_T$  scaling in  $J/\psi + \eta_c$  is  $p_T^{-7}$ . The extra  $p_T$  suppression of  $J/\psi + \eta_c$  compared to double- $J/\psi$ production at NLO\* likely comes from the presence of t-channel exchange topologies for  $J/\psi + J/\psi$  and absence in  $J/\psi + \eta_c$ . Owing to the  $p_T^2$  enhancement at NLO\* for  $J/\psi + J/\psi$  in CSM and double CO LDMEs suppression in  ${}^3\Sigma_1^{[8]} + {}^3\Sigma_1^{[8]}$ , we observe that the CSM contribution is dominant in the double  $J/\psi$  yield compared to the CO one. At  $p_T = 50$  GeV, the CSM NLO\* result is still ten times larger than that of production process is sensitive to the values of the LDMEs. The order of the LDMEs used here is same with that extracted in prompt  $J/\psi$  production process, which was already done in the first section of this chapter. Anyway, we do not want to draw a strong conclusion here, because a more careful analysis including the mixed CO+CS contributions is necessary. Such a analysis is beyond the scope of this section, and we leave it for the future studies.

#### 4.3.1.2 Kinematic Correlations

We study the azimuthal correlation and invariant-mass distribution here. These kinematic correlations are useful to study DPS contributions in the associated quarkonium production processes. In DPS, the azimuthal distribution is flat if we do not consider any smearing effect from initial states, because the two-parton scattering processes can be viewed as two independent scattering processes.

Because the magnitudes of the distributions usually suffer from large uncertainties due to various parameters setup, we normalize all of the kinematic distributions in this subsection to unity. It is fine because the shapes are indeed the primarily interested things. In the following, we will perform such a normalization in each distribution. The treatment has the virtue of significantly reducing the theoretical uncertainties. We show the plots in Fig. 4.18.

At LO, the  $J/\psi$  pair is completely anti-correlated with a peak at  $\Delta\phi_{J/\psi-J/\psi}=\pi$ , because the  $2\to 2$  kinematics make  $J/\psi$  back-to-back produced. In the presence of an additional final-state patron, the far "away" side  $\Delta\phi=\pi$  is not anymore the only populated region, which can be observed in Fig. 4.18. With the intrinsic  $k_T$  for the initial partons [70], it would create a natural imbalance but decrease as  $\langle k_T \rangle/p_T$ , which can be seen clearly from the first plot in Fig. 4.18. This observation was already pointed out in Ref. [56], and the authors suggested to impose a  $p_T$  cutoff to avoid such  $k_T$  smearing effects in azimuthal correlations. As we have already pointed out, the configurations in  $J/\psi+\eta_c$  are not  $p_T$ -enhanced. In contrary, for  $J/\psi+J/\psi$  at NLO\*, the  $J/\psi$  pair recoils against a parton in  $p_T$ -enhanced t-channel exchange topologies at large enough transverse momentum. The charmonia approach each other and the distribution peaks at  $\Delta\phi_{J/\psi-J/\psi}\sim 0$ . Moreover, the away-side peak decreases as the transverse momentum increases. Therefore, we think the introduction of a  $p_T$  cutoff may be still not enough to make clear comparison between DPS and single-parton scattering (SPS) signals.

For the invariant-mass distribution (see the second plot in Fig. 4.18), we have taken the same normalization to cancel the large charm mass and scale uncertainties. We compare our result with the measurement performed by LHCb collaboration [64].

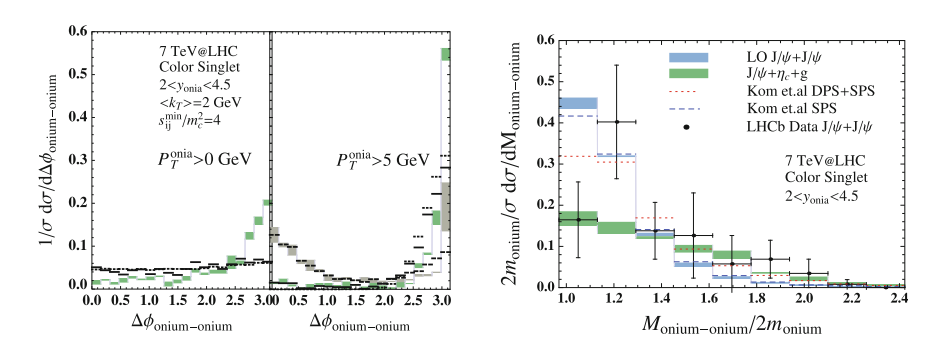


**Fig. 4.18**  $d\sigma/d\Delta\phi$  and  $d\sigma/d\Delta M_{\text{pair}}$  at 7 TeV for  $J/\psi + J/\psi$  at LO and NLO\*, and for  $J/\psi + \eta_c$ 

At LO in  $J/\psi + J/\psi$ , we recover the shape of the SPS result in Refs. [56, 57]. The theoretical result agrees with the data except the first bin. However, we do not entirely share the observation made in Ref. [56] that SPS disagrees with the data. The reason relies on the uncertainties. We think the uncertainties in SPS normalization were underestimated in Ref. [56]. It is not clear that whether the peak in the second bin or the dip in the first bin is just a fluctuation or a feature of the distribution. We hope the forthcoming data will clarify the situation. Here, we think the NLO\* is not significant if no  $p_T$  cutoff applies.

#### 4.3.1.3 Polarization

Polarization is also very interesting and may be crucial to revealing the quarkonium production mechanism. Hence, we study the polar anisotropy  $\lambda_{\theta}$  in the helicity frame in this subsubsection. We compare the  $\lambda_{\theta}$  of  $J/\psi$  accompanied by an  $\eta_c$  with that accompanied by another  $J/\psi$ . For the first time, we give the NLO\* results of the polarization in such processes. The results presented here should produce the exact NLO results accurately when  $p_T > 5$  GeV.

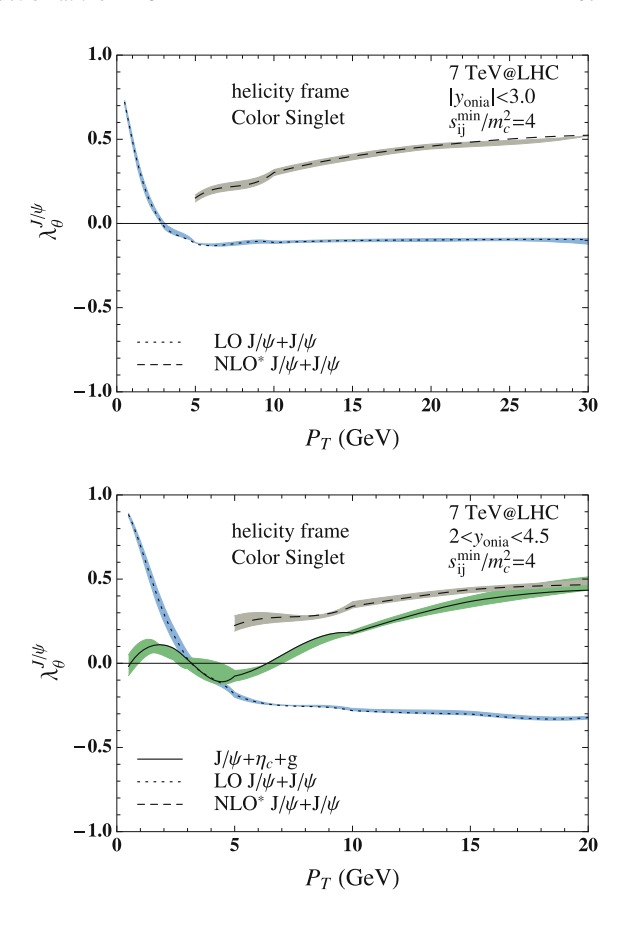
Our theoretical results in the central rapidity and forward rapidity intervals are shown in Fig. 4.19. We only plot the curve for  $J/\psi + \eta_c$  in the LHCb fiducial region, because we believe it is only possible for the LHCb experiment to measure it especially for reconstructing  $\eta_c$  via  $p\bar{p}$  in the future. At high  $p_T$  regime, the NLO\* polarization of a  $J/\psi$  is quite different than that at LO. It is a little bit transverse at NLO\*, while at LO it is longitudinal. It can be understood at moderate and high  $p_T$ , where the NLO\* is dominated by novel topologies. It is interesting to see that the curve of NLO\* result for  $J/\psi + J/\psi$  coincides at high  $p_T$  with that for  $J/\psi + \eta_c$ .

### 4.3.1.4 Final Remarks

Finally, we want to give some remarks on the  $p_T$  spectra we presented in this section. In our analysis, we only give the  $p_T$  distributions of the "first"  $J/\psi$  in  $J/\psi$ -pair events. People have no way to distinguish the two identical  $J/\psi$  in the  $J/\psi$ -pair production process. Then, is it possible for experimentalists to compare our theoretical results? The answer, of course, is yes by following the below steps:

- Measure the  $p_T$  for the two  $J/\psi$  in the reconstructed  $J/\psi$ -pair events.
- Count the number of events as  $N_i^{\text{same}}$  if both transverse momenta of the  $J/\psi$ -pair are in the bin  $p_{Ti} < p_T < p_{Ti+1}$ .
- Count the number of events as  $N_i^{\text{diff}}$  if one and only one transverse momentum of the  $J/\psi$ -pair is in the bin  $p_{Ti} < p_T < p_{Ti+1}$ .
- Then the total number of events in  $p_{Ti} < p_T < p_{Ti+1}$  related to the "first"  $J/\psi p_T$  spectrum is  $N_i^{\text{same}} + N_i^{\text{diff}}/2$ .

**Fig. 4.19** Polarization observable  $\lambda_{\theta}$  of  $J/\psi$  in the helicity frame at 7 TeV for  $J/\psi + J/\psi$  at LO and NLO\*, and for  $J/\psi + \eta_{c}$ 



Although we only use such  $p_T$  differential distributions here, the main conclusion should not alter if we consider other  $p_T$  distributions like leading or subleading  $p_T$  of the  $J/\psi$ -pair. In any case, we are able to provide the experimentalists our unweighted event samples in their fiducial regions.

Recently, after our publication, a new preprint [71] on the measurements of the prompt double  $J/\psi$  production by CMS collaboration appears. Moreover, ATLAS collaboration also contacted us to give them our event samples. We will leave such careful analysis about the CMS and ATLAS experiments for the future works.

### 4.3.2 Y-pair Production

Following the same line, we present the  $p_T$  distributions for the yields and polarizations of  $\Upsilon$ -pair hadroproduction. The results presented here are completely new.

The setup for  $\Upsilon$ -pair production is similar to that for  $J/\psi$ -pair production in Sect. 4.3.1. The CS LDME is estimated via potential model  $\langle \mathcal{O}^{J/\psi}(\mathring{S}_1^{[1]})\rangle = \frac{2N_c|R(0)|^2}{4\pi}$ , where  $|R(0)|^2 = 19.431 \text{ GeV}^3$ . We only use the  $|R(0)|^2$  for  $\Upsilon(1S)$  here, since one is able to make a simple rescaling to obtain the curves for other excited states. The theoretical uncertainty comes from the combined variations of bottom quark mass  $m_b = 4.75 \pm 0.1 \text{ GeV}$  and the factorization scale  $\mu_F$  and renormalization scale  $\mu_R$  as  $0.5\mu_0 \leq \mu_F = \mu_R \leq 2\mu_0$ , where  $\mu_0 = \sqrt{(4m_b)^2 + p_T^2}$ .

In order to see the convergence of the IR cutoff  $s_{ij}^{\min}$ , we plot  $s_{ij}^{\min}$  dependence in Fig. 4.20. It is observed that at  $p_T/(2m_b) \sim 3$ , the  $s_{ij}^{\min}$  is almost negligible, whereas at  $p_T/(2m_b) \sim 2$  the situation is similar to the  $J/\psi$ -pair case at  $p_T = 5$  GeV. On the other side, one can imagine that NLO corrections to  $\Upsilon$ -pair production at small  $p_T$  is only an  $\mathscr{O}(\alpha_S)$  correction. After considering the large theoretical uncertainties, we are able to give a  $p_T$  distribution in the whole  $p_T$  regime by interpolating the high and low  $p_T$  theoretical results. Finally, we show the yields and polarizations of  $\Upsilon$  in

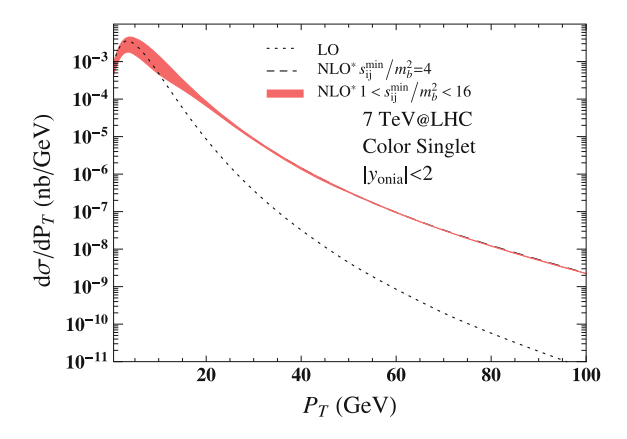


**Fig. 4.20**  $s_{ii}^{\min}$  dependence for  $\Upsilon + \Upsilon$  production at NLO\*

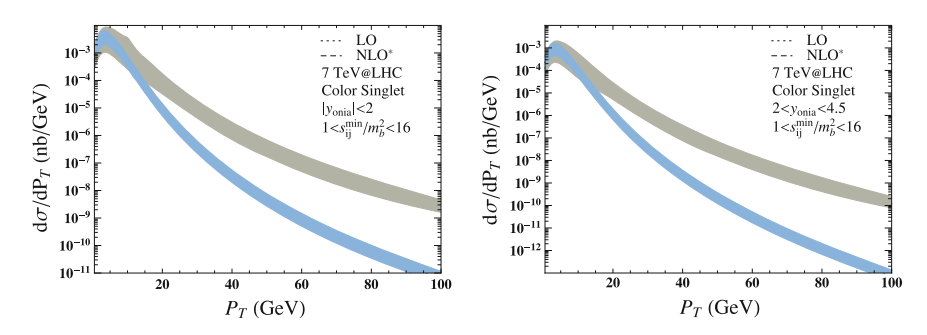
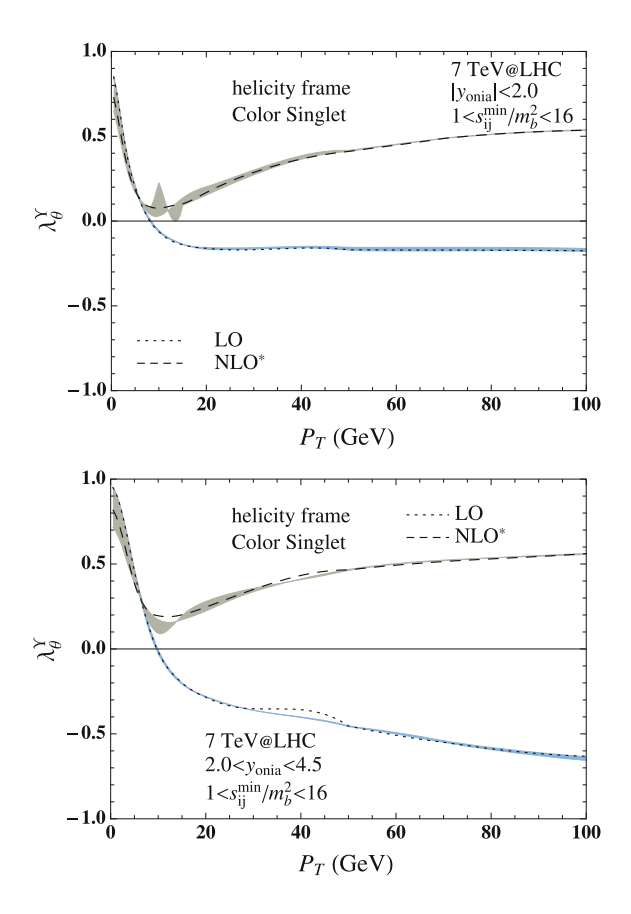


**Fig. 4.21**  $d\sigma/dp_T$  for  $\Upsilon + \Upsilon$  at LO and NLO\* at the LHC with  $\sqrt{S} = 7$  TeV

**Fig. 4.22** The polarization observable  $\lambda_{\theta}$  of  $\Upsilon$  in the helicity frame at 7 TeV for  $\Upsilon + \Upsilon$  production at LO and NLO\*



Figs. 4.21 and 4.22 at the LHC with the center-of-mass energy  $\sqrt{S} = 7$  TeV. Results in two rapidity intervals |y| < 2 and 2 < y < 4.5 are given in order to cover the regions of the CMS and ATLAS detectors and of the LHCb detector.

### References

- H.S. Shao, H. Han, Y.Q. Ma, C. Meng, Y.J. Zhang, K.T. Chao, JHEP 05, 103 (2015). doi:10. 1007/JHEP05(2015)103
- M. Butenschoen, B.A. Kniehl, Phys. Rev. Lett. 106, 022003 (2011). doi:10.1103/PhysRevLett. 106.022003
- Y.Q. Ma, K. Wang, K.T. Chao, Phys. Rev. Lett. 106, 042002 (2011). doi:10.1103/PhysRevLett. 106.042002
- Y.Q. Ma, K. Wang, K.T. Chao, Phys. Rev. D 83, 111503 (2011). doi:10.1103/PhysRevD.83. 111503
- 5. M. Butenschoen, B.A. Kniehl, Phys. Rev. Lett. 108, 172002 (2012)
- 6. K.T. Chao, Y.Q. Ma, H.S. Shao, K. Wang, Y.J. Zhang, Phys. Rev. Lett. 108, 242004 (2012)

- 7. B. Gong, L.P. Wan, J.X. Wang, H.F. Zhang, Phys. Rev. Lett. 110, 042002 (2013)
- 8. H.S. Shao, K.T. Chao, Phys. Rev. D **90**(1), 014002 (2014). doi:10.1103/PhysRevD.90.014002
- G.T. Bodwin, H.S. Chung, U.R. Kim, J. Lee, Phys. Rev. Lett. 113(2), 022001 (2014). doi:10. 1103/PhysRevLett.113.022001
- P. Faccioli, V. Knnz, C. Lourenco, J. Seixas, H.K. Whri. Phys. Lett. B736, 98 (2014). doi:10. 1016/j.physletb.2014.07.006
- 11. J. Pumplin, D. Stump, J. Huston, H. Lai, P.M. Nadolsky et al., JHEP **0207**, 012 (2002)
- 12. K. Nakamura, et al., J. Phys. G G37, 075021 (2010). doi:10.1088/0954-3899/37/7A/075021
- 13. R. Li, J.X. Wang, Phys. Rev. D 89(11), 114018 (2014). doi:10.1103/PhysRevD.89.114018
- H.S. Shao, Y.Q. Ma, K. Wang, K.T. Chao, Phys. Rev. Lett. 112(18), 182003 (2014). doi:10. 1103/PhysRevLett.112.182003
- 15. E.J. Eichten, C. Quigg, Phys. Rev. D 52, 1726 (1995). doi:10.1103/PhysRevD.52.1726
- 16. W. Buchmuller, S. Tye, Phys. Rev. D 24, 132 (1981). doi:10.1103/PhysRevD.24.132
- 17. A. Abulencia et al., Phys. Rev. Lett. 98, 232001 (2007). doi:10.1103/PhysRevLett.98.232001
- Y.Q. Ma, K. Wang, K.T. Chao, Phys. Rev. D 84, 114001 (2011). doi:10.1103/PhysRevD.84. 114001
- 19. D. Acosta et al., Phys. Rev. D 71, 032001 (2005). doi:10.1103/PhysRevD.71.032001
- 20. T. Aaltonen et al., Phys. Rev. D 80, 031103 (2009). doi:10.1103/PhysRevD.80.031103
- 21. S. Chatrchyan et al., JHEP 02, 011 (2012). doi:10.1007/JHEP02(2012)011
- 22. R. Aaij et al., Eur. Phys. J. C 72, 2100 (2012). doi:10.1140/epjc/s10052-012-2100-4
- 23. T.A. collaboration, (2013)
- 24. A. Abulencia et al., Phys. Rev. Lett. 99, 132001 (2007). doi:10.1103/PhysRevLett.99.132001
- 25. S. Chatrchyan et al., Phys. Lett. B 727, 381 (2013). doi:10.1016/j.physletb.2013.10.055
- 26. R. Aaij et al., Eur. Phys. J. C **74**(5), 2872 (2014). doi:10.1140/epjc/s10052-014-2872-9
- 27. G. Aad et al., Nucl. Phys. B **850**, 387 (2011). doi:10.1016/j.nuclphysb.2011.05.015
- 28. R. Aaij et al., Eur. Phys. J. C 71, 1645 (2011). doi:10.1140/epjc/s10052-011-1645-y
- 29. R. Aaij et al., Phys. Lett. B **718**, 431 (2012). doi:10.1016/j.physletb.2012.10.068
- 30. R. Aaij et al., Eur. Phys. J. C **73**(11), 2631 (2013). doi:10.1140/epjc/s10052-013-2631-3
- 31. B. Abelev et al., Phys. Rev. Lett. 108, 082001 (2012). doi:10.1103/PhysRevLett.108.082001
- 32. H.S. Shao, Comput. Phys. Commun. 184, 2562 (2013). doi:10.1016/j.cpc.2013.05.023
- B.A. Kniehl, G. Kramer, C.P. Palisoc, Phys. Rev. D 68, 114002 (2003). doi:10.1103/PhysRevD. 68.114002
- P. Faccioli, C. Lourenco, J. Seixas, H.K. Wohri, Phys. Rev. D 83, 096001 (2011). doi:10.1103/ PhysRevD.83.096001
- 35. M. Artuso et al., Phys. Rev. D **80**, 112003 (2009)
- G. Karl, S. Meshkov, J.L. Rosner, Phys. Rev. Lett. 45, 215 (1980). doi:10.1103/PhysRevLett. 45.215
- M.G. Olsson, C.J. Suchyta III, A.D. Martin, W.J. Stirling, Phys. Rev. D31, 1759 (1985). doi:10. 1103/PhysRevD.31.1759
- 38. R. Aaij et al., Phys. Lett. B **714**, 215 (2012). doi:10.1016/j.physletb.2012.06.077
- 39. S. Chatrchyan et al., Eur. Phys. J. C 72, 2251 (2012). doi:10.1140/epjc/s10052-012-2251-3
- J.M. Campbell, F. Maltoni, F. Tramontano, Phys. Rev. Lett. 98, 252002 (2007). doi:10.1103/ PhysRevLett.98.252002
- 41. P. Artoisenet, J. Lansberg, F. Maltoni, Phys. Lett. B **653**, 60 (2007). doi:10.1016/j.physletb. 2007.04.031.13 pages, 5 figures
- B. Gong, J.X. Wang, Phys. Rev. Lett. 100, 232001 (2008). doi:10.1103/PhysRevLett.100. 232001
- 43. B. Gong, J.X. Wang, Phys. Rev. D 78, 074011 (2008). doi:10.1103/PhysRevD.78.074011
- P. Artoisenet, J.M. Campbell, J. Lansberg, F. Maltoni, F. Tramontano, Phys. Rev. Lett. 101, 152001 (2008). doi:10.1103/PhysRevLett.101.152001
- 45. J. Lansberg, Eur. Phys. J. C **61**, 693 (2009). doi:10.1140/epjc/s10052-008-0826-9
- S.J. Brodsky, J.P. Lansberg, Phys. Rev. D 81, 051502 (2010). doi:10.1103/PhysRevD.81. 051502
- 47. H.S. Shao, JHEP **04**, 182 (2014)

References 71

48. J.P. Lansberg, H.S. Shao, Phys. Rev. Lett. **111**, 122001 (2013). doi:10.1103/PhysRevLett.111. 122001

- 49. V. Kartvelishvili, S. Esakiya, Yad. Fiz. 38, 722 (1983)
- 50. B. Humpert, P. Mery, Z. Phys. C 20, 83 (1983). doi:10.1007/BF01577721
- 51. C.F. Qiao, Phys. Rev. D 66, 057504 (2002). doi:10.1103/PhysRevD.66.057504
- R. Li, Y.J. Zhang, K.T. Chao, Phys. Rev. D 80, 014020 (2009). doi:10.1103/PhysRevD.80. 014020
- 53. C.F. Qiao, L.P. Sun, P. Sun, J. Phys. **G37**, 075019 (2010). doi:10.1088/0954-3899/37/7/075019
- C.F. Qiao, J. Wang, Y.h. Zheng. Chin. Phys. C35, 209 (2011). doi:10.1088/1674-1137/35/3/ 001
- 55. P. Ko, C. Yu, J. Lee, JHEP **1101**, 070 (2011). doi:10.1007/JHEP01(2011)070
- C. Kom, A. Kulesza, W. Stirling, Phys. Rev. Lett. 107, 082002 (2011). doi:10.1103/ PhysRevLett.107.082002
- A. Berezhnoy, A. Likhoded, A. Luchinsky, A. Novoselov, Phys. Rev. D 84, 094023 (2011). doi:10.1103/PhysRevD.84.094023
- 58. C.F. Qiao, L.P. Sun, Chin. Phys. C 37, 033105 (2013). doi:10.1088/1674-1137/37/3/033105
- 59. Y.J. Li, G.Z. Xu, K.Y. Liu, Y.J. Zhang, JHEP 1307, 051 (2013). doi:10.1007/JHEP07(2013)051
- 60. J. Lansberg, Int. J. Mod. Phys. A 21, 3857 (2006), doi:10.1142/S0217751X06033180
- 61. J. Lansberg, J. Phys. **G38**, 124110 (2011). doi:10.1088/0954-3899/38/12/124110
- 62. J. Lansberg, Phys. Lett. B 679, 340 (2009). doi:10.1016/j.physletb.2009.07.067
- 63. R. Aaij et al., JHEP 1206, 141 (2012). doi:10.1007/JHEP06(2012)141
- 64. R. Aaij et al., Phys. Lett. B **707**, 52 (2012). doi:10.1016/j.physletb.2011.12.015
- 65. J. Badier et al., Phys. Lett. B 114, 457 (1982). doi:10.1016/0370-2693(82)90091-0
- 66. J. Badier et al., Phys. Lett. B 158, 85 (1985). doi:10.1016/0370-2693(85)90745-2
- 67. R. Vogt, S. Brodsky, Phys. Lett. B 349, 569 (1995). doi:10.1016/0370-2693(95)00306-6
- A. Berezhnoy, A. Likhoded, A. Luchinsky, A. Novoselov, Phys. Rev. D 86, 034017 (2012). doi:10.1103/PhysRevD.86.034017
- B. Gong, J.P. Lansberg, C. Lorce, J. Wang, JHEP 1303, 115 (2013). doi:10.1007/ JHEP03(2013)115
- K. Sridhar, A.D. Martin, W.J. Stirling, Phys. Lett. B 438, 211 (1998). doi:10.1016/S0370-2693(98)00956-3
- 71. C. Collaboration, (2013)

# **Chapter 5**

# Inclusive $J/\psi$ Production at B Factories

**Abstract** In this chapter, we will use HELAC-ONIA to study the prompt  $J/\psi$  inclusive production at B factories. In particular, the initial state radiation (ISR) effect to the  $J/\psi$  production in electron–positron annihilation is discussed. The main result of this chapter was already published in Ref. [1].

### 5.1 Background

The first measurement of the prompt  $J/\psi$  inclusive production cross section at B factories with the center-of-mass energy  $\sqrt{s}\approx 10.6$  GeV was reported by BABAR collaboration over a decay ago, which is  $\sigma_{prompt}(e^-e^+ \to J/\psi + X) = 2.52 \pm 0.21 \pm 0.21$  pb [2]. Later on, similar measurement for this process was done by the BELLE collaboration, but the cross section is smaller  $\sigma_{prompt}(e^-e^+ \to J/\psi + X) = 1.47 \pm 0.10 \pm 0.13$  pb [3]. On the theoretical side, the earlier calculations [4–9] of the prompt  $J/\psi$  inclusive production in CSM show the cross section is only 0.3–0.5 pb depending on the input parameters. Obviously, it is much lower than the experimental measurements. People suggested that there might be significant CO contributions in the prompt  $J/\psi$  process. Moreover, later, Belle collaboration reported another measurement on  $e^-e^+ \to J/\psi + c\bar{c}$  [10]. The measured value is  $\sigma_{prompt}(e^-e^+ \to J/\psi + c\bar{c} + X) = 0.87^{+0.21}_{-0.19} \pm 0.17$  pb. It is larger than the LO NRQCD results [4, 6–9, 11] by at least a factor of 5. The LO NRQCD result [12] of the cross-sectional ratio

$$R_{c\bar{c}} \equiv \frac{\sigma(e^-e^+ \to J/\psi + c\bar{c} + X)}{\sigma(e^-e^+ \to J/\psi + X)},\tag{5.1}$$

which is expected to have less uncertainties both from theory and experiments, is also found to underestimate the Belle measurement  $0.59^{+0.15}_{-0.13} \pm 0.12$  [10]. The CO contribution [11] and the relativistic correction [13] to  $e^-e^+ \rightarrow J/\psi + c\bar{c} + X$  only

<sup>&</sup>lt;sup>1</sup>The process can be reconstructed by detecting another open-charm meson in companying with a  $J/\psi$ .

<sup>©</sup> Springer Science+Business Media Singapore 2016 H.-S. Shao, *Heavy Quarkonium Production Phenomenology and Automation of One-Loop Scattering Amplitude Computations*, Springer Theses,

enhance its cross section a little. These large discrepancies have promoted several theoretical studies in the next few years [14–16].

An important step toward reducing the discrepancy is the NLO correction in  $\alpha_S$  to the process  $e^-e^+ \to J/\psi + c\bar{c} + X$  [17]. It gains a factor of 1.8 enhancement compared to the LO result. This result was also confirmed later by other authors [18]. In Ref. [17], the authors use the  $J/\psi$  leptonic decay width [19] to extract the wave function at the origin R(0) of  $J/\psi$  at NLO level. They estimate the CS LDME as  $\langle \mathcal{O}^{J/\psi}({}^3\!\zeta_1^{[1]})\rangle = \frac{2N_c|R(0)|^2}{4\pi}$ . Its value is larger than the pure Buchmuller–Tye potential model value by a factor of  $\sim$ 1.25, which is estimated in Ref. [20]. After combining other important contributions especially the feed-down contribution from  $\psi(2S)$ , it is obtained that the cross section of prompt  $J/\psi$  production in  $e^-e^+ \to J/\psi + c\bar{c} + X$  is 0.51 pb at NLO level. Although it still suffers large uncertainties from the errors in  $m_c$ ,  $|R(0)|^2$  and the choice of renormalization scale, the NLO QCD correction to  $e^-e^+ \to J/\psi + c\bar{c} + X$  in CSM significantly reduces the discrepancy between experiments and theory.

Along the same line, both NLO corrections in  $\alpha_S$  [21, 22] and in  $v^2$  [23, 24] in CSM were performed later on. It is shown that these corrections enhance the LO CS cross section  $\sigma(e^-e^+ \to J/\psi + gg + X)$  by about 20–30%, which is already comparable to the Belle measurement of  $\sigma_{\text{prompt}}(e^-e^+ \to J/\psi + X_{\text{non}-c\bar{c}}) = 0.43 \pm 0.09 \pm 0.09$  pb [25]. At NLO in  $\alpha_S$ , the renormalization scale dependence is improved in comparison with that at LO. Moreover, the  $J/\psi$  momentum spectrum significantly changes at NLO QCD level, especially near the kinematic endpoint. It makes the momentum spectrum compatible with the Belle measurement [25]. The  $J/\psi$  momentum spectrum is thought as an important observable to probe the components of CO channels.

The CO contribution to  $e^-e^+ \to J/\psi + X_{\mathrm{non}-c\bar{c}}$  at LO in  $\alpha_S$  and at LO in  $v^2$  is  $e^-e^+ \to c\bar{c}[^1S_0^{[8]}, ^3P_J^{[8]}] + g$ . Due to the 2-body final kinematics, there is an enhancement near the kinematic endpoint  $z \equiv E_{c\bar{c}}/E_{c\bar{c}}^{\mathrm{max}} \to 1$  [26], where  $E_{c\bar{c}}$  and  $E_{c\bar{c}}^{\mathrm{max}}$  are the energy and maximum energy of the  $c\bar{c}$  pair, respectively. The authors of Ref. [14] pointed out that resummation of  $v^2$  and  $\log(1-z)$  near the endpoint would smear out the peak near z=1. However, their resummation procedure is heavily depending on a non-perturbative shape function. A comparison of NRQCD result with the up-to-date Belle measurement [25] is performed in Ref. [27]. The authors extract a strong constraint on the non-perturbative CO matrix elements [27]

$$\langle \mathcal{O}^{J/\psi}({}^{\rm [S[8]}_0)\rangle + 4.0 \frac{\langle \mathcal{O}^{J/\psi}({}^3\!P_0^{[8]})\rangle}{m_c^2} < (2.0 \pm 0.6) \times 10^{-2} \,{\rm GeV}^3,$$
 (5.2)

which is apparently in contradiction with the high  $p_T$  hadronic results in NRQCD at NLO in  $\alpha_S$  level [28–33].<sup>2</sup>

<sup>&</sup>lt;sup>2</sup>We want to point out that the values of the LDMEs extracted by authors in Refs. [34–36] satisfy this constraint. However, in their  $\chi^2$  fit, they have also included the small  $p_T$  yields data, and they predict a completely wrong polarization of  $J/\psi$  and  $\psi(2S)$  at the LHC.

5.1 Background 75

We will study the ISR effect to prompt  $J/\psi$  inclusive production at B factories in this chapter, which is already presented in a public write-up [1]. ISR is a very important ingredient that should be understood well in investigating physics in electron positron collisions. Two representative Feynman diagrams for  $e^-e^+ \rightarrow J/\psi + c\bar{c} + X$ and  $e^-e^+ \rightarrow J/\psi + gg + X$  with ISR are shown in Fig. 5.1. Due to the smallness of the electron mass, ISR does happen very often, which is understood because there is a large logarithm  $\log(m_s^2/s)$  to make up the suppression of the electromagnetic fine structure constant  $\alpha$ . After ISR, the annihilating electron and positron are no more in a head-on collision, because they may deviate from the beam axis by the radiation. The center-of-mass energy after ISR  $\sqrt{\hat{s}}$  may be smaller than that before showering  $\sqrt{s} = 10.6$  GeV. If the cross section is sensitive to the value of  $\sqrt{\hat{s}}$ , the ISR effect will really impact the final result. We show the dependence of  $\sqrt{\hat{s}}$  for the LO CS cross sections of  $e^-e^+ \to J/\psi + c\bar{c} + X$  and  $e^-e^+ \to J/\psi + gg + X$  in Fig. 5.2. It is observed that the cross section for  $e^-e^+ \to J/\psi + gg + X$  is sensitive to  $\sqrt{\hat{s}}$ , whereas it is not for  $e^-e^+ \rightarrow J/\psi + c\bar{c} + X$  at least not faraway from 10.6 GeV. Hence, we expect that ISR will significantly change the cross section of the former one, whereas it will change the distributions in the latter process very mildly. Moreover,

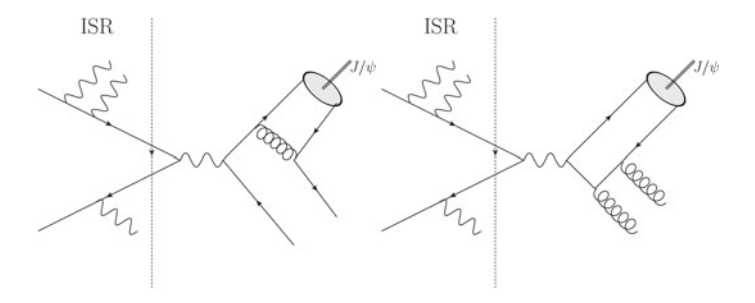
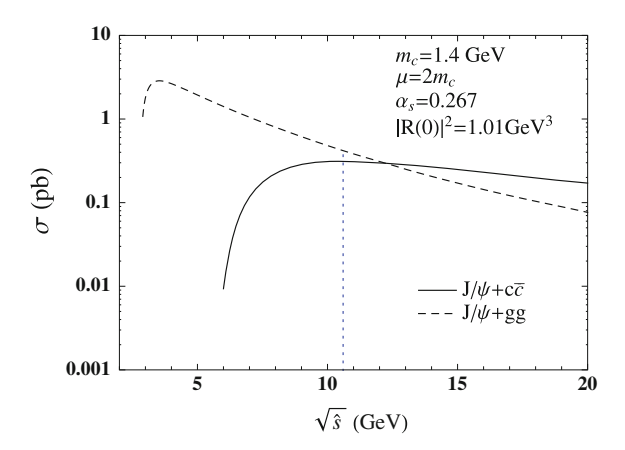


Fig. 5.1 Two representative Feynman diagrams with ISR

**Fig. 5.2** Cross sections as functions of center-of-mass energy  $\sqrt{\hat{s}}$ 



we point out that ISR is factorized out with QCD and relativistic corrections in  $J/\psi$  production.

In the next section, we will demonstrate how one can include the ISR effect into the theoretical results by combing HELAC- ONIA with other external programs.

### 5.2 Photon Shower from $e^{\pm}$ Beams

ISR is a very important ingredient that should be understood well in the  $e^\pm$  annihilation processes. Usually, ISR can be implemented by the structure function of the initial electron–positron, which is very likely the PDFs in hadronic collisions. The structure function method is easy to be realized. However, in general, by using a Monte Carlo generator, it is possible not only to predict the correct total cross sections for annihilation processes but also to provide the opportunity to maintain all the photon information from ISR and give any distribution over any kinematical variable. Therefore, a lot of researches [37–45] are dedicated to developing Monte Carlo generators with photon radiation. In this chapter, we will interface HELAC- ONIA to a general photon shower program QEDPS [43–45] to study ISR in the inclusive  $J/\psi$  production processes at B factories. The aim of this section is to review the main formulation of QEDPS briefly. We refer the interested reader to Refs. [43–45] for more details.

The starting point of the whole story is the renormalization group equation of the structure function of an electron. For an electron with the virtuality  $Q^2$  and the momentum fraction x, its structure function  $F(x,Q^2)$  obeys the Dokshitzer–Gribov–Lipatov–Altarelli–Parisi (DGLAP) [46–48] equation in leading-logarithm approximation as [49, 50]

$$\frac{dF(x,Q^2)}{d\log Q^2} = \frac{\alpha}{2\pi} \int_{x}^{1} P_{+}(x/y)F(y,Q^2),$$
 (5.3)

where  $P_{+}(x)$  is Altarelli–Parisi splitting function [48].  $P_{+}(x)$  can be written in a modified form

$$P_{+}(x) \simeq \theta(1 - \varepsilon - x)P(x) - \delta(1 - x) \int_{0}^{1 - \varepsilon} dy P(y),$$

$$P(x) \equiv \frac{1 + x^{2}}{1 - x},$$
(5.4)

where  $\theta(x)$  is the Heaviside theta function,  $\delta(x)$  is the Dirac delta function, and  $\varepsilon$  is a small quantity that will be specified later. Then, the Eq. (5.3) can be solved as

$$F(x, Q^{2}) = \Delta(Q^{2}, Q_{0}^{2})F(x, Q_{0}^{2}) + \frac{\alpha}{2\pi} \int_{Q_{0}^{2}}^{Q^{2}} \frac{dK^{2}}{K^{2}} \Delta(Q^{2}, K^{2}) \int_{x}^{1-\varepsilon} \frac{dy}{y} P(y)F(x/y, K^{2}),$$
 (5.5)

where  $\Delta$  is the Sudakov form factor of the electron

$$\Delta(Q^2, Q_0^2) \equiv \exp(-\frac{\alpha}{2\pi} \int_{Q_0^2}^{Q^2} \frac{dK^2}{K^2} \int_0^{1-\varepsilon} dx P(x)), \tag{5.6}$$

which indicates the probability that no branching<sup>3</sup>  $e^{\pm} \rightarrow e^{\pm} \gamma$  happens from the initial scale  $Q_0$  to the scale Q. For simplicity, no running of  $\alpha$  with  $Q^2$  is understood in Eq. (5.5). One is able to treat the right-hand side of Eq. (5.5) in a successive way as follows [43–45]:

- 1. Set z = 1, where z is the fraction of the collinear momentum of the initial electron.
- 2. Set  $Q_0^2 = m_e^2 e$ , i.e., the initial scale  $Q_0$  is taken as the order of the physical mass of the electron. The Euler's number e is settled to take into account effectively the constant term -1 of  $\beta \equiv (2\alpha/\pi)(\log(s/m_e^2) 1) = (2\alpha/\pi)\log(s/(m_e^2 e))$ .
- 3. Choose a random number r. If it is smaller than  $\Delta(Q^2, Q_0^2)$ , where  $Q^2$  is the virtuality of the initial state  $e^{\pm}$ , the evolution stops. Otherwise, try to find the virtuality  $K^2$  that satisfies  $r = \Delta(K^2, Q_0^2)$ . Branching  $e^{\pm} \rightarrow e^{\pm} \gamma$  happens at virtuality  $K^2$ .
- 4. Fix x according to the probability P(x) between 0 and  $1 \varepsilon$  and replace z by xz.
- 5. Set  $Q_0^2 = K^2$  and go to step 3 until it stops.

Following the algorithm, each branching of a photon is dealt with as

$$e^{\pm}(z, -K^2) \to e^{\pm}(xz, -K'^2) + \gamma((1-x)z, Q_s^2).$$
 (5.7)

where a cutoff  $Q_s^2 = 10^{-12}$  is introduced to avoid the IR divergence. In QEDPS [43–45], the variable  $\varepsilon$  is fixed as

$$\varepsilon \equiv Q_s^2 / K^2. \tag{5.8}$$

Finally, we want to emphasize that a double cascade scheme [51] to ensure the symmetry of the radiation between  $e^-$  and  $e^+$  beams is used in QEDPS, which was proven to be mathematically equivalent to the single-cascade scheme in the leading-logarithm approximation [45].

<sup>&</sup>lt;sup>3</sup>The Sudakov form factor already contains the soft photon emission contributions and the loop corrections in all orders of the leading logarithmic terms.

# 5.3 Numerical Results: QCD, Relativistic and ISR Corrections

Let us present our main numerical results in this section [1]. We will study the ISR effects in  $e^-e^+ \to J/\psi + c\bar{c} + X$  first and then have a look at  $e^-e^+ \to J/\psi + gg + X$ .

$$5.3.1 \ e^-e^+ \to J/\psi + c\bar{c} + X$$

The newest measurement of the cross section for  $e^-e^+ \to J/\psi + c\bar{c} + X$  at B factories was performed by Belle collaboration [25], where they reported

$$\sigma_{prompt}(e^-e^+ \to J/\psi + c\bar{c} + X) = 0.74 \pm 0.08^{+0.09}_{-0.08} \text{ pb.}$$
 (5.9)

Authors of Ref. [27] calculated its CS cross section at NLO in  $\alpha_S$ . They found it was 0.33(0.47) pb when  $m_c = 1.5(1.4)$  GeV and  $\mu = 2m_c$ ,  $|R(0)|^2 = 1.01$  GeV<sup>3</sup>. Moreover, the QED and double photon diagrams also contribute the cross section by 8 + 29 fb [27]. Besides QCD correction, the second important contribution comes from  $\psi(2S)$  feed-down contribution, which enhances the cross section by a factor of 1.355. The contribution from  $\chi_c$  decay is only 21 fb [11, 27]. The CO contribution is very small, and it only contributes 21 fb [11]. The relativistic correction is negligible [13].

In principle, the physical cross section should contain ISR contribution in electron–positron annihilation processes. The distribution of the number of ISR photon in  $e^-e^+ \to J/\psi + c\bar{c} + X$  is shown in Fig. 5.3. As expected, the probability for radiating at least one photon is not small. The average number of ISR photon in each event is about 0.88, which means that it radiates almost one photon in each event. It can be imagined because the probability is estimated roughly as  $\frac{\alpha}{\pi} \log \frac{\hat{s}}{m_e^2}$ . In order to have a good look at the  $\sqrt{\hat{s}}$  distribution after showering, we also plot the  $\sqrt{\hat{s}}/\sqrt{s}$  distribution in Fig. 5.3. The average value of  $\sqrt{\hat{s}}/\sqrt{s}$  is about 0.98. It is quite close to 1 and indicates ISR effect is not important in  $e^-e^+ \to J/\psi + c\bar{c} + X$ .

Figure 5.4 shows the ISR effect in the  $J/\psi$  momentum distribution. We obtain the curves for NLO and NLO + ISR via multiplying the corresponding LO and LO + ISR<sup>4</sup> results with a NLO K factor from Ref. [27]. It is reasonable because the K factor changes mildly in the  $p_{J/\psi}^*$  and  $\sqrt{\hat{s}}$  [18] spectra. Here, we take  $m_c = 1.4$  GeV,  $\mu = 2 \text{m}_c$ ,  $|R(0)|^2 = 1.01$  GeV<sup>3</sup>. ISR shifts the momentum spectrum only by a little amount. To make things clear, we also present the  $K^{\text{ISR}} = \sigma^{\text{LO}+\text{ISR}}/\sigma^{\text{LO}}$  as a function of  $p_{J/\psi}^*$  in the right panel of Fig. 5.4. ISR makes the  $J/\psi$  momentum distribution a little softer near the endpoint. We have compared the Belle measure-

 $<sup>^4</sup>$ Note that, LO + ISR means LO result plus ISR effects. LO result has already included QCD and QED diagrams.

<sup>&</sup>lt;sup>5</sup>Here,  $p_{{\rm J/}\psi}^*$  means the momentum of  ${\rm J/}\psi$  in the rest frame of initial  $e^-e^+$  beams before showering.

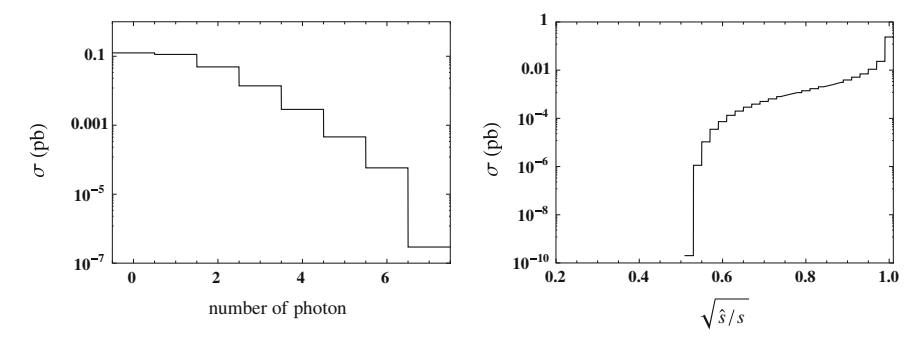


Fig. 5.3 Cross section as functions of number of photon and  $\sqrt{\hat{s}}/\sqrt{s}$  in  $e^-e^+ \to J/\psi + c\bar{c} + X$ 

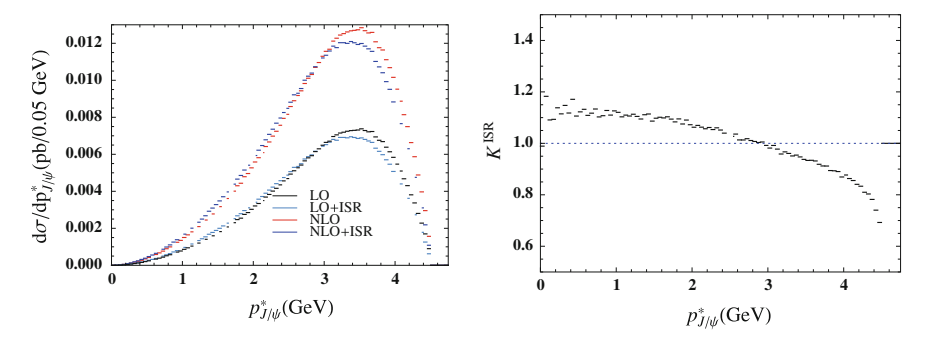


Fig. 5.4 Cross sections and  $K^{\rm ISR}=\sigma^{\rm LO+ISR}/\sigma^{\rm LO}$  as functions of  $J/\psi$  momentum  $p_{J/\psi}^*$  in the rest frame of the initial  $e^-e^+$ . We take the parameter set as  $m_c=1.4$  GeV,  $\mu=2{\rm m_c}$ , in  $e^-e^+\to J/\psi+c\bar c+X$ 

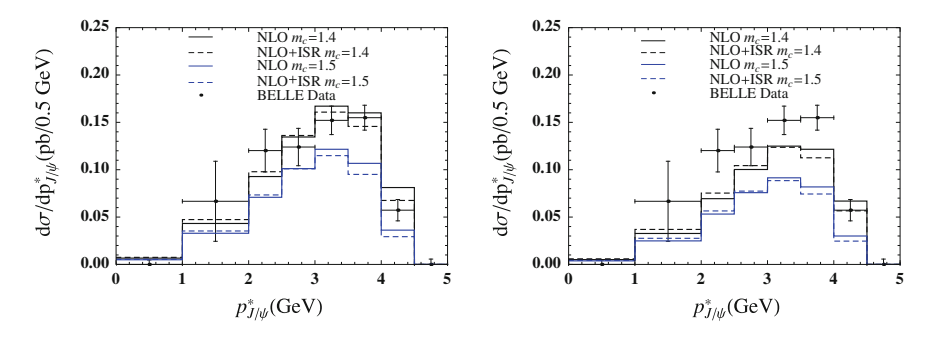


Fig. 5.5 Comparisons of the theoretical predictions and BELLE measurement [25] with  $\mu=2m_c$  (left-panel) and  $\mu=\sqrt{\hat{s}}/2$  (right-panel), respectively, in  $e^-e^+\to J/\psi+c\bar{c}+X$ . We have multiplied a factor 1.355 to account for the feed-down contribution from  $\psi(2S)\to J/\psi+X$ 

		* .	NLO (pb)	NLO + ISR (pb)
$m_c = 1.4 \text{ GeV}, \mu = 2m_c$	0.45	0.44	0.77	0.75
$m_c = 1.5 \text{ GeV}, \mu = 2m_c$	0.31	0.30	0.54	0.53
$m_c = 1.4 \text{ GeV}, \mu = \sqrt{\hat{s}/2}$	0.31	0.31	0.59	0.59
$m_c = 1.5 \text{ GeV}, \mu = \sqrt{\hat{s}/2}$	0.23	0.22	0.42	0.42

**Table 5.1** Cross sections of  $e^-e^+ \rightarrow J/\psi + c\bar{c} + X$  in different parameter sets

ment [25] with the theoretical prompt results in Fig. 5.5. Because of the uncertainties in the input parameters like the charm quark mass  $m_c$  and the renormalization scale  $\mu$ , we compare the experimental result with the theoretical ones in different parameter sets. It is shown that  $m_c = 1.4$  GeV,  $\mu = 2 m_c$ , is the closest set to the Belle data [25]. One should bear in mind that there are large uncertainties both in experimental data and in theoretical results. The total cross sections for prompt  $J/\psi$  production in various parameter sets are summarized in Table 5.1, from which we see that ISR decreases the total cross section of  $e^-e^+ \to J/\psi + c\bar{c} + X$  only a little.

### $5.3.2 \quad e^-e^+ \to J/\psi + gg + X$

For the process  $e^-e^+ \to J/\psi + X_{\rm non-c\bar{c}}$ , Belle collaboration has measured the cross section as [25]

$$\sigma_{prompt}(e^+e^- \to J/\psi + X_{\text{non-}c\bar{c}}) = 0.43 \pm 0.09 \pm 0.09 \text{ pb.}$$
 (5.10)

In the CSM, the NLO QCD correction enhances the cross section for prompt  $J/\psi$  production in  $e^-e^+ \to J/\psi + gg + X$  to be 0.67(0.53) pb when  $m_c = 1.4$  GeV,  $\mu = 2.8(5.3)$  GeV,  $|R(0)|^2 = 1.01$  GeV [21, 22]. The K factor for QCD correction is about 1.2–1.3. Relativistic correction also contributes a factor of 1.20–1.3 compared to the LO one [23, 24]. Hence, roughly, the CS contribution has already saturated the Belle data.

However, this is not the most sever problem. As we have discussed, ISR may also change the cross section substantially. Similar to the case in  $e^-e^+ \to J/\psi + c\bar{c} + X$  production, we plot the number of ISR photon distribution and  $\sqrt{\hat{s}}/\sqrt{s}$  distribution in Fig. 5.6. Unlike  $e^-e^+ \to J/\psi + c\bar{c} + X$ , there is a larger probability to radiate a photon from  $e^\pm$  beams in  $e^-e^+ \to J/\psi + gg + X$ . It can be attributed to the fact that the cross section  $\sigma(e^-e^+ \to J/\psi + gg + X)$  increases when  $\sqrt{\hat{s}}$  becomes smaller near 10.6 GeV. Thus, the average number of photon in each event is enlarging to 1.04, and the average  $\sqrt{\hat{s}}/\sqrt{s}$  becomes 0.93. As expected, ISR is more important in  $e^-e^+ \to J/\psi + gg + X$  than in  $e^-e^+ \to J/\psi + c\bar{c} + X$ .

After including QCD correction and relativistic correction, we obtain the final result in CSM with ISR. Because the QCD correction in  $e^-e^+ \rightarrow J/\psi + gg + X$ 

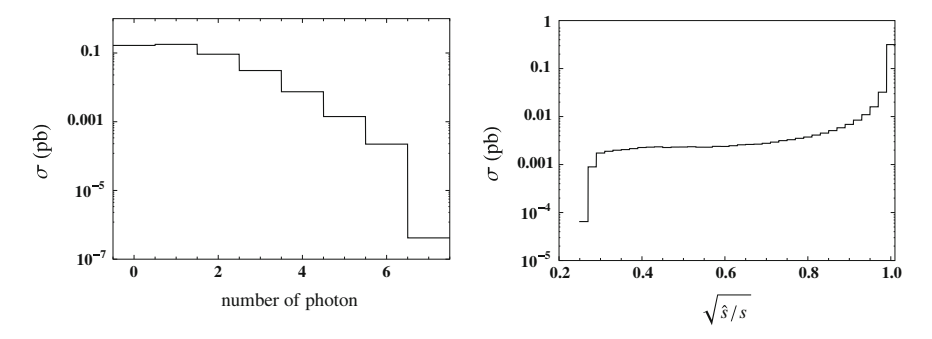


Fig. 5.6 Cross section as functions of number of photon and  $\sqrt{\hat{s}}/\sqrt{s}$  in  $e^-e^+ \to J/\psi + gg + X$ 

makes the  $J/\psi$  momentum  $p_{J/\psi}^*$  distribution much softer than the LO one near the endpoint [21], we use the differential K factor of QCD correction to take into account the QCD correction.<sup>6</sup> Moreover, the relativistic correction does not shift the LO spectrum, and it only enhances the spectrum by a simple constant. We use the formula

$$\frac{d\sigma^{\text{NLO}}}{dp_{J/\psi}^*} = (K^{\text{NLO}(\alpha_s)} + K^{\text{NLO}(v^2)} - 1) \frac{d\sigma^{\text{LO}}}{dp_{J/\psi}^*} 
K^{\text{NLO}(\alpha_s)} = \frac{d\sigma^{\text{NLO}(\alpha_s)}}{dp_{J/\psi}^*} / \frac{d\sigma^{\text{LO}}}{dp_{J/\psi}^*}, 
K^{\text{NLO}(v^2)} = \frac{d\sigma^{\text{NLO}(v^2)}}{dp_{J/\psi}^*} / \frac{d\sigma^{\text{LO}}}{dp_{J/\psi}^*},$$
(5.11)

to get the fixed-order result with QCD and relativistic corrections. Similar formula is applied to the result with ISR

$$\frac{d\sigma^{\text{NLO+ISR}}}{dp_{J/\psi}^*} = (K^{\text{NLO}(\alpha_s)} + K^{\text{NLO}(v^2)} - 1) \frac{d\sigma^{\text{LO+ISR}}}{dp_{J/\psi}^*}, \tag{5.12}$$

which is justified by the fact that ISR and QCD/relativistic correction can be factorized out and the K factors of QCD and relativistic corrections change mildly with  $\sqrt{\hat{s}}$  [22, 23]. Our result is shown in Fig. 5.7. Like the QCD correction, ISR makes the  $J/\psi$  momentum spectrum softer, which is much clear from  $K^{\rm ISR} = \sigma^{\rm LO+ISR}/\sigma^{\rm LO}$  distribution in the right panel of Fig. 5.7. Another interesting thing is whether the K factors are sensitive to  $m_c$  values. We establish two plots in Fig. 5.8. It is easily seen that both of  $K^{\rm ISR} = \sigma^{\rm LO+ISR}/\sigma^{\rm LO}$  and  $K^{\rm NLO} = K^{\rm NLO(\alpha_s)} + K^{\rm NLO(v^2)} - 1$  are indeed insensitive to  $m_c$  when varying  $m_c$  from 1.4 GeV to 1.5 GeV.

<sup>&</sup>lt;sup>6</sup>Although the resummation of  $\log(1-E_{J/\psi}/E_{J/\psi}^{max})$  near the endpoint changes the LO spectrum significantly, it is found that this effect is very small at NLO in  $\alpha_S$  level [21].

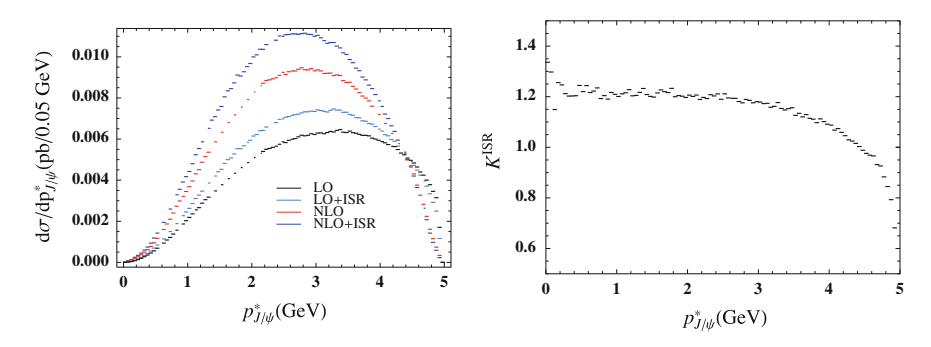
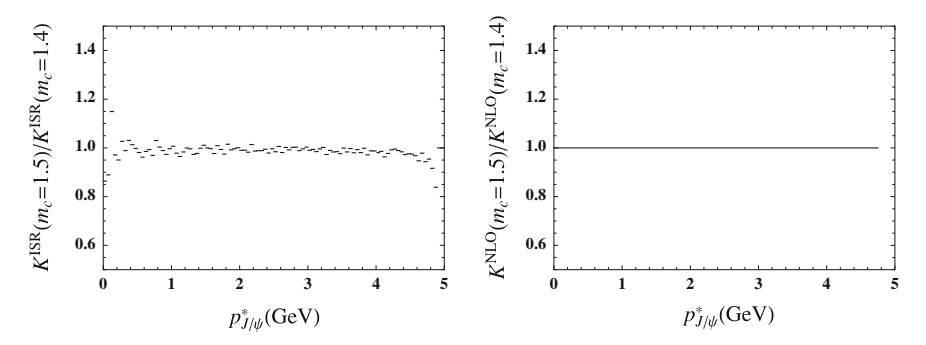


Fig. 5.7 Cross sections and  $K^{\rm ISR}=\sigma^{\rm LO+ISR}/\sigma^{\rm LO}$  as functions of  $J/\psi$  momentum  $p_{J/\psi}^*$  in the rest frame of initial  $e^-e^+$ . We take the parameter set as  $m_c=1.4$  GeV,  $\mu=2{\rm m_c}$  in  $e^-e^+\to J/\psi+gg+X$ 



**Fig. 5.8**  $K^{\rm ISR} = \sigma^{\rm LO+ISR}/\sigma^{\rm LO}$  (*left*) and  $K^{\rm NLO} = \sigma^{\rm NLO}/\sigma^{\rm LO}$  (*right*) as functions of  $J/\psi$  momentum  $p_{J/\psi}^*$  with  $m_c = 1.5$  GeV and  $m_c = 1.4$  GeV and  $\mu = 2m_c$  in  $e^-e^+ \to J/\psi + gg + X$  than in  $e^-e^+ \to J/\psi + c\bar{c} + X$ 

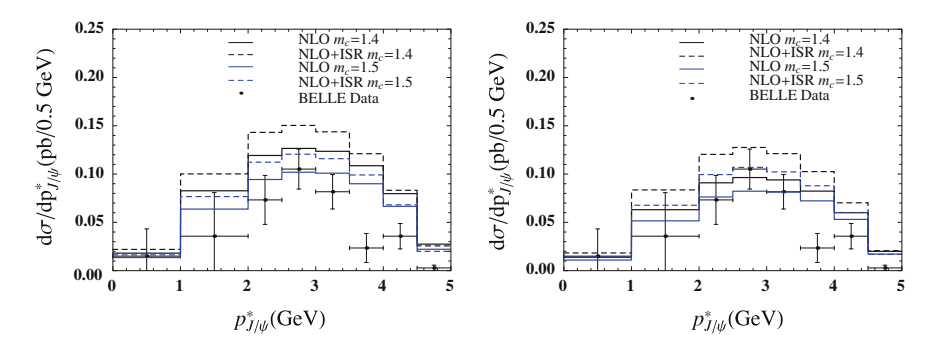


Fig. 5.9 Comparisons of the theoretical predictions and BELLE measurement [25] with  $\mu=2m_c$  (left-panel) and  $\mu=\sqrt{\hat{s}}/2$  (right-panel), respectively, in  $e^-e^+\to J/\psi+gg+X$ . We have multiplied a factor 1.355 to account for the feed-down contribution from  $\psi(2S)\to J/\psi+X$ 

In order to compare the theoretical result with the Belle measurement, we take the same bin size as theirs. The  $J/\psi$  momentum spectrum is shown in Fig. 5.9. We take four different input parameter sets. The CS result is already saturating the experimental data. After combining the OCD correction, relativistic correction and ISR correction, there is a more stringent constraint for CO contribution in  $J/\psi + X_{\text{non-cc}}$ . The total theoretical cross sections for  $e^-e^+ \to J/\psi + gg + X$  in various parameter sets are summarized in Table 5.2. ISR enlarges the cross section of  $e^-e^+ \rightarrow J/\psi + gg + X$  about 15–25 %. We want to point out that although the cross section is a little larger than the experimental data [25], considering large theoretical uncertainties, there is still room to make the theoretical result lower. For example, one can take a lower value of  $|R(0)|^2$  as done in Ref. [22] or from the potential model estimation [20]. However, the ratio  $R_{c\bar{c}}$  is independent of the value of  $|R(0)|^2$  in CSM. We present the theoretical  $R_{c\bar{c}}$  values in Table 5.3. We take the same parameter set in  $e^-e^+ \rightarrow J/\psi + c\bar{c} + X$  and  $e^-e^+ \rightarrow J/\psi + gg + X$  and assume  $\sigma(e^-e^+ \to J/\psi + gg + X) = \sigma(e^-e^+ \to J/\psi + X_{non-c\bar{c}})$ . It seems that the theoretical result is lower than Belle measurement, but it is still within 2 standard deviations. Therefore, we expect that a more precise measurement will clarify the situation. Finally, we also list the total cross section  $\sigma(e^-e^+ \to J/\psi + X) = \sigma(e^-e^+ \to J/\psi + X)$  $J/\psi + c\bar{c} + X$ ) +  $\sigma(e^-e^+ \rightarrow J/\psi + gg + X)$  in Table 5.4. It is compatible with the

**Table 5.2** Cross sections of  $e^-e^+ \rightarrow J/\psi + gg + X$  in different parameter sets

Parameter sets	LO (pb)	LO+ISR (pb)	NLO (pb)	NLO+ISR (pb)
$m_c = 1.4 \text{ GeV}, \mu = 2\text{m}_c$	0.57	0.65	0.79	0.91
$m_c = 1.5 \text{ GeV}, \mu = 2m_c$	0.45	0.50	0.63	0.72
$m_c = 1.4 \text{ GeV}, \mu = \sqrt{\hat{s}/2}$	0.35	0.45	0.60	0.77
$m_c = 1.5 \text{ GeV}, \mu = \sqrt{\hat{s}}/2$	0.30	0.37	0.51	0.64

**Table 5.3** Comparisons of  $R_{c\bar{c}}$  in different parameter sets with BELLE measurement [25]

Parameter sets	LO	LO+ISR	NLO	NLO+ISR	BELLE
$m_c = 1.4 \text{ GeV}, \mu = 2\text{m}_c$	0.44	0.41	0.49	0.45	$0.63 \pm 0.11$
$m_c = 1.5 \text{ GeV}, \mu = 2\text{m}_c$	0.41	0.38	0.46	0.42	$0.63 \pm 0.11$
$m_c = 1.4 \text{ GeV}, \mu = \sqrt{\hat{s}/2}$	0.47	0.41	0.50	0.44	$0.63 \pm 0.11$
$m_c = 1.5 \text{ GeV}, \mu = \sqrt{\hat{s}}/2$	0.43	0.38	0.45	0.40	$0.63 \pm 0.11$

**Table 5.4** Cross sections of  $e^-e^+ \rightarrow J/\psi + X$  in different parameter sets

Parameter sets	LO (pb)	LO + ISR (pb)	NLO (pb)	NLO + ISR (pb)
$m_c = 1.4 \text{ GeV}, \mu = 2\text{m}_c$	1.02	1.09	1.55	1.66
$m_c = 1.5 \text{ GeV}, \mu = 2\text{m}_c$	0.76	0.80	1.17	1.25
$m_c = 1.4 \text{ GeV}, \mu = \sqrt{\hat{s}/2}$	0.66	0.76	1.19	1.36
$m_c = 1.5 \text{ GeV}, \mu = \sqrt{\hat{s}}/2$	0.52	0.59	0.93	1.05

Belle experiment [25] value  $\sigma_{\text{prompt}}(e^-e^+ \to J/\psi + X) = 1.17 \pm 0.02 \pm 0.07$  pb. We look forward to the future measurements at the super B factories.

### References

- 1. H.S. Shao, JHEP **04**, 182 (2014)
- 2. B. Aubert et al., Phys. Rev. Lett. 87, 162002 (2001). doi:10.1103/PhysRevLett.87.162002
- 3. K. Abe et al., Phys. Rev. Lett. 88, 052001 (2002). doi:10.1103/PhysRevLett.88.052001
- V. Kiselev, A. Likhoded, M. Shevlyagin, Phys. Lett. B332, 411 (1994). doi:10.1016/0370-2693(94)91273-4
- 5. F. Yuan, C.F. Qiao, K.T. Chao, Phys. Rev. D56, 321 (1997). doi:10.1103/PhysRevD.56.321
- 6. P.L. Cho, A.K. Leibovich, Phys. Rev. D54, 6690 (1996). doi:10.1103/PhysRevD.54.6690
- 7. S. Baek, P. Ko, J. Lee, H. Song, J. Korean Phys. Soc. 33, 97 (1998)
- 8. G.A. Schuler, Eur. Phys. J. C8, 273 (1999). doi:10.1007/s100529900948
- K.Y. Liu, Z.G. He, K.T. Chao, Phys. Rev. D68, 031501 (2003). doi:10.1103/PhysRevD.68. 031501
- 10. K. Abe et al., Phys. Rev. Lett. 89, 142001 (2002). doi:10.1103/PhysRevLett.89.142001
- K.Y. Liu, Z.G. He, K.T. Chao, Phys. Rev. D69, 094027 (2004). doi:10.1103/PhysRevD.69. 094027
- K. Hagiwara, E. Kou, Z. Lin, C. Qiao, G. Zhu, Phys. Rev. D70, 034013 (2004). doi:10.1103/ PhysRevD.70.034013
- 13. Z.G. He, Y. Fan, K.T. Chao, Phys. Rev. D75, 074011 (2007). doi:10.1103/PhysRevD.75.074011
- S. Fleming, A.K. Leibovich, T. Mehen, Phys. Rev. D68, 094011 (2003). doi:10.1103/ PhysRevD.68.094011
- 15. Z.H. Lin, G.h. Zhu. Phys. Lett. **B597**, 382 (2004). doi:10.1016/j.physletb.2004.07.037
- 16. A.K. Leibovich, X. Liu, Phys. Rev. D76, 034005 (2007). doi:10.1103/PhysRevD.76.034005
- Y.J. Zhang, K.T. Chao, Phys. Rev. Lett. 98, 092003 (2007). doi:10.1103/PhysRevLett.98. 092003
- 18. B. Gong, J.X. Wang, Phys. Rev. **D80**, 054015 (2009). doi:10.1103/PhysRevD.80.054015
- 19. W. Yao et al., J. Phys. **G33**, 1 (2006). doi:10.1088/0954-3899/33/1/001
- 20. E.J. Eichten, C. Quigg, Phys. Rev. **D52**, 1726 (1995). doi:10.1103/PhysRevD.52.1726
- Y.Q. Ma, Y.J. Zhang, K.T. Chao, Phys. Rev. Lett. 102, 162002 (2009). doi:10.1103/ PhysRevLett.102.162002
- B. Gong, J.X. Wang, Phys. Rev. Lett. 102, 162003 (2009). doi:10.1103/PhysRevLett.102. 162003
- 23. Z.G. He, Y. Fan, K.T. Chao, Phys. Rev. D81, 054036 (2010). doi:10.1103/PhysRevD.81.054036
- 24. Y. Jia, Phys. Rev. **D82**, 034017 (2010). doi:10.1103/PhysRevD.82.034017
- 25. P. Pakhlov et al., Phys. Rev. **D79**, 071101 (2009), doi:10.1103/PhysRevD.79.071101
- 26. E. Braaten, Y.Q. Chen, Phys. Rev. Lett. 76, 730 (1996). doi:10.1103/PhysRevLett.76.730
- Y.J. Zhang, Y.Q. Ma, K. Wang, K.T. Chao, Phys. Rev. D81, 034015 (2010). doi:10.1103/ PhysRevD.81.034015
- Y.Q. Ma, K. Wang, K.T. Chao, Phys. Rev. Lett. 106, 042002 (2011). doi:10.1103/PhysRevLett. 106.042002
- Y.Q. Ma, K. Wang, K.T. Chao, Phys. Rev. D84, 114001 (2011). doi:10.1103/PhysRevD.84. 114001
- 30. K.T. Chao, Y.Q. Ma, H.S. Shao, K. Wang, Y.J. Zhang, Phys. Rev. Lett. 108, 242004 (2012)
- 31. B. Gong, L.P. Wan, J.X. Wang, H.F. Zhang, Phys. Rev. Lett. 110, 042002 (2013)
- 32. G.T. Bodwin, H.S. Chung, U.R. Kim, J. Lee, Phys. Rev. Lett. **113**(2), 022001 (2014). doi:10. 1103/PhysRevLett.113.022001
- P. Faccioli, V. Knnz, C. Lourenco, J. Seixas, H.K. Whri, Phys. Lett. B736, 98 (2014). doi:10. 1016/j.physletb.2014.07.006

References 85

 M. Butenschoen, B.A. Kniehl, Phys. Rev. Lett. 106, 022003 (2011). doi:10.1103/PhysRevLett. 106.022003

- M. Butenschoen, B.A. Kniehl, Phys. Rev. D84, 051501 (2011). doi:10.1103/PhysRevD.84. 051501
- 36. M. Butenschoen, B.A. Kniehl, Phys. Rev. Lett. 108, 172002 (2012)
- G. Bonvicini, L. Trentadue, Nucl. Phys. B323, 253 (1989). doi:10.1016/0550-3213(89)90142-
- 38. S. Jadach, B. Ward, Comput. Phys. Commun. **56**, 351 (1990). doi:10.1016/0010-4655(90)90020-2
- S. Jadach, E. Richter-Was, B. Ward, Z. Was, Comput. Phys. Commun. 70, 305 (1992). doi:10. 1016/0010-4655(92)90196-6
- 40. H. Dahmen, P. Manakos, T. Mannel, T. Ohl, Z. Phys. C50, 75 (1991). doi:10.1007/BF01558560
- 41. M. Caffo, H. Czyz, E. Remiddi, Nuovo Cim. A105, 277 (1992). doi:10.1007/BF02826033
- M. Caffo, E. Remiddi, H. Czyz, Int. J. Mod. Phys. C4, 591 (1993). doi:10.1142/ S0129183193000574
- 43. J. Fujimoto, Y. Shimizu, T. Munehisa, Prog. Theor. Phys. **91**, 333 (1994). doi:10.1143/PTP.91.
- J. Fujimoto, Y. Shimizu, T. Munehisa, Prog. Theor. Phys. 90, 177 (1993). doi:10.1143/PTP.90.
   177
- T. Munehisa, J. Fujimoto, Y. Kurihara, Y. Shimizu, Prog. Theor. Phys. 95, 375 (1996). doi:10. 1143/PTP.95.375
- 46. V. Gribov, L. Lipatov, Sov. J. Nucl. Phys. **15**, 438 (1972)
- 47. Y.L. Dokshitzer. Sov. Phys. JETP 46, 641 (1977)
- 48. G. Altarelli, G. Parisi, Nucl. Phys. B126, 298 (1977). doi:10.1016/0550-3213(77)90384-4
- 49. R. Odorico, Nucl. Phys. **B172**, 157 (1980). doi:10.1016/0550-3213(80)90165-0
- 50. G. Marchesini, B. Webber, Nucl. Phys. **B238**, 1 (1984). doi:10.1016/0550-3213(84)90463-2
- 51. K. Kato, T. Munehisa, Phys. Rev. D39, 156 (1989). doi:10.1103/PhysRevD.39.156

# **Chapter 6 Summary and Outlooks of Part I**

In the first part of this thesis, we have presented our studies on quarkonium production mechanism, which provides a good way to study the non-perturbative QCD. Quarkonium production processes are typical multiscale processes. Its investigation provides us a good opportunity to study non-perturbative QCD physics via perturbative computations. The state-of-the-art theory to describe quarkonium production is NRQCD. However, there are still several challenges in it. We summarize them as follows:

- It is still lacking the proof of the factorization theorem.
- It suffers from very large K factors of high-order QCD corrections.
- It confronts the rich experimental data to test.

The novel feature of NRQCD effective theory is that it also predicts the COM in quarkonium production processes besides CS production mechanism. However, to be honest, it is still unclear whether COM is really important in describing quarkonium production processes, which of course should be answered by experiments. In the first part of this thesis, we have presented the following studies on the quarkonium production processes

- 1. We develop a Monte Carlo generator HELAC-ONIA for quarkonium production based on recursion relation. It can be applied to study one or more quarkonium production processes in SM. The Fock states can be up to P-waves. Moreover, it also provides the user more flexible observables to study quarkonium physics, like the SDMEs of quarkonium. We have also interfaced the parton shower Monte Carlo generators with HELAC-ONIA. It provides us a very powerful tool to study the quarkonium physics in the following aspects.
- 2. With HELAC-ONIA, we have presented the state-of-the-art perturbative computations to various quarkonium production processes at hadron colliders. All the processes are promoted to NLO level in  $\alpha_S$ . They include the yields and

- polarizations of prompt  $J/\psi$ ,  $\psi(2S)$ ,  $\chi_c$ , and the  $J/\psi$ -pair production. Except the  $J/\psi$ -pair production process, the COM are very crucial in describing the high- $p_T$  LHC data (both yields and polarizations) in above processes. It may indicate that NRQCD factorization is not valid at low momentum transfer regime. This strong statement should be confirmed by other quarkonium production processes and the measurements of other observables in the future experiments. Theoretically, it is also very crucial to make the progress in proving the NRQCD factorization conjecture. All of these observations should be understood at least at NLO level.
- 3. We also study the prompt  $J/\psi$  production in electron–positron annihilation at B factories. We found beside QCD and relativistic corrections, ISR effect is also very important. It gives a very stringent constraint to the CO contribution to  $J/\psi$  production at B factories. Combining with other studies, it seems that at low momentum transfer regime, CS mechanism is already enough, and it is satisfactory to describe the experimental data. Of course, this conjecture should also be verified by more accurate experiments and theoretical results.

In the future, it may be very useful to extend HELAC-ONIA to be applicable to other aspects of physics (e.g., heavy ion collisions, transverse momentum-dependent factorization, and quarkonium decay). It is also very important to develop it to perform higher-order calculations. We can compare more quarkonium production processes with experiments. Theoretically, the NRQCD factorization proof is very important and may be urgent. Finally, we want to point out that it is very interesting to know which mechanism is able to describe the quarkonium production at the intermediate  $p_T$  regime.

# Part II Automation of One-Loop Scattering Amplitudes Computations

# **Chapter 7 NLO Computations and Automation Philosophy**

**Abstract** In this chapter, we will give a brief introduction to the relevant background of the second part. It consists of three aspects. After we present some general remarks in Sect. 7.1, we will introduce the basic concepts of NLO computations, including IR and ultraviolet (UV) divergences cancellations. Finally, we will emphasize the automation philosophy.

### 7.1 General Remarks

Phenomenological analysis of collider physics is already heavily relying on the perturbative calculations of scattering amplitudes in QFT. With the large samples accumulated at the LHC, many experimental measurements have entered into the precision era, which promotes us to be not satisfied with the rough LO theoretical estimations anymore. There are two shortcomings of theoretical results at LO level: LO results usually suffer from large theoretical uncertainties and sometimes (not barely) predict wrong cross sections and/or shapes. Hence, it is often demanded to present theoretical results by taking into account the NLO quantum corrections (e.g., QCD corrections or QED/EW corrections) in the SM.

More than a decade ago, it was still a challenge to present a NLO prediction for a  $2 \rightarrow n (n \ge 3)$  process. The situation radically changes since the rapid development in the studies of NLO computations in the recent 10 years. The main improvements are classified into the following aspects:

- The evolution of one-loop integrals evaluations with the so-called unitary-based methods [1–8].
- The introduction of the universal formalisms for the cancellation of IR divergences [9–19].
- The developments of more efficient algorithms for computing multileg processes at tree level [20–23].

Moreover, these new techniques are also written into various programs, which allows people to get rid of the shackles of the limitations of the human brains and to perform practical and complex phenomenological analysis for the multileg processes

at various colliders. The automatic or semi-automatic NLO programs on the market are: FormCalc/FeynArts [24–26], BlackHat/Sherpa [27–31], MadDipole [32, 33], Rocket [34], Helac-Nlo [16, 35], MadFkS4/MadLoop4 [36, 37], AutoDipole [38], GoSam [3, 39], OpenLoops [40], MadGolem [41, 42], Recola [43], NGLuon/NJet [44, 45], MadGraph5\_AMC@Nlo[46].

Apart from the progress in the fixed-order calculations, there are also significant developments in Monte Carlo simulations, in which it provides us a mimic way to describe the dynamics and the kinematics of the strong-interactive particles at the detector level. There are several reasons to emphasize why Monte Carlo simulation is important in describing particles production processes at high energy colliders. First, it provides a relatively good description of QCD radiation in the non-perturbative regime (in the soft and/or collinear regime), where the fixed-order calculations are not reliable anymore. By accounting for the so-called Sudakov factor via a Markov chain process, it is able to include the leading important contribution up to all orders in  $\alpha_S$ . Second, the determination of the efficiencies and acceptances of the experiments is usually required for Monte Carlo simulations. Third, the Monte Carlo simulation is necessary to present an exclusive OCD prediction. Hence, it provides a better and precise theoretical result after combining the fixed-order calculations with Monte Carlo results. This task is in principle trivial at LO, while it is not so straightforward at NLO level. Two main approaches for matching the NLO matrix elements to the Monte Carlo event generators are available: the MC@NLO [47] and the POWHEG [48] methods.

# 7.2 Basic Concepts of NLO Computations

The basic procedures of the NLO computations for any scattering process are text-book like and standard. It consists of three groups of scattering amplitudes: Born, one-loop and real emission. For example, let us assume a n-body final states process. The relevant amplitudes are denoted as

Born: 
$$\mathscr{A}^{(n,0)} \Longrightarrow n$$
-body tree-level Feynman diagrams (7.1) one-loop:  $\mathscr{A}^{(n,1)} \Longrightarrow n$ -body one-loop Feynman diagrams real-emission:  $\mathscr{A}^{(n+1,0)} \Longrightarrow (n+1)$ -body tree-level Feynman diagrams.

Without losing generality, a NLO level cross section can be written as

$$\sigma^{\text{NLO}} \equiv \int_{n} |\mathscr{A}^{(n,0)}|^{2} + \int_{n} 2\Re\{\mathscr{A}^{(n,1)}\mathscr{A}^{(n,0)*}\} + \int_{n+1} |\mathscr{A}^{(n+1,0)}|^{2}, \tag{7.2}$$

where  $\int_n$  is a *n*-body phase space integration. Situation is complicated because there are divergences in the last two terms of Eq. (7.2). Hence, regularization schemes are necessary to regulate these divergences. The most notable regularization method is

the dimensional regularization [49], which is based on the fact that the scattering amplitudes are the analytic functions of the dimensions of the space-time. In dimensional regularization, the dimensions of the space-time are continued to  $d=4-2\varepsilon$ . The final physical results are obtained after taking the limitation of  $\varepsilon \to 0$ , i.e., after recovering the physical four-dimensional space-time.

Let us take a simple example. The divergences are much apparent from integrating a simple 2-point one-loop integral

$$B_0 \equiv \int d^d \bar{\ell} \frac{1}{(\bar{\ell}^2)^2} = \int d\bar{\ell}_0 d^{d-1} \bar{\ell} \frac{1}{(\bar{\ell}_0^2 - |\bar{\ell}|^2)^2}.$$
 (7.3)

After Wick rotation  $\bar{\ell}_0 \to i\bar{\ell}_0$  and transforming into d-dimensional spherical coordinates, the integral becomes

$$B_{0} = i \int d\Omega_{d} \int_{0}^{+\infty} d|\bar{\ell}||\bar{\ell}|^{d-5} = i \frac{2\pi^{d/2}}{\Gamma(d/2)} \times \int_{0}^{+\infty} d|\bar{\ell}||\bar{\ell}|^{d-5}$$

$$= i \frac{2\pi^{d/2}}{\Gamma(d/2)} \times \left(\int_{1}^{+\infty} d|\bar{\ell}||\bar{\ell}|^{d-5} + \int_{0}^{1} d|\bar{\ell}||\bar{\ell}|^{d-5}\right). \tag{7.4}$$

The first piece in the parentheses of Eq. (7.4) is finite only when d < 4, whereas the second piece is finite only when d > 4. Both of them are divergent when  $d \to 4$ . Due to the different sources, the divergences in the first and second terms are called the UV and IR divergences, respectively. To avoid the possible confusions, we denote  $d = 4 - 2\varepsilon_{\rm UV}$  and  $d = 4 - 2\varepsilon_{\rm IR}$  in the two pieces, respectively. We have

$$B_0 = i \frac{2\pi^{d/2}}{\Gamma(d/2)} \times \left(-\frac{1}{-2\varepsilon_{\text{UV}}} + \frac{1}{-2\varepsilon_{\text{IR}}}\right) = i\pi^2 \times \left(\frac{1}{\varepsilon_{\text{UV}}} - \frac{1}{\varepsilon_{\text{IR}}}\right), \tag{7.5}$$

where we have taken  $d \to 4$  in the last equal sign. From the above example, we understand that the UV divergence  $\frac{1}{\varepsilon_{\rm UV}}$  comes from the large momentum mode  $|\bar{\ell}| \sim +\infty$ , whereas the IR divergence  $\frac{1}{\varepsilon_{\rm IR}}$  originates from the small momentum mode  $|\bar{\ell}| \sim 0$ . Such a situation will not be altered for a general loop integral.

The UV divergences in the one-loop amplitudes should be removed via a so-called renormalization procedure, which implies that the impacts of the unknown high scale  $|\bar{\ell}| \sim +\infty$  physics should be absorbed into the measured observables of the lowenergy effective theory. It results into a decoupling form between the unknown high scale physics and the known low-energy effective theory. We refer the interested reader to Ref. [50] for more renormalization-related discussions. In the following, we call the renormalized one-loop part as the virtual part.

Due to the IR safety of the cross section, the IR divergences in the virtual part (the second piece of Eq. (7.2)) can be canceled by those in the real-emission part (the

third piece of Eq. (7.2)), which is guaranteed by Kinoshita–Lee–Nauenberg (KLN) theorem [51, 52]. Schematically, we have the combination

$$2\Re\{\mathscr{A}^{(n,1)}\mathscr{A}^{(n,0)*}\} + \int_{1} |\mathscr{A}^{(n+1,0)}|^{2}$$
 (7.6)

to be finite. This fact is easy to be understood from the Feynman's Tree Theorem [53–55], which relates perturbative scattering amplitudes and Green functions at the loop level with the analogous quantities at the tree level. This relation follows an elementary relation between the loop integrals and the phase-space integrals. It guarantees the two parts in Eq. (7.6) share the same magnitude IR divergence, but they are in opposite signs.

Let us consider a simple example, in which we have

$$|\mathscr{A}^{(n,0)}|^{2} = B,$$

$$2\Re\{\mathscr{A}^{(n,1)}\mathscr{A}^{(n,0)*}\} = \frac{\alpha_{X}}{\pi} (\frac{B}{2\varepsilon_{\text{IR}}} + V),$$

$$|\mathscr{A}^{(n+1,0)}|^{2} = \frac{\alpha_{X}}{\pi} \frac{R(x)}{x},$$
(7.7)

where we have assumed that  $\int_1$  is only an integration of variable x and the perturbative expansion is via  $\frac{\alpha_x}{\pi}$ . From Eq. (7.7), one sees that the IR divergence in virtual is proportional to the Born one, which is the exact case in QED. The form has a generalization in the non-abelian gauge theories such as QCD (see e.g. Ref. [36]). For an arbitrary IR safe observable  $\mathcal{O}$ , one has

$$\lim_{x \to 0} \mathcal{O}(x)R(x) = \mathcal{O}(0)B. \tag{7.8}$$

Then, the quantity

$$\mathcal{O}(0)2\Re\{\mathcal{A}^{(n,1)}\mathcal{A}^{(n,0)*}\} + \int_{1} \mathcal{O}(x)|\mathcal{A}^{(n+1,0)}|^{2}$$

$$= \frac{\alpha_{X}}{\pi} \left[ \mathcal{O}(0)(\frac{B}{2\varepsilon_{IR}} + V) + \int_{0}^{1} dx x^{-1-2\varepsilon_{IR}} \mathcal{O}(x) R(x) \right]$$

$$= \frac{\alpha_{X}}{\pi} \left[ \mathcal{O}(0)(\frac{B}{2\varepsilon_{IR}} + V) + \left( -\mathcal{O}(0) \frac{B}{2\varepsilon_{IR}} + \int_{0}^{1} dx \left( \frac{1}{x} \right)_{+} \mathcal{O}(x) R(x) \right) \right]$$

$$= \frac{\alpha_{X}}{\pi} \left[ \mathcal{O}(0)V + \int_{0}^{1} dx \left( \frac{1}{x} \right)_{+} \mathcal{O}(x) R(x) \right]$$

$$(7.9)$$

is IR finite, where we have used

$$x^{-1-2\varepsilon_{\rm IR}} = -\frac{1}{2\varepsilon_{\rm IR}}\delta(x) + \left(\frac{1}{x}\right)_{\perp} - 2\varepsilon_{\rm IR}\left(\frac{\log x}{x}\right)_{\perp} + O(\varepsilon_{\rm IR}^2). \tag{7.10}$$

The plus functions are defined as

$$\left(\frac{1}{x}\right)_{+} f(x) \equiv \frac{f(x) - f(0)}{x},$$

$$\left(\frac{\log x}{x}\right)_{+} f(x) \equiv \frac{(f(x) - f(0))\log x}{x},$$
(7.11)

and  $\delta(x)$  is the Dirac function.

For a practical process, because of the complicities in the amplitudes and in the kinematics, the integration of the one-body phase space in Eq. (7.6) is difficult. Two main approaches are usually adopted by people to separate IR divergences in the real-emission part. One is the phase space slicing method [56-59] and the other one is the IR subtraction method [9-19, 60-62].

In the phase space slicing method, the real-emission phase space is divided into various regions and approximations are taken in the unresolved regions. In our example, we can introduce a small parameter  $\varepsilon$  and obtain

$$\int_{0}^{1} dx x^{-1-2\varepsilon_{\mathrm{IR}}} \mathscr{O}(x) R(x) = \left(\int_{0}^{\varepsilon} + \int_{\varepsilon}^{1}\right) dx x^{-1-2\varepsilon_{\mathrm{IR}}} \mathscr{O}(x) R(x)$$

$$= \left(-\mathscr{O}(0) \frac{B}{2\varepsilon_{\mathrm{IR}}} \varepsilon^{-2\varepsilon_{\mathrm{IR}}} + O(\varepsilon)\right)$$

$$+ \left(\int_{\varepsilon}^{1} dx x^{-1} \mathscr{O}(x) R(x) + O(\varepsilon_{\mathrm{IR}})\right)$$

$$= \left(-\mathscr{O}(0) \frac{B}{2\varepsilon_{\mathrm{IR}}} + \mathscr{O}(0) B \log \varepsilon + O(\varepsilon, \varepsilon_{\mathrm{IR}})\right)$$

$$+ \left(\int_{\varepsilon}^{1} dx x^{-1} \mathscr{O}(x) R(x) + O(\varepsilon_{\mathrm{IR}})\right)$$

$$= -\mathscr{O}(0) \frac{B}{2\varepsilon_{\mathrm{IR}}} + \mathscr{O}(0) B \log \varepsilon$$

$$+ \int_{0}^{1} dx x^{-1} \mathscr{O}(x) R(x) + O(\varepsilon), \tag{7.12}$$

where we have ignored the vanishing terms when  $\varepsilon_{\rm IR} \to 0$  in the last equal sign. One notices that the accuracy in the phase space slicing method is at best  $O(\varepsilon)$  due to their ignorance. Another disadvantage in the phase space slicing method is that numerical accuracy will lose due to large cancellation between  $\mathcal{O}(0)B\log\varepsilon$  and  $\int_{-1}^{1} dx x^{-1} \mathcal{O}(x) R(x)$ .

The IR subtraction method is the most commonly used method to handle IR divergences especially in multileg processes. The basic idea is to find a relatively simple

and universal form S, which shares the same singular behavior with  $|\mathscr{A}^{(n+1,0)}|^2$  but is easier to be integrated analytically

$$\int_{1} S. \tag{7.13}$$

Then, one can do the following subtraction

$$2\Re\{\mathscr{A}^{(n,1)}\mathscr{A}^{(n,0)*}\} + \int_{1} |\mathscr{A}^{(n+1,0)}|^{2} = (2\Re\{\mathscr{A}^{(n,1)}\mathscr{A}^{(n,0)*}\} + \int_{1} S) + \int_{1} (|\mathscr{A}^{(n+1,0)}|^{2} - S)$$

$$(7.14)$$

to make the two part IR finite. In principle, the functional form of *S* in the non-singular region is not restricted. Different choices of *S* result in different subtraction schemes. In our above example, we can choose

$$S(x) = \frac{\alpha_X}{\pi} \mathscr{O}(0) B\Theta(\xi - x), \tag{7.15}$$

where  $\xi$  is an arbitrary number between  $0 < \xi \le 1$  and  $\Theta$  is the Heaviside function. The integrated subtraction term is

$$\int_0^1 dx x^{-1-2\varepsilon_{\rm IR}} S(x) = \frac{\alpha_X}{\pi} \left( -\mathscr{O}(0) \frac{B}{2\varepsilon_{\rm IR}} + \mathscr{O}(0) B \log \xi \right). \tag{7.16}$$

Then,

$$\mathcal{O}(0)2\Re\{\mathcal{A}^{(n,1)}\mathcal{A}^{(n,0)*}\} + \int_{1} \mathcal{O}(x)|\mathcal{A}^{(n+1,0)}|^{2}$$

$$= \frac{\alpha_{X}}{\pi}\mathcal{O}(0)\left(V + B\log\xi\right)$$

$$+ \frac{\alpha_{X}}{\pi}\int_{0}^{1} dx \frac{\mathcal{O}(x)R(x) - \mathcal{O}(0)B\Theta(\xi - x)}{x}.$$
(7.17)

By contrast to the phase space slicing method, the subtraction method is free of any large numerical cancellation or any approximation.

# 7.3 Why Automation

The aim of this section is to establish the advantages of automation, which has been realized recently at NLO level [46]. The automation advances the physical study. We summarize the advantages in the following aspects

- Automation saves people a lot of time and man power. During the past 15 years, a
  lot of physicists devoted themselves to NLO computations. Their efforts make a lot
  of progress in the computational techniques and physical understanding. Thanks
  to the past efforts, automatic analysis at NLO level plus parton shower simulation
  is already feasible. A NLO level phenomenological analysis does not require you
  to be an expert on the NLO calculations in OFT.
- Automation also has the advantage in avoiding (repeated and sometimes stupid) mistakes.
- It is very convenient for people to share the state-of-the-art techniques in the whole physics community. For example, people have proposed a standard interface between Monte Carlo tools and one-loop programs, which is called Binoth Les Houches Accord (BLHA) format [63, 64].
- Finally, automation makes people to focus on their physics study and phenomenological analysis only.

### References

- G. Ossola, C.G. Papadopoulos, R. Pittau, Nucl. Phys. B 763, 147 (2007). doi:10.1016/j. nuclphysb.2006.11.012
- 2. F. del Aguila, R. Pittau, JHEP 07, 017 (2004). doi:10.1088/1126-6708/2004/07/017
- P. Mastrolia, G. Ossola, T. Reiter, F. Tramontano, JHEP 1008, 080 (2010). doi:10.1007/ JHEP08(2010)080
- Z. Bern, L.J. Dixon, D.C. Dunbar, D.A. Kosower, Nucl. Phys. B 425, 217 (1994). doi:10.1016/ 0550-3213(94)90179-1
- R. Britto, F. Cachazo, B. Feng, Nucl. Phys. B 725, 275 (2005). doi:10.1016/j.nuclphysb.2005. 07.014
- 6. R.K. Ellis, W. Giele, Z. Kunszt, JHEP 0803, 003 (2008). doi:10.1088/1126-6708/2008/03/003
- R.K. Ellis, W.T. Giele, Z. Kunszt, K. Melnikov, Nucl. Phys. B 822, 270 (2009). doi:10.1016/j.nuclphysb.2009.07.023
- W.T. Giele, Z. Kunszt, K. Melnikov, JHEP 0804, 049 (2008). doi:10.1088/1126-6708/2008/ 04/049
- S. Frixione, Z. Kunszt, A. Signer, Nucl. Phys. B 467, 399 (1996). doi:10.1016/0550-3213(96)00110-1
- 10. S. Frixione, Nucl. Phys. B **507**, 295 (1997), doi:10.1016/S0550-3213(97)00574-9
- 11. S. Frixione, JHEP 1109, 091 (2011). doi:10.1007/JHEP09(2011)091
- 12. S. Catani, M. Seymour, Nucl. Phys. B 485, 291 (1997). doi:10.1016/S0550-3213(96)00589-5
- S. Catani, S. Dittmaier, M.H. Seymour, Z. Trocsanyi, Nucl. Phys. B 627, 189 (2002). doi:10. 1016/S0550-3213(02)00098-6
- 14. S. Dittmaier, Nucl. Phys. B **565**, 69 (2000). doi:10.1016/S0550-3213(99)00563-5
- 15. L. Phaf, S. Weinzierl, JHEP **0104**, 006 (2001)
- M. Czakon, C. Papadopoulos, M. Worek, JHEP 0908, 085 (2009). doi:10.1088/1126-6708/ 2009/08/085
- 17. D.A. Kosower, Phys. Rev. D 57, 5410 (1998). doi:10.1103/PhysRevD.57.5410
- 18. D.A. Kosower, Phys. Rev. D 71, 045016 (2005). doi:10.1103/PhysRevD.71.045016
- J.M. Campbell, M. Cullen, E.N. Glover, Eur. Phys. J. C 9, 245 (1999). doi:10.1007/ s100529900034
- F.A. Berends, W.T. Giele, Nucl. Phys. B 306, 759 (1988). doi:10.1016/0550-3213(88)90442-7

- R. Britto, F. Cachazo, B. Feng, Nucl. Phys. B 715, 499 (2005). doi:10.1016/j.nuclphysb.2005. 02.030
- R. Britto, F. Cachazo, B. Feng, E. Witten, Phys. Rev. Lett. 94, 181602 (2005). doi:10.1103/ PhysRevLett.94.181602
- F. Maltoni, K. Paul, T. Stelzer, S. Willenbrock, Phys. Rev. D 67, 014026 (2003). doi:10.1103/ PhysRevD.67.014026
- T. Hahn, M. Perez-Victoria, Comput. Phys. Commun. 118, 153 (1999). doi:10.1016/S0010-4655(98)00173-8
- 25. T. Hahn, Comput. Phys. Commun. 140, 418 (2001). doi:10.1016/S0010-4655(01)00290-9
- S. Agrawal, T. Hahn, E. Mirabella, J. Phys. Conf. Ser. 368, 012054 (2012). doi:10.1088/1742-6596/368/1/012054
- C. Berger, Z. Bern, L. Dixon, F. Febres Cordero, D. Forde, et al. Phys. Rev. D78, 036003 (2008). doi:10.1103/PhysRevD.78.036003
- 28. T. Gleisberg, F. Krauss, Eur. Phys. J. C 53, 501 (2008). doi:10.1140/epjc/s10052-007-0495-0
- S. Hoche, F. Krauss, M. Schonherr, F. Siegert, JHEP 1104, 024 (2011). doi:10.1007/ JHEP04(2011)024
- Z. Bern, G. Diana, L. Dixon, F. Febres Cordero, S. Hoeche, et al. Phys. Rev. Lett. 109, 042001 (2012). doi:10.1103/PhysRevLett.109.042001
- Z. Bern, L.J. Dixon, F. Febres Cordero, S. Hche, H. Ita, D.A. Kosower, D. Matre, K.J. Ozeren.
   J. Phys. Conf. Ser. 523, 012051 (2014). doi:10.1088/1742-6596/523/1/012051
- R. Frederix, T. Gehrmann, N. Greiner, JHEP 0809, 122 (2008). doi:10.1088/1126-6708/2008/ 09/122
- 33. R. Frederix, T. Gehrmann, N. Greiner, JHEP 1006, 086 (2010). doi:10.1007/JHEP06(2010)086
- 34. W. Giele, G. Zanderighi, JHEP **0806**, 038 (2008). doi:10.1088/1126-6708/2008/06/038
- 35. G. Bevilacqua, M. Czakon, M. Garzelli, A. van Hameren, A. Kardos et al., Comput. Phys. Commun. **184**, 986 (2013). doi:10.1016/j.cpc.2012.10.033
- R. Frederix, S. Frixione, F. Maltoni, T. Stelzer, JHEP 0910, 003 (2009). doi:10.1088/1126-6708/2009/10/003
- V. Hirschi, R. Frederix, S. Frixione, M.V. Garzelli, F. Maltoni et al., JHEP 1105, 044 (2011). doi:10.1007/JHEP05(2011)044
- K. Hasegawa, S. Moch, P. Uwer, Comput. Phys. Commun. 181, 1802 (2010). doi:10.1016/j. cpc.2010.06.044
- 39. G. Cullen, et al., Eur. Phys. J. C (2012) 72 (1889)
- F. Cascioli, P. Maierhofer, S. Pozzorini, Phys. Rev. Lett. 108, 111601 (2012). doi:10.1103/ PhysRevLett.108.111601
- T. Binoth, D. Goncalves Netto, D. Lopez-Val, K. Mawatari, T. Plehn, et al. Phys. Rev. D84, 075005 (2011). doi:10.1103/PhysRevD.84.075005
- 42. D. Goncalves-Netto, D. Lopez-Val, K. Mawatari, T. Plehn, I. Wigmore, Phys. Rev. D 87, 014002 (2013). doi:10.1103/PhysRevD.87.014002
- S. Actis, A. Denner, L. Hofer, A. Scharf, S. Uccirati, JHEP 1304, 037 (2013). doi:10.1007/ JHEP04(2013)037
- S. Badger, B. Biedermann, P. Uwer, V. Yundin, Comput. Phys. Commun. 184, 1981 (2013). doi:10.1016/j.cpc.2013.03.018
- S. Badger, B. Biedermann, P. Uwer, V. Yundin, J. Phys. Conf. Ser. 523, 012057 (2014). doi:10. 1088/1742-6596/523/1/012057
- J. Alwall, R. Frederix, S. Frixione, V. Hirschi, F. Maltoni, O. Mattelaer, H.S. Shao, T. Stelzer,
   P. Torrielli, M. Zaro, JHEP 07, 079 (2014). doi:10.1007/JHEP07(2014)079
- 47. S. Frixione, B.R. Webber, JHEP **0206**, 029 (2002). doi:10.1088/1126-6708/2002/06/029
- 48. P. Nason, JHEP **0411**, 040 (2004). doi:10.1088/1126-6708/2004/11/040
- 49. G. 't Hooft, M.J.G. Veltman, Nucl. Phys. **B44**, 189 (1972). doi:10.1016/0550-3213(72)90279-9
- 50. J.C. Collins, (1984)
- 51. T. Kinoshita, J. Math. Phys. 3, 650 (1962). doi:10.1063/1.1724268
- 52. T. Lee, M. Nauenberg, Phys. Rev. 133, B1549 (1964). doi:10.1103/PhysRev.133.B1549

References 99

- 53. R. Feynman, Acta Phys. Polon. 24, 697 (1963)
- 54. R. Feynman, (1972)
- 55. R. Feynman, L. Brown, (2000)
- K. Fabricius, I. Schmitt, G. Kramer, G. Schierholz, Z. Phys. C 11, 315 (1981). doi:10.1007/ BF01578281
- 57. G. Kramer, B. Lampe, Fortsch. Phys. 37, 161 (1989)
- H. Baer, J. Ohnemus, J. Owens, Phys. Rev. D 40, 2844 (1989). doi:10.1103/PhysRevD.40.
   2844
- 59. B.W. Harris, J.F. Owens, Phys. Rev. D 65, 094032 (2002). doi:10.1103/PhysRevD.65.094032
- R.K. Ellis, D. Ross, A. Terrano, Nucl. Phys. B 178, 421 (1981). doi:10.1016/0550-3213(81)90165-6
- 61. Z. Kunszt, P. Nason, G. Marchesini, B. Webber, (1989)
- 62. M.L. Mangano, P. Nason, G. Ridolfi, Nucl. Phys. B **373**, 295 (1992). doi:10.1016/0550-3213(92)90435-E
- 63. T. Binoth, F. Boudjema, G. Dissertori, A. Lazopoulos, A. Denner et al., Comput. Phys. Commun. **181**, 1612 (2010). doi:10.1016/j.cpc.2010.05.016
- 64. S. Alioli, S. Badger, J. Bellm, B. Biedermann, F. Boudjema et al., Comput. Phys. Commun. **185**, 560 (2014). doi:10.1016/j.cpc.2013.10.020

## **Chapter 8**

# **One-Loop Computations: OPP Versus TIR**

**Abstract** In this chapter, we compared two methods for calculating one-loop Feynman integrals: one is called Ossola–Papadopolous–Pittau (OPP) method [1] and the other one is the Tensor Integral Reduction (TIR) method. We will also introduce the calculation of rational terms in one-loop computations.

#### 8.1 Generalities

Let us consider a generic N-point one-loop Feynman amplitude in dimensional regularization, which can be written as

$$\mathscr{A}_{N}^{1-\text{loop}} = \int d^{d}\bar{\ell} \frac{\bar{N}(\bar{\ell})}{\bar{D}_{0}\bar{D}_{1}\cdots\bar{D}_{N-1}},\tag{8.1}$$

where the denominators are

$$\bar{D}_i = (\bar{\ell} + k_i)^2 - m_i^2, \quad i = 0, \dots, N - 1.$$
 (8.2)

We keep the notation  $k_i$  as the external momenta flowing into the loop and the notation  $m_i$  as the mass of the ith loop line. Hence, in general we have  $k_i^2 \neq m_i^2$ . Due to the conservation of momenta, we can always assume  $k_0 = 0$ . In Eq. (8.1), the numerator function  $\bar{N}(\bar{\ell})$  is process dependent and much involved.  $\bar{N}(\bar{\ell})$  is in general a polynomial of the loop momentum  $\bar{\ell}$ . Although in principle it is possible to calculate the integral directly in (very few) relatively simple cases, in most of the cases especially in non-abelian gauge theories (e.g., QCD), it is a nightmare to integrate each new encountered integrals directly case by case. Hence, a smart method is necessary for a practical phenomenological analysis, for example, if one is able to reduce a general integral into a minimal basis of the Feynman integrals. Since the pioneer work done by Passarino and Veltman [2], many one-loop reduction methods have been proposed. They can mainly be classified into three categories: TIR [2–15], integrand reduction [16–18], and generalized unitarity reduction [19–22]. TIR

is the earliest method to perform a general one-loop reduction. However, due to large algebraic expressions in the reduction intermediate steps, TIR may be slower than the latter two reduction methods, which is usually the case for sufficiently complicated processes. The latter two methods are modern alternative reduction methods, which are aiming at improving the speed of one-loop integral reduction. Both methods have achieved several significant results. So far, the groups using integrand reduction method have mainly focused on studies of massive final states [23–27], whereas the generalized unitary method focuses on high-multiplicity final states [28–32]. Because only TIR and the integrand reduction are used in Madloop5, we will not discuss anything about the third method in the following of this chapter.

Before proceeds, it is useful to decompose a  $d=4-2\varepsilon$ -dimensional quantity (like  $\bar{\ell}^{\mu}$  or  $\bar{g}^{\mu\nu}$ ) into the sum of a 4-dimensional part and a  $(-2\varepsilon)$ -dimensional part. It is legal in dimensional regularization, which maintain d>4. Therefore, we have

$$\bar{\ell}^{\mu} = \ell^{\mu} + \tilde{\ell}^{\mu}, \, \bar{g}^{\mu\nu} = g^{\mu\nu} + \tilde{g}^{\mu\nu}, 
\bar{\ell}^{\mu}g_{\mu\nu} = \ell_{\nu}, \quad \bar{\ell}^{\mu}\tilde{g}_{\mu\nu} = \tilde{\ell}_{\nu}, \quad \ell^{\mu}\tilde{g}_{\mu\nu} = 0, \qquad \tilde{\ell}^{\mu}g_{\mu\nu} = 0, 
\bar{\ell} \cdot \ell = \ell^{2}, \quad \bar{\ell} \cdot \tilde{\ell} = \tilde{\ell}^{2}, \quad \ell \cdot \tilde{\ell} = 0, 
\bar{g}^{\mu}_{\mu} = d, \quad g^{\mu}_{\mu} = 4, \quad \tilde{g}^{\mu}_{\mu} = -2\varepsilon.$$
(8.3)

From the viewpoint of numerical automation, it is quite inefficient and inconvenient to calculate the numerator  $\bar{N}(\bar{\ell})$  in an non-integer dimensions. Therefore, we decompose the  $d=4-2\varepsilon$ -dimensional numerator function into a 4-dimensional part and a remainder

$$\tilde{N}(\ell, \tilde{\ell}^2, \varepsilon) \equiv \bar{N}(\bar{\ell}) - N(\ell),$$
 (8.4)

where

$$N(\ell) \equiv \lim_{\epsilon \to 0} \bar{N}(\bar{\ell} = \ell; \bar{\gamma}^{\mu} = \gamma^{\mu}, \bar{g}^{\mu\nu} = g^{\mu\nu}). \tag{8.5}$$

Then, the amplitude  $\mathcal{A}_N^{1-\text{loop}}$  can be written into two parts

$$\mathscr{A}_{N}^{1-\text{loop}} = \mathscr{A}_{N,\text{non-}R_{2}}^{1-\text{loop}} + R_{2},$$
 (8.6)

where

$$\mathcal{A}_{N,\text{non-}R_2}^{1-\text{loop}} \equiv \int d^d \bar{\ell} \frac{N(\ell)}{\bar{D}_0 \bar{D}_1 \cdots \bar{D}_{N-1}},$$

$$R_2 \equiv \int d^d \bar{\ell} \frac{\tilde{N}(\ell, \tilde{\ell}^2, \varepsilon)}{\bar{D}_0 \bar{D}_1 \cdots \bar{D}_{N-1}}.$$
(8.7)

Here, we use the same notation  $R_2$  in the OPP reduction method [1] for the rational term that originates from the  $(-2\varepsilon)$ -dimensional part of the numerator function. One

8.1 Generalities 103

can show that the computation of  $R_2$  is equivalent to that of a tree-level amplitude, constructed with a universal set of theory-dependent Feynman rules and can be derived once for all, which will be discussed in the next section.

## 8.2 Rational Terms $R_2$

In this section, we will introduce the  $R_2$  terms. For the interested reader, one can refer to Refs. [1, 33–40] for more details. Because  $R_2$  comes from the remainder  $N(\ell, \ell)$ , which is of course process- and kinematic-dependent, an easy way to derive it is by computing tree-level  $R_2$  amplitude. With the UV nature of  $R_2$  [33, 41, 42], one is able to establish Feynman rules in each model. In fact, this approach is more efficient than applying the D-dimensional unitary reduction in practical calculations [43]. However, the disadvantage is also obvious. For each new model considered, one has to derive a new set of Feynman rules for  $R_2$ . There are already some sets of  $R_2$  Feynman rules available in specific models. One can see Ref. [34] for the QCD corrections in SM, Refs. [35, 36] for the EW corrections in SM, Ref. [39] for the QCD corrections in minimal supersymmetric SM (MSSM) and Ref. [40] for the QCD corrections in Higgs effective field theory (HEFT). From the technical point of view, the derivation of  $R_2$  Feynman rules is at least not as difficult as the derivation of the Feynman rules for UV counterterm vertices. In the future, all the UV and  $R_2$  Feynman rules can be derived automatically by the new version of FEYNRULES [44, 45]. It is an important supplementary to the automation of NLO computations, which is already successfully used in the MADGRAPH5\_AMC@NLO framework [46].

Since  $R_2$  is always related to the UV divergences, the derivation of the Feynman rules for  $R_2$  effective vertices can be obtained from all possible one-particle irreducible Green functions. In a renormalizable theory, it is enough to consider the Green functions up to 4 external legs. Because of the nature of the 4-dimensional numerator  $N(\ell)$ , the only dimensional regularization scheme-dependent part in the one-loop amplitude is the  $R_2$  term. In order to maintain the advantages of the helicity method for loop calculations, we choose the four-dimensional helicity (FDH) [47–50] and 't Hooft-Veltman (HV) [51] schemes in MADLOOP5. We have

$$R_{2}\Big|_{\text{HV}} \equiv \int d^{d}\bar{\ell} \frac{\tilde{N}(\ell, \tilde{\ell}^{2}, \varepsilon)}{\bar{D}_{0}\bar{D}_{1} \cdots \bar{D}_{N-1}},$$

$$R_{2}\Big|_{\text{FDH}} \equiv \int d^{d}\bar{\ell} \frac{\tilde{N}(\ell, \tilde{\ell}^{2}, \varepsilon = 0)}{\bar{D}_{0}\bar{D}_{1} \cdots \bar{D}_{N-1}}.$$
(8.8)

Let us take an example from Ref. [39] to illustrate how to derive  $R_2$  Feynman rules. In Fig. 8.1, we consider the one-loop Feynman diagrams that contribute to

<sup>&</sup>lt;sup>1</sup>The default scheme for MADLOOP5 is HV scheme.

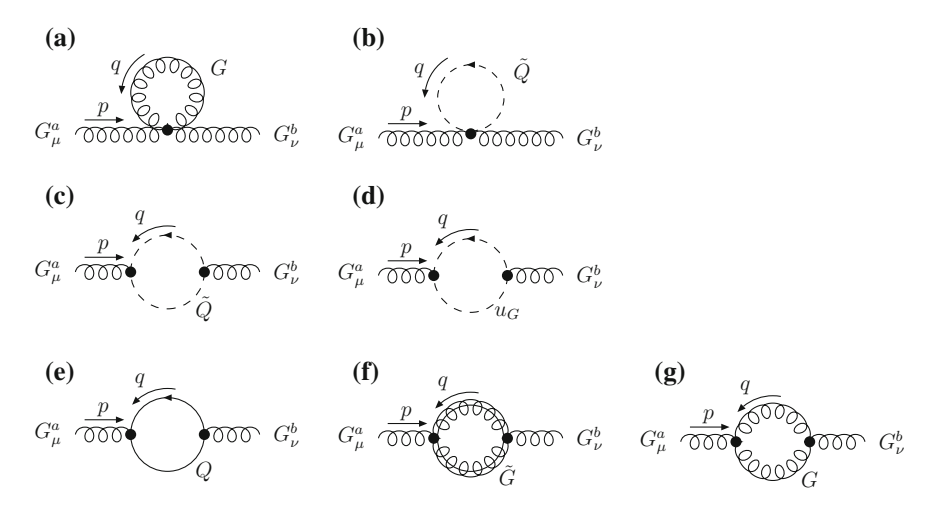


Fig. 8.1 Feynman diagrams contributing to the gluon self-energy in the MSSM QCD

the gluon self-energy in the MSSM QCD. The contribution of diagram (a) vanishes because it is a massless tadpole. For diagrams (b) to (d), the internal scalar loops cannot give a nonvanishing contribution to the  $R_2$  because the vertices are always contracted with external four-dimensional polarization vectors. For the quark loop with two external gluons, the numerator can be read as

$$\bar{N}(\bar{\ell}) = -\frac{\alpha_S}{(2\pi)^3} \delta_{ab} \text{Tr}[\gamma^{\mu}(\bar{\ell} + m_Q)\gamma^{\nu}(\bar{\ell} + p + m_Q)], \tag{8.9}$$

where external indices  $\mu$  and  $\nu$  have been taken into four dimensions. After performing some Clifford algebra, one arrives at

$$\tilde{N}(\tilde{\ell}^2) = 4 \frac{\alpha_S}{(2\pi)^3} \delta_{ab} g^{\mu\nu} \tilde{\ell}^2. \tag{8.10}$$

After integrating it with the help of any one-loop integral reduction algorithm, this quark loop contribution can be obtained. The last two diagrams are gluino loop and gluon loop. Similar procedure can be applied to deal with these loops. After combining all these contributions, we get [39]

$$G_{\mu}^{a} \xrightarrow{p} \sim \frac{i\alpha_{S}}{12\pi} C_{A} \delta^{ab} \left[ \frac{p^{2}}{2} g_{\mu\nu} + \lambda_{HV} \left( g_{\mu\nu} p^{2} - p_{\mu} p_{\nu} \right) + \sum_{Q} \left( \frac{p^{2} - 6m_{Q}^{2}}{N_{c}} g_{\mu\nu} \right) + \left( p^{2} - 6m_{\tilde{G}}^{2} \right) g_{\mu\nu} \right],$$
(8.11)

where  $C_A = N_c$  and  $\lambda_{HV} = 1(0)$  in HV (FDH) scheme.

8.2 Rational Terms  $R_2$  105

We want to emphasize here that although the decomposition of Eq. (8.6) is inspired by the OPP reduction method, it is universal and the definition of  $R_2$  has nothing to do with OPP but rather with the interplay of d-dimensional quantities and their 4dimensional counterparts. There are several alternative approaches, but the majority of them do not lend themselves to the numerical computation of the rational part. Two methods which have been used in numerical simulations are bootstrap [52] and D-dimensional unitary method [53–55]. Based on the recursion relations, their complexity does not grow exponentially. However, they still involve rather nontrivial issues, such as the presence of spurious singularities for bootstrap and the necessity of performing additional computations in 6 and 8 dimensions for Ddimensional unitary. The problem for D-dimensional unitary can be bypassed by means of a mass shift [56], which, however, might imply additional complications in the case of axial couplings in massive theories. Therefore, because of the advantages and disadvantages in each of these approaches, we point out that  $R_2$  should not really be an extra issue in the context of a complete computation, because one has to carry out renormalization procedure anyhow, which is similar to  $R_2$  but more involved.

## 8.3 The Ossola-Papadopolous-Pittau Reduction

The first integrand reduction method was proposed by Ossola, Papadopolous, and Pittau [16]. The algorithm has already been implemented in a public package Cuttools [57].

The key point in OPP method is expanding the numerator function  $N(\ell)$  into denominators  $\bar{D}_0, \ldots, \bar{D}_{N-1}$ . Due to the dimensionality of  $\ell$ ,  $N(\ell)$  can be directly decomposed into 4-dimensional denominator  $D_i \equiv \bar{D}_i - \tilde{\ell}^2$  first as [16]

$$\begin{split} N(\ell) &= \sum_{0 \leq i_0 < i_1 < i_2 < i_3 \leq N-1} [d_{i_0 i_1 i_2 i_3} + \hat{d}_{i_0 i_1 i_2 i_3}(\ell)] \prod_{\substack{i=0 \\ i \neq i_0, i_1, i_2, i_3}}^{N-1} D_i \\ &+ \sum_{0 \leq i_0 < i_1 < i_2 \leq N-1} [c_{i_0 i_1 i_2} + \hat{c}_{i_0 i_1 i_2}(\ell)] \prod_{\substack{i=0 \\ i \neq i_0, i_1, i_2}}^{N-1} D_i \\ &+ \sum_{0 \leq i_0 < i_1 \leq N-1} [b_{i_0 i_1} + \hat{b}_{i_0 i_1}(\ell)] \prod_{\substack{i=0 \\ i \neq i_0, i_1}}^{N-1} D_i \\ &+ \sum_{0 \leq i_0 \leq N-1} [a_{i_0} + \hat{a}_{i_0}(\ell)] \prod_{\substack{i=0 \\ i \neq i_0}}^{N-1} D_i \end{split}$$

$$+ \hat{P}(\ell) \prod_{i=0}^{N-1} D_i. \tag{8.12}$$

The terms proportional to coefficients  $\hat{d}$ ,  $\hat{c}$ ,  $\hat{b}$ ,  $\hat{a}$ , and  $\hat{P}$  vanish upon integration. They are called spurious terms. The functional forms of  $\ell$  in these spurious coefficients are proven and exploited in Ref. [16] for any renormalizable theory. There are  $\{1, 6, 8, 4\}$  terms for each spurious coefficient  $\{\hat{d}, \hat{c}, \hat{b}, \hat{a}\}$ , and  $\hat{P}$  is a polynomial of  $\ell$ . In principle, one is able to derive these coefficients and d, c, b, a by solving the master equation Eq. (8.12) with enough number of numerical (complex)  $\ell$  values. A smart way of solving Eq. (8.12) was also proposed in Ref. [16], which is achieved by putting denominators on-shell:

1. First, solve all of the 4-point coefficients d,  $\hat{d}$ . Choose a set of  $\{i_0, i_1, i_2, i_3\}$ , and determine two complex solutions  $\ell = \ell^{\pm}$  by solving

$$D_{i_0}(\ell) = D_{i_1}(\ell) = D_{i_2}(\ell) = D_{i_3}(\ell) = 0.$$
 (8.13)

In this case, all terms without coefficients  $d_{i_0i_1i_2i_3}$ ,  $\hat{d}_{i_0i_1i_2i_3}(\ell)$  on the right-hand side of Eq. (8.12) vanish. Then, it is easier to determine the coefficients of  $d_{i_0i_1i_2i_3}$ ,  $\hat{d}_{i_0i_1i_2i_3}(\ell)$ . Successively, exhaust all possible sets of  $\{i_0, i_1, i_2, i_3\}$  and determine all of the coefficients  $d_{i_0i_1i_2i_3}$ ,  $\hat{d}_{i_0i_1i_2i_3}(\ell)$ . After such a procedure, the master equation becomes

$$N(\ell) - \sum_{0 \leq i_{0} < i_{1} < i_{2} < i_{3} \leq N-1} [d_{i_{0}i_{1}i_{2}i_{3}} + \hat{d}_{i_{0}i_{1}i_{2}i_{3}}(\ell)] \prod_{\substack{i=0\\i \neq i_{0}, i_{1}, i_{2}, i_{3}}}^{N-1} D_{i}$$

$$= \sum_{0 \leq i_{0} < i_{1} < i_{2} \leq N-1} [c_{i_{0}i_{1}i_{2}} + \hat{c}_{i_{0}i_{1}i_{2}}(\ell)] \prod_{\substack{i=0\\i \neq i_{0}, i_{1}, i_{2}}}^{N-1} D_{i}$$

$$+ \sum_{0 \leq i_{0} < i_{1} \leq N-1} [b_{i_{0}i_{1}} + \hat{b}_{i_{0}i_{1}}(\ell)] \prod_{\substack{i=0\\i \neq i_{0}, i_{1}}}^{N-1} D_{i}$$

$$+ \sum_{0 \leq i_{0} \leq N-1} [a_{i_{0}} + \hat{a}_{i_{0}}(\ell)] \prod_{\substack{i=0\\i \neq i_{0}}}^{N-1} D_{i}$$

$$+ \hat{P}(\ell) \prod_{i=0}^{N-1} D_{i}. \tag{8.14}$$

2. Second, solve all of the 3-point coefficients c,  $\hat{c}$ . After choosing a set of values for  $\{i_0, i_1, i_2\}$ , determine 7 independent<sup>2</sup> complex solutions  $\ell = \ell_1, \ldots, \ell_7$ , which satisfy

$$D_{i_0}(\ell) = D_{i_1}(\ell) = D_{i_2}(\ell) = 0.$$
(8.15)

Solve the linear equations for coefficients  $c_{i_0i_1i_2}$ ,  $\hat{c}_{i_0i_1i_2}(\ell)$  in Eq. (8.14). After exhausting all possible  $\{i_0, i_1, i_2\}$ , one arrives a new equation

$$N(\ell) - \sum_{0 \le i_{0} < i_{1} < i_{2} < i_{3} \le N-1} [d_{i_{0}i_{1}i_{2}i_{3}} + \hat{d}_{i_{0}i_{1}i_{2}i_{3}}(\ell)] \prod_{\substack{i=0\\i \ne i_{0}, i_{1}, i_{2}, i_{3}}}^{N-1} D_{i}$$

$$- \sum_{0 \le i_{0} < i_{1} < i_{2} \le N-1} [c_{i_{0}i_{1}i_{2}} + \hat{c}_{i_{0}i_{1}i_{2}}(\ell)] \prod_{\substack{i=0\\i \ne i_{0}, i_{1}, i_{2}}}^{N-1} D_{i}$$

$$= \sum_{0 \le i_{0} < i_{1} \le N-1} [b_{i_{0}i_{1}} + \hat{b}_{i_{0}i_{1}}(\ell)] \prod_{\substack{i=0\\i \ne i_{0}, i_{1}}}^{N-1} D_{i}$$

$$+ \sum_{0 \le i_{0} \le N-1} [a_{i_{0}} + \hat{a}_{i_{0}}(\ell)] \prod_{\substack{i=0\\i \ne i_{0}}}^{N-1} D_{i}$$

$$+ \hat{P}(\ell) \prod_{i=0}^{N-1} D_{i}. \tag{8.16}$$

3. Similar procedure is iteratively applied to determine the coefficients b,  $\hat{b}$ , and a. One is aware that since  $\hat{a}$ ,  $\hat{P}$  vanish upon integration and they do not contribute terms to determine the wanted d, c, b, a, it is not necessary to determine them in a practical computation.

To match the dimensionality of denominators, one has to use the following substitution

$$D_i(\ell) = \bar{D}_i(\bar{\ell}) - \tilde{\ell}^2 \tag{8.17}$$

into the master equation Eq. (8.12). The numerator  $N(\ell)$  can be decomposed into [1]

$$N_{R_1}(\ell, \tilde{\ell}^2) \equiv N(\ell) - N_{cc}(\ell, \tilde{\ell}^2), \tag{8.18}$$

where

<sup>&</sup>lt;sup>2</sup>Because the number of constraints is less than the degree of freedom in  $\ell$ , it is not straightforward to determine independent solutions. One improvement is done in Ref. [58] by using a projection-technique based on the discrete Fourier transform.

$$N_{cc}(\ell, \tilde{\ell}^2) \equiv N(\ell) \Big|_{D_i \to \bar{D}_i}$$
 (8.19)

Therefore, the non- $R_2$  amplitude  $\mathcal{A}_{N,\text{non-}R_2}^{1-\text{loop}}$  defined in Eq. (8.7) can be decomposed into two parts

$$\mathscr{A}_{N,\text{non}-R_2}^{1-\text{loop}} = \mathscr{A}_{N,cc}^{1-\text{loop}} + R_1,$$
 (8.20)

where we have defined the cut-constructible amplitude

$$\mathscr{A}_{N,cc}^{1-\text{loop}} \equiv \int d^d \bar{\ell} \frac{N_{cc}(\ell, \tilde{\ell}^2)}{\bar{D}_0 \bar{D}_1 \cdots \bar{D}_{N-1}}$$
(8.21)

and another rational term

$$R_{1} \equiv \int d^{d}\bar{\ell} \frac{N_{R_{1}}(\ell, \tilde{\ell}^{2})}{\bar{D}_{0}\bar{D}_{1}\cdots\bar{D}_{N-1}}.$$
 (8.22)

After combing Eqs. (8.12), (8.19), we reduce the cut-constructible amplitude into one-loop master integrals (i.e., up to 4-point scalar integrals)

$$\mathcal{A}_{N,cc}^{1-\text{loop}} = \sum_{0 \le i_0 < i_1 < i_2 < i_3 \le N-1} d_{i_0 i_1 i_2 i_3} \mathcal{I}_0(i_0 i_1 i_2 i_3)$$

$$+ \sum_{0 \le i_0 < i_1 < i_2 \le N-1} c_{i_0 i_1 i_2} \mathcal{I}_0(i_0 i_1 i_2)$$

$$+ \sum_{0 \le i_0 < i_1 \le N-1} b_{i_0 i_1} \mathcal{I}_0(i_0 i_1)$$

$$+ \sum_{0 \le i_0 < N-1} a_{i_0} \mathcal{I}_0(i_0), \tag{8.23}$$

where the one-loop master integrals are

$$\mathcal{I}_{0}(i_{0}i_{1}i_{2}i_{3}) \equiv \int d^{d}\bar{\ell} \frac{1}{\bar{D}_{i_{0}}\bar{D}_{i_{1}}\bar{D}_{i_{2}}\bar{D}_{i_{3}}}, 
\mathcal{I}_{0}(i_{0}i_{1}i_{2}) \equiv \int d^{d}\bar{\ell} \frac{1}{\bar{D}_{i_{0}}\bar{D}_{i_{1}}\bar{D}_{i_{2}}}, 
\mathcal{I}_{0}(i_{0}i_{1}) \equiv \int d^{d}\bar{\ell} \frac{1}{\bar{D}_{i_{0}}\bar{D}_{i_{1}}}, 
\mathcal{I}_{0}(i_{0}) \equiv \int d^{d}\bar{\ell} \frac{1}{\bar{D}_{i}}.$$
(8.24)

Because all the coefficients d, c, b, a and  $\hat{d}$ ,  $\hat{c}$ ,  $\hat{b}$ ,  $\hat{a}$ ,  $\hat{P}$  do not change, both the cut-constructible amplitude and rational term  $R_1$  can be computed in CutTools [57]. Moreover, we want to emphasize that  $R_1$  and  $R_2$  are gauge dependent individually, but  $R_1 + R_2$  are gauge independent.

## 8.4 Tensor Integral Reduction and IREGI

Recently, thanks to an independent OPENLOOPS [59] techniques implemented in MADLOOP5 [46], we have managed to implement a general interface to TIR libraries in the unpublished version of MADLOOP5. Two TIR libraries PJFRY++ [60, 61] and IREGI [62] have been successfully used. The aim of this section is to introduce the basic procedure used in TIR [2–15] and in particular by the program IREGI,<sup>3</sup> which is already extensively validated. IREGI is the only self-contained TIR library in the current version of MADLOOP5.

The starting point of TIR is the observation that the numerator  $\bar{N}(\bar{\ell})$  can be decomposed as

$$\bar{N}(\bar{\ell}) = \sum_{r=0}^{r_{\text{max}}} \bar{c}_{\mu_1 \cdots \mu_r}^{(r)} \bar{\ell}^{\mu_1} \cdots \bar{\ell}^{\mu_r}, \tag{8.25}$$

where the maximal rank  $r_{\max}$  in  $\bar{N}(\bar{\ell})$  is a nonnegative integer.  $r_{\max}$  may vary diagram by diagram. In a renormalizable theory, we have a general constraint  $r_{\max} \leq N$ . The coefficients  $\bar{c}_{\mu_1\cdots\mu_r}^{(r)}$  are independent of loop momentum  $\bar{\ell}$ . Thus, the amplitude can be decomposed as

$$\mathscr{A}_{N}^{1-\text{loop}} = \sum_{r=0}^{r_{\text{max}}} \bar{c}_{\mu_{1}\cdots\mu_{r}}^{(r)} \int d^{d}\bar{\ell} \frac{\bar{\ell}^{\mu_{1}}\cdots\bar{\ell}^{\mu_{r}}}{\bar{D}_{0}\cdots\bar{D}_{N-1}}.$$
 (8.26)

Conceptually, the coefficients  $\bar{c}_{\mu_1\cdots\mu_r}^{(r)}$  can be determined through a few algebra procedures. However, technically, it is not easy and efficient to achieve it. The remaining obstacle to obtain the value of  $\mathscr{A}_N^{1-\mathrm{loop}}$  is to calculate the so-called rank r tensor integral

$$\bar{\mathscr{J}}^{\mu_1\cdots\mu_r}(\{k_i\},\{m_i\}) = \int d^d\bar{\ell} \frac{\bar{\ell}^{\mu_1}\cdots\bar{\ell}^{\mu_r}}{\bar{D}_0\cdots\bar{D}_{N-1}}.$$
 (8.27)

It is quite cumbersome to calculate the integral directly when N and/or r increase. Therefore, a clever method is necessary to perform a practical application.

Thanks to the pioneer work done by Passarino and Veltman [2], we understand that the general one-loop tensor integral  $\bar{\mathcal{I}}^{\mu_1\cdots\mu_r}(\{k_i\},\{m_i\})$  can be reduced to a

<sup>&</sup>lt;sup>3</sup>The acronym stands for "Integral REduction with General positive propagator Indices".

minimal basis of up to N=4 scalar integrals plus some additional rational terms. It is schematically written as

$$\bar{\mathcal{J}}^{\mu_{1}\cdots\mu_{r}}(\{k_{i}\},\{m_{i}\}) = \sum_{0 \leq i_{0} < i_{1} < i_{2} < i_{3} \leq N-1} \bar{d}^{\mu_{1}\cdots\mu_{r}}(i_{0}i_{1}i_{2}i_{3};\{k_{i}\},\{m_{i}\}) \mathscr{I}_{0}(i_{0}i_{1}i_{2}i_{3}) 
+ \sum_{0 \leq i_{0} < i_{1} < i_{2} \leq N-1} \bar{c}^{\mu_{1}\cdots\mu_{r}}(i_{0}i_{1}i_{2};\{k_{i}\},\{m_{i}\}) \mathscr{I}_{0}(i_{0}i_{1}i_{2}) 
+ \sum_{0 \leq i_{0} < i_{1} \leq N-1} \bar{b}^{\mu_{1}\cdots\mu_{r}}(i_{0}i_{1};\{k_{i}\},\{m_{i}\}) \mathscr{I}_{0}(i_{0}i_{1}) 
+ \sum_{0 \leq i_{0} \leq N-1} \bar{a}^{\mu_{1}\cdots\mu_{r}}(i_{0};\{k_{i}\},\{m_{i}\}) \mathscr{I}_{0}(i_{0}) + R,$$
(8.28)

where the one-loop master integrals  $\mathcal{J}_0(i_0i_1i_2i_3)$ ,  $\mathcal{J}_0(i_0i_1i_2)$ ,  $\mathcal{J}_0(i_0i_1)$ ,  $\mathcal{J}_0(i_0)$  have already been defined in Eq. (8.24) and R represents the rational term. Then, the only mission is to integrate these basis scalar integrals, which have been investigated a lot in the literature [63–70]. In IREGI, we use two public packages QCDLoop [67] and ONELOOP [70] to calculate these scalar integrals.

This important observation can be understood into two steps. First, due to the Lorentz invariance, the Lorentz indices in the tensor integral  $\bar{\mathcal{J}}^{\mu_1\cdots\mu_r}(\{k_i\},\{m_i\})$  can be shared by external momenta  $k_i$  and metric tensor  $\bar{g}^{\mu\nu}$ . Considering the orderless of  $\mu_1,\ldots,\mu_r$ , this step can be performed as follows

$$\bar{\mathscr{J}}^{\mu_1\cdots\mu_r}(\{k_i\},\{m_i\}) = \sum_{\substack{2j+i_0+i_1+\cdots+i_{N-1}=r\\ \mathscr{I}_{ji_0\cdots i_{N-1}}(\{k_i\},\{m_i\}),}} \{[\bar{g}]^j [k_0]^{i_0}\cdots [k_{N-1}]^{i_{N-1}}\}^{\mu_1\cdots\mu_r}$$
(8.29)

where the symmetric tensor form  $\{[\bar{g}]^j[k_0]^{i_0}\cdots[k_{N-1}]^{i_{N-1}}\}^{\mu_1\cdots\mu_r}$  is defined in such a way that all non-equivalent permutations of the Lorentz indices  $\mu_1,\ldots,\mu_r$  on j metric tensors  $\bar{g}$  and  $i_s$  external momentum  $k_s$  contribute with weight one. For example, we have

$$\{ [\bar{g}]^{2} [k_{0}]^{0} [k_{1}]^{0} \}^{\mu_{1} \cdots \mu_{4}} = \bar{g}^{\mu_{1} \mu_{2}} \bar{g}^{\mu_{3} \mu_{4}} + \bar{g}^{\mu_{1} \mu_{3}} \bar{g}^{\mu_{2} \mu_{4}} + \bar{g}^{\mu_{1} \mu_{4}} \bar{g}^{\mu_{2} \mu_{3}},$$

$$\{ [\bar{g}]^{1} [k_{0}]^{0} [k_{1}]^{2} \}^{\mu_{1} \cdots \mu_{4}} = \bar{g}^{\mu_{1} \mu_{2}} k_{1}^{\mu_{3}} k_{1}^{\mu_{4}} + \bar{g}^{\mu_{1} \mu_{3}} k_{1}^{\mu_{2}} k_{1}^{\mu_{4}} + \bar{g}^{\mu_{1} \mu_{4}} k_{1}^{\mu_{2}} k_{1}^{\mu_{3}},$$

$$\{ [\bar{g}]^{0} [k_{0}]^{0} [k_{1}]^{4} \}^{\mu_{1} \cdots \mu_{4}} = k_{1}^{\mu_{1}} k_{1}^{\mu_{2}} k_{1}^{\mu_{3}} k_{1}^{\mu_{4}},$$

$$\{ [\bar{g}]^{0} [k_{0}]^{1} [k_{1}]^{2} \}^{\mu_{1} \mu_{2} \mu_{3}} = k_{0}^{\mu_{1}} k_{1}^{\mu_{2}} k_{1}^{\mu_{3}} + k_{0}^{\mu_{2}} k_{1}^{\mu_{1}} k_{1}^{\mu_{3}} + k_{0}^{\mu_{3}} k_{1}^{\mu_{1}} k_{1}^{\mu_{2}}.$$

$$(8.30)$$

In general, there are several methods to determine the scalar function  $\mathscr{I}_{ji_0\cdots i_{N-1}}(\{k_i\},\{m_i\})$  in Eq. (8.29). One way is based on the fact that any linear combination of  $\bar{\ell}^2$ ,  $\bar{\ell} \cdot k_i$  can be expressed into denominators and loop momentum independent terms, because we have

$$\bar{\ell}^2 = \bar{D}_0 + m_0^2,$$

$$\bar{\ell} \cdot k_i = (\bar{D}_i - \bar{D}_0 + m_i^2 - m_0^2)/2.$$
(8.31)

Then, one is able to contract one Lorentz index by external momenta  $k_i$  and/or two Lorentz indices by metric tensor  $\bar{g}$  at the left-hand side of Eq. (8.29). After a contraction, we can express the original integral by lower-rank and/or lower-point tensor integrals. The way doing so can be found in several literature (see, e.g., in Ref. [4]).

An alternative way is attributed to Davydychev by finding a relation between integral in different dimensions [3]. One can extend the tensor integral  $\bar{\mathscr{I}}^{\mu_1\cdots\mu_r}(\{k_i\},\{m_i\})$  in a more general way

$$\bar{\mathscr{J}}^{\mu_1\cdots\mu_r}(d,\{\nu_i\},\{k_i\},\{m_i\}) = \frac{(\mu^2)^{2-d/2}}{(2\pi)^d} \int d^d\bar{\ell} \frac{\bar{\ell}^{\mu_1}\cdots\bar{\ell}^{\mu_r}}{\bar{D}_0^{\nu_0}\bar{D}_1^{\nu_1}\cdots\bar{D}_{N-1}^{\nu_{N-1}}}, \quad (8.32)$$

where the propagator indices  $v_0, v_1, \dots, v_{N-1}$  are integers. In particular, the generalized scalar integral is

$$\mathscr{I}_0(d, \{\nu_i\}, \{k_i\}, \{m_i\}) = \frac{(\mu^2)^{2-d/2}}{(2\pi)^d} \int d^d \bar{\ell} \frac{1}{\bar{D}_0^{\nu_0} \bar{D}_1^{\nu_1} \cdots \bar{D}_{N-1}^{\nu_{N-1}}}, \tag{8.33}$$

We have introduced a prefactor  $\frac{(\mu^2)^{2-d/2}}{(2\pi)^d}$  in Eqs. (8.32), (8.33) for convenience. Then,

$$\bar{\mathcal{J}}^{\mu_{1}\cdots\mu_{r}}(\{k_{i}\},\{m_{i}\}) \sim \bar{\mathcal{J}}^{\mu_{1}\cdots\mu_{r}}(d,\{\nu_{i}\},\{k_{i}\},\{m_{i}\}) \Big|_{d=4-2\varepsilon,\nu_{0}=\nu_{1}=\cdots=\nu_{N-1}=1}.$$
(8.34)

Based on the Feynman parameter representations

$$\widetilde{\mathscr{I}}^{\mu_{1}\cdots\mu_{r}}(d,\{\nu_{i}\},\{k_{i}\},\{m_{i}\}) = \frac{i}{(4\pi)}(4\pi\mu^{2})^{2-d/2} \sum_{2j+i_{0}+\cdots+i_{N-1}=r} \{[\bar{g}]^{j}[k_{0}]^{i_{0}}\cdots[k_{N-1}]^{i_{N-1}}\}^{\mu_{1}\cdots\mu_{r}} \\
\times (-1)^{\sum_{i}\nu_{i}+r-j} \frac{\Gamma(\sum_{i}\nu_{i}-d/2-j)}{2^{j}\prod_{i}\Gamma(\nu_{i})} \int_{0}^{1}\prod_{i}dy_{i}y_{i}^{\nu_{i}+i_{i}-1} \\
\times \delta(\sum_{i}y_{i}-1) \left[-\sum_{i< j}y_{i}y_{j}(k_{i}-k_{j})^{2}+\sum_{i}y_{i}m_{i}^{2}\right]^{j+d/2-\sum_{i}\nu_{i}} ,$$

$$\mathscr{I}_{0}(d,\{\nu_{i}\},\{k_{i}\},\{m_{i}\}) = \frac{i}{(4\pi)}(4\pi\mu^{2})^{2-d/2} \frac{\Gamma(\sum_{i=0}^{N-1}\nu_{i}-d/2)}{\prod_{i=0}^{N-1}\Gamma(\nu_{i})}(-1)^{\sum_{i=0}^{N-1}\nu_{i}} \\
\times \int_{0}^{1}\prod_{i=0}^{N-1}dy_{i}y_{i}^{\nu_{i}-1}\delta(\sum_{i=0}^{N-1}y_{i}-1) \\
\times \left[-\sum_{i< j}y_{i}y_{j}(k_{i}-k_{j})^{2}+\sum_{i=0}^{N-1}y_{i}m_{i}^{2}\right]^{d/2-\sum_{i=0}^{N-1}\nu_{i}} , \quad (8.35)$$

one can derive the following relation

$$\mathcal{J}^{\mu_{1}\cdots\mu_{r}}(d,\{\nu_{i}\},\{k_{i}\},\{m_{i}\}) = \sum_{2j+i_{0}+\cdots+i_{N-1}=r} \{[\bar{g}]^{j}[k_{0}]^{i_{0}}\cdots[k_{N-1}]^{i_{N-1}}\}^{\mu_{1}\cdots\mu_{r}} \\
\times \frac{(4\pi\,\mu^{2})^{r-j}}{(-2)^{j}} \left(\prod_{i=0}^{N-1} \frac{\Gamma(\nu_{i}+i_{i})}{\Gamma(\nu_{i})}\right) \\
\times \mathcal{J}_{0}(d+2(r-j),\{\nu_{i}+i_{i}\},\{k_{i}\},\{m_{i}\}). \quad (8.36)$$

After combing Eqs. (8.36) and (8.29), a quick by-product is a general relation

$$\mathcal{I}_{ji_0\cdots i_{N-1}}(\{k_i\}, \{m_i\}) = \left[\frac{(\mu^2)^{2-d/2}}{(2\pi)^d}\right]^{-1} \frac{(4\pi\mu^2)^{r-j}}{(-2)^j} \left(\prod_{i=0}^{N-1} \frac{\Gamma(1+i_i)}{\Gamma(1)}\right) \\
\times \mathcal{I}_0(d+2(r-j), \{1+i_i\}, \{k_i\}, \{m_i\}), \\
\text{with } d=4-2\varepsilon. \tag{8.37}$$

With Eq. (8.35), one is also able to derive relations for scalar integrals in different dimensions. For instance, a relation (Eq. (6)) in Ref. [3] is straightforward to derive

$$\mathscr{I}_0(d-2,\{\nu_i\},\{k_i\},\{m_i\}) = -(4\pi\mu^2) \sum_{s=0}^{N-1} \nu_s \mathscr{I}_0(d,\{\nu_i+\delta_{is}\},\{k_i\},\{m_i\}).$$
 (8.38)

Moreover, more recursion relations for scalar integrals  $\mathcal{I}_0(d, \{v_i\}, \{k_i\}, \{m_i\})$  can be obtained with the help of the integration by parts method [15, 71]

$$\int d^{d}\bar{\ell} \frac{\partial}{\partial \bar{\ell}^{\mu}} \left( \frac{P^{\mu}(\bar{\ell}, \{k_{i}\})}{\bar{D}_{0}^{\nu_{0}} \bar{D}_{1}^{\nu_{1}} \cdots \bar{D}_{N-1}^{\nu_{N-1}}} \right) = 0, \tag{8.39}$$

which is due to the integral is translational invariance in dimensional regularization. The function  $P^{\mu}(\bar{\ell}, \{k_i\})$  is a polynomial of  $\bar{\ell}$  and  $k_i$ .

We have implemented two methods mainly proposed in Refs. [4, 71] in IREGI. Although in principle we can directly reduce the one-loop amplitude  $\mathscr{A}_N^{1-\text{loop}}$  with TIR methods, its realization is not so simple if we aim at an efficient numerical solution. The reason is because the loop momentum  $\bar{\ell}$  is living in  $d=4-2\varepsilon$  dimensions, the determination of its coefficients  $\bar{c}_{\mu_1\cdots\mu_r}^r$  in Eq. (8.25) will be much more involved than that in 4 dimensions. It is much convenient to express the numerator function in 4 dimensions  $N(\ell)$ . The decomposition of  $N(\ell)$  is similar

$$N(\ell) = \sum_{r=0}^{r_{\text{max}}} c_{\mu_1 \cdots \mu_r}^{(r)} \ell^{\mu_1} \cdots \ell^{\mu_r}.$$
 (8.40)

And we can take the Lorentz indices  $\mu_1, \ldots, \mu_r = 0, 1, 2, 3$ . The new rank r tensor integral becomes

$$\mathscr{J}^{\mu_1 \cdots \mu_r}(\{k_i\}, \{m_i\}) = \int d^d \bar{\ell} \frac{\ell^{\mu_1} \cdots \ell^{\mu_r}}{\bar{D}_0 \cdots \bar{D}_{N-1}}.$$
 (8.41)

 $\mathscr{I}^{\mu_1\cdots\mu_r}(\{k_i\},\{m_i\})$  is the exact quantity what is calculated in IREGI. We have a similar decomposition of Eq. (8.29) to  $\mathscr{I}^{\mu_1\cdots\mu_r}(\{k_i\},\{m_i\})$  but replacing d-dimensional metric tensor  $\bar{g}$  with the 4-dimensional one g

$$\mathscr{I}^{\mu_1\cdots\mu_r}(\{k_i\},\{m_i\}) = \sum_{\substack{2j+i_0+i_1+\cdots+i_{N-1}=r\\ \mathscr{I}_{ji_0\cdots i_{N-1}}(\{k_i\},\{m_i\}).}} \{[g]^j[k_0]^{i_0}\cdots[k_{N-1}]^{i_{N-1}}\}^{\mu_1\cdots\mu_r}$$

$$(8.42)$$

Given that the scalar functions  $\mathcal{I}_{ji_0\cdots i_{N-1}}(\{k_i\}, \{m_i\})$  are independent of the dimensionality of the numerator, as easily been understood from Eq. (8.37), we can always use the algebra reduction relations of  $\mathcal{I}_{ji_0\cdots i_{N-1}}(\{k_i\}, \{m_i\})$  derived in d dimension to reduce them. In other words, we can reduce  $\mathcal{I}^{\mu_1\cdots \mu_r}(\{k_i\}, \{m_i\})$  into two steps:

- First, one can decompose it by using Eq. (8.42).
- Afterward, the scalar functions  $\mathscr{I}_{ji_0\cdots i_{N-1}}(\{k_i\}, \{m_i\})$  can be reduced by using the relations of different  $\mathscr{I}_{ji_0\cdots i_{N-1}}(\{k_i\}, \{m_i\})$  derived in d dimensions.

The remainder is known as a rational term  $R_2$ . Finally, the computation of one-loop amplitude can be performed as follows:

$$\mathcal{A}_{N}^{1-\text{loop}} = \int d^{d}\bar{\ell} \frac{N(\ell)}{\bar{D}_{0}\bar{D}_{1}\cdots\bar{D}_{N-1}} + R_{2},$$

$$= \sum_{r=0}^{r_{\text{max}}} c_{\mu_{1}\cdots\mu_{r}}^{(r)} \mathcal{I}^{\mu_{1}\cdots\mu_{r}}(\{k_{i}\},\{m_{i}\}) + R_{2}.$$
(8.43)

It is worth to mention that there are rational terms left in the reduction of  $\mathscr{I}^{\mu_1\cdots\mu_r}(\{k_i\},\{m_i\})$ .

IREGI can use either of two methods in Refs. [4, 71] for the recursive reduction, where the actual choice is made by the calling external program (e.g., Madloop5). The default method in the Madgraph5\_aMC@NLO framework [46] is the reduction scheme proposed in Ref. [4]. It is straightforward to change the reduction scheme since it is simply controlled by a parameter in an input card. IREGI has a minimal internal stability test. If it finds the scheme proposed in Ref. [4] suffers from the numerical instability issue, the program will turn to using the method presented in Ref. [71] alternatively. IREGI is extensively validated though it is still not published. Besides its internal checks, it also compares with other programs especially Cuttols [57]. We establish the cross check results by using Madloop5 in the Appendix B.

## 8.5 Comparison Between OPP and TIR

One pitfall in OPP reduction [58] is that it heavily uses the numerical inversion of Gram determinant.<sup>4</sup> It potentially affects the numerical accuracy when the Gram determinant approaches to zero. For up to N=4 point integrals, this happens only near various thresholds on the edge of the phase space. However, for N=5 point integrals, the regions where the Gram determinants are small or zero can overlap with the phase space.<sup>5</sup> In additional to conventional Passarino–Veltman reduction [2], modern alternative methods [4–12, 15] for multileg processes still suffer from numerical cancellation in the different regions of the same physical phase space, which makes it difficult to choose a best scheme in a process-by-process way and forces us to resort to numerical reduction instead of analytical reduction. Hence, the numerical stability issue is one of our motivations to use TIR libraries in addition to OPP in MADLOOP5. It is much easier for TIR to choose the best reduction schemes on *per phase space point* basis.

Another advantage of TIR compared to OPP is that it can be used to improve the efficiency of one-loop computation for loop-induced processes (e.g., Higgs pair production via gluon–gluon fusion) [46, 73]. In OPP, the calling of reduction program like CutTools is dependent on each helicity configuration, which requires heavy computations in CutTools. However, from the definition in Sect. 8.4, the rank r tensor integral  $\mathscr{I}^{\mu_1\cdots\mu_r}(\{k_i\},\{m_i\})$  is independent of any helicity configuration, which means that each integral is only computed once and it is caching into memory. It paves the way for improving the efficiency of loop-induced process computations.

The advantage of OPP compared to TIR is obviously faster in reduction especially for multileg processes, which is the primary motivation of constructing OPP algorithm. It means that if the integral is in the scope of the Cuttools, the best solution is always first using OPP, and only when it encounters instability, it turns to TIR reduction schemes. Of course if the integral is beyond the scope of Cuttools (e.g., in a non-renormalizable theory) or TIR (e.g., very high N), the program only adopts the available solution.

### References

- G. Ossola, C.G. Papadopoulos, R. Pittau, JHEP 05, 004 (2008). doi:10.1088/1126-6708/2008/ 05/004
- G. Passarino, M.J.G. Veltman, Nucl. Phys. B160, 151 (1979). doi:10.1016/0550-3213(79)90234-7
- 3. A.I. Davydychev, Phys. Lett. **B263**, 107 (1991). doi:10.1016/0370-2693(91)91715-8
- 4. A. Denner, S. Dittmaier, Nucl. Phys. **B734**, 62 (2006). doi:10.1016/j.nuclphysb.2005.11.007

<sup>&</sup>lt;sup>4</sup>The Gram determinant is defined, e.g., in Ref. [72].

<sup>&</sup>lt;sup>5</sup>For  $N \ge 6$  point integrals, due to dimensionality of space-time, the Gram determinant is identical to zero. Hence, it is not necessary to introduce the inverse of Gram determinant in the reduction.

References 115

T. Diakonidis, J. Fleischer, J. Gluza, K. Kajda, T. Riemann et al., Phys. Rev. D80, 036003 (2009). doi:10.1103/PhysRevD.80.036003

- 6. J. Fleischer, T. Riemann, Phys. Rev. D83, 073004 (2011). doi:10.1103/PhysRevD.83.073004
- T. Binoth, J. Guillet, G. Heinrich, Nucl. Phys. B572, 361 (2000). doi:10.1016/S0550-3213(00)00040-7
- T. Binoth, J.P. Guillet, G. Heinrich, E. Pilon, C. Schubert, JHEP 0510, 015 (2005). doi:10. 1088/1126-6708/2005/10/015
- Z. Bern, L.J. Dixon, D.A. Kosower, Nucl. Phys. B412, 751 (1994). doi:10.1016/0550-3213(94)90398-0
- J.M. Campbell, E.N. Glover, D. Miller, Nucl. Phys. B498, 397 (1997). doi:10.1016/S0550-3213(97)00268-X
- J. Fleischer, F. Jegerlehner, O. Tarasov, Nucl. Phys. B566, 423 (2000). doi:10.1016/S0550-3213(99)00678-1
- 12. W. Giele, E.N. Glover, JHEP 0404, 029 (2004). doi:10.1088/1126-6708/2004/04/029
- 13. R.G. Stuart, Comput. Phys. Commun. 48, 367 (1988). doi:10.1016/0010-4655(88)90202-0
- R.G. Stuart, A. Gongora, Comput. Phys. Commun. 56, 337 (1990). doi:10.1016/0010-4655(90)90019-W
- 15. O. Tarasov, Phys. Rev. **D54**, 6479 (1996). doi:10.1103/PhysRevD.54.6479
- G. Ossola, C.G. Papadopoulos, R. Pittau, Nucl. Phys. B763, 147 (2007). doi:10.1016/j. nuclphysb.2006.11.012
- 17. F. del Aguila, R. Pittau, JHEP 07, 017 (2004). doi:10.1088/1126-6708/2004/07/017
- P. Mastrolia, G. Ossola, T. Reiter, F. Tramontano, JHEP 1008, 080 (2010). doi:10.1007/ JHEP08(2010)080
- Z. Bern, L.J. Dixon, D.C. Dunbar, D.A. Kosower, Nucl. Phys. B425, 217 (1994). doi:10.1016/ 0550-3213(94)90179-1
- R. Britto, F. Cachazo, B. Feng, Nucl. Phys. B725, 275 (2005). doi:10.1016/j.nuclphysb.2005. 07.014
- 21. R.K. Ellis, W. Giele, Z. Kunszt, JHEP 0803, 003 (2008). doi:10.1088/1126-6708/2008/03/003
- R.K. Ellis, W.T. Giele, Z. Kunszt, K. Melnikov, Nucl. Phys. B822, 270 (2009). doi:10.1016/j. nuclphysb.2009.07.023
- G. Ossola, C.G. Papadopoulos, R. Pittau, JHEP 07, 085 (2007). doi:10.1088/1126-6708/2007/ 07/085
- G. Bevilacqua, M. Czakon, C.G. Papadopoulos, R. Pittau, M. Worek, JHEP 09, 109 (2009). doi:10.1088/1126-6708/2009/09/109
- G. Bevilacqua, M. Czakon, A. van Hameren, C.G. Papadopoulos, M. Worek, JHEP 02, 083 (2011). doi:10.1007/JHEP02(2011)083
- G. Bevilacqua, M. Czakon, C. Papadopoulos, M. Worek, Phys. Rev. D84, 114017 (2011). doi:10.1103/PhysRevD.84.114017
- G. Bevilacqua, M. Czakon, C.G. Papadopoulos, M. Worek, Phys. Rev. Lett. 104, 162002 (2010). doi:10.1103/PhysRevLett.104.162002
- R. Frederix, S. Frixione, K. Melnikov, G. Zanderighi, JHEP 1011, 050 (2010). doi:10.1007/ JHEP11(2010)050
- 29. C.F. Berger et al., Phys. Rev. Lett. 106, 092001 (2011). doi:10.1103/PhysRevLett.106.092001
- Z. Bern, L. Dixon, F. Febres Cordero, S. Hche, H. Ita et al., Phys. Rev. D88(1), 014025 (2013). doi:10.1103/PhysRevD.88.014025
- S. Badger, B. Biedermann, P. Uwer, V. Yundin, Phys. Rev. D89, 034019 (2014). doi:10.1103/ PhysRevD.89.034019
- 32. W. Giele, G. Zanderighi, JHEP 0806, 038 (2008). doi:10.1088/1126-6708/2008/06/038
- 33. T. Binoth, J.P. Guillet, G. Heinrich, JHEP **02**, 013 (2007). doi:10.1088/1126-6708/2007/02/
- P. Draggiotis, M.V. Garzelli, C.G. Papadopoulos, R. Pittau, JHEP 04, 072 (2009). doi:10.1088/ 1126-6708/2009/04/072
- 35. M.V. Garzelli, I. Malamos, R. Pittau, JHEP **01**, 040 (2010). doi:10.1007/JHEP01(2010)040
- 36. M.V. Garzelli, I. Malamos, R. Pittau, JHEP **01**, 029 (2011). doi:10.1007/JHEP01(2011)029

- 37. H.S. Shao, Y.J. Zhang, K.T. Chao, JHEP 09, 048 (2011). doi:10.1007/JHEP09(2011)048
- 38. R. Pittau, JHEP 1202, 029 (2012). doi:10.1007/JHEP02(2012)029
- 39. H.S. Shao, Y.J. Zhang, JHEP 1206, 112 (2012). doi:10.1007/s13130-012-4240-2
- 40. B. Page, R. Pittau, JHEP 1309, 078 (2013). doi:10.1007/JHEP09(2013)078
- A. Bredenstein, A. Denner, S. Dittmaier, S. Pozzorini, JHEP 08, 108 (2008). doi:10.1088/ 1126-6708/2008/08/108
- 42. A. Bredenstein, A. Denner, S. Dittmaier, S. Pozzorini, JHEP **03**, 021 (2010). doi:10.1007/JHEP03(2010)021
- 43. J.R. Andersen, et al., (2010)
- N.D. Christensen, C. Duhr, Comput. Phys. Commun. 180, 1614 (2009). doi:10.1016/j.cpc. 2009.02.018
- A. Alloul, N.D. Christensen, C. Degrande, C. Duhr, B. Fuks, Comput. Phys. Commun. 185, 2250 (2014). doi:10.1016/j.cpc.2014.04.012
- J. Alwall, R. Frederix, S. Frixione, V. Hirschi, F. Maltoni, O. Mattelaer, H.S. Shao, T. Stelzer,
   P. Torrielli, M. Zaro, JHEP 07, 079 (2014). doi:10.1007/JHEP07(2014)079
- 47. Z. Bern, D.A. Kosower, Nucl. Phys. **B379**, 451 (1992). doi:10.1016/0550-3213(92)90134-W
- 48. Z. Kunszt, A. Signer, Z. Trocsanyi, Nucl. Phys. **B411**, 397 (1994). doi:10.1016/0550-3213(94)90456-1
- S. Catani, M.H. Seymour, Z. Trocsanyi, Phys. Rev. D55, 6819 (1997). doi:10.1103/PhysRevD. 55.6819
- Z. Bern, A. De Freitas, L.J. Dixon, H.L. Wong, Phys. Rev. D66, 085002 (2002). doi:10.1103/ PhysRevD.66.085002
- G. 't Hooft, M.J.G. Veltman, Nucl. Phys. B44, 189 (1972). doi:10.1016/0550-3213(72)90279-9
- Z. Bern, L.J. Dixon, D.A. Kosower, Phys. Rev. D73, 065013 (2006). doi:10.1103/PhysRevD. 73.065013
- C. Anastasiou, R. Britto, B. Feng, Z. Kunszt, P. Mastrolia, Phys. Lett. B645, 213 (2007). doi:10. 1016/j.physletb.2006.12.022
- C. Anastasiou, R. Britto, B. Feng, Z. Kunszt, P. Mastrolia, JHEP 0703, 111 (2007). doi:10. 1088/1126-6708/2007/03/111
- W.T. Giele, Z. Kunszt, K. Melnikov, JHEP 0804, 049 (2008). doi:10.1088/1126-6708/2008/ 04/049
- 56. S. Badger, JHEP **0901**, 049 (2009). doi:10.1088/1126-6708/2009/01/049
- G. Ossola, C.G. Papadopoulos, R. Pittau, JHEP 03, 042 (2008). doi:10.1088/1126-6708/2008/ 03/042
- P. Mastrolia, G. Ossola, C.G. Papadopoulos, R. Pittau, JHEP 06, 030 (2008). doi:10.1088/ 1126-6708/2008/06/030
- F. Cascioli, P. Maierhofer, S. Pozzorini, Phys. Rev. Lett. 108, 111601 (2012). doi:10.1103/ PhysRevLett.108.111601
- 60. V. Yundin, Massive loop corrections for collider physics. Ph.D. thesis, Humboldt-Universitat zu Berlin (2012). http://edoc.hu-berlin.de/docviews/abstract.php?id=39163
- 61. J. Fleischer, T. Riemann, V. Yundin, PoS LL2012, 020 (2012)
- 62. H.S. Shao, unpublished
- 63. G. 't Hooft, M. Veltman, Nucl. Phys. **B153**, 365 (1979). doi:10.1016/0550-3213(79)90605-9
- 64. G. van Oldenborgh, J. Vermaseren, Z. Phys. C46, 425 (1990). doi:10.1007/BF01621031
- G. van Oldenborgh, Comput. Phys. Commun. 66, 1 (1991). doi:10.1016/0010-4655(91)90002-3
- T. Hahn, M. Perez-Victoria, Comput. Phys. Commun. 118, 153 (1999). doi:10.1016/S0010-4655(98)00173-8
- 67. R.K. Ellis, G. Zanderighi, JHEP 02, 002 (2008), doi:10.1088/1126-6708/2008/02/002
- D.T. Nhung, L.D. Ninh, Comput. Phys. Commun. 180, 2258 (2009). doi:10.1016/j.cpc.2009. 07.012
- 69. A. Denner, S. Dittmaier, Nucl. Phys. B844, 199 (2011). doi:10.1016/j.nuclphysb.2010.11.002
- 70. A. van Hameren, Comput. Phys. Commun. 182, 2427 (2011). doi:10.1016/j.cpc.2011.06.011

References 117

- 71. G. Duplancic, B. Nizic, Eur. Phys. J. C35, 105 (2004). doi:10.1140/epjc/s2004-01723-7
- 72. D. Melrose, Nuovo Cim. 40, 181 (1965). doi:10.1007/BF02832919
- 73. V. Hirschi, Automation of one-loop computations for scattering amplitudes and applications to collider phenomenology. Ph.D. thesis, Ecole Polytechnique Federale de Lausanne (2013), http://infoscience.epfl.ch/record/186388/files/EPFL\_TH5736.pdf

# Chapter 9 MadLoop5

Abstract In this chapter, we describe the techniques for automatic one-loop scattering amplitude computations by using MADGRAPH5 [1], which is dubbed as MADLOOP5. It is an important component in the MADGRAPH5\_AMC@NLO [2] framework. In order to avoid possible confusions between MADLOOP5 and the original MADLOOP4 [3], we want to emphasize here that the core functionalities relevant to the handling of tree-level amplitudes are inherited from MADGRAPH4 [4] in MADLOOP4, whereas MADLOOP5 uses MADGRAPH5. There are significant improvements in MADLOOP5 compared to MADLOOP4. Some of them are still not public.

#### 9.1 Notations and Conventions

Given an arbitrary  $2 \to n$  partonic process, an ordered list of the identities of its 2+n external legs  $r \equiv (\mathcal{I}_1, \mathcal{I}_2, \dots, \mathcal{I}_{n+2})$  represents one of the subprocesses. For example, for a process  $pp \to W^+ + j$ , r can be  $(u, \bar{d}, W^+, g)$ ,  $(u, g, W^+, d)$ , etc. One is able to demand MADLOOP5 to evaluate the following virtual quantity:

$$\mathcal{V}(r) \equiv 2\overline{\sum_{\substack{\text{color}\\\text{spin}}}} \Re{\{\mathcal{A}^{(n,1)}(r)\mathcal{A}^{(n,0)}(r)^*\}},\tag{9.1}$$

where  $\mathscr{A}^{(n,1)}$  is the renormalized one-loop scattering amplitude and  $\mathscr{A}^{(n,0)}$  is the Born scattering amplitude. In Eq. (9.1), the summation means that we have already taken the average of color and spin quantum numbers for the initial states and the summation of those for the final states. In general, the virtual  $\mathscr V$  is regularization

<sup>&</sup>lt;sup>1</sup>MADLOOP4 is written in C++, whereas MADLOOP5 is completely rewritten in Python and output in Fortran

<sup>&</sup>lt;sup>2</sup>I joined in the MADGRAPH5\_AMC@NLO project from September 2012. Under ERC grant LHC theory, I stayed at CERN for one year. Since then, I am collaborating with Dr. Valentin Hirschi in developing MADLOOP5.

<sup>©</sup> Springer Science+Business Media Singapore 2016 H.-S. Shao, *Heavy Quarkonium Production Phenomenology and Automation of One-Loop Scattering Amplitude Computations*, Springer Theses, DOI 10.1007/978-981-10-1624-0\_9

scheme dependent.<sup>3</sup> In default, MadLoop5 uses the HV scheme [7] in dimensional regularization. Moreover, a standard prefactor  $\frac{(4\pi)^\epsilon}{\Gamma(1-\epsilon)}$  is contained in  $\mathscr V$ . After specifying a phase space point from an external program (such as MadFKS5 in the MadGraph5\_AMC@NLO [2] framework), MadLoop5 returns double pole, single pole, and finite term in the virtual part.

For the loop-induced processes (e.g.,  $gg \to HH$ ), the Born scattering amplitude vanishes and only one-loop scattering amplitude survives. MADLOOP5 provides the following quantity:

$$\mathcal{Y}_{LI}(r) \equiv \overline{\sum_{\substack{\text{color} \\ \text{spin}}}} \left| \mathscr{A}^{(n,1)}(r) \right|^2,$$
 (9.2)

which is UV and IR finite. We want to emphasize that although  $\mathcal{A}^{(n,1)}(r)$  is UV finite (no need of UV renormalization counterterms), it may be UV divergent for a single-loop diagram. Therefore,  $R_2$  is still necessary in computing loop-induced processes.

In a process with non-vanishing Born amplitude, the virtual amplitude can be written as

$$\mathscr{A}^{(n,1)} = \mathscr{A}_0^{(n,1)} + \mathscr{A}_{IIV}^{(n,1)}, \tag{9.3}$$

where  $\mathscr{A}_{\mathrm{UV}}^{(n,1)}$  is the amplitude with UV renormalization counterterms.  $\mathscr{A}_{0}^{(n,1)}$  is the unrenormalized amplitude. It is composed of one-loop diagrams only

$$\mathscr{A}_0^{(n,1)} \equiv \sum_{\text{diagrams}} \mathscr{C},\tag{9.4}$$

where symbol  $\mathscr C$  denotes the contribution of a single one-loop Feynman diagram. The one-loop integral in  $\mathscr C$  should be reduced to a minimal basis of one-loop master integrals by reduction methods. Schematically, it is<sup>4</sup>

$$\mathscr{C} = \operatorname{Red}[\mathscr{C}] = \sum_{i} c_{i}(\mathscr{C}) \mathscr{J}_{i}^{(\operatorname{Red})} + R(\mathscr{C})$$
(9.5)

with  $\mathcal{J}_i^{(\text{Red})}$  up to 4-point one-loop scalar integrals. The coefficients  $c_i$  and R are functions of external momenta and of masses. We assume  $\mathscr{C}$  is a N-point one-loop diagram  $\mathscr{A}_N^{1-\text{loop}}$ , which is defined in Eq. (8.1). With Eq. (8.6), one is able to write  $\mathscr{C}$  into two terms

$$\mathscr{C} = \mathscr{C}_{\text{non}-R_2} + \mathscr{C}_{R_2} \tag{9.6}$$

<sup>&</sup>lt;sup>3</sup>The reader who is interested in regularization schemes can refer to Refs. [5, 6] and references therein.

<sup>&</sup>lt;sup>4</sup>We follow the notations in Ref. [2].

with

$$\mathcal{C}_{\text{non}-R_2} \equiv \int d^d \bar{\ell} \frac{N(\ell)}{\prod_{i=0}^{N-1} \bar{D}_i},$$

$$\mathcal{C}_{R_2} \equiv \int d^d \bar{\ell} \frac{\tilde{N}(\ell, \tilde{\ell}^2, \epsilon)}{\prod_{i=0}^{N-1} \bar{D}_i}.$$
(9.7)

### 9.2 Basic Procedures

Let us first present the basic procedures of calculating virtual corrections in MAD-LOOP5. The performance of MADLOOP5 follows the below steps:

- 1. A NLO extensive model should be provided by user or a third-party code (e.g., FEYNRULES<sup>5</sup>) following the Universal FeynRules Output (UFO) format [8]. In the public version of MADGRAPH5\_AMC@NLO, a NLO UFO model loop\_sm is available for QCD corrections to SM processes. In the private version, two extensively validated NLO UFO models loop\_qcd\_qed\_sm and loop\_qcd\_qed\_sm\_Gmu are established for QCD and/or QED/EW corrections in SM. The former one is in  $(\alpha(m_Z), m_Z, m_W)$  input scheme, and the EW coupling constant is renormalized in  $\alpha(m_Z)$ -scheme [9]. The latter one is in  $(G_\mu, m_Z, m_W)$  input scheme, and the EW coupling constant is renormalized in  $G_\mu$ -scheme [9, 10]. A NLO model includes tree-level vertices as well as UV renormalized and  $R_2$  vertices.
- 2. Inherited from the way using MadGraph5, it calls a module called Automatic Libraries Of Helicity Amplitudes for Feynman Diagram Computations (ALOHA) [11] to construct amplitudes starting from a given UFO model.
- 3. MadLoop5 generates one-loop amplitudes by cutting one and only one loop leg and then uses MadGraph5 to generate all corresponding tree-level diagrams. This strategy is also adopted in MadLoop4 [3] and HELAC-1LOOP [12]. Such diagrams are called L-cut diagrams. Special attention should be paid to avoid double counting and maximal recycling. The interested reader can refer to Refs. [3, 13] for the details.
- 4. Construct the numerator function  $N(\ell)$  and the loop propagator information from the L-cut diagrams and output the amplitude into the format that is needed by the loop reduction libraries. At the meantime, all of the UV and  $R_2$  amplitudes are also obtained and outputted. There are two modes available in MadLoop5 to output. One way, which is called the *default mode*, only uses CutTools [14], and no optimization is implemented. Another way, called the *optimized mode*, the code being already optimized a lot, is in which both CutTools [14] and TIR libraries (now it is still restricted to PJFRY++ [15, 16] and IREGI [17])<sup>7</sup> are available.

<sup>&</sup>lt;sup>5</sup>The new version of FEYNRULES for generating NLO model will be published in the near future.

 $<sup>{}^{6}</sup>G_{\mu}$  is the fermion constant.

<sup>&</sup>lt;sup>7</sup>TIR interface is only available in the private version. It will be contained in the future release.

5. For a single phase space point provided by a user or a third-party event generator, the reduction libraries are called to calculate the loop integrals. With the same kinematic configuration, UV and  $R_2$  amplitudes are also computed.

6. Numerical stability test is performed to the given kinematic configuration. If an unstable phase space point is found, MADLOOP5 tries to rescue it in a proper way. In the default mode, it turns to quadruple precision arithmetic, whereas in the optimized mode, it uses other reduction libraries first and then turns to quadruple precision arithmetic.

## 9.3 Improvements Compared to MadLoop4

In this section, we will mainly establish the improvements in MADLOOP5 compared to the original MADLOOP4, which is also described in Ref. [2]. Because of the technically awkward limitation of MADGRAPH4, MADLOOP4 cannot generate a process whose Born amplitude contains a four-gluon vertex. This limitation is completely lifted in MAD-Loop5 by using the UFO/ALOHA chain in MADGRAPH5. Due to the limitation of unitary gauge only adopted in MADGRAPH4, MADLOOP4 cannot compute some loops that feature massive vector bosons. It is overcome now in MADGRAPH5 as well as MADLOOP5 by providing alternatives to Feynman gauge. Moreover, complex mass scheme [18] is also implemented in MADLOOP5 to include the finite-width effects in loops. In the case of mixed corrections (like QCD+EW corrections), MadLoop5 is designed in an efficient way to separate specific orders. For example, in  $uu \rightarrow uu$  process, at LO, there are three gauge-invariant part  $\mathcal{O}(\alpha_s^2)$ ,  $\mathcal{O}(\alpha_s\alpha)$ , and  $\mathcal{O}(\alpha^2)$  at matrix elementsquared level. The corresponding virtual correction has  $\mathcal{O}(\alpha_S^3)$ ,  $\mathcal{O}(\alpha_S^2\alpha)$ ,  $\mathcal{O}(\alpha_S\alpha^2)$ , and  $\mathcal{O}(\alpha^3)$  parts. MadLoop5 provides the results in different orders to the external program (e.g., MADFKS5 in MADGRAPH5\_AMC@NLO), which is necessary to cancel the IR poles with the corresponding IR subtraction terms.

## 9.4 Optimizations

A lot of optimizations have been done in MADLOOP5 in the optimized mode. In this section, we will discuss the main ones.

Let us recall how one-loop integral is calculated in MADLOOP4. For a Born amplitude in the helicity configuration h, it can be decomposed in a color basis as

$$\mathscr{A}_{h}^{(n,0)} = \sum_{b} \lambda_{b}^{(0)} \mathscr{B}_{h,b}, \tag{9.8}$$

<sup>&</sup>lt;sup>8</sup>It is only available in optimized mode of the private version.

9.4 Optimizations 123

where  $\lambda_b^{(0)}$  is a color factor and subscript *b* runs over all possible color factors. Here,  $\mathcal{B}_{h,b}$  can be understood as a scalar quantity without any color index. The similar color decomposition can also be applied to the one-loop integrals as follows:

$$N(\ell) \to \lambda_l^{(1)} \mathcal{N}_{h,l}(\ell),$$

$$\bar{D}_i \to \bar{D}_{i,l}, \tag{9.9}$$

where we have added a subscript index l for each color–structure subamplitude. Then, one easily arrives at

$$\mathcal{A}_{\text{non}-R_{2}}^{(n,1)} \mathcal{A}^{(n,0)*} = \sum_{\text{color}} \sum_{h} \left( \sum_{l} \lambda_{l}^{(1)} \int d^{d} \bar{\ell} \frac{\mathcal{N}_{h,l}(\ell)}{\prod_{i=0}^{l-1} \bar{D}_{i,l}} \right) \left( \sum_{b} \lambda_{b}^{(0)} \mathcal{B}_{h,b} \right)^{*}$$

$$= \sum_{h} \sum_{l} \sum_{b} \int d^{d} \bar{\ell} \frac{\mathcal{N}_{h,l}(\ell)}{\prod_{i=0}^{N_{l}-1} \bar{D}_{i,l}} \Lambda_{lb} \mathcal{B}_{h,b}^{*}$$
(9.10)

where

$$\mathscr{A}_{\text{non}-R_2}^{(n,1)} \equiv \sum_{\text{diagrams}} \mathscr{C}_{\text{non}-R_2},$$

$$\Lambda_{h,b} \equiv \sum_{\text{color}} \lambda_l^{(1)} \lambda_b^{(0)*}.$$
(9.11)

The one-loop integral reduction procedure of MADLOOP4 follows the following way:

$$\mathscr{A}_{\text{non}-R_{2}}^{(n,1)}\mathscr{A}^{(n,0)*} = \sum_{h} \sum_{l} \sum_{b} \text{Red} \left[ \int d^{d} \bar{\ell} \frac{\mathscr{N}_{h,l}(\ell)}{\prod_{i=0}^{N_{l}-1} \bar{D}_{i,l}} \right] \Lambda_{lb} \mathscr{B}_{h,b}^{*}. \quad (9.12)$$

The operation Red in MadLoop4 is restricted to OPP or Cuttools. The reduction in Eq. (9.12) is quite inefficient and requires heavy computations of the most complicated numerator functions  $\mathcal{N}_{h,l}(\ell)$  calling by Cuttools. The reduction in Cuttools is called  $\#h \times \#l$  times for each kinematic configuration. Moreover, each of these calls involves the recomputation of  $\mathcal{N}_{h,l}$  for a large number of times (it is recomputed by Cuttools  $\sim 50$  times for a box integral) in OPP, but it only involves changing the numerical complex value of loop momentum  $\bar{\ell}$ .

It is straightforward to improve the computational efficiency by summing helicities with the Born one

$$\mathscr{A}_{\text{non}-R_{2}}^{(n,1)}\mathscr{A}^{(n,0)*} = \sum_{l} \text{Red} \left[ \int d^{d} \bar{\ell} \frac{\sum_{h} \sum_{b} \mathscr{N}_{h,l}(\ell) \Lambda_{lb} \mathscr{B}_{h,b}^{*}}{\prod_{i=0}^{N_{l}-1} \bar{D}_{i,l}} \right], \quad (9.13)$$

because the Born amplitude is irrelevant to  $\ell$  and the reduction procedure. Another optimization is by grouping the different one-loop diagrams sharing the same

denominators into one topology set t

$$\prod_{i=0}^{N_l-1} \bar{D}_{i,l} = \prod_{i=0}^{N_p-1} \bar{D}_{p,l}, \quad \forall l, p \in t.$$
 (9.14)

Then, the computation becomes

$$\mathscr{A}_{\text{non}-R_{2}}^{(n,1)}\mathscr{A}^{(n,0)*} = \sum_{t} \text{Red} \left[ \int d^{d} \bar{\ell} \frac{\sum_{h} \sum_{l \in t} \sum_{b} \mathscr{N}_{h,l}(\ell) \Lambda_{lb} \mathscr{B}_{h,b}^{*}}{\prod_{i=0}^{N_{l_{i}}-1} \bar{D}_{i,l_{i}}} \right]. \quad (9.15)$$

The number of calling OPP reduces from  $\#h \times \#l$  to #t with  $\#t \leq \#l$ . However, it is easy to realize that the optimization presented here is not applicable to the loop-induced processes.

The solution of the second issue is attributed to the techniques explored in Open-Loops [19]. One observes that the numerator  $\mathcal{N}_{h,l}(\ell)$  is a polynomial of  $\ell$  (at least in Feynman gauge)

$$\mathcal{N}_{h,l}(\ell) = \sum_{r=0}^{r_{\text{max}}} c_{\mu_1 \cdots \mu_r;h,l}^{(r)} \ell^{\mu_1} \cdots \ell^{\mu_r}.$$
 (9.16)

The coefficients  $c_{\mu_1\cdots\mu_r;h,l}^{(r)}$  are independent of  $\ell$ . Hence, the numerical recomputation of  $\mathcal{N}_{h,l}(\ell)$  is much faster in the OPP reduction after changing the value of  $\ell$ , because the coefficients  $c_{\mu_1\cdots\mu_r;h,l}^{(r)}$  are only calculated once in each phase space point. It also paves the way to use TIR libraries. In the loop-induced processes, TIR is mandatory to improve the computation efficiency in Madloop5. Because of the failure of Eq. (9.15) for loop-induced processes, the number of calling OPP cannot be at best  $\#h\times\#t$ . With TIR, one is able to reduce the number of reducing loop integrals to #t, because the tensor integrals are independent of helicity configurations. Finally, we stress that the expansion in Eq. (9.16) will lose its advantages if it does not use recursion relations (like in Openloops [19]) or efficient caching systems (like in Madloop5 [2]). To avoid the possible confusions, the implementation of such algorithms in Madloop5 is completely in an independent way and irrelevant to any detail code of the unpublic Openloops.

## 9.5 General UV Renormalization and $R_2$ Contribution

In this section, we will discuss the general UV renormalization strategy and describe how MadLoop5 calculates UV and  $R_2$  contributions.

As far as UV renormalization is concerned, MadLoop4 is limited to consider QCD corrections in SM. It allows significant simplifications. For example, the wave function renormalization of the external massive particles is always proportional

to the helicity-summed Born amplitude-squared [3]. This simplification will not be satisfied in EW corrections and in a general BSM. The wave function renormalization of external quarks is chiral dependent in EW corrections, which means that the EW wave function renormalization constants of the left-handed top quark and right-handed top quark are different. It makes the UV contribution from wave function renormalization not proportional to the Born amplitude-squared anymore. The new general strategy of UV renormalization in Madloop5 follows the Bogoliubov–Parasiuk–Hepp–Zimmermann (BPHZ) renormalization procedures. The wave function renormalization constants are completely absorbed into the UV renormalized vertices and the renormalized mass insertion. This strategy is the current choice for the extension of FeynRules to NLO level.

The computation of the UV and  $R_2$  contributions in MADLOOP5 can be schematically written as

$$2\overline{\sum_{\substack{\text{color}\\\text{spin}}}} \Re\{\mathscr{A}_X^{(n,1)}(r)\mathscr{A}^{(n,0)}(r)^*\}$$
(9.17)

with  $X=R_2$  or UV. The computation of  $\mathscr{A}_X^{(n,1)}(r)$  is performed in the similar manner as that of Born amplitude  $\mathscr{A}^{(n,0)}(r)$ , by imposing that  $\mathscr{A}_X^{(n,1)}(r)$  contain one and only one X-type vertex. Because we always use on-shell renormalization in MADLOOP5, we have excluded the diagrams with the 2-point UV- or  $R_2$ -type vertex attached on the external legs.

In order to increase the flexibility of MadLoop5, in particular for what concerns the exclusion of the contributions of certain loop integrals, a more extensive loop-matching construction has been implemented. Given the physics contents of a generic UV and  $R_2$  counterterm G, we have

$$G \equiv \left\{ \left\{ \mathcal{J}_{1}^{(e)} \cdots \mathcal{J}_{m}^{(e)} \right\}; \left\{ \mathcal{J}_{1}^{(l_{k})} \cdots \mathcal{J}_{n_{k}}^{(l_{k})} \right\}_{k=1}^{k_{\text{loop}}}; \mathcal{W}, L, \lambda, o, X \right\},$$
(9.18)

where L and  $\lambda$  are lists of Lorentz structures and color structures, respectively, o is a list of coupling orders,  $\mathcal{W}$  is a list of couplings for the counterterm, and  $\mathcal{I}_i^{l_k}$  is the identity of particles in the loop. G is an effective vertex with its external particles' identities  $\{\mathcal{I}_1^{(e)}\cdots\mathcal{I}_m^{(e)}\}$ . For example, for a  $X=R_2$  vertex ggg, there are several one-loop diagrams corresponding to it as shown in Fig. 9.1, where Q=u,d,s,c,b,t. We have

$$\left\{ \mathcal{J}_{1}^{(e)} \cdots \mathcal{J}_{m}^{(e)} \right\} = \left\{ g, g, g \right\}, 
\left\{ \mathcal{J}_{1}^{(l_{k})} \cdots \mathcal{J}_{n_{k}}^{(l_{k})} \right\}_{k=1}^{k_{\text{loop}}} = \left\{ g \right\}, \left\{ u \right\}, \left\{ d \right\}, \left\{ s \right\}, \left\{ c \right\}, \left\{ b \right\}, \left\{ t \right\}.$$
(9.19)

Although in principle  $R_2$  and loop Feynman diagrams can be one-to-one correspondence, we gather the one-loop diagrams with the same loop particle content together. In our example, the Fig. 9.1a and b share the same loop particle content and they

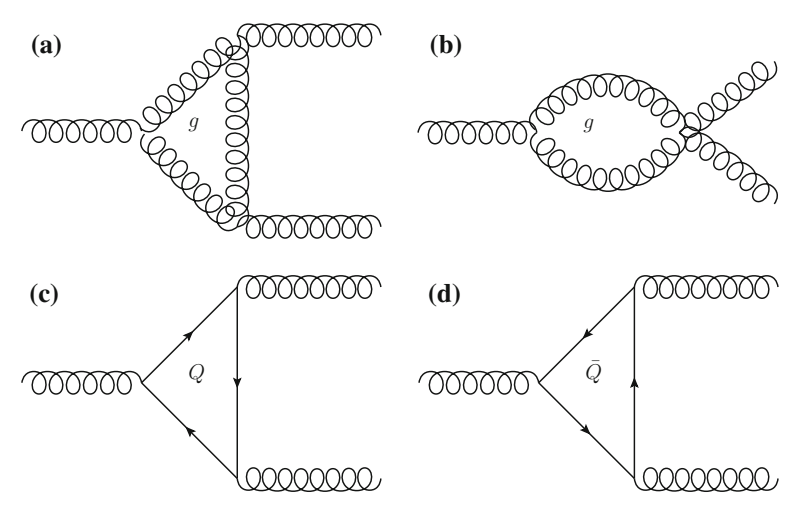


**Fig. 9.1** Feynman diagrams contributing to  $R_2$  vertex ggg

are combined together in G. The situation to UV is more involved than  $R_2$  because of the new general UV renormalization. For example, for a UV vertex  $gu\bar{u}$ , the renormalization vertex is

$$\delta V_{gu\bar{u}} \sim \delta g_S + \delta Z_g / 2 + \delta Z_u, \tag{9.20}$$

where  $\delta g_S$ ,  $\delta Z_g$ , and  $\delta Z_u$  are the renormalization constants for the strong coupling constant  $g_S \equiv \sqrt{4\pi\alpha_S}$ , the gluon wave function, and the u or  $\bar{u}$  quark wave function. The loop particles for  $\delta g_S$  and  $\delta Z_u$  are  $\{g, u\}$ , whereas those for  $\delta Z_g$  are  $\{g\}$ ,  $\{u\}$ ,  $\{d\}$ ,  $\{s\}$ ,  $\{c\}$ ,  $\{b\}$ ,  $\{t\}$ . Therefore, for the X = UV vertex  $gu\bar{u}$ , we have

$$\begin{cases}
\mathscr{I}_{1}^{(e)} \cdots \mathscr{I}_{m}^{(e)} \\
\end{cases} = \{g, u, \bar{u}\}, 
\begin{cases}
\mathscr{I}_{1}^{(l_{k})} \cdots \mathscr{I}_{n_{k}}^{(l_{k})} \\
\rbrace_{k=1}^{k_{\text{loop}}} = \{g, u\}, \{g\}, \{u\}, \{d\}, \{s\}, \{c\}, \{b\}, \{t\}.
\end{cases} (9.21)$$

We discuss how MadLoop5 exploits such informations. If one wants to exclude some loops from his/her calculation (e.g., one wants to leave out some heavy-flavor quark contributions or decouple the photon contribution in EW corrections), it is convenient for MadLoop5 to exclude the corresponding contributions from UV and  $R_2$  with the loop particle information in G. The corresponding loops are discarded at the L-cut diagram generation time. The presence of  $\{\mathcal{I}_1^{(l_k)} \cdots \mathcal{I}_{n_k}^{(l_k)}\}$  in G allows one to discard the contributions when computing the UV and  $R_2$  ones. In specific, if the set  $\{\mathcal{I}_1^{(l_k)} \cdots \mathcal{I}_{n_k}^{(l_k)}\}$  contains the particle that should be dropped, the corresponding diagrams are not included in  $\mathcal{A}_X^{(n,1)}$ . This way of filtering diagrams is called *loop content filtering* in Ref. [2].

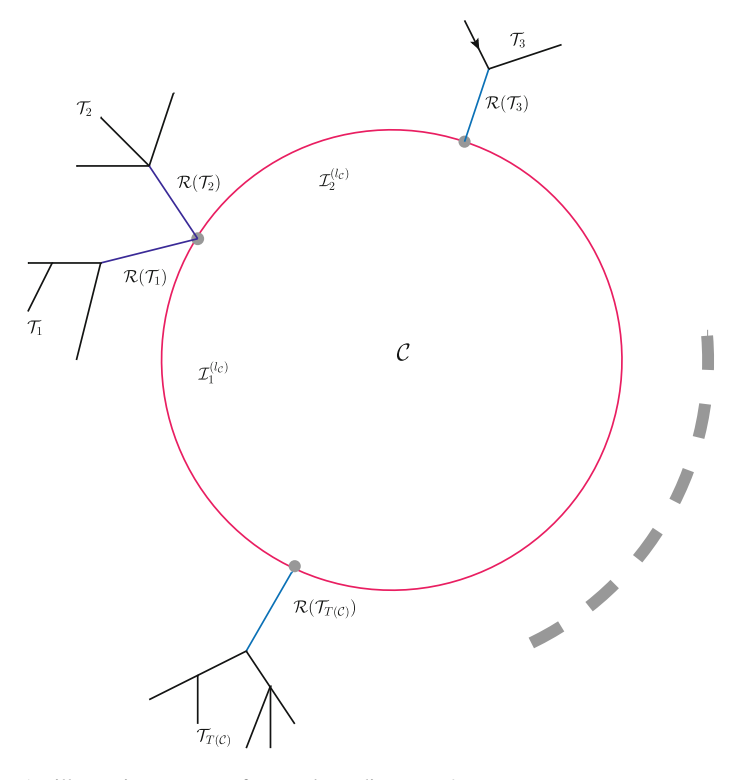


**Fig. 9.2** An illustrative structure for one-loop diagram  $\mathscr{C}$ 

Apart from the loop content filtering, MADLOOP5 also provides another filtering way, which is actually used for UV mass insertion and  $R_2$  ones. Let us start from a loop diagram  $\mathscr{C}$ . Its associated tree topology  $\Gamma^{(\mathscr{C})}$  can be determined

$$\mathscr{C} \to \Gamma^{(\mathscr{C})} \equiv \left( \left\{ \mathscr{T}_1 \cdots \mathscr{T}_{T(\mathscr{C})} \right\}, \left\{ \mathscr{I}_1^{(l_{\mathscr{C}})} \cdots \mathscr{I}_n^{(l_{\mathscr{C}})} \right\} \right).$$
 (9.22)

The notation here means that there are  $T(\mathscr{C})$  subtrees  $\mathscr{T}_{\alpha}$  attached to the loop in diagram  $\mathscr{C}$  (see Fig. 9.2).  $\left\{\mathscr{I}_{1}^{(l_{\mathscr{C}})}\cdots\mathscr{I}_{n}^{(l_{\mathscr{C}})}\right\}$  is the set of particles flowing in the loop. MADLOOP5 collects all the different subtree topologies relevant to the computation and selects all of the counterterm vertices G that fulfill the following relation:

$$\left\{ \mathcal{I}_{1}^{(e)} \cdots \mathcal{I}_{m}^{(e)} \right\} = \left\{ \mathcal{R}(\mathcal{T}_{1}) \cdots \mathcal{R}(\mathcal{T}_{T_{\mathscr{C}}}) \right\}, \tag{9.23}$$

where we have denoted  $\mathcal{R}(\mathcal{T}_{\alpha})$  as the root of the  $\alpha$ th subtree  $\mathcal{T}_{\alpha}$ . Furthermore, MADLOOP5 only selects the ones that fulfill the equation

$$\left\{ \mathcal{J}_1^{(l_k)} \cdots \mathcal{J}_{n_k}^{(l_k)} \right\} = \left\{ \mathcal{J}_1^{(l_{\mathscr{C}})} \cdots \mathcal{J}_n^{(l_{\mathscr{C}})} \right\}. \tag{9.24}$$

It guarantees a rather strict relationship between a generated loop diagram and its counterterm. It is quite useful in establishing the correctness of a new model.

## 9.6 Stability

Numerical stability issue is very crucial in any numerical program. It not only affects the accuracy but also changes the convergence of the result and the total time costing. MADLOOP5 has a very solid self-diagnostic and recovery strategy. Unlike MADLOOP4 [3, 20], MADLOOP5 is implemented a completely reduction library-independent diagnostic tool. MADLOOP5 is redesigned to judge the unstable phase space at the whole amplitude-squared level instead of loop-by-loop basis in MADLOOP4. The advantage is obvious that when a negligible loop integral is reported to be unstable, MADLOOP5 ignores it since it does not indeed affect the accuracy of the final result.

Let us describe the stability diagnostic procedure in MADLOOP5. Back to Eq. (9.1), the quantity calculated by MADLOOP5 is

$$\mathscr{V}(r) = \frac{(4\pi)^{\epsilon}}{\Gamma(1-\epsilon)} \left(\frac{\mu_F^2}{Q_{FS}^2}\right)^{\epsilon} \left(\frac{c_{-2}}{\epsilon^2} + \frac{c_{-1}}{\epsilon} + c_0\right),\tag{9.25}$$

where  $Q_{\rm ES}$  is the Ellis–Sexton scale [21]. For any given phase space point, the coefficients  $c_j(j=-2,-1,0)$  in Eq. (9.25) are computed  $1+n_{\rm test}$  times. We denote the coefficients  $c_j$  in i+1th evaluation as  $c_j^{(i)}$  with  $i=0,1,\ldots,n_{\rm test}$ . Then, the average and the difference can be defined as

$$\bar{c}_{j} \equiv \frac{1}{2} \left( \max \left\{ \left| c_{j}^{(i)} \right| \right\}_{i=0}^{n_{\text{test}}} + \min \left\{ \left| c_{j}^{(i)} \right| \right\}_{i=0}^{n_{\text{test}}} \right),$$

$$\Delta c_{j} \equiv \max \left\{ \left| c_{j}^{(i)} \right| \right\}_{i=0}^{n_{\text{test}}} - \min \left\{ \left| c_{j}^{(i)} \right| \right\}_{i=0}^{n_{\text{test}}}.$$
(9.26)

The relative accuracy defined in MADLOOP5 is

$$\chi \equiv \frac{\sum_{j=-2}^{0} \Delta c_j}{\sum_{j=-2}^{0} \bar{c}_j}.$$
(9.27)

A phase space point is flagged as unstable when the relative accuracy  $\chi$  is larger than a threshold  $\varepsilon$ , i.e.,

$$\chi > \varepsilon$$
. (9.28)

9.6 Stability 129

We call the corresponding kinematic configuration as an unstable phase space (UPS) point. The threshold  $\varepsilon$  can be defined by the user via the input card MadLoopParams.dat. Its default value in MadLoop5 is  $10^{-3}$ .

The first calculated coefficients  $c_j^{(0)}$  are the results by applying the loop reduction library with the given kinematic configuration. The other coefficients  $c_j^{(>0)}$  are obtained in two different manners. One is using a new kinematic configuration by taking a Lorentz boost to the original one, which is called *Lorentz test*. Because the amplitudes are Lorentz invariant, it should return the same result if the point is stable. Another one, called *direction test*, is using a different ordering of the loop propagators  $\bar{D}_i$  as input to the loop reduction libraries. This is very useful because the reduction procedure of the loop integral completely changes. From the viewpoint of efficiency, the advantage of the *direction test* is that the program is able to reuse the values of  $c_{\mu_1\cdots\mu_r;h,l}^{(r)}$  (see Eq. (9.16)) that has been evaluated in the first time. Hence, it is faster than *Lorentz test*. The numbers of *Lorentz test* and *direction test* can be assigned by the user via MadLoopParams .dat. By default, MadLoop5 sets  $n_{\text{test}}=2$  and performs exact one *Lorentz test* and one *direction test*. In *Lorentz test*, the kinematic for each external leg is rotated as

$$\{E, p_x, p_y, p_z\} \to \{E, p_z, -p_x, -p_y\},$$
 (9.29)

whereas in *direction test*, the order of the loop denominators is reversed

$$\bar{D}_0 \bar{D}_1 \cdots \bar{D}_{N-1} \to \bar{D}_{N-1} \cdots \bar{D}_1 \bar{D}_0.$$
 (9.30)

When an UPS is found, MadLoop5 has two ways to rescue it in the optimized mode. It starts from changing the integral reduction procedure if there are several integral reduction libraries are available. For example, if the entry MLReductionLib in MadLoopParams.dat is specified as follows:

```
! This file is for the user to set the different parameters of MadLoop.
! The name of the variable to define must start with the '#' sign and then
! the value should be put immediately on the next line.

!
#MLReductionLib
1|2|3
! Default :: 1|2|3
! The tensor integral reduction library. The current choices are:
! 1 | CutTools
! 2 | PJFry++
! 3 | IREGI
! One can use the combinations to reduce integral, e.g.
! 1|2|3 means first use CutTools, if it is not stable, use PJFry++,
! if it is still unstable, use IREGI. If it failed, use QP of CutTools.
```

MADLOOP5 first uses CUTTOOLS to reduce the integral (the first number "1"). If the result is unstable, the program uses the second available library PJFRY++ (the second number "2"). If the integral is beyond the scope of PJFRY++ or the result is still unstable,

the program turns to the third available library IREGI (the third number "3"). The order is completely up to the user. For example, one can specify 2|1|3 instead of 1|2|3. Then, the order of calling reduction libraries becomes

$$PJFRYPP++ \rightarrow CUTTOOLS \rightarrow IREGI.$$
 (9.31)

Only when all of the reduction libraries cannot give a stable result in double precision, the program goes into quadruple precision evaluations. If at some point the integral is stable, the program, of course, will not go further. We point out that the evaluation speed in quadruple precision is much slower than that in double precision. If the result is again classified to be unstable, the phase space point is called an exceptional phase space (EPS) point and Madloop5 sets the coefficients  $c_j$  to be zero and proceeds to the next kinematic configuration. In the practical calculations, the case of EPS extremely rarely happens after using quadruple precision. As we have pointed out for several times, TIR is only available in the private version. Hence, in the public version of Madloop5, only the second recovery strategy is used to rescue UPS.

#### 9.7 Illustrative Stand-Alone Results

In this section, we want to present some stand-alone results to illustrate the ability of MADLOOP5. The results presented here are indeed the ones given in Ref. [2].

We denote the Born amplitude-squared as

$$a_0 \equiv \overline{\sum_{\substack{\text{color} \\ \text{spin}}}} \left| \mathscr{A}^{(n,0)}(r) \right|^2. \tag{9.32}$$

The coefficients  $c_j$ , j = -2, -1, 0 for the virtual part are already defined in Eq. (9.25). Throughout this section, we set

$$\mu_F = \mu_R = Q_{\rm ES} = \sqrt{s},\tag{9.33}$$

where  $\sqrt{s}$  is the invariant mass of the initial particles. For simplicity, all particle widths are equal to zero, the leptons that circulate in the loops are massless, and the Cabibbo–Kobayashi–Maskawa (CKM) matrix is diagonal. In order to maximize the numerical accuracy, the results reported here are calculated by using quadruple precision arithmetics, <sup>9</sup> though in double precision they are already stable. Moreover, we want to remind the reader that all results are computed in HV scheme.

<sup>&</sup>lt;sup>9</sup>The accuracy of the coefficients  $c_i$  reported here in quadruple precision is beyond 17 digits.

# 9.7.1 High-Multiplicity QCD Process: $gg \rightarrow d\bar{d}b\bar{b}t\bar{t}$

First, we consider a high-multiplicity and multiscale QCD process, i.e.,  $gg \rightarrow d\bar{d}b\bar{b}t\bar{t}$ . It is a 2  $\rightarrow$  6 process that contains up to 8-point one-loop integrals. There are three scales involved in it: the top quark mass, the bottom quark mass, and the partonic center-of-mass energy. Only, pure QCD loops, UV, and  $R_2$  terms are considered. There are totally 54614 one-loop diagrams and 8190 topologies generating. The relevant input parameters in this process are

Parameter	Value	Parameter	Value
$\alpha_S$	0.118	$n_{lf}$	4
$m_t$	173.0	$m_b$	4.7

A chosen random kinematic configuration generated by RAMBO [22], in the unit of GeV, is

```
p_{\varrho} = (500
                          , 0
                                               , 0
                                                                        , 500)
p_g = (500)
                          , 0
                                                , 0
                                                                         , -500)
p_d = (159.884957663500 \quad , -100.187853644511 \quad , \ 83.9823400815702 \quad \  , \ 92.0465111972672)
p_{\bar{d}} = (203.546206153656 , -154.329441032052 , -0.512510195103158 , 132.714803257139)
p_b = (81.9036633616240 , 4.56741073895954 , -80.4386221767117 , 13.9601895942747)
                          ,\; 6.99982274816896 \quad ,\; 9.96034329509376 \qquad ,\; 39.4277395334349)
p_{\bar{b}} = (41.5312244194448)
                          ,\ 84.0110736983121 \qquad ,\ 18.3862699981019 \qquad ,\ -142.325385396572)
p_t = (239.961310957973)
p_{\bar{t}} = (273.172637443802 , 158.938987491122 , -31.3778210029510 , -135.823858185543)
```

There are only  $\mathscr{O}(\alpha_S^6)$  Born contribution and  $\mathscr{O}(\alpha_S^7)$  virtual contribution. The results are

$gg \rightarrow d\bar{d}b\bar{b}t\bar{t}$	MADLOOP5
$a_0$	1.7614866952133752e-14
<i>c</i> <sub>0</sub>	7.1888721656398052e-14
$c_{-1}$	-3.8948541926529643e-15
$c_{-2}$	-2.8670389920110557e-15

The coefficients  $c_{-1}$  and  $c_{-2}$  have been checked with the analytical known forms in Ref. [23]. It can be achieved with the MADGRAPH5\_AMC@NLO-shell generation command:

```
MG5_aMC > generate g g > d d\sim b b\sim t t\sim [virt=QCD]
```

It demonstrates that MADLOOP5 shows good performances for QCD corrections to any SM process from this example.

# 9.7.2 Mixed-Coupling Expansion I: $u\bar{d} \rightarrow d\bar{d}W^+ZH$

We have pointed out that QCD and QED/EW corrections for any SM process are already checked extensively in the private version of MadLoop5. Here, we consider the first process  $u\bar{d}\to d\bar{d}W^+ZH$  with QCD+EW corrections. The results are expanded into various orders. For Born  $a_0$ , there are  $\mathcal{O}(\alpha_S^2\alpha^3)$ ,  $\mathcal{O}(\alpha_S\alpha^4)$ , and  $\mathcal{O}(\alpha^5)$  contributions, whereas for virtual, there are  $\mathcal{O}(\alpha_S^2\alpha^3)$ ,  $\mathcal{O}(\alpha_S^2\alpha^4)$ ,  $\mathcal{O}(\alpha_S\alpha^5)$ , and  $\mathcal{O}(\alpha^6)$  parts. MadLoop5 is already designed to be able to efficiently split the contributions into different orders. We have performed our computation in  $(\alpha(m_Z), m_Z, m_W)$  input scheme and used  $\alpha(m_Z)$ -scheme for the EW coupling constant renormalization. For this process, we have generated 187138 one-loop diagrams. After grouping, there are remaining 8098 topologies, which show a lot of simplifications. The relevant input parameters are

Parameter	Value	Parameter	Value
$\alpha_S$	0.118	$n_{lf}$	5
$m_t$	173.0	$y_t$	173.0
$m_W$	80.419	$m_Z$	91.188
$m_H$	125.0	$\alpha^{-1}$	132.507

The chosen kinematic configuration (in GeV units) is

```
p_u = (500
                            . 0
                                                  . 0
                                                                         , 500)
                                                  , 0
 p_{\bar{d}} = (500)
                            , 0
                                                                         , -500)
 p_d = (77.3867935143263)
                          , -13.6335837243927 , 33.7255664483738
                                                                         , -68.3039338032245)
 p_{\bar{d}} = (251.029839835656 , -74.4940380485791 , -235.871950829717
                                                                        , 42.7906718212678)
p_{W^+} = (139.739680522225)
                           , -81.0565319364851
                                                  , -74.5408139008771
                                                                         , 30.5527158347332)
 p_Z = (382.164100735946)
                            . 208.038848497860
                                                  . 298.200182616267
                                                                         . -74.3682536477996)
 p_H = (149.679585391847)
                            , -38.8546947884028 , -21.5129843340470
                                                                        , 69.3287997950232)
```

The Born results in various orders are

$u\bar{d} \rightarrow d\bar{d}W^+ZH$	$a_0$
$\mathscr{O}(\alpha_S^2 \alpha^3)$	2.8791434190645365e-16
$\mathcal{O}(\alpha_S \alpha^4)$	-4.2378807039987007e-17
$\mathscr{O}(\alpha^5)$	5.8013051661550053e-18

701	cc ·			1	- 1	
Tha	coathorante	0	110	anch	order	Ora
1110	coefficients	(, i	111	Cacii	OLUCI	aic

$u\bar{d} \to d\bar{d}W^+ZH$	$\mathscr{O}(\alpha_S^3 \alpha^3)$	$\mathscr{O}(\alpha_S^2 \alpha^4)$
$c_0$	-4.9670212643498834e-17	3.5197577360529166e-18
$c_{-1}$	-1.0437771535958436e-16	1.5619709675879874e-17
$c_{-2}$	-2.8837935481452971e-17	3.9757576347989499e-18
	$\mathscr{O}(\alpha_S \alpha^5)$	$\mathscr{O}(\alpha^6)$
$c_0$	2.3220780285374270e-18	-1.4592469761033279e-18
$c_{-1}$	-1.8146075843176133e-18	-5.0799804067050324e-21
$\overline{c_{-2}}$	-5.4147748433007504e-19	-5.4195415714279579e-21

The coefficients  $c_{-1}$  and  $c_{-2}$  have been checked with the analytical known forms in Ref. [23] and its generalization to EW correction. One can generate the process with the MADGRAPH5 AMC@NLO-shell generation command:

```
MG5_aMC> generate u d\sim > d d\sim w+ z h QCD=99 QED=99 [virt=QCD QED]
```

The QCD=99 QED=99 coupling order specification means that all contributions must be considered, whereas the [virt=QCD QED] syntax demands for both QCD and QED/EW type of corrections.

# 9.7.3 Mixed-Coupling Expansion II: $u\bar{u} \rightarrow d\bar{d}t\bar{t}$

We consider the second example for mixed QCD+EW corrections to  $u\bar{u} \to d\bar{d}t\bar{t}$ . Due to the fact that the Born diagrams have three quark lines, the mixed-coupling expansion here is wider. There are 10947 one-loop Feynman diagrams generated. They are grouped into 811 topologies. It is an another example to illustrate the power of optimization presented in Sect. 9.4. We choose the same parameters and same renormalization scheme as done in Sect. 9.7.2. The chosen kinematic configuration is

```
p_u = (500)
                                                                          , 500)
p_{\bar{u}} = (500)
                           , 0
                                                  , 0
                                                                          , -500)
p_d = (77.6887158960956)
                          , -19.3895923374881 , 35.1636848900680
                                                                          , -66.5063572263756)
p_{\bar{d}} = (288.053156184158)
                           , -91.1103505191485 , -264.895455921162
                                                                          , 67.1112676698377)
p_t = (218.623451637725)
                           , -92.8925122931906 , -85.7235692614867
                                                                          , 43.4702707482150)
p_{\bar{t}} = (415.634676282022)
                           , 203.392455149827
                                                  , 315.455340292580
                                                                          ,-44.0751811916771)
```

The following is the Born results $a_0$ in	

$u\bar{u} \rightarrow d\bar{d}t\bar{t}$	$a_0$
$\mathscr{O}(\alpha_S^4)$	8.0443110796911884e-10
$\mathcal{O}(\alpha_S^3 \alpha^1)$	-4.1964024114099949e-11
$\mathscr{O}(\alpha_S^2\alpha^2)$	3.2368049995513863e-11
$\mathcal{O}(\alpha_S^1 \alpha^3)$	-7.9030872133243511e-13
$\mathcal{O}(\alpha^4)$	1.8667390802029741e-13

whereas the renormalized one-loop results are

$u\bar{u} \to d\bar{d}t\bar{t}$	$\mathscr{O}(\alpha_S^5)$	$\mathscr{O}(\alpha_S^4 \alpha^1)$
$c_0$	2.7744575300036875e-10	-6.1309409133299879e-11
<i>c</i> <sub>-1</sub>	-2.4891722473717473e-10	5.1973614496390480e-12
$c_{-2}$	-8.0573035150936874e-11	3.1296167547367972e-12
	$\mathscr{O}(\alpha_S^3 \alpha^2)$	$\mathscr{O}(\alpha_S^2\alpha^3)$
$\overline{c_0}$	1.2122291790182845e-11	-4.0611498141889722e-12
$c_{-1}$	-8.6161115635612362e-12	4.3209683736654367e-15
<i>c</i> <sub>-2</sub>	-3.1860291930204890e-12	3.5961341456741816e-14
	$\mathscr{O}(\alpha_S^1 \alpha^4)$	$\mathscr{O}(\alpha^5)$
$c_0$	-3.8642357648130340e-14	-1.1866388556893426e-14
$c_{-1}$	-3.6050223887148020e-14	-4.7983631557836333e-16
$c_{-2}$	-1.7642824564621470e-14	-2.4912793041300221e-16

The results have been cross-checked by using both CutTools and IREGI. We have also checked the coefficients  $c_{-1}$  and  $c_{-2}$  with the analytical known forms in Ref. [23] and its generalization to EW correction. The process can be generated with the MADGRAPH5 AMC@NLO-shell generation command:

```
MG5_aMC> generate u u\sim > d d\sim t t\sim QCD=99 QED=99 [virt=QCD QED]
```

# 9.7.4 A BSM Example: QCD Correction to $gg \rightarrow \tilde{t}_1 \tilde{t}_1^{\star} g$

MADLOOP5 is designed as a general framework to do any type of correction to any BSM. Hence, it extends the future usage of MADGRAPH5\_AMC@NLO. Here, we give an example about the QCD correction to a  $2 \to 3$  process  $gg \to \tilde{t}_1\tilde{t}_1^*g$  in a fully fledged BSM model MSSM. Given the complication of the NLO MSSM UFO model, the model is generated by using a development version of Feynrules, <sup>10</sup> which has been validated recently by a completely independent and private MATHEMATICA program. We want to point out that it is indeed a far non-trivial example. Some

<sup>&</sup>lt;sup>10</sup>I want to thank Celine Degrande and Benjamin Fuks here for providing us the model.

elementary expressions and structures in this example do not appear in the SM processes. For example, due to the presence of Majorana fermions in the model, MADLOOP5 is designed well to handle the so-called fermion flow violating currents. There are totally 3952 one-loop diagrams and 437 topologies. The results (as well as some other processes in MSSM) presented here are completely cross-checked by a private MATHEMATICA program.

The coupling renormalization follows the same strategy in, e.g., Ref. [24]: All massive modes are subtracted at zero momentum to avoid possible large logarithms. The input parameters are

Parameter	Value	Parameter	Value
$\alpha_S$	0.118	$n_{lf}$	4
$m_b$	4.75	$m_t$	175
$m_W$	79.82901	$m_Z$	91.1876
$m_{\tilde{g}}$	607.7137	$\tan \beta$	9.748624
$m_{\tilde{u}_1}$	561.119	$m_{\tilde{u}_2}$	549.2593
$m_{\tilde{c}_1}$	561.119	$m_{\tilde{c}_2}$	549.2593
$\overline{m_{\tilde{t}_1}}$	399.6685	$m_{\tilde{t}_2}$	585.7858
$m_{\tilde{d}_1}$	568.4411	$m_{\tilde{d}_2}$	545.2285
$m_{\tilde{s}_1}$	568.4411	$m_{\tilde{s}_2}$	545.2285
$m_{\tilde{b}_1}$	513.0652	$m_{\tilde{b}_2}$	543.7267

with the diagonal quark-mixing matrices. We randomly choose a phase space point

and obtain the final results

$gg \to \tilde{t}_1 \tilde{t}_1^{\star} g$	MADLOOP5
$a_0$	-2.839872059757065e-4
$c_0$	-2.081163174420354e-5
$\overline{c_{-1}}$	-1.550338075591894e-4
$\overline{c_{-2}}$	-4.800024159745521e-5

One can use the following MADGRAPH5\_AMC@NLO-shell commands to generate the process

```
MG5_aMC> import model loop_MSSM
MG5_aMC> generate g g > t1 t1~ g [virt=QCD]
```

We emphasize that only the private version of MADLOOP5 is able to handle this process and the UFO model loop\_MSSM is not yet public.

## 9.8 Summary of New Features in MadLoop5

Let us summarize the new features in MadLoop5 before closing this chapter. They mainly include the following aspects:

- It has been exploited a lot for QCD corrections to SM processes. Several optimizations have been implemented to improve the efficiency. Especially, an independent OPENLOOPS technique is implemented to improve the efficiency of the code.
- New and general NLO UFO format is exploited for any type of corrections in SM and BSM.
- We have generalized MADLOOP5 to be capable of handling EW corrections to any SM process. Of course, it should be applicable to the EW corrections to any BSM process if the corresponding NLO UFO model is available.
- For the mixed-order processes, MADLOOP5 has been designed in an efficient way to calculate the results in different orders.
- Complex mass scheme is used and validated at least in QCD corrections to SM processes.
- We have generalized MADLOOP5 to a format for SUSY processes. Especially, we have fixed the fermion flow violating issue.
- Apart from OPP or CutTools, TIR is also implemented in MadLoop5. With the help of TIR, it is very useful in improving the numerical accuracy. Moreover, it is mandatory to efficiently calculate the loop-induced processes.

#### References

- J. Alwall, M. Herquet, F. Maltoni, O. Mattelaer, T. Stelzer, JHEP 06, 128 (2011). doi:10.1007/ JHEP06(2011)128
- J. Alwall, R. Frederix, S. Frixione, V. Hirschi, F. Maltoni, O. Mattelaer, H.S. Shao, T. Stelzer, P. Torrielli, M. Zaro, JHEP 07, 079 (2014). doi:10.1007/JHEP07(2014)079
- V. Hirschi, R. Frederix, S. Frixione, M.V. Garzelli, F. Maltoni et al., JHEP 1105, 044 (2011). doi:10.1007/JHEP05(2011)044
- 4. J. Alwall et al., JHEP 09, 028 (2007). doi:10.1088/1126-6708/2007/09/028
- H.S. Shao, Y.J. Zhang, K.T. Chao, Phys. Rev. D 84, 094021 (2011). doi:10.1103/PhysRevD. 84.094021
- 6. H.S. Shao, Y.J. Zhang, K.T. Chao, JHEP 1201, 053 (2012), doi:10.1007/JHEP01(2012)053
- 7. G. 't Hooft, M.J.G. Veltman, Nucl. Phys. **B44**, 189 (1972). doi:10.1016/0550-3213(72)90279-9
- 8. C. Degrande, C. Duhr, B. Fuks, D. Grellscheid, O. Mattelaer et al., Comput. Phys. Commun. **183**, 1201 (2012). doi:10.1016/j.cpc.2012.01.022
- S. Dittmaier, Kramer, Michael. Phys. Rev. D 65, 073007 (2002). doi:10.1103/PhysRevD.65. 073007
- 10. A. Denner, Fortschr. Phys. 41, 307 (1993)
- P. de Aquino, W. Link, F. Maltoni, O. Mattelaer, T. Stelzer, Comput. Phys. Commun. 183, 2254 (2012). doi:10.1016/j.cpc.2012.05.004
- A. van Hameren, C. Papadopoulos, R. Pittau, JHEP 0909, 106 (2009). doi:10.1088/1126-6708/ 2009/09/106

References 137

13. V. Hirschi, Automation of one-loop computations for scattering amplitudes and applications to collider phenomenology. Ph.D. thesis, Ecole Polytechnique Federale de Lausanne (2013). http://infoscience.epfl.ch/record/186388/files/EPFL\_TH5736.pdf

- G. Ossola, C.G. Papadopoulos, R. Pittau, JHEP 03, 042 (2008). doi:10.1088/1126-6708/2008/ 03/042
- 15. V. Yundin, Massive loop corrections for collider physics. Ph.D. thesis, Humboldt-Universitat zu Berlin (2012). http://edoc.hu-berlin.de/docviews/abstract.php?id=39163
- 16. J. Fleischer, T. Riemann, V. Yundin, PoS LL2012, 020 (2012)
- 17. H.S. Shao, unpublished
- A. Denner, S. Dittmaier, M. Roth, L.H. Wieders, Nucl. Phys. B 724, 247 (2005). doi:10.1016/j.nuclphysb.2005.06.033
- F. Cascioli, P. Maierhofer, S. Pozzorini, Phys. Rev. Lett. 108, 111601 (2012). doi:10.1103/ PhysRevLett.108.111601
- 20. R. Pittau, Comput. Phys. Commun. 181, 1941 (2010). doi:10.1016/j.cpc.2010.09.013
- 21. R.K. Ellis, J. Sexton, Nucl. Phys. B 269, 445 (1986). doi:10.1016/0550-3213(86)90232-4
- R. Kleiss, W. Stirling, S. Ellis, Comput. Phys. Commun. 40, 359 (1986). doi:10.1016/0010-4655(86)90119-0
- R. Frederix, S. Frixione, F. Maltoni, T. Stelzer, JHEP 0910, 003 (2009). doi:10.1088/1126-6708/2009/10/003
- W. Beenakker, S. Dittmaier, M. Kramer, B. Plumper, M. Spira et al., Nucl. Phys. B 653, 151 (2003). doi:10.1016/S0550-3213(03)00044-0

## **Chapter 10 Automation of NLO Computations**

**Abstract** In this chapter, we present a brief introduction to the MADGRAPH5\_AMC @NLO [1] framework, which is the first public code to perform NLO level computation and match to parton shower automatically. For the users who are interested in the details, we suggest them to read our recent publication Ref. [1].

## 10.1 MadGraph5\_aMC@NLO in a Nutshell

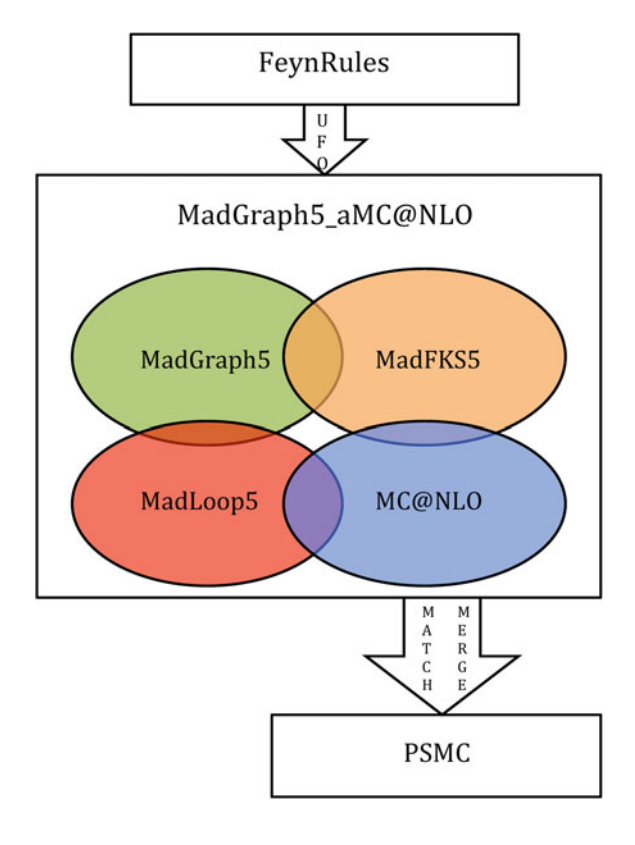
We first describe the basic structure of the code MADGRAPH5 AMC@NLO, which was released in 16 December 2013. It is the first public code (and so far also the only one) to perform NLO computation and match the fixed-order NLO result to parton shower (with MC@NLO formalism [2]) in an automatic way. Let us briefly describe its main structure. All of the fixed-order calculations are based on the MadGraph5 [3] framework. For the purpose of the LO computation and its interface to parton shower Monte Carlo (PSMC), such as the Fortran codes PYTHIA6 [4], HERWIG [5, 6] and their C++ successors PYTHIA8 [7], HERWIG++ [8, 9], MADGRAPH5 AMC@NLO framework is relegated to the original MADGRAPH5. At the NLO level, the new versions of MADLOOP5 and MADFKS5, 2 the successors of the original MADLOOP4 [10] and MADFKS4 [11], are in charge of the virtual and real calcularespectively. As have already discussed we previous chapter, MADLOOP5 has a lot of developments compared to MADLOOP4. MADFKS uses the Frixione-Kunszt-Signer (FKS) [12, 13] subtraction scheme to subtract the IR divergences in the real part. It also provides an event generator at NLO level, which is an extension of the original MADEVENT [14]. There are several novelties of the new version of MADFKS5 in MADGRAPH5 AMC@NLO with respect to its previous version MADFKS4 [11]. We refrain ourselves to describe them here and guide the interested reader to Ref. [1]. All tree-level features are based on MadGraph5. Since the NLO matrix elements are not bounded in the whole phase space, without matching to parton shower (e.g., the MC@NLO

<sup>&</sup>lt;sup>1</sup>It can be downloaded from the Web page http://amcatnlo.web.cern.ch/amcatnlo.

<sup>&</sup>lt;sup>2</sup>Both of them have inherited features of MADGRAPH5.

<sup>©</sup> Springer Science+Business Media Singapore 2016 H.-S. Shao, *Heavy Quarkonium Production Phenomenology and Automation of One-Loop Scattering Amplitude Computations*, Springer Theses,

Fig. 10.1 Structure of MADGRAPH5\_AMC@NLO and the flowchart of automatic NLO computation and matching to parton shower with MADGRAPH5\_AMC@NLO



[2, 15, 16] and POWHEG [17–19] methods) or introducing an unphysical cutoff, it is unable to generate unweighted events at NLO level. MADGRAPH5\_AMC@NLO adopts the MC@NLO method, which is proposed in Ref. [2]. Therefore, it is apparent that MADGRAPH5\_AMC@NLO framework is mainly composed of four parts: MADGRAPH5, MADLOOP5, MADFKS5 and MC@NLO. The structure is shown in Fig. 10.1. We also illustrate a flowchart for the automation of NLO computations in a BSM in the figure. If one wants to perform a phenomenological analysis at NLO level in a BSM theory, he/she can use the FEYNRULES<sup>3</sup> to generate a NLO UFO [21] model for the dedicated theory, and then feed it into MADGRAPH5\_AMC@NLO. MADGRAPH5\_AMC@NLO automatically performs a fixed-order NLO or NLO plus parton shower analysis.<sup>4</sup>

Another important issue in the MADGRAPH5\_AMC@NLO project is that it can also merge the matched samples that differ by light-parton multiplicities. The aim of merging is that of combining samples in different parton multiplicities in a consistent manner. It avoids double counting after parton showering. Over a decade ago, three main

<sup>&</sup>lt;sup>3</sup>As we have emphasized for several times, it is still not public but is expected to be released in the future. Maybe in the future, an alternative choice is also provided, e.g., SARAH [20].

<sup>&</sup>lt;sup>4</sup>Certainly, one can also perform a fixed-order LO or LO plus parton shower analysis with MAD-GRAPH5\_AMC@NLO.

merging schemes such as Michelagelo. L. Mangano (MLM) scheme [22, 23], Catani-Krauss-Kuhn-Webber (CKKW) scheme [24, 25], and Lönnblad<sup>5</sup> scheme [26–28] were proposed to merge the LO samples in different light-parton multiplies. MAD-GRAPH5\_AMC@NLO uses a hybrid version of those available in Sherpa [29] and Alpgen [30], which is called shower- $k_T$  MLM scheme [31]. At NLO level, more complexities appear due to an extra parton radiation in the matrix elements. During the recent years, the merging techniques have been applied to NLO computations [32–40]. In MADGRAPH5\_AMC@NLO, Frederix-Frixione (FxFx) procedure has been implemented. The samples can be merged in a (semi-)automatic way.<sup>6</sup>

Finally, we also want to point out that the current MADGRAPH5\_AMC@NLO framework has superseded both the current versions of MADGRAPH5 and of AMC@NLO. Hence, it should be considered as a successor instead of a plugin of MADGRAPH5, which is unlike other MADGRAPH projects.

## 10.2 How to Use MadGraph5\_aMC@NLO

In this section, we will show how to run the code to perform a phenomenological analysis in a basic way. As it has been described already in Ref. [1], the computation of a cross section by MADGRAPH5\_AMC@NLO mainly consists of three phases, i.e., *generation*, *output*, and *running*. In this section, we will only focus on the description of NLO computation, whereas that of LO computation we refer the readers to the MADGRAPH5 paper [3] and the MADGRAPH5\_AMC@NLO paper [1]. The running of the code starts with a shell script by commanding<sup>7</sup>

```
> ./bin/mg5_aMC
```

Then, the user will see the interactive prompt

```
MG5_aMC>
```

The syntax of the three steps is

```
MG5_aMC> generate PROCESS
MG5_aMC> output (output file)
MG5_aMC> launch (options)
```

where PROCESS is the interested process, (options) in the last step is the optional options specified by user for the command launch, and (output file) is the optional file the user tells the program where to output the numerical code. Let us

<sup>&</sup>lt;sup>5</sup>The Lönnblad scheme is also usually called CKKW-L scheme, which is similar to CKKW scheme but differs in the way of constructing the shower history.

<sup>&</sup>lt;sup>6</sup>See http://amcatnlo.web.cern.ch/amcatnlo/FxFx\_merging.htm.

<sup>&</sup>lt;sup>7</sup>We assume the user is working in the main directory of MADGRAPH5\_AMC@NLO here.

give a quick example. If one is interested in the QCD correction to the top quark pair and a jet production at the LHC, one can type the following commands

```
MG5_aMC> generate p p > t t~ j [QCD]
MG5_aMC> output pp2ttjQCD
MG5_aMC> launch -f
```

Symbols p and j are multiparticle definitions. Both of them consist of all massless QCD patrons. For instance, in 4 flavor scheme,  $p, j = u, d, s, c, g, \bar{u}, \bar{d}, \bar{s}, \bar{c}$ . The bracket [QCD] means we are considering a process with QCD correction. The numerical code will be outputted in the file pp2ttjQCD. The option -f in companion with the command launch forces the program to use the default setup (e.g., the default parameters and kinematic cutoffs).

Let us explain the steps in a detail way.

• In the *generation* phase, MADGRAPH5\_AMC@NLO constructs all of the building blocks of the process information, including import of model information, generation, and filter of the relevant Feynman diagrams. Let us take the example of  $pp \rightarrow t\bar{t} + j$ 

```
■ MG5_aMC > generate p p > t t\sim j [mode=QCD]
```

There are three choices for the option mode:all, real, virt. They correspond to

- all: both Born, virtual and FKS-subtracted real emission are included.
- real: only Born and FKS-subtracted real emission are included.
- virt: only Born and virtual are included.

If one does not specify mode, it is understood as the default one all. There are more flexible usage to apply MADGRAPH5\_AMC@NLO in a wider way. By default, the program imports the model loop\_sm if one specifies QCD in the bracket. However, if one is interested in a BSM, for example MSSM, he/she should import the corresponding model before generation as follows:

```
MG5_aMC> import model loop_MSSM
MG5_aMC> generate p p > t t~ j [mode=QCD]
```

If one is interested in another type of correction, he/she should specify the keyword of the correction in the bracket. For example, QED/EW correction,

```
MG5_aMC> generate p p > t t\sim j [mode=QED]
```

or QCD plus QED/EW corrections,

```
MG5_aMC> generate p p > t t\sim j [mode=QCD QED]
```

By default, when the program finds the keyword QED in the command, it will use the model loop\_qcd\_qed\_sm, which is renormalized in  $\alpha(m_Z)$ -scheme. If one wants to use  $G_u$ -scheme, one can do the following

```
MG5_aMC> import model loop_qcd_qed_sm_Gmu
MG5_aMC> generate p p > t t~ j [mode=QCD QED]
```

There are more options to specify the coupling orders of the generated amplitudes. We refer the reader to Ref. [1] and the examples presented in the previous chapter.

• In the *output* phase, MADGRAPH5\_AMC@NLO generates all of the HELAS [41] routines, <sup>8</sup> calculates color matrices, draws Feynman diagrams, and outputs the numerical code as well as other auxiliary files on the disk. In the above case, one can either specify an output directory, for example pp2ttjQCD

```
MG5_aMC > output pp2ttjQCD
or not
MG5_aMC > output
```

In the later case, the program automatically generates a new directory PROCNLO\_Model\_X, where Model is the choosing model (e.g., loop\_sm in the example) and X is a non-negative number to uniquely identify the directory.

• In the running phase, MADGRAPH5\_AMC@NLO performs the phase space integration, generates the unweighted events via MC@NLO formula, interfaces to PSMC to do parton shower, and plots the user-defined differential distributions. We want to emphasize again that the unweighted events can only be generated after including parton shower at NLO level. The choice is available to the user by not forcing option −f as follows:

```
MG5_aMC > launch
```

#### An interactive talk to prompt opens

<sup>&</sup>lt;sup>8</sup>As we have emphasized before, they are created by ALOHA [42] on the fly.

One can choose the level of the results. MADGRAPH5\_AMC@NLO also provides the choices to the user to use their own setup, which are mainly in param card.dat, run card.dat, and shower card.dat

From the above description, we see that MADGRAPH5\_AMC@NLO provides its usage in a very user-friendly way and it does not lose its maximal flexibility and extensions. The aim of MADGRAPH5\_AMC@NLO framework was available to the ones who are even not familiar with QFT. The best way of learning to use it is following the examples presented here or in Ref. [1].

#### 10.3 Selected Results

Since its release on 16 December 2013, MADGRAPH5\_AMC@NLO has managed to calculate and/or validate more than 100 SM processes with QCD corrections up to  $2 \rightarrow 4$  at Born level. It has reproduced the majority of the current NLO results in the literature. Hence, it is the largest number of NLO processes available in a single framework ever. We point out that the fixed-order results in the literature have also been extended by matching to parton shower. Several new results are also obtained.

The aim of this section was to show the power of MADGRAPH5\_AMC@NLO framework with several specific examples. All of the examples below are obtained from Ref. [1].

#### 10.3.1 Total Cross Sections

First, we give some examples on computing the total cross sections with MAD-GRAPH5\_AMC@NLO. The main physical parameters in the calculation are as follows:

- $\alpha^{-1} = 132.507$ ,  $m_H = 125$  GeV,  $m_t = 173.2$  GeV,  $m_Z = 91.188$  GeV,  $m_W = 80.419$  GeV. In 4-flavor scheme,  $m_b = 4.75$  GeV, while in 5-flavor scheme,  $m_b = 0$  GeV. The widths of unstable particles are set as zero and the CKM matrix is set to be diagonal.
- MSTW 2008 NLO PDFs [43, 44] with errors at 68 % confidential level. They are also applied to obtain the LO results.
- Independent scale variations of renormalization scale  $\mu_R$  and factorization scale  $\mu_F$  as  $0.5\mu_0 \le \mu_R$ ,  $\mu_F \le 2\mu_0$ , where  $\mu_0 = H_T/2$ , with  $H_T$  the scalar sum of the transverse masses  $m_T \equiv \sqrt{p_T^2 + m^2}$  of all final state particles.
- Final jets are defined by anti- $k_T$  algorithm [45] with  $R = 0.5, p_{Tj} > 30$  GeV and  $|n_i| < 4$ .
- Final photons are identified via Frixione isolation [46] with  $R = 0.7, p_{T\gamma} > 20$  GeV and  $|\eta_{\gamma}| < 2$ .

10.3 Selected Results 145

We present Tables 10.1 and 10.2. The fixed-order NLO results in Table 10.1 are already available in the literature, whereas the results in Table 10.2 are completely new. The statistical errors from Monte Carlo generator have been controlled under 0.3 %. The remaining uncertainties in the results come from the scale and PDF uncertainties, which are obtained by using the reweighing method proposed in Ref. [47]. More extensive tables are available in Ref. [1].

## 10.3.2 Differential Distributions

In this subsection, we want to show that the results from MADGRAPH5\_AMC@NLO are completely differential. Hence, all differential distributions of user-defined observables are provided at both fixed-order NLO and fixed-order NLO+parton shower levels. We choose one representative example

$$pp \to t (\to e^+ \nu_e b) \bar{t} (\to e^- \bar{\nu}_e \bar{b}) W^- (\to \mu^- \bar{\nu}_\mu) W^+ (\to \mu^+ \nu_\mu)$$

from Ref. [1]. This example is new. The parameters and kinematic cutoffs are the same with those in the total cross-sectional case. The decays of the top quarks and W bosons are achieved either by MADSPIN [93] or by the internal PYTHIA8 routine.

**Table 10.1** Samples of LO and NLO rates for selected 2 → 4 processes at the LHC with center-of-mass energy 13 TeV (within cutoffs) by MADGRAPH5\_AMC@NLO

Process	Cross section (pb)	Cross section (pb)		
	LO 13 TeV	NLO 13 TeV		
$pp \to W^{\pm}jjj$	$1.821 \pm 0.002 \times 10^{3}  ^{+41.0 \%}_{-27.1 \%}  ^{+0.5 \%}_{-0.5 \%}$	$2.005 \pm 0.008 \times 10^{3}  ^{+0.9 \%}_{-6.7 \%}  ^{+0.6 \%}_{-0.5 \%}$		
$pp \rightarrow Zjjj$	$6.314 \pm 0.008 \times 10^{2}  ^{+40.8 \%}_{-27.0 \%}  ^{+0.5 \%}_{-0.5 \%}$	$6.996 \pm 0.028 \times 10^{2}  ^{+1.1\%}_{-6.8\%}  ^{+0.5\%}_{-0.5\%}$		
$pp \to W^+W^+jj$	$1.484 \pm 0.006 \times 10^{-1}  ^{+25.4 \%}_{-18.9 \%}  ^{+2.1 \%}_{-1.5 \%}$	$2.251 \pm 0.011 \times 10^{-1}  {}^{+10.5 \%}_{-10.6 \%}  {}^{+2.2 \%}_{-1.6 \%}$		
$pp \rightarrow W^-W^-jj$	$ \begin{array}{ c c c c c c c c c c c c c c c c c c c$	$1.003 \pm 0.003 \times 10^{-1}  {}^{+10.1\%}_{-10.4\%}  {}^{+2.5\%}_{-1.8\%}$		
$\begin{array}{ccc} pp & \rightarrow & W^+W^-jj \\ \text{(4f)} & & \end{array}$	$1.144 \pm 0.002 \times 10^{1}$ $^{+27.2\%}_{-19.9\%}$ $^{+0.7\%}_{-0.5\%}$	$1.396 \pm 0.005 \times 10^{1}$ $^{+5.0 \%}_{-6.8 \%}$ $^{+0.7 \%}_{-0.6 \%}$		
$pp \to \gamma \gamma W^{\pm} j$	$\begin{array}{ c c c c c c c c c c c c c c c c c c c$	$\begin{array}{ c c c c c c c c c c c c c c c c c c c$		
$pp \rightarrow t\bar{t}jj$	$1.361 \pm 0.001 \times 10^{2}$ $^{+61.4\%}_{-35.6\%}$ $^{+2.6\%}_{-3.0\%}$	$1.795 \pm 0.006 \times 10^{2}  {}^{+9.3  \%}_{-16.1  \%}  {}^{+2.4  \%}_{-2.9  \%}$		
$pp \to t\bar{t}t\bar{t}$	$4.505 \pm 0.005 \times 10^{-3}  ^{+63.8 \%}_{-36.5 \%}  ^{+5.4 \%}_{-5.7 \%}$	$9.201 \pm 0.028 \times 10^{-3} $ $^{+30.8 \%}_{-25.6 \%} $ $^{+5.5 \%}_{-5.9 \%}$		
$pp \to t\bar{t}b\bar{b}$	$6.119 \pm 0.004 \times 10^{0} \begin{array}{c} +62.1 \% & +2.9 \% \\ -35.7 \% & -3.5 \% \end{array}$	$1.452 \pm 0.005 \times 10^{1}  ^{+37.6 \%}_{-27.5 \%}  ^{+2.9 \%}_{-3.5 \%}$		

All cross sections except  $pp \to W^+W^-jj$  and  $pp \to t\bar{t}b\bar{b}$  are in the 5-flavor scheme, whereas the exceptional ones are in 4-flavor scheme. These processes are also available in the literature up to NLO level: Z/W plus jets [48–66], VV+jets [67–81],  $\gamma\gamma W^{\pm}$ +jet [82],  $t\bar{t}$ +jets [68, 83–88],  $t\bar{t}t\bar{t}$  [89],  $t\bar{t}b\bar{b}$  [90–92]

Process	Cross section (pb)		
	LO 13 TeV	NLO 13 TeV	
$pp \rightarrow \gamma Zjj$	$3.260 \pm 0.009 \times 10^{0} \begin{array}{cccc} +24.3 \% & +0.6 \% \\ -18.4 \% & -0.6 \% \end{array}$	$\begin{array}{ c c c c c c c c c c c c c c c c c c c$	
$pp \to \gamma W^{\pm} jj$	$1.233 \pm 0.002 \times 10^{1}  ^{+24.7 \%}_{-18.6 \%}  ^{+0.6 \%}_{-0.6 \%}$	$1.448 \pm 0.005 \times 10^{1}  ^{+3.6\%}_{-5.4\%}  ^{+0.6\%}_{-0.7\%}$	
$\begin{array}{c} pp \to W^+W^- \\ W^{\pm}j \text{ (4f)} \end{array}$	$9.167 \pm 0.010 \times 10^{-2}  {}^{+15.0 \%}_{-12.2 \%}  {}^{+1.0 \%}_{-0.7 \%}$	$1.197 \pm 0.004 \times 10^{-1}  ^{+5.2 \%}_{-5.6 \%}  ^{+1.0 \%}_{-0.8 \%}$	
$pp \to ZW^+W^-j$ (4f)	$8.340 \pm 0.010 \times 10^{-2}$ $^{+15.6 \%}_{-12.6 \%}$ $^{+1.0 \%}_{-0.7 \%}$	$1.066 \pm 0.003 \times 10^{-1}  ^{+4.5 \%}_{-5.3 \%}  ^{+1.0 \%}_{-0.7 \%}$	
$pp \to ZZW^{\pm}j$	$\begin{array}{ c c c c c c c c c c c c c c c c c c c$	$3.660 \pm 0.013 \times 10^{-2} $ $^{+4.8\%}_{-5.6\%} $ $^{+1.0\%}_{-0.7\%}$	
$pp \rightarrow ZZZj$	$\begin{array}{ c c c c c c c c c c c c c c c c c c c$	$\begin{array}{ c c c c c c c c c c c c c c c c c c c$	
$\begin{array}{c} pp \rightarrow W^+W^- \\ W^+W^- \text{ (4f)} \end{array}$	$\begin{array}{ c c c c c c c c c c c c c c c c c c c$	$9.959 \pm 0.035 \times 10^{-4}  {}^{+7.4 \%}_{-6.0 \%}  {}^{+1.7 \%}_{-1.2 \%}$	
$pp \rightarrow ZZZZ$	$1.989 \pm 0.002 \times 10^{-5}  {}^{+3.8\%}_{-3.6\%}  {}^{+2.2\%}_{-1.7\%}$	$\begin{array}{ c c c c c c c c c c c c c c c c c c c$	
$pp \to t\bar{t} Zj$	$3.953 \pm 0.004 \times 10^{-1}$ $^{+46.2\%}_{-29.5\%}$ $^{+2.7\%}_{-3.0\%}$	$5.074 \pm 0.016 \times 10^{-1}$ $^{+7.0\%}_{-12.3\%}$ $^{+2.5\%}_{-2.9\%}$	

**Table 10.2** Samples of LO and NLO rates for selected  $2 \rightarrow 4$  processes at the LHC with center-of-mass energy 13 TeV (within cutoffs) by MADGRAPH5\_AMC@NLO

All cross sections except  $pp \to W^+W^-W^\pm j$ ,  $pp \to ZW^+W^-j$  and  $pp \to W^+W^-W^+W^-$  are in the 5-flavor scheme, whereas the exceptional ones are in 4-flavor scheme. All processes are calculated for the first time at NLO level

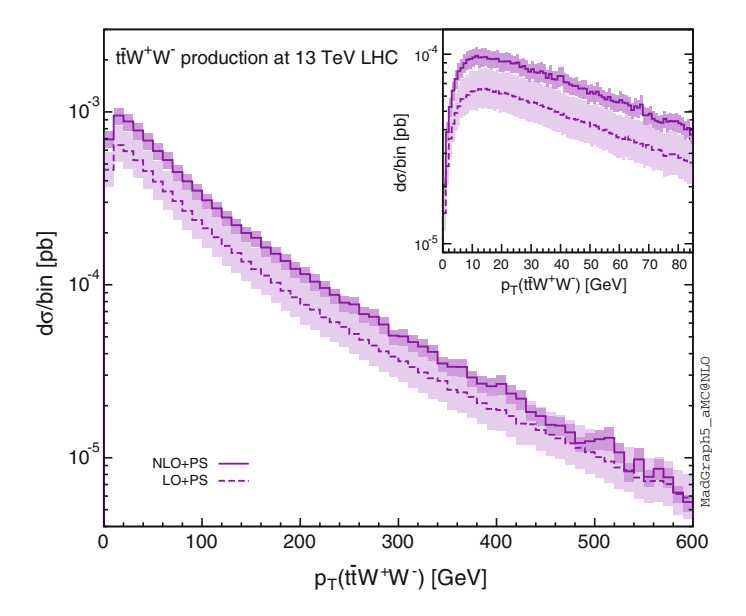


Fig. 10.2 Transverse momentum distribution of  $t\bar{t}W^+W^-$  in  $pp\to t\bar{t}W^+W^-+X$  at LHC 13 TeV. It uses PYTHIA8 as PSMC

10.3 Selected Results 147

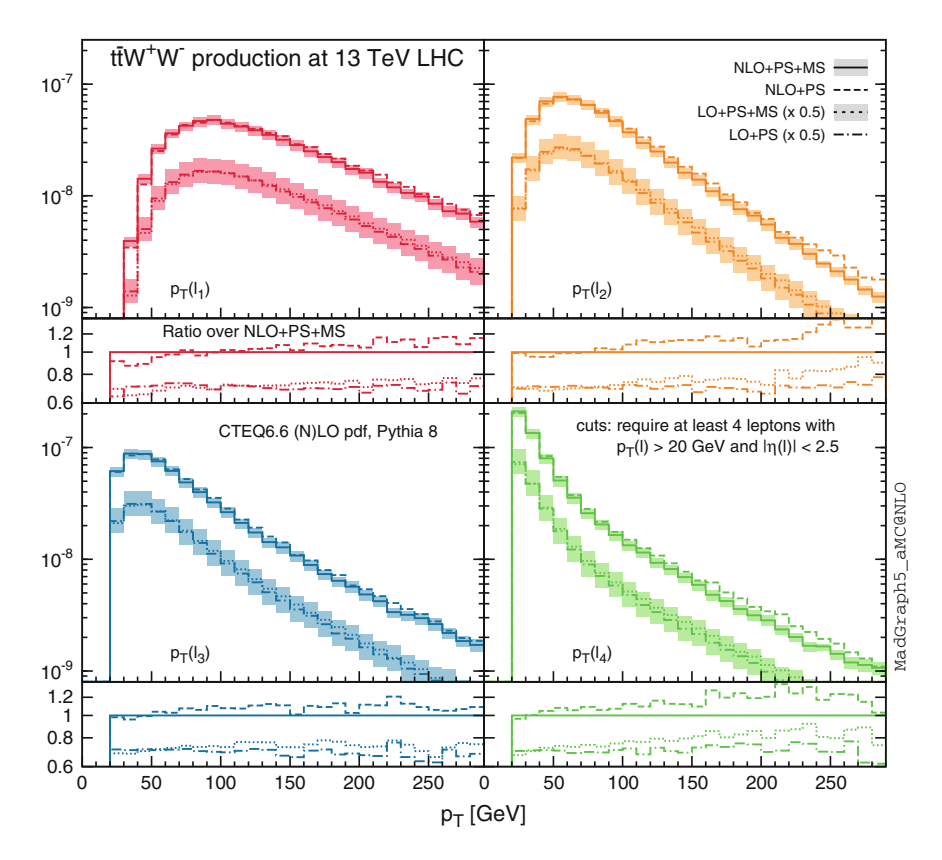


Fig. 10.3 Transverse momentum distributions of the hardest four charged leptons in  $pp \to t\bar{t}W^+W^- + X$  at LHC 13 TeV. The corresponding decay branching ratios have been included. It uses PYTHIA8 as PSMC. The results are NLO+PS with MADSPINdecays (*solid lines*), NLO+PS with PYTHIA8 decays (*dashed lines*), LO+PS with PYTHIA8 decays (dotted lines)

Both methods are able to correctly take account for the decay spin correlations. In Fig. 10.2, the transverse momentum distribution of the system of the four primary final states in this process is displayed. At small- $p_T$ , the behavior is dominated by PSMC effects. The uncertainty bands represent for the scale dependence only. As expected, the scale dependence improves from LO to NLO. In Fig. 10.3, we show the  $p_T$  distributions for the first four hardest charged leptons. The leptons are required to pass the cutoffs  $p_{T\ell} > 20$  GeV and  $|\eta_\ell| < 2.5$ . All of these results indicate that NLO corrections are significant and the production spin correlations are sizable.

### References

- J. Alwall, R. Frederix, S. Frixione, V. Hirschi, F. Maltoni, O. Mattelaer, H.S. Shao, T. Stelzer, P. Torrielli, M. Zaro, JHEP 07, 079 (2014). doi:10.1007/JHEP07(2014)079
- 2. S. Frixione, B.R. Webber, JHEP **0206**, 029 (2002). doi:10.1088/1126-6708/2002/06/029
- J. Alwall, M. Herquet, F. Maltoni, O. Mattelaer, T. Stelzer, JHEP 06, 128 (2011). doi:10.1007/ JHEP06(2011)128
- T. Sjostrand, S. Mrenna, P.Z. Skands, JHEP 0605, 026 (2006). doi:10.1088/1126-6708/2006/ 05/026
- G. Corcella, I. Knowles, G. Marchesini, S. Moretti, K. Odagiri et al., JHEP 0101, 010 (2001). doi:10.1088/1126-6708/2001/01/010
- 6. G. Corcella, I. Knowles, G. Marchesini, S. Moretti, K. Odagiri et al. (2002)
- T. Sjostrand, S. Mrenna, P.Z. Skands, Comput. Phys. Commun. 178, 852 (2008). doi:10.1016/j.cpc.2008.01.036
- 8. M. Bahr, S. Gieseke, M. Gigg, D. Grellscheid, K. Hamilton et al., Eur. Phys. J. **C58**, 639 (2008). doi:10.1140/epjc/s10052-008-0798-9
- 9. J. Bellm, S. Gieseke, D. Grellscheid, A. Papaefstathiou, S. Platzer et al. (2013)
- V. Hirschi, R. Frederix, S. Frixione, M.V. Garzelli, F. Maltoni et al., JHEP 1105, 044 (2011). doi:10.1007/JHEP05(2011)044
- R. Frederix, S. Frixione, F. Maltoni, T. Stelzer, JHEP 0910, 003 (2009). doi:10.1088/1126-6708/2009/10/003
- S. Frixione, Z. Kunszt, A. Signer, Nucl. Phys. B467, 399 (1996). doi:10.1016/0550-3213(96)00110-1
- 13. S. Frixione, Nucl. Phys. **B507**, 295 (1997). doi:10.1016/S0550-3213(97)00574-9
- 14. F. Maltoni, T. Stelzer, JHEP 0302, 027 (2003). doi:10.1088/1126-6708/2003/02/027
- S. Frixione, P. Nason, B.R. Webber, JHEP 0308, 007 (2003). doi:10.1088/1126-6708/2003/ 08/007
- S. Frixione, F. Stoeckli, P. Torrielli, B.R. Webber, JHEP 1101, 053 (2011). doi:10.1007/ JHEP01(2011)053
- 17. P. Nason, JHEP **0411**, 040 (2004). doi:10.1088/1126-6708/2004/11/040
- S. Frixione, P. Nason, C. Oleari, JHEP 0711, 070 (2007). doi:10.1088/1126-6708/2007/11/ 070
- 19. S. Alioli, P. Nason, C. Oleari, E. Re, JHEP 1006, 043 (2010). doi:10.1007/JHEP06(2010)043
- 20. F. Staub, Comput. Phys. Commun. 184, 1792 (2013). doi:10.1016/j.cpc.2013.02.019
- C. Degrande, C. Duhr, B. Fuks, D. Grellscheid, O. Mattelaer et al., Comput. Phys. Commun. 183, 1201 (2012). doi:10.1016/j.cpc.2012.01.022
- F. Caravaglios, M.L. Mangano, M. Moretti, R. Pittau, Nucl. Phys. B539, 215 (1999). doi:10. 1016/S0550-3213(98)00739-1
- M.L. Mangano, M. Moretti, R. Pittau, Nucl. Phys. B632, 343 (2002). doi:10.1016/S0550-3213(02)00249-3
- 24. S. Catani, F. Krauss, R. Kuhn, B. Webber, JHEP **0111**, 063 (2001)
- 25. F. Krauss, JHEP **0208**, 015 (2002). doi:10.1088/1126-6708/2002/08/015
- 26. L. Lonnblad, JHEP **0205**, 046 (2002). doi:10.1088/1126-6708/2002/05/046
- 27. N. Lavesson, L. Lonnblad, JHEP 0507, 054 (2005). doi:10.1088/1126-6708/2005/07/054
- 28. L. Lonnblad, S. Prestel, JHEP 1203, 019 (2012). doi:10.1007/JHEP03(2012)019
- T. Gleisberg, S. Hoeche, F. Krauss, A. Schalicke, S. Schumann et al., JHEP 0402, 056 (2004). doi:10.1088/1126-6708/2004/02/056
- 30. M.L. Mangano, M. Moretti, F. Piccinini, R. Pittau, A.D. Polosa, JHEP 0307, 001 (2003)
- 31. J. Alwall, S. Hoche, F. Krauss, N. Lavesson, L. Lonnblad et al., Eur. Phys. J. C53, 473 (2008). doi:10.1140/epjc/s10052-007-0490-5
- 32. K. Hamilton, P. Nason, JHEP **1006**, 039 (2010). doi:10.1007/JHEP06(2010)039
- S. Hoche, F. Krauss, M. Schonherr, F. Siegert, JHEP 1108, 123 (2011). doi:10.1007/ JHEP08(2011)123

References 149

- 34. N. Lavesson, L. Lonnblad, JHEP 0812, 070 (2008), doi:10.1088/1126-6708/2008/12/070
- 35. L. Lnnblad, S. Prestel, JHEP 1303, 166 (2013). doi:10.1007/JHEP03(2013)166
- T. Gehrmann, S. Hoche, F. Krauss, M. Schonherr, F. Siegert, JHEP 1301, 144 (2013). doi:10. 1007/JHEP01(2013)144
- S. Hoeche, F. Krauss, M. Schonherr, F. Siegert, JHEP 1304, 027 (2013). doi:10.1007/ JHEP04(2013)027
- 38. R. Frederix, S. Frixione, JHEP 1212, 061 (2012). doi:10.1007/JHEP12(2012)061
- 39. L. Lonnblad, S. Prestel, JHEP 1302, 094 (2013). doi:10.1007/JHEP02(2013)094
- K. Hamilton, P. Nason, E. Re, G. Zanderighi, JHEP 1310, 222 (2013). doi:10.1007/ JHEP10(2013)222
- 41. H. Murayama, I. Watanabe, K. Hagiwara (1992)
- 42. P. de Aquino, W. Link, F. Maltoni, O. Mattelaer, T. Stelzer, Comput. Phys. Commun. 183, 2254 (2012). doi:10.1016/j.cpc.2012.05.004
- A. Martin, W. Stirling, R. Thorne, G. Watt, Eur. Phys. J. C63, 189 (2009). doi:10.1140/epjc/ s10052-009-1072-5
- A. Martin, W. Stirling, R. Thorne, G. Watt, Eur. Phys. J. C70, 51 (2010). doi:10.1140/epjc/ s10052-010-1462-8
- M. Cacciari, G.P. Salam, G. Soyez, JHEP 04, 063 (2008). doi:10.1088/1126-6708/2008/04/ 063
- 46. S. Frixione, Phys. Lett. **B429**, 369 (1998). doi:10.1016/S0370-2693(98)00454-7
- R. Frederix, S. Frixione, V. Hirschi, F. Maltoni, R. Pittau et al., JHEP 1202, 099 (2012). doi:10. 1007/JHEP02(2012)099
- 48. J.M. Campbell, R.K. Ellis, Phys. Rev. D65, 113007 (2002). doi:10.1103/PhysRevD.65.113007
- J.M. Campbell, R.K. Ellis, D.L. Rainwater, Phys. Rev. D68, 094021 (2003). doi:10.1103/ PhysRevD.68.094021
- J.M. Campbell, R.K. Ellis, P. Nason, G. Zanderighi, JHEP 1308, 005 (2013). doi:10.1007/ JHEP08(2013)005
- J.M. Campbell, R.K. Ellis, F. Febres, Cordero, F. Maltoni, L. Reina et al. Phys. Rev. D79, 034023 (2009). doi:10.1103/PhysRevD.79.034023
- J.M. Campbell, R.K. Ellis, F. Maltoni, S. Willenbrock, Phys. Rev. D69, 074021 (2004). doi:10. 1103/PhysRevD.69.074021
- 53. J.M. Campbell, R.K. Ellis, F. Maltoni, S. Willenbrock, Phys. Rev. D 73, 054007 (2006). doi:10. 1103/PhysRevD.77.019903, doi:10.1103/PhysRevD.73.054007
- J.M. Campbell, R.K. Ellis, F. Maltoni, S. Willenbrock, Phys. Rev. D75, 054015 (2007). doi:10. 1103/PhysRevD.75.054015
- J. Campbell, F. Caola, F. Febres, Cordero, L. Reina, D. Wackeroth. Phys. Rev. D86, 034021 (2012). doi:10.1103/PhysRevD.86.034021
- S. Alioli, P. Nason, C. Oleari, E. Re, JHEP 0807, 060 (2008). doi:10.1088/1126-6708/2008/ 07/060
- 57. S. Alioli, P. Nason, C. Oleari, E. Re, JHEP 1101, 095 (2011). doi:10.1007/JHEP01(2011)095
- 58. E. Re, JHEP **1210**, 031 (2012). doi:10.1007/JHEP10(2012)031
- R.K. Ellis, K. Melnikov, G. Zanderighi, JHEP 0904, 077 (2009). doi:10.1088/1126-6708/2009/ 04/077
- K. Melnikov, G. Zanderighi, Phys. Rev. D81, 074025 (2010). doi:10.1103/PhysRevD.81. 074025
- C. Berger, Z. Bern, L.J. Dixon, F. Febres, Cordero, D. Forde et al. Phys. Rev. Lett. 102, 222001 (2009). doi:10.1103/PhysRevLett.102.222001
- 62. C.F. Berger et al., Phys. Rev. **D80**, 074036 (2009). doi:10.1103/PhysRevD.80.074036
- 63. C.F. Berger et al., Phys. Rev. **D82**, 074002 (2010). doi:10.1103/PhysRevD.82.074002
- 64. C.F. Berger et al., Phys. Rev. Lett. 106, 092001 (2011). doi:10.1103/PhysRevLett.106.092001
- H. Ita, Z. Bern, L. Dixon, F. Febres, Cordero, D. Kosower et al. Phys. Rev. D85, 031501 (2012). doi:10.1103/PhysRevD.85.031501
- S. Hoeche, F. Krauss, M. Schonherr, F. Siegert, Phys. Rev. Lett. 110, 052001 (2013). doi:10. 1103/PhysRevLett.110.052001

- T. Melia, K. Melnikov, R. Rontsch, G. Zanderighi, JHEP 12, 053 (2010). doi:10.1007/ JHEP12(2010)053
- T. Melia, P. Nason, R. Rontsch, G. Zanderighi, JHEP 1111, 078 (2011). doi:10.1007/ JHEP11(2011)078
- P. Nason, G. Zanderighi, Eur. Phys. J. C74, 2702 (2014). doi:10.1140/epjc/s10052-013-2702-
- V. Del Duca, F. Maltoni, Z. Nagy, Z. Trocsanyi, JHEP 0304, 059 (2003). doi:10.1088/1126-6708/2003/04/059
- T. Gehrmann, N. Greiner, G. Heinrich, Phys. Rev. Lett. 111, 222002 (2013). doi:10.1103/ PhysRevLett.111.222002
- 72. S. Badger, A. Guffanti, V. Yundin, JHEP 1403, 122 (2014). doi:10.1007/JHEP03(2014)122
- Z. Bern, L.J. Dixon, F. Febres Cordero, S. Hoeche, H. Ita, D.A. Kosower, N.A. Lo Presti, D. Maitre, in *Proceedings, 11th International Symposium on Radiative Corrections Application* of Quantum Field Theory to Phenomenology (RADCOR 2013) (2013), http://inspirehep.net/ record/1267007/files/arXiv:1312.0592.pdf
- Z. Bern, L.J. Dixon, F. Febres, Cordero, S. Hoeche, H. Ita, D.A. Kosower, N.A. Lo Presti, D. Maitre. Phys. Rev. D90(5), 054004 (2014). doi:10.1103/PhysRevD.90.054004
- F. Campanario, M. Kerner, L.D. Ninh, D. Zeppenfeld, Phys. Rev. D89, 054009 (2014). doi:10. 1103/PhysRevD.89.054009
- 76. J.M. Campbell, H.B. Hartanto, C. Williams, JHEP **1211**, 162 (2012). doi:10.1007/JHEP11(2012)162
- F. Campanario, M. Kerner, L.D. Ninh, D. Zeppenfeld, Eur. Phys. J. C74(5), 2882 (2014). doi:10.1140/epjc/s10052-014-2882-7
- 78. F. Campanario, M. Kerner, L.D. Ninh, D. Zeppenfeld, in *Rencontres du Vietnam: Windows on the Universe Quy Nhon, Binh Dinh, Vietnam, August 11–17, 2013* (2013), http://inspirehep.net/record/1260556/files/arXiv:1310.4369.pdf
- F. Campanario, C. Englert, M. Spannowsky, D. Zeppenfeld, Europhys. Lett. 88, 11001 (2009). doi:10.1209/0295-5075/88/11001
- F. Campanario, C. Englert, M. Spannowsky, Phys. Rev. D83, 074009 (2011). doi:10.1103/ PhysRevD.83.074009
- F. Campanario, C. Englert, S. Kallweit, M. Spannowsky, D. Zeppenfeld, JHEP 1007, 076 (2010). doi:10.1007/JHEP07(2010)076
- 82. F. Campanario, C. Englert, M. Rauch, D. Zeppenfeld (2011)
- 83. S. Dittmaier, P. Uwer, S. Weinzierl, Phys. Rev. Lett. **98**, 262002 (2007). doi:10.1103/ PhysRevLett.98.262002
- K. Melnikov, A. Scharf, M. Schulze, Phys. Rev. D85, 054002 (2012). doi:10.1103/PhysRevD. 85.054002
- 85. S. Alioli, S.O. Moch, P. Uwer, JHEP 1201, 137 (2012). doi:10.1007/JHEP01(2012)137
- G. Bevilacqua, M. Czakon, C.G. Papadopoulos, M. Worek, Phys. Rev. Lett. 104, 162002 (2010). doi:10.1103/PhysRevLett.104.162002
- 87. M. Schnherr, S. Hche, J. Huang, G. Luisoni, J. Winter. PoS EPS-HEP2013, 246 (2013)
- 88. S. Hoeche, F. Krauss, P. Maierhoefer, S. Pozzorini, M. Schonherr, F. Siegert, Phys. Lett. **B748**, 74 (2015). doi:10.1016/j.physletb.2015.06.060
- 89. G. Bevilacqua, M. Worek, JHEP 1207, 111 (2012). doi:10.1007/JHEP07(2012)111
- G. Bevilacqua, M. Czakon, C.G. Papadopoulos, R. Pittau, M. Worek, JHEP 09, 109 (2009). doi:10.1088/1126-6708/2009/09/109
- 91. A. Bredenstein, A. Denner, S. Dittmaier, S. Pozzorini, Phys. Rev. Lett. 103, 012002 (2009). doi:10.1103/PhysRevLett.103.012002
- A. Bredenstein, A. Denner, S. Dittmaier, S. Pozzorini, JHEP 03, 021 (2010). doi:10.1007/ JHEP03(2010)021
- P. Artoisenet, R. Frederix, O. Mattelaer, R. Rietkerk, JHEP 1303, 015 (2013). doi:10.1007/ JHEP03(2013)015

## **Chapter 11 Summary and Prospects of Part II**

In the second part of this thesis, we mainly focus on the realization of automatically calculating one-loop scattering amplitudes in any theory. With the state-of-the-art techniques, we have developed a one-loop program Madloop5 based on Madgraph5. It is an important part in the Madgraph5\_AMC@NLO, which is the first realization of automation of NLO computations including the fixed-order calculations, its matching to parton shower (via MC@NLO formalism) and its merging of the matched samples in different parton multiplicities. It is a milestone, and we can claim that the theoretical frontier now is next-to-next-to-leading order. We summarize the following aspects presented in this part of the thesis

- 1. We first contribute ourselves to study the modern one-loop integral reduction techniques. It also establishes the main algorithms of one-loop integral reduction adopted in MadLoop5.
- 2. In the next chapter, we describe how the one-loop scattering amplitudes can be computed automatically in MadLoop5. It is general enough to be applicable to any theory and any type of quantum correction. We have also presented some examples to its applications to QCD and EW corrections in SM processes and OCD corrections to BSM processes.
- 3. We briefly describe the MADGRAPH5\_AMC@NLO framework. It has all features of phenomenological analysis for collider physics up to NLO level. We describe its main structure and its usage and present some examples.
  - Before closing this part, we establish some of our plans here.
- Apply MadGraph5\_aMC@NLO to QCD+EW corrections to SM and BSM processes.
- Extend MADGRAPH5\_AMC@NLO to loop-induced processes. There are two key ingredients missing: optimize MADLOOP5 for loop-induced processes; construct multichannel phase space integration for loop-induced processes.

- Extend MADGRAPH5\_AMC@NLO to higher multiplicity processes  $2 \rightarrow n (n \ge 5)$ .
- Generalize MADLOOP5 to decay processes.
- Apply MadLoop5 to quarkonium production processes.

## Appendix A Advanced Usage of HELAC-Onia

## A.1 Program Structure

In this section, we will describe briefly the program structure of HELAC-ONIA for future development. The main files contained in the program are already described in the README file of the tar-ball. The files in the program are mainly included in several subdirectories, which are displayed in Fig. A.1. There are mainly six subdirectories under the main directory of HELAC-ONIA. Let us explain them in detail:

- input. All of the input files that required by the program are contained in this subdirectory. They are:
  - user.inp: a file for a user to specify his/her input parameters.
  - default.inp: a file that includes all of the default values for the input parameters.
  - process.inp: a file for a user to tell the program the process information.
  - ho configuration.txt: configuration file for HELAC-ONIA.
  - seed.input: seed for random number generators.
- output. All of the output files will be generated here. Initially, it is empty.
- src. It contains all of the main source files of the program. They can be mainly divided into two parts. One part is for the matrix elements generator and the other part is for the phase space integration and events generation.
  - 1. Matrix elements generation.
    - Helac\_Global.f90: It is a file which contains all of the global variables.
    - Helac Func 1.f90: In it, many helper functions and subroutines are defined.
    - alfas\_functions.f90: Running of  $\alpha_S$  which is used in MCFM.
    - Projectors.f90: It is a file in which the Clebsch-Gordan coefficients are defined.
    - Constants.90: Several subroutines are defined for reading input parameters.
    - SM FeynRule Helac.f90: It contains all of the Feynman rules of the SM.

**Fig. A.1** Program structure of HELAC-ONIA with version 1.2.X



- Feynman\_Helac.f90: A useful subroutine is written in this file for reconstructing all Feynman diagrams.
- Helac wavef.90: It is a file to define all of the external wave functions.
- Helac\_pan2.f90: Definition of vertices to be used in Helac\_pan1.f90.
- Helac\_pan1.f90: Off-shell currents generation by using recursion relation.
- Helac\_master.f90: It is the main file of computing helicity amplitudes.
- 2. Phase space integration and events generation. It is based on several adapted Monte Carlo programs.

#### a. PHEGAS:

- Phegas.f90: It is an extended version of PHEGAS to deal with quarkonium kinematics. It is also rewritten in FORTRAN 90.
- Phegas\_Choice.f90: Some helper functions are defined here for the calling by Phegas.f90.

#### b. VEGAS:

- MC VEGAS.f90: A FORTRAN 90 version of VEGAS.
- Func\_PSI.f90: Some helper functions of phase space integration are written in this file.
- Colliders\_PSI1.f90: Phase space integration with VEGAS for  $2 \rightarrow n(n \ge 1)$  at hadron colliders.
- Colliders\_PSI2.f90: Phase space integration with VEGAS for  $2 \rightarrow n(n \ge 2)$  at electron-positron colliders.

#### c. MINT:

mint-integrator.f90: It is a FORTRAN 90 version of MINT.

### d. Internal FORTRAN 90 PDF files:

- CTEQ6PDF.f90:CTEQ6 PDF file in FORTRAN 90 version.
- Structf\_PDFs.f90: A file for calling PDFs.

#### e. LHAPDF file:

 Structf\_LHAPDF.f90: A file for calling PDFs from LHAPDF. User should specify "lhapdf=/path/to/lhapdf-config" in input/ho\_configuration.txt.

#### f. Others:

- Helac\_ranmar.f90: A random number generation program RANMAR in FORTRAN 90.
- MC PARNI Weight.f90: PARNI in FORTRAN 90, but it is not used.
- MC\_RAMBO.f90: RAMBO in FORTRAN 90.

- MC Helac GRID.f90: A grid file.
- Helac\_unwei.f90: There are some subroutines for dealing with unweighted events in this file.
- ADAPT.f90: It is for optimization by using an adaptation procedure.
- Phegas\_Durham.f90: Durham in FORTRAN 90. It can only be used to generate phase space points for the massless external particles.
- MC\_Func.f90: There are some helper functions and subroutines for Monte Carlo integrations.
- Kinetic Func.f90: Some kinematical variables are defined in this file.
- Cuts Module.f90: It is a file to provide users to impose kinematical cutoff.
- KT\_Clustering.f90: k<sub>T</sub> clustering and reweighting factor for MLM merging.
- setscale.f90: It provides the user to specify his/her renormalization and factorization scales.
- setscale\_default.f90: It is only a default set scale.f90 file for backup.
- Helac\_histo.f90: Histogram drawing file in HELAC.
- SinglePro.f90: It is the main file for phase space integration and events generation.
- Summation\_Pro.f90: A file for the summation mode, which is not used yet.
- unweight\_lhe.f90: A file for writing out LHE files.
- FO\_plot.f90: A file for fixed-order plots. In this case, unweighted events generation is not necessary.
- Main Test.f90: The FORTRAN 90 main program.
- pdf. More extended internal PDFs are in this subdirectory.
  - pdf list.txt: A summary of internal PDFs in HELAC-ONIA.
  - make\_opts,makefile\_pdf: Files of makefile for compiling PDF library. A library libpdf.a will be generated in lib subdirectory.
  - opendata.f: A file in FORTRAN 77 for opening PDF data.
  - Partonx5.f: Standalone FORTRAN 77 Partonx function.
  - CTEQ files: They include cteq3.f,Ctq4Fn.f,Ctq5Par.f,Ctq5Pdf.f,Ctq6Pdf.f.
  - MRST files: They include mrs98.f,mrs98ht.f,mrs98lo.f,mrs99.f,mrst2001.f, jeppe02.f.
- shower. The shower files are contained in this subdirectory.
  - QEDPS: It contains the file of QEDPS for ISR photon shower from initial  $e^{\pm}$  beams.
  - HERWIG6: HERWIG6 subsubdirectory.
  - interface: All interface files are included in this sub subdirectory. For example,
     QEDPS interface.f90 is a file to interface HELAC-ONIA to QEDPS.
- analysis. A subdirectory for analysis.
  - hbook: hbook files for plotting.
  - user: user defined plot files,like plot\_user.f90.

There are other subdirectories under the main directory. All generated libraries will be put in lib subdirectory. All module (object) files will be put in mod (obj) subdirectory. Executable files will be generated in subdirectory bin.

## A.2 How to Perform a Single Phase Space Point Computation with HELAC-Onia

The version 1.2.X of HELAC-ONIA also provides the user to perform a single phase space point computation without convolution of PDF, which might be very helpful in cross check with other programs. In this section, we will demonstrate how can we use it in such a mode. Again, first of all, one should specify the process information in input/process.inp and set the parameters in input/user.inp. Especially, one should make sure ranhel is 0, gener is -1, ptdisQ is F and alphasrun is 0.1 Moreover, one should also supply his/her phase space point in a file with name PS. input and put it into the input subdirectory. For example, if we have a  $2 \rightarrow 2$  process and the ith 4-momentum is  $P_i \equiv (E_i, p_{ix}, p_{iy}, p_{iz})$ , the PS. input should be in the form of

$$E_1$$
  $p_{1x}$   $p_{1y}$   $p_{1z}$   
 $E_2$   $p_{2x}$   $p_{2y}$   $p_{2z}$   
 $E_3$   $p_{3x}$   $p_{3y}$   $p_{3z}$   
 $E_4$   $p_{4x}$   $p_{4y}$   $p_{4z}$ 

Then one just runs the program with shell command

and get the result from screen output.

 $<sup>^1</sup>$ Supply your  $\alpha_S$  and/or  $\alpha$  values with the parameters alphas2 and alphaem if you want to use your own values.

<sup>&</sup>lt;sup>2</sup>Since we always assume the first two particles are initial states while the rest ones are final states, we have the momentum conservation  $P_1 + P_2 = P_3 + P_4$ .

## Appendix B

## Validation of IREGI

In this appendix, we present the comparisons between IREGI [1] results and CUTTOOLS [2] in the framework of MADLOOP5. These comparisons are an essential part of the validation of IREGI, and it also allows us to cross-check the results with other programs.

We compute the renormalized virtual part as

$$\begin{split} \mathcal{V} &\equiv 2 \overline{\sum_{\text{color}}} \Re \{ (\mathscr{A}^{1-\text{loop}} + \mathscr{A}^{\text{UV}}) (\mathscr{A}^{\text{Born}})^* \} \\ &= \sup_{\text{spin}} \\ &= \frac{\alpha_S a_0}{2\pi} \frac{(4\pi)^{\varepsilon}}{\Gamma(1-\varepsilon)} \left( \frac{\mu_F^2}{Q_{\text{FS}}^2} \right)^{\varepsilon} \left( \frac{c_{-2}}{\varepsilon^2} + \frac{c_{-1}}{\varepsilon^1} + c_0 \right), \end{split} \tag{B.1}$$

where the Born matrix element squared is

$$a_0 \equiv \overline{\sum_{\text{color}}} |\mathscr{A}^{\text{Born}}|^2,$$
 (B.2)

and  $Q_{\rm ES}$  is the Ellis-Sexton scale [3]. In the above equations, the summation symbol  $\overline{\sum}$  represents averages over initial-state color and helicity and summations over final-state color and helicity.

In the following validations, we assume

$$\mu_R = \mu_F = Q_{\rm ES} = \sqrt{s} \tag{B.3}$$

and take the CKM matrix to be diagonal. The results are in HV scheme and the masses not in the parameter tables are understood as zero.

## **B.1** Processes with QCD Corrections

We used the following set of parameters:

Parameter	Value	Parameter	Value
$\alpha_S$	0.118	$n_{lf}$	4
$\overline{m_t}$	174.3	$y_t$	174.3
$m_b$	4.62	$y_b$	4.62
$m_{\tau}$	1.777	$y_{\tau}$	1.777
$m_W$	80.419	$m_Z$	91.188
$m_H$	120.0	$\alpha^{-1}$	132.50698

There are total 30 processes checked. All of them are in good agreement in double precision. We summarized the checked processes in Table B.1.

Next, we will establish the results for the two  $2 \rightarrow 4$  processes for example.

## B.1.1 $gg \rightarrow HHt\bar{t}$

The chosen kinematic configuration, in GeV, is

$p_g = (1000$	, 0	, 0	, 1000)
$p_g = (1000$	, 0	, 0	, –1000)
$p_H = (2.0539224638e+02)$	, -4.1602895162e+01	, 7.5448264745e+01	, -1.4269804951e+02)
$p_H = (6.2959722787e+02)$	, -1.9548912091e+02	, -5.6836769385e+02	, 1.4399596363e+02)
$p_t = (3.3561331875e+02$	, -1.9931298106e+02	, -1.8393108028e+02	, 9.3271126340e+01)
$p_{\bar{t}} = (8.2939720700e+02)$	, 4.3640499712e+02	, 6.7685050939e+02	, -9.4569040464e+01)

Table B.1 Summary of the validated processes with QCD corrections by using IREGI and CUTTOOLS

Processes	Processes	Processes	Processes
$d\bar{d}  o W^+W^-g$	$u\bar{d} \rightarrow W^+ gg$	$u\bar{u} \rightarrow W^+W^-Z$	gg  o gg
$d\bar{d}  ightarrow \gamma gg$	$gg \rightarrow \gamma t\bar{t}$	$u\bar{u} \rightarrow ZZZ$	$\bar{d}d  o g\gamma$
$d\bar{d}  o Zgg$	$gg \rightarrow gt\bar{t}$	$u\bar{u} \to d\bar{d}$	$\bar{u}u \rightarrow gZ$
$d\bar{d}  o ZZg$	$gg \rightarrow HHt\bar{t}$	$dg \rightarrow dg$	$e^+e^-  o d\bar{d}$
$gg \rightarrow Zt\bar{t}$	$gg \rightarrow W^- \bar{d}u$	$\bar{d}\bar{u}  o \bar{d}\bar{u}$	$d\bar{u} \rightarrow W^- g$
$gg \rightarrow Ht\bar{t}$	$gg \rightarrow Zc\bar{c}$	$g\bar{u} \rightarrow g\bar{u}$	$\bar{d}d \rightarrow gZ$
$gs \rightarrow e^- \bar{\nu}_e c$	$s\bar{s} \rightarrow \gamma Zg$	$gg  o d\bar{d}$	
$u\bar{d} \to Ht\bar{b}$	$u\bar{u} \rightarrow W^+W^-b\bar{b}$	$gg \rightarrow t\bar{t}$	

#### The results are

$gg \rightarrow HHt\bar{t}$	CUTTOOLS	IREGI	Relative difference
$a_0$	7.6718349690e-12	7.6718349690e-12	0.000000000e+00
$\overline{c_{-2}}$	-6.0000000000e+00	-6.0000000000e+00	2.4533708398e-12
$\overline{c_{-1}}$	-4.9348538318e+00	-4.9348538316e+00	2.1115155094e-11
$c_0$	2.1609406234e+01	2.1609410055e+01	8.8416736662e-08

## $B.1.2 \quad u\bar{u} \rightarrow W^+W^-b\bar{b}$

The chosen kinematic configuration, in GeV, is

$p_u = (1000$	, 0	, 0	, 1000)
$p_{\bar{u}} = (1000$	, 0	, 0	, –1000)
$p_{W^+} = (1.9268605143e+02$	, -4.3702044719e+01	, 7.9255143831e+01	, -1.4989813850e+02)
$p_{W^-} = (6.5420231049e+02)$	, -2.0535287918e+02	, -5.9704571705e+02	, 1.5126154123e+02)
$p_b = (3.0130931053e+02$	, -2.0936967914e+02	, -1.9321165665e+02	, 9.7977290244e+01)
$p_{\bar{b}} = (8.5180232756e+02)$	, 4.5842460304e+02	, 7.1100222987e+02	, -9.9340692981e+01)

#### The results are

$u\bar{u} \rightarrow W^+W^-b\bar{b}$	CUTTOOLS	IREGI	Relative difference
$a_0$	1.1869091909e-11	1.1869091909e-11	8.4392641888e-15
$c_{-2}$	-2.6666666667e+00	-2.6666666659e+00	1.3590936711e-10
$c_{-1}$	1.6986902388e+01	1.6986902387e+01	3.4859229497e-11
$c_0$	2.0824345522e+02	2.0824343491e+02	4.8758156539e-08

## **B.2** Processes with QED/EW Corrections

We used the following set of parameters:

Parameter	Value	Parameter	Value
$\alpha_S$	0.118	$n_{lf}$	5
$m_t$	174.3	$y_t$	174.3
$m_W$	80.419	$m_Z$	91.188
$m_H$	120.0	$\alpha^{-1}$	132.50698

Processes	Processes	Processes	Processes
$\gamma \gamma \to t \bar{t}$	$HH \rightarrow HH$	$u\bar{u} \rightarrow ZZ$	$gg \rightarrow t\bar{t}H$
$\gamma\gamma \to W^+W^-$	$t\bar{t} \rightarrow W^+W^-$	$v_e \bar{v}_e \rightarrow e^+ e^-$	$HH \rightarrow HHH$
$e^+e^-  o t\bar{t}\gamma$	$u\bar{u} \rightarrow \gamma \gamma$	$W^+W^-  o HH$	$\bar{u}d \rightarrow W^-Z$
$e^+e^- \rightarrow t\bar{t}g$	$u\bar{u} \rightarrow e^+e^-$	$\gamma \gamma  o t \bar{t} \gamma$	$\bar{u}u \rightarrow W^+W^-$
$gg \rightarrow t\bar{t}$	$u\bar{u} \rightarrow W^+W^-$	$\bar{d}d \rightarrow W^+W^-$	$\bar{u}u \to ZZ$
$gg \rightarrow t\bar{t}g$	$u\bar{u} \rightarrow Z\gamma$	$\bar{d}d \rightarrow ZZ$	

**Table B.2** Summary of the validated processes with QED/EW corrections by using IREGI and CUTTOOLS

We have set leptons to be massless and the CKM matrix to be diagonal. The renormalization procedure follows Ref. [4]. Especially for the coupling constant renormalization, we use  $\alpha(m_Z)$  renormalization scheme [5] (we want to point out that the  $G_{\mu}$ -scheme [4, 5] is also available in MADLOOP5).

In Table B.2, we summarized the total 23 validated processes with QED/EW corrections. For instance, we choose  $\gamma\gamma\to t\bar{t}\gamma$  and  $HH\to HHH$  here to present the explicit results.

## $B.2.1 \quad \gamma \gamma \rightarrow t\bar{t}\gamma$

The chosen kinematic configuration, in GeV, is

$p_{\gamma} = (500$	, 0	, 0	, 500)
$p_{\gamma} = (500$	, 0	, 0	, –500)
$p_t = (1.8532118462e+02$	, 3.0437958333e+01	, -5.5083775653e+01	, 1.6612710311e+00)
$p_{\bar{t}} = (3.9710407423e+02)$	, 1.7551456272e+02	, -2.9693655639e+02	, -9.1293348717e+01)
$p_{\nu} = (4.1757474115e+02)$	, -2.0595252105e+02	, 3.5202033204e+02	, 8.9632077686e+01)

#### The results are

$\gamma\gamma \to t\bar{t}\gamma$	CUTTOOLS	IREGI	Relative difference
$a_0$	3.3998008154e-08	3.3998008154e-08	3.2560709591e-12
$c_{-1}$	8.7520121350e-01	8.7520121345e-01	5.7129724419e-11
$c_0$	-1.6920547939e+00	-1.6920548155e+00	1.2765543971e-08

Because there is no soft-collinear divergence in  $\gamma \gamma \to t \bar{t} \gamma$ ,  $c_{-2}$  is zero.

## $B.2.2 \quad HH \rightarrow HHH$

The chosen kinematic configuration, in GeV, is

$p_H = (500$	, 0	, 0	, 4.8538644398e+02)
$p_H = (500$	, 0	, 0	, -4.8538644398e+02)
$p_H = (2.8487875044e+02$	, -2.0209461376e+02	, 1.5512548791e+02	, 4.3008749625e+01)
$p_H = (4.5606319356e+02$	, 2.0741430639e+02	, -3.5666887273e+02	, -1.5284062696e+02)
$p_H = (2.5905805600e+02)$	, -5.3196926339e+00	, 2.0154338483e+02	, 1.0983187734e+02)

### The results are

$\gamma \gamma \to t \bar{t} \gamma$	CUTTOOLS	IREGI	Relative difference
$a_0$	8.6599627528e-08	8.6599627528e-08	4.6189578929e-12
<i>c</i> <sub>0</sub>	7.7243279942e+01	7.7243279942e+01	5.1784444342e-12

Because there is no IR divergences in  $HH \rightarrow HHH$ ,  $c_{-2}$  and  $c_{-1}$  are zero.

# Appendix C Timing Scale of MadLoop5

We presented a table of timing scale in Madloop5 for several processes. It is shown in Table C.1. The time presented in the table is obtained by running Madloop5 on a single core of a 2.3 GHz i7 CPU, with the gfortran compiler version 4.6.2 without optimization flags. All of these processes have been corrected by QCD corrections and QED/EW corrections. The corresponding times are the columns "(un)polarized QCD" and "(un)polarized QED" respectively. The "polarized" columns are the times of calculating only one non-zero helicity, whereas the "unpolarized" columns the times of evaluating the helicity-summed results. We point out here that though for the most complicated process  $u\bar{u} \rightarrow W^+W^-W^+W^-$  with EW corrections is a little bit time consuming in the helicity-summed case. It is still possible to calculate it with Madloop5 by using the efficient Monte Carlo over helicities method adopted in Madgraph5\_AMC@NLO [6], because the time for computing one helicity result is only about one second.

**Table C.1** The typical time costs in MADLOOP5 to calculate a randomly phase space point

Processes	Polarized QCD	Polarized QED	Unpolarized QCD	Unpolarized QED
$e^+e^-  o t\bar{t}$	0.0705 ms	1.54 ms	0.132 ms	3.58 ms
$gg \to t\bar{t}$	1.45 ms	2.4 ms	3.1 ms	6.75 ms
$gg \rightarrow t\bar{t}H$	9.72 ms	21.9 ms	38 ms	85.4 ms
$\gamma \gamma \to t \bar{t} H$	4.09 ms	31.1 ms	12 ms	156 ms
$u\bar{u} \rightarrow W^+W^-Z$	2.77 ms	50.9 ms	28.1 ms	866 ms
$ \begin{array}{c} e^+e^- \to \\ W^+W^-e^+e^- \end{array} $	_	424 ms	_	8.02 s
$ \begin{array}{c} u\bar{u} \to \\ W^+W^-W^+W^- \end{array} $	23.6 ms	1.27 s	968 ms	72.5 s

The word "polarized" means only one non-zero helicity is computed, whereas the word "unpolarized" represents we have summed the helicities

### References

- 1. H.S. Shao, unpublished
- G. Ossola, C.G. Papadopoulos, R. Pittau, JHEP 03, 042 (2008). doi:10.1088/1126-6708/2008/ 03/042
- 3. R.K. Ellis, J. Sexton, Nucl. Phys. B 269, 445 (1986). doi:10.1016/0550-3213(86)90232-4
- 4. A. Denner, Fortschr. Phys. 41, 307 (1993)
- S. Dittmaier, Kramer. Michael. Phys. Rev. D 65, 073007 (2002). doi:10.1103/PhysRevD.65. 073007
- J. Alwall, R. Frederix, S. Frixione, V. Hirschi, F. Maltoni, O. Mattelaer, H.S. Shao, T. Stelzer, P. Torrielli, M. Zaro, JHEP 07, 079 (2014). doi:10.1007/JHEP07(2014)079

## Index

 $\mathbf{A}$ 

A factorization theorem, 10	Complex mass scheme, 122
ALOHA, 121, 143	Confinement, 1
Angular distribution, 52	CS states, 12
Asymptotic freedom, 2	CTEQ6, 33
Automatic Libraries Of Helicity Amplitudes	Cut-constructible amplitude, 108
for Feynman Diagram Computations,	•
121	
	D
	Dark matter, 2
B	D-dimensional unitary method, 105
Benchmark processes, 31	Derivation index, 27
Berends-Giele off-shell recursive relation,	Dimensional regularization, 93, 101-103,
21	120
Beyond the Standard Model (BSM), 1	Direction test, 129
Binary representation, 23	Discrete Fourier Transform, 107
Binoth Les Houches Accord, 97	Double-parton-scattering (DPS), 60, 62, 65
Bjorken fractions, 38	Double-quarkonium production, 58
Bootstrap, 105	DURHAM, 29
BPHZ, 125	Dyson–Schwinger equations, 21
Buchmuller-Tye potential model, 40	
	E
C	Electro-Weak (EW), 1, 30
CKKW, 141	Ellis-Sexton scale, 128
Clifford algebra, 104	Extra-Dimensional Models (EDM), 1
Collinear factorization theorem, 12	
Collins-Soper frame, 31	
Color projectors, 26	F
Color-evaporation model (CEM), 10, 11	Factorization, 2
Color-flow, 26	FDH, 103
Color-flow basis, 24	Feed-down, 47, 48
Color-octet (CO) states, 12	Feynman's Tree Theorem, 94
Color-singlet, 9	Finite-width effects, 122
Color-singlet model (CSM), 10, 62	Fixed-target experiments, 33
CO mechanism (COM), 12	Fock states, 26, 37
© Springer Science+Business Media Singapore 2016	165
HS. Shao, Heavy Quarkonium Production Phenome	
of One-Loop Scattering Amplitude Computations, Sp	
DOI 10.1007/978-981-10-1624-0	5

Completeness relation, 26

166 Index

Fragmentation-function (FF), 10, 12	Lorentz test, 129
Frixione-Kunszt-Signer (FKS), 139	Lorentz-invariant phase space measurement,
FxFx, 141	38
	Low-momentum transfer, 10
G	
Gell-Mann, 26	M
Gottfried-Jackson frame, 31	MC@NLO, 92, 139
Gram determinant, 114	MINT, 32
	Mixed corrections, 122
	MLM, 141
Н	Monte Carlo generator, 29
Heavy ion collisions, 33	Monte Carlo sampling over the helicity con-
Heavy quarkonium production mechanism,	figurations, 25, 29
9, 39	Monte Carlo simulations, 92
HELAS, 143	MSSM, 103
Helicity frame, 31, 40, 41, 50, 66, 67	Multi-channel techniques, 34
Hierarchy problem, 2	Multi-leg, 31
Higgs boson, 2	
Higgs Effective Field Theory, 103	
Higgs mechanism, 1	N
Higher-order QCD corrections, 33	Next-to-leading order (NLO), 2
HV, 103	NLO computations, 92
HV scheme, 120, 130	NLO NRQCD, 43–49
	NLO*, 60
	NNLO* QCD corrections, 33
I	Non-relativistic QCD, 10
Identity numbers, 28, 29	NRQCD, 10, 12, 37
Infrared (IR) safety, 2	NRQCD factorization, 13, 40, 44, 51, 56
Initial radiation, 33	NRQCD factorization theorem, 15
Integration-by-parts method, 112	Nucleon collisions, 33
Intrinsic charm, 60	Numerical stability test, 122
IR subtraction method, 95	- · · · · · · · · · · · · · · · · · · ·
	0
K	Off-shell current, 21
Kinoshita-Lee-Nauenberg (KLN) theorem,	One-loop master integrals, 108, 120
94	One-particle irreducible Green functions,
	103
	On-shell renormalization, 125
L	Ossola-Papadopolous-Pittau (OPP), 101
Large Hadron Collider (LHC), 2	
Lattice QCD, 2	
L-cut diagrams, 121, 126	P
Leading- $p_T$ resummation contribution, 38	Parton model, 1
Les Houches Event (LHE) format, 31	PDFs, 38
LHAPDF, 30, 32, 33	Perturbative QCD, 10
Little Higgs Models (LHM), 1	Phase space slicing method, 95
Long-distance matrix elements (LDMEs),	Plus functions, 95
10, 38, 40–42	Polar angular distribution, 39
Lönnblad, 141	Polarization, 45
Loop content filtering, 126, 127	Polarization puzzle, 16
Loop-induced processes, 114, 120	POWHEG, 92, 140
Lorentz invariance, 110	Production mechanism, 37
	·

Index 167

Projection method, 26	Spurious terms, 106
Prompt $\psi(2S)$ hadroproduction, 43	Stability diagnostic procedure, 128
Prompt $J/\psi$ , 46	Standard Model (SM), 1
Prompt $J/\psi$ production, 37, 45	Strong coupling constant, 30
P-wave currents, 27	Sudakov form factor, 77
	SUper-SYmmetric (SUSY), 1
0	
QCD Sum Rules, 2	Tr.
QED photon showering, 33	T
QEDPS, 31–33, 76	Target frame, 31
Quantum ChromoDynamics (QCD), 1, 30	Tensor integral, 109
Quantum ElectroDynamics (QED), 1, 30  Quantum ElectroDynamics (QED), 30	Tensor Integral Reduction (TIR), 101, 121
Quantum Field Theories (QFT), 2	Third party codes, 32
Quark model, 1	Transverse momentum factorization, 33
Quark-hadron duality, 11	Tree-level, 31
Quarkonium production mechanism, 58, 66	
Quarkonium production mechanism, 50, 00	
	U
R	Unitary-based methods, 91
RAMBO, 29, 32	Universal FeynRules Output (UFO), 121
Recursion relation, 31	
Renormalization, 124	
Renormalization procedure, 93	V
F,	VEGAS, 29, 32, 33
	Velocity scaling rule, 13
S	
SARAH, 140	
SDMEs, 50	W
Short-distance coefficients (SDCs), 10, 38,	Wave function at origin, 40, 74 Wick rotation, 93
Single-quark radiation hypothesis, 54	•
Soft-Collinear Effective Theory, 12	
Spin projectors, 26	Y
Spin symmetry relation, 51	Yields, 44, 46
Spin Symmetry rotation, ST	110100,, 10